University of Reading

Understanding the function of structural domains of CACHD1, a Ca_V3 calcium channel modulator

Mária Rožňovcová

PhD Thesis

May 2024

Supervisors

Prof. Gary J. Stephens

Dr. Graeme S. Cottrell

Dr. Paul Wright (LifeArc Ltd.)

School of Pharmacy, University of Reading

DECLARATION

I confirm that this thesis is my own work and the use of all materials from other sources has been properly and fully acknowledged. No part of this thesis was previously submitted for another degree at this or any other institution.

Mária Rožňovcová

3rd May 2024

ACKNOWLEDGMENTS

First and foremost, I would like to extend my deepest gratitude to my supervisors, Dr. Graeme Cottrell and Prof. Gary Stephens for giving me the opportunity to join their research groups. Your infinite patience, guidance and unparallel scientific expertise have been invaluable, shaping me into the scientist I am today. Thank you for your remarkable mentorship and for being such wonderful supervisors!

I would also like to thank Dr. Maria Maiarú and Dr. Silvia Amadesi for always making me feel welcome and supported, especially when I first joined during the Covid-19 lockdown. Additionally, I want to thank LifeArc and Dr. Paul Wright for supporting my PhD project.

A special thank you goes to Prof. Manoj Patel for inviting me to his lab at University of Virginia. His invaluable mentorship and expert guidance in patch-clamp electrophysiology have been pivotal in broadening my scientific knowledge. Additionally, I want to thank Tyler Deutsch for helping me complete a crucial set of electrophysiology experiments described in this thesis.

I want to thank all who supported me in Reading, particularly the wonderful group of people in the office. Special thanks go to Kamila, Tate, and Kathryn for making the lab a better and more joyful place to come to every day. Of course, I cannot forget our lunchtime (or really anytime) discussions about pretty much anything, that became the highlights during the longest lab days.

Lastly, I want to thank my partner Lewis, whose unwavering support and willingness to move across the country and embark on this journey with me have been a constant source of strength and motivation. Thank you for your encouragement and patience, but most importantly, for always believing in me. I simply could not have done it without you!

ABSTRACT

CACHD1 is classified as a member of the α2δ protein family due to their shared organisation of structural motifs and domains. However, unlike α2δ, CACHD1 has been characterised as a modulator of the Ca_V3 low-voltage-activated voltage-gated Ca^{2+} channels (LVA VGCCs), distinguishing it as the sole auxiliary subunit of LVA VGCCs. As a relatively unstudied protein, CACHD1 research has primarily focused on its functional effects on LVA VGCCs and its potential role in disease. This study represents the first investigation into the mechanisms by which specific motifs govern CACHD1 modulation of LVA VGCCs, and its trafficking pathways. This thesis tested the hypothesis that structural motifs within CACHD1 play crucial roles in regulating its expression, sub-cellular localisation, trafficking, and function as a modulator of LVA VGCCs.

This study first characterised the role of the variant MIDAS motif (D^{234}xGxS) on CACHD1 expression, sub-cellular localisation, and function as a modulator of Ca_V3 channels, using western blotting, immunocytochemistry, and whole-cell patch clamp electrophysiology. Interestingly, mutagenesis of the G^{236} residue to Ser showed similar CACHD1 expression and sub-cellular localisation in the absence of $Ca_V3.1$ compared to wild-type CACHD1 (CACHD1-wt). Moreover, like CACHD1-wt, CACHD1-G236S significantly increased the current density and G_{max} of rat $Ca_V3.1$ ($rCa_V3.1$) VGCCs. In contrast, mutating all three key residues to Ala (DxGxS to AxAxA) led to significant reduction in CACHD1 expression levels and disrupted trafficking to cell surface. Additionally, the AxAxA mutant resulted in a significant decrease in $rCa_V3.1$ currents and G_{max}, underscoring the important role of an intact MIDAS motif in CACHD1 function.

Next, this study investigated the internalisation, and post-endocytic mechanisms used by CACHD1. The use of endocytic inhibitors showed that methyl-β-cyclodextrin (MβCD), a cholesterol depleting agent, inhibited CACHD1 internalisation. Moreover, cholesterol recovery post-MβCD treatment restored CACHD1 internalisation, suggesting a caveolae pathway dependent on cholesterol was used by CACHD1. Additionally, CACHD1 co-localised with EEA1, Rab5, and Rab11, indicating CACHD1 recycling back to the membrane via a Rab11-associated pathway. Further analysis identified a tyrosine internalisation motif (Y^{1197}STM) present in the intracellular C-terminal tail of CACHD1. Mutagenesis of the Y^{1197} residue to Ala and Phe showed that the Y1197F slowed CACHD1 internalisation. Surprisingly, the removal of

the C-terminal tail, thus the YSTM signal motif, had no discernible effect on CACHD1 internalisation, indicating the involvement of multiple motifs. Moreover, removal of the transmembrane domain led to intracellular retention of CACHD1, but modification of the natural signal peptide to Igκ signal peptide facilitated protein secretion, enabling the purification of soluble CACHD1 protein.

LAY SUMMARY

CACHD1 is a protein that belongs to a protein family involved in important cellular functions like muscle contraction, hormone release, and neuronal response to signals. What makes CACHD1 unique is its role in regulating a specific type of calcium channels known as low-voltage-activated voltage-gated calcium channels (LVA VGCCs), which play a crucial role in the process of how neurons respond to signals in our body. However, despite its importance, CACHD1 has not been studied in depth, and researchers are only beginning to understand how it works.

This study explored how different parts of the CACHD1 protein influence its behaviour and function. A specific part of the protein, called the MIDAS motif, is essential for CACHD1 to function properly. When the MIDAS motif was altered, the CACHD1 protein failed to reach the cell surface where it is needed to regulate the function of calcium channels, leading to reduced activity of LVA VGCCs.

This study also examined how CACHD1 moves and recycles within cells, finding that cholesterol played a key role in its movement. CACHD1 was shown to use specific pathways to return to the cell surface after being internalised. Another part of CACHD1 called the tyrosine internalisation motif, could help regulate how quickly CACHD1 is internalised by the cellular machinery.

These findings have several important implications. First, they enhance our understanding of how LVA VGCCs are regulated. This could lead to new insights into diseases linked to LVA VGCCs dysfunction, including many neurological diseases. If abnormalities in CACHD1 are found to contribute to these diseases, this protein could become a target for new disease treatments.

TABLE OF CONTENTS

ABBREVIATIONS

5-HT	5-hydroxytryptaine
AID	α-interaction domain
AIS	atomic ion spectroscopy
Ala	alanine
AMPA	α-amino-3-hydroxy-5-methyl-4-isoxazolepropionic acid
APS	ammonium persulphate
AP-1	adaptor protein-1
AP-2	adaptor protein-2
AP-3	adaptor protein-3
AP-4	adaptor protein-4
APP	amyloid precursor protein
AQP4	aquaporin-4
ASIC	acid-sensing ion channel
ASS	atomic absorption spectroscopy
BACE1	β-site amyloid precursor protein cleaving enzyme 1
BCA	bicinchoninic acid
BID	β-interaction domain
BSA	bovine serum albumin
BVL	bovine leukaemia virus
CA	cornu ammonis
Ca^{2+}	calcium
CACHD1	Ca^{2+} channel and chemotaxis receptor domain containing 1
cAMP	cyclic adenosine monophosphate
Ca_V	voltage-gated calcium channel
CHO	Chinese hamster ovary
C_M	membrane capacitance
Cryo-EM	cryogenic electron microscopy
CTLA4	cytotoxic T-lymphocyte associated protein 4
Cx	connexin
DAPI	4’6-diamidino-2-phenylindole
ddH2O	distilled deionised water

DG	dendate gyrus
DHP	1,4-dihydropyridine
DMEM	Dulbecco's modified eagle's serum
DMSO	dimethyl sulphoxide
DNA	deoxyribonucleic acid
dNTP	deoxyribonucleotide triphosphate
DPBC-CM	Dulbecco's phosphate buffered saline without Ca^{2+} and Mg^{2+}
DPBS	Dulbecco's phosphate buffered saline
DPBS+CM	Dulbecco's phosphate buffered saline with Ca^{2+} and Mg^{2+}
DRG	dorsal root ganglion
ECACC	European Collection of Authenticated Cell Cultures
ECL	enhanced chemiluminescence
ECS	extracellular solution
EDTA	ethylenediaminetetraacetic acid
EEA1	early endosomal antigen-1
EGFP	enhanced green fluorescent protein
EHD2	EH-domain-containing protein 2
ELISA	enzyme-linked immunosorbent assay
Endo H	endoglycosidase H
ETX	ethosuximide
FACS	fluorescence-activated cell sorting
FBS	foetal bovine serum
FFA1	free fatty acid receptor 1
FFA4	free fatty acid receptor 4
FRET	fluorescence resonance energy transfer
GDP	guanosine diphosphate
GFP	green fluorescent protein
G_{max}	maximal conductance
GPCR	G protein-coupled receptor
GPI	glycosyl-phosphatidylinositol
GTP	guanosine triphosphate
H^+/K^+-ATPase	hydrogen potassium adenosine triphosphatase
HA	hemagglutinin

HCN	hyperpolarisation-activated cyclic nucleotide-gated channel
HEK	human embryonic kidney
HEPES	4-(2-hydroxyethyl)-1-piperazineethanesulfonic acid
His	histidine
HRP	horseradish peroxidase
HVA	high-voltage-activated
ICC	immunocytochemistry
ICS	intracellular solution
IgG	immunoglobulin G
IP3R	inositol triphosphate receptor
IUPAC	International Union of Pure and Applied Chemistry
KLHL1	kelch-like 1
KO	knockout
K_V	voltage-gated potassium channel
LB	loading buffer
LRP1	low density lipoprotein receptor-related protein-1
LTR	long terminal repeat
LVA	low-voltage-activated
MIDAS	metal ion-dependent adhesion site
MβCD	methyl-β-cyclodextrin
Na_V	voltage-gated sodium channel
NHS	normal horse serum
Ni-NTA	nickel-nitrilotriacetic acid
NMDAR	N-methyl-D-aspartate receptor
NMR	nuclear magnetic resonance
NSS	natural signal sequence
PAR-1	protease-activated receptor 1
PBS	phosphate buffered saline
PBST	phosphate buffered saline – Tween 20
PCR	polymerase chain reaction
PEI	polyethyleneimine
PFA	paraformaldehyde
Phe	phenylalanine

PIPES	piperazine-1,2-bis[2-ethanesulforic acid
PLA	proximity ligation assay
PLC	phospholipase C
PNGase F	peptide-N-glycosidase F
PrP	prior protein
PVDF	polyvinylidene difluoride
RAP	receptor-associated protein
RC	resistor-capacitor
$rCa_V3.1$	rat voltage-gated 3.1 calcium channel
R_M	membrane resistance
rtTA	reverse tetracycline transactivator
RyR	ryanodine receptor
SARS-CoV	severe acute respiratory syndrome - coronavirus
SD	standard deviation
SDS	sodium dodecyl sulphate
SDS-PAGE	sodium dodecyl sulphate polyacrylamide gel electrophoresis
SEC	size exclusion chromatography
SEM	standard error of the mean
SERCA	sarcoendoplasmic reticulum Ca2+ ATPase
SH3	*src* homology-3
SOB	super optimal broth
SOC	super optimal broth with catabolite repression medium
SP	sodium pyruvate
SPR	surface plasmon resonance
Stac1	stac adaptor protein 1
TAE	tris-acetate EDTA
TB	transformation buffer
Tet	tetracycline
TetO	tetracycline operator
TetON	tetracycline-ON
TetR	tetracycline repressor
TFR	transferrin receptor
TGF-β	transforming growth factor-β

TMD	transmembrane domain
TRH	thyrotropin-releasing hormone
TRP	transient receptor potential
TSP	thrombospondin
Tyr	tyrosine
TyrIM	tyrosine internalisation motif
$V_{1/2}$	midpoint activation
VGCC	voltage-gated calcium channel
V_{rev}	reversal potential
VWA	von Willebrand Factor A domain
YAP1	yes-associated protein 1

LIST OF FIGURES

LIST OF TABLES

1. INTRODUCTION

1.1 Intracellular calcium signalling and dynamics

Calcium ions (Ca^{2+}) are involved in several cellular processes, ranging from muscle contraction to neurotransmitter release, hormone secretion, cell proliferation, and gene expression. Intracellular Ca^{2+} signalling is typically initiated by external stimuli that trigger increase in intracellular Ca^{2+} levels which subsequently leads to downstream Ca^{2+} signalling pathways. An example of downstream signalling pathway activated by Ca^{2+} is the calmodulin and Ca^{2+}/calmodulin-dependent kinase II (CaMKII) pathway. The signalling pathway often begins with the activation of cell surface receptors, such as G protein-coupled receptors (GPCRs), followed by a series of events, often involving phospholipase C (PLC) and inositol triphosphate receptors (IP3Rs) which mediate the release of Ca^{2+} ions from intracellular stores into the cytoplasm (Islam, 2019; Klocke *et al*., 2023). Ca^{2+} binds to calmodulin, causing a conformational change that allows it to interact with target proteins. One key target of the Ca^{2+}/calmodulin complex is CaMKII. When Ca^{2+}/calmodulin binds to CaMKII, it activates the kinase by exposing its active site. As Ca^{2+} levels decrease, calmodulin releases Ca^{2+} and returns to its inactive state. However, once CaMKII is activated and undergoes autophosphorylation, it can remain active even in the absence of Ca^{2+} until dephosphorylated by a protein phosphatase (Villalobo and Berchtold, 2020). This sustained activation of CaMKII therefore provides a molecular memory of the Ca^{2+} signal, playing an important role in processes like memory and learning (Lucchesi *et al*., 2011; Coultrap and Bayer, 2012).

Additionally, activation of Ca^{2+}-permeable AMPA receptors (Barron and Kim, 2019) and N-methyl-D-aspartate receptors (NMDARs) (Lüscher and Malenka, 2012), as well as ligand-gated transient receptor potential (TRP) ion channels (Vangeel and Voets, 2019) leads to further increase in intracellular Ca^{2+} levels. Simultaneously, depolarisation of presynaptic neurons triggers Ca^{2+} influx from the extracellular environment through voltage-gated calcium channels (VGCCs). The elevation of cytosolic Ca^{2+} level can also lead to further depolarisation of membrane potential and subsequent activation of other ion channels. The rise in intracellular Ca^{2+} triggers the fusion of synaptic vesicles containing neurotransmitters with the presynaptic membrane, facilitating neurotransmitter release into the synaptic cleft. Neurotransmitters then bind to receptors on postsynaptic neurons, initiating various

downstream signalling events that lead to excitatory or inhibitory effects on the postsynaptic cell. Intracellular Ca^{2+} functions as an important secondary messenger, regulating neurotransmitter release, neuronal excitability, and synaptic plasticity, thus playing a crucial role in neuronal function.

1.2 Regulation of intracellular calcium

Ca^{2+} is essential for various cellular functions, and intracellular Ca^{2+} concentration is at significantly lower levels than outside the cell (Islam, 2019) to maintain Ca^{2+} homeostasis. This balance is meticulously regulated by a multitude of membrane pumps and channel proteins permeable to Ca^{2+} ions, such as sarcoendoplasmic reticulum Ca^{2+} ATPase (SERCA; Xu and Van Remmen, 2021), Na^{+}/Ca^{2+} exchangers (Ottolia *et al*., 2013), ryanodine receptors (RyR), IP3Rs (Woll and Van Petegem, 2021) and VGCCs (Zamponi *et al*., 2015). This project further focuses on VGCCs as the key regulators of intracellular Ca^{2+} levels.

1.3 Voltage-gated calcium channels

Voltage-gated calcium channels represent a class of transmembrane proteins important in cellular physiology, facilitating Ca^{2+} influx in response to changes in membrane potential. VGCCs are widely distributed across excitable cell types, including neurons, muscle cells and endocrine cells, where they fulfil diverse cellular functions, including but not limited to hormone secretion, transmitter release (Catterall *et al*., 2013), and excitation-contraction coupling (Bannister and Beam, 2013).

VGCCs were first studied and purified in 1987 from transverse T-tubule membranes found in skeletal muscle (Takahashi *et al*., 1987). Analysis of the purified protein complex revealed it was composed of five distinct components: α1, α2, β, δ, and γ subunits. Out of these subunits, α1 subunit showed the ability to bind Ca^{2+} channel blockers 1,4-dihydropyridines (DHPs) and was therefore established as the pore-forming subunit within the VGCC complex. The remaining subunits (α2, β, δ, and γ) were classified as auxiliary subunits due to their supportive roles in channel assembly and modulation. The study by Takahashi *et al*. (1987) led to the identification and cloning of the first VGCC, and thus it was termed $Ca_V1.1$. Subsequent studies resulted in the cloning of ten α1 subunits, four β subunits, and four α2δ subunits, further expanding the knowledge on VGCCs (Zamponi *et al*., 2015). In this chapter, the structure, function, biophysical properties, and classification of VGCCs will be described in more detail.

1.3.1 General structure of VGCCs

Structurally, VGCCs are multi-subunit protein complexes composed of the α1 pore-forming subunit and auxiliary subunits, each contributing to channel assembly, expression, and modulation. All VGCCs contain a main α1 pore-forming subunit which consists of four homologous domains (I-IV), each containing six transmembrane segments (S1-S6) with voltage-sensing residues (positively charged lysine/arginine residues) present within the S4 segment of each domain, and hairpin-like loop between S5 and S6 segments as shown in Figure 1.1 (Weiss and Zamponi, 2020). These voltage-sensing residues serve as the voltage sensor and facilitate channel opening/closing in response to membrane depolarisation, and thereby regulate Ca^{2+} influx into the cell (Zamponi *et al*., 2015). Most types of VGCCs also require the auxiliary subunits to function correctly, and Figure 1.1 shows the general interaction sites of β and α2δ subunits.

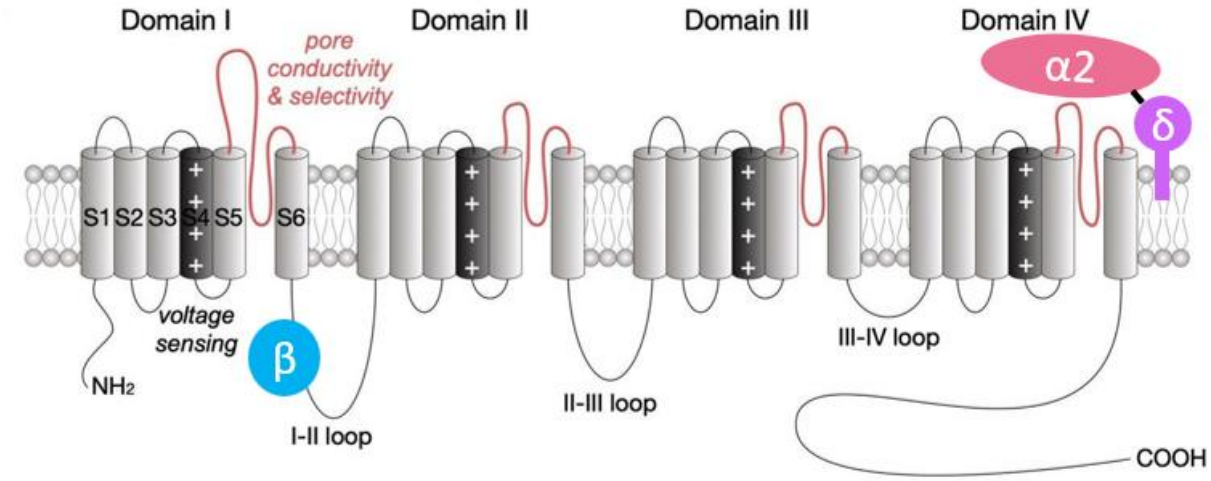

Figure 1.1 Schematic representation of the general membrane topology of VGCCs α1 pore-forming subunit. The α1 pore-forming subunit of VGCCs contains four homologous domains (I-IV). Each of these domains consists of six transmembrane segments (S1-6). Positively charged residues (lysine and arginine) in the S4 transmembrane segment form the voltage sensor, and the loop between segments S5 and S6 determines ion conductance and selectivity. The α1 subunit contains intracellular N-terminus and C-terminus. In general, β subunit binds to the intracellular I-II loop, while α2δ subunit associates with the α1 subunit extracellularly. The α2δ subunit consists of an extracellular α2 subunit (pink) linked to a membrane-associated δ subunit (purple) via disulphide bonds. (Adapted from: Weiss and Zamponi, 2020).

1.3.2 Classification of VGCCs

Depending on the voltage threshold required for channel activation, VGCCs are classified into high-voltage-activated (HVA) and low-voltage-activated (LVA) VGCCs, with LVA VGCCs requiring smaller depolarisation for activation compared to HVA VGCCs (Carbone and Lux, 1984). VGCCs are further categorised into three main families based on their α1 pore-forming subunit: Ca_V1 and Ca_V2 as HVA VGCCs, and Ca_V3 as LVA VGCCs (Catterall *et al*., 2005). Moreover, each VGCC family exhibits distinct subtypes in terms of the type of current associated with the subunit, such as L-type, N-type, P/Q-type, and T-type currents, each with specific cellular distribution, function, and biophysical properties as summarised in Tables 1.1 and 1.2. This complex categorisation underscores the diversity and specialisation of VGCCs, and while VGCCs possess distinctive properties, they do share structural and sequence similarities as shown by a phylogenetic tree of the α1 pore-forming subunits (Figure 1.2).

Table 1.1 Physiological properties of HVA and LVA VGCCs.

Voltage-gated Ca^{2+} channel type		Gene (chromosome)	Localisation	Function
HVA VGCCs	**$Ca_V1.1$**	*CACNA1S* (1q31-32)	skeletal muscle	skeletal muscle contraction
	$Ca_V1.2$	*CACNA1C* (12p13)	neurons, cardiomyocytes, pancreatic islets, adrenal chromaffin cells, intestinal/bladder smooth muscle	normal brain function, pacemaking activity, hormone release, excitation-contraction coupling
	$Ca_V1.3$	*CACNA1D* (3p14.3)	neurons, auditory and vestibular hair cells, cardiomyocytes, pancreatic islets, adrenal chromaffin cells, adrenal cortex	normal brain function, neurotransmitter release, pacemaking activity, β-cell mass maintenance, hormone release
	$Ca_V1.4$	*CACNA1F* (Xp11.23)	retina	normal visual function, neurotransmitter release
	$Ca_V2.1$	*CACNA1A* (19p13.1)	presynaptic nerve terminals, dendrites, neuroendocrine cells	evoked synaptic transmission, action potential, neurotransmitter release, hormone release, dendritic Ca^{2+} transients, gene transcription regulation
	$Ca_V2.2$	*CACNA1B* (9q34)		
	$Ca_V2.3$	*CACNA1E* (1q25-31)		
LVA VGCCs	**$Ca_V3.1$**	*CACNA1G* (17q22)	neuronal cell bodies dendrites, cardiomyocytes, smooth muscle myocytes	neuronal excitability regulation, evoked hormone secretion, pacemaking activity, neurotransmitter release, sleep-wake cycle, gene transcription regulation
	$Ca_V3.2$	*CACNA1H* (16p13.3)		
	$Ca_V3.3$	*CACNA1I* (22q13)	neuronal cell bodies, dendrites	

Compiled from: Catterall *et al*., 2005; Zamponi *et al.,* 2015; Zamponi, 2016; Weiss and Zamponi, 2020.

Table 1.2 Structural and biophysical properties of HVA and LVA VGCCs.

Voltage-gated Ca^{2+} channel type		Structure		Electrophysiological properties			
		Pore-forming subunit	Auxiliary subunits	Current	Activation potential	Inactivation potential	Inactivation rate
HVA VGCCS	**$Ca_V1.1$**	α1S	β, α2δ, γ	L	-20 mV to +10 mV	-50 mV to -10 mV	slow
	$Ca_V1.2$	α1C					
	$Ca_V1.3$	α1D					
	$Ca_V1.4$	α1F					
	$Ca_V2.1$	α1A	β, α2δ	P/Q	-30 mV to +10 mV	-70 mV to +10 mV	slow / moderate
	$Ca_V2.2$	α1B		N			moderate
	$Ca_V2.3$	α1E		R			fast
LVA VGCCs	**$Ca_V3.1$**	α1G	CACHD1	T	-50 mV to -10 mV	-70 mV to -10 mV	fast
	$Ca_V3.2$	α1H					
	$Ca_V3.3$	α1I					

Compiled from: Catterall *et al*., 2005; Yagami *et al.*, 2012; Dolphin, 2018.

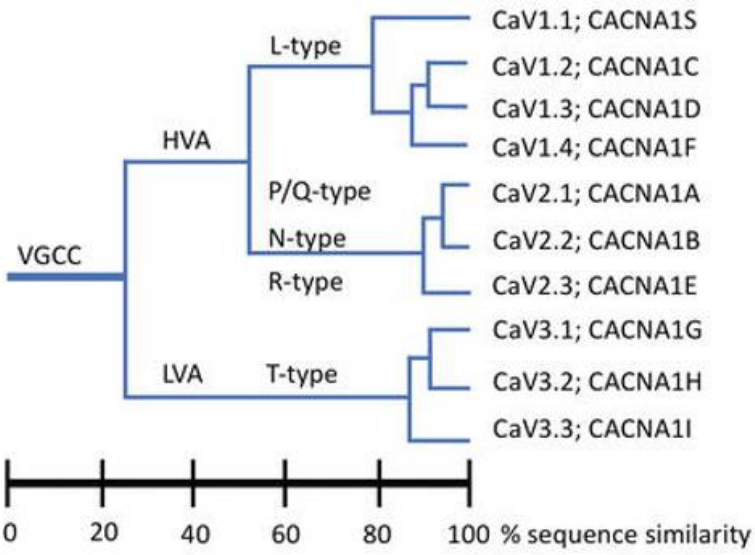

Figure 1.2 Dendrogram showing evolutionary relationship and sequence similarity among the members of VGCC family. (From: Feng *et al*., 2017).

1.3.3 Modulation of VGCCs

Mammalian VGCCs exhibit high functional diversity across the body, mainly due to the number of different subunit isoforms, including ten α1 pore-forming subunits, along with four α2δ, four β, and multiple γ subunits (Dolphin, 2012). VGCCs have been shown to be regulated through various modulation pathways. These pathways include GPCR inhibition of neuronal VGCCs, cyclic adenosine monophosphate (cAMP)-dependent phosphorylation of L-type VGGCs, and Ca^{2+}-calmodulin control of Ca^{2+}-dependent inactivation of L-type and P-type VGCCs (Dolphin, 2018), amongst others. This section further describes the modulation of VGCCs by the auxiliary subunits α2δ, β, and γ, with focus on α2δ subunits.

1.3.3.1 Beta (β) subunits

Initially cloned from skeletal muscle and termed β_1 (Ruth *et al*., 1989), the β subunit family has since seen the identification of three more isoforms, β_2, β_3, and β_4, each having multiple splice variants. For example, the β_1 isoform has two distinct variants, with β_{1a} primarily associated with skeletal muscle, while β_{1b} is a non-muscle variant (Pragnell *et al*., 1991).

β subunits are cytoplasmic proteins that interact with the intracellular loop between domains I and II of the HVA VGCCs α1 pore-forming subunit, via their variable β-interaction domain (BID) (Van Petegem *et al*., 2008). This interaction is facilitated by an 18-amino acid binding motif termed α-interaction domain (AID) located in the proximal part of the I-II linker (Pragnell *et al*., 1994). Structurally, β subunits contain a conserved *Src* homology-3 (SH3) and a guanylate kinase-like domains linked by a flexible loop, although due to mutations in the active site the guanylate kinase-like domain lacks kinase activity (Hanlon *et al*., 1999). Further structural studies revealed that the AID interaction site is situated in a groove of the guanylate kinase-like domain (Van Petegem *et al*., 2004).

Functionally, β subunits are considered VGCC chaperones, facilitating correct folding and trafficking of the α1 subunits. β subunits have been shown to play important roles in the expression of Ca_V1 and Ca_V2 channels, whereas Ca_V3 channels do not appear to require β subunits for their expression (Berrow *et al*., 1995; Qin *et al*., 1998). Additionally, β subunits act as modulators of channel biophysical properties through direct interaction with VGCCs and by interacting with other proteins such as G proteins, in particular Gβγ dimers GPCRs (Meir *et al*., 2000; Dolphin, 2003b).

1.3.3.2 Gamma (γ) subunit

The γ subunit, now termed γ1 subunit, has been shown to be associated exclusively with the skeletal calcium channel complex (Takahashi *et al*., 1987). Additionally, there are seven γ-like subunits, although their specific roles in relation to VGCCs have been subject to controversy. While the γ1 subunit has been shown to be involved in the modulation of VGCCs, other members of the γ subunit family are known for functions unrelated to VGCCs, including their role as trafficking proteins and modulators of the AMPA glutamate receptors (Tomita *et al*., 2003).

1.3.3.3 Alpha-2-delta (α2δ) subunit

α2δ genes and proteins

The first α2δ subunit was cloned from skeletal muscle (Takahashi *et al*., 1987), and now the α2δ family consists of four isoforms, α2δ-1, α2δ-2, α2δ-3, α2δ-4, encoded by the *CACNA2D1*, *CACNA2D2*, *CACNA2D3*, and *CACNA2D4* genes, respectively (Gao *et al*., 2000; Barclay *et al*., 2001; Qin *et al*., 2002). The *CACNA2D* genes undergo alternative splicing, thereby expanding the α2δ protein family and their functional roles.

The α2 and δ proteins are encoded by the same gene and form the α2δ precursor protein linked via disulphide bonds (De Jongh *et al*., 1990). This precursor protein is post-translationally cleaved by the metalloprotease ADAM17 into α2 and δ peptides (Figure 1.3), which remain linked by disulphide bonds formed prior to the cleavage (De Jongh *et al*., 1990; Jay et al., 1991; Wu *et al*., 2016). Further post-translational modifications of α2δ proteins include glycosylation and cleavage of the N-terminal signal peptide, and ultimately lead to a mature form of α2δ proteins (Ablinger *et al*., 2024). All these post-translational modifications have been shown to be essential for proper α2δ trafficking and function as a VGCC modulator (Kadurin *et al*., 2017).

Bioinformatics analysis revealed several recognisable protein domains in α2δ, including a von Willebrand Factor A (VWA) domain involved in protein-protein interactions between the extracellular matrix and cell-adhesion proteins, generally through a metal ion-dependent adhesion site (MIDAS) motif which coordinates a divalent cation binding (Ca^{2+}, Mg^{2+} or Mn^{2+}) (Whittaket and Hynes, 2002). Moreover, the VWA domain was shown to be essential for the trafficking of α2δ subunits, as well as the α2δ-associated effects on the trafficking of the α1 pore-forming subunit (Cantí *et al*., 2005; Hoppa *et al*., 2012; Cassidy *et al*., 2014). Surprisingly,

α2δ are predicted to contain cache domains which are normally found in bacteria and are used in a process called chemotaxis (Anantharaman and Aravind, 2000). Additionally, α2δ contain a short hydrophobic domain at their C-terminal, which classifies them into a type I transmembrane protein group; however, many proteomic studies suggest that α2δ proteins are linked to the plasma membrane through a glycosyl-phosphatidylinositol (GPI)-anchor as all α2δ subunits, especially α2δ-3 and α2δ-4, have a short or absent C-terminal cytoplasmic domain (Davies *et al*., 2010; Ablinger *et al*., 2024). Moreover, the cryo-EM (cryogenic electron microscopy) α2δ structure reported by Wu *et al*. (2016) and Chen *et al*. (2023) shows that the α2δ protein is entirely extracellular, with δ peptide linked to the plasma membrane via a glycophosphatidyl molecule, further supporting GPI-anchoring of α2δ. There is some evidence suggesting that α2δ-1, but not α2δ-2 or α2δ-3, interact with NMDARs via the C-terminus of α2δ-1, surprisingly after the GPI-anchor cleavage site (Chen *et al*., 2018). This would indicate that NMDARs interact with either a transmembrane version of α2δ-1 intracellularly, or with the C-terminal peptide of α2δ-1 that is cleaved off during GPI-anchor attachment (Hooper, 2001).

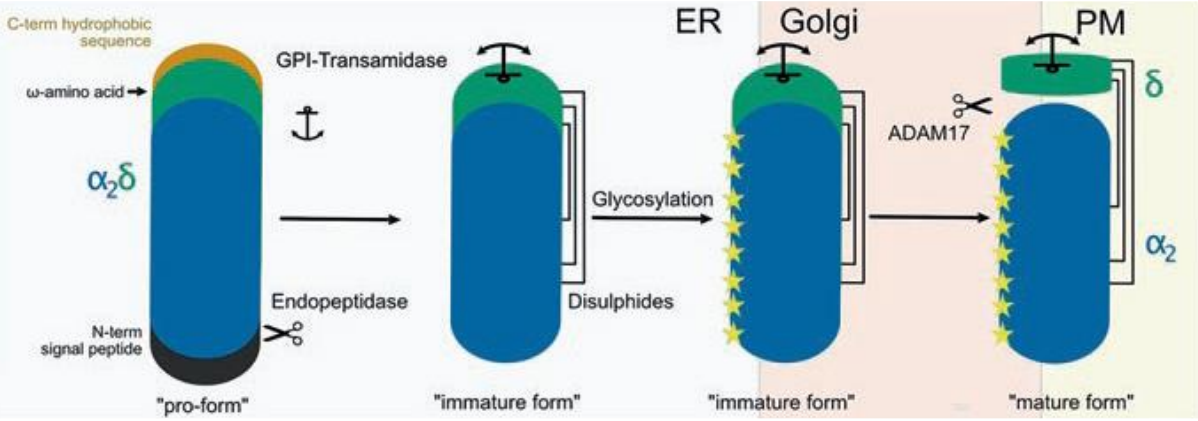

Figure 1.3 Post-translational modifications of α2δ proteins. The pro-form of α2δ is post-translationally modified within the endoplasmic reticulum (ER), including disulphide formations during translation, replacing the C-terminal hydrophobic sequence (orange) with a GPI-anchor by the GPI-transamidase, cleavage of N-terminal signal peptide by an endopeptidase, and addition of several glycan moieties (yellow stars) in the Golgi apparatus. The metalloprotease ADAM17 is proposed to cleave α2δ into the mature disulphide-linked α2 and δ subunit found at the plasma membrane (PM). (From: Ablinger *et al*., 2024).

α2δ expression

The α2δ isoforms, particularly α2δ1-3, are widespread across the central and peripheral nervous systems while showing distinct but partially overlapping distribution patterns (Ablinger *et al*., 2024). α2δ-1 is expressed in various neuronal cell types (Urao *et al*., 2001), including dorsal root ganglion (DRG) neurons (Bauer *et al*., 2009). On the other hand, α2δ-2 is predominantly expressed in GABAergic neurons, such as cerebellar Purkinje neurons (Barclay *et al*., 2001; Cole *et al*., 2005), while α2δ-3 is expressed in cerebral cortex and caudate putamen (Cole *et al*., 2005). In contracts, α2δ-4 exhibits a more restricted expression pattern, primarily found in photoreceptor cells of the retina (Wang *et al*., 2017).

With regard to subcellular localisation, α2δ-1 and α2δ-2 are mainly localised to presynaptic terminals, with some expression in cell bodies (Taylor and Garrido, 2008) and the plasma membrane of primary afferent neurons (Bauer *et al*., 2009). Although there is limited evidence, some studies suggest that α2δ-3 can also target VGCCs to specific presynaptic sites (Dickman *et al*., 2008; Saheki and Bargmann, 2009).

α2δ function as a modulator of VGCCs

α2δ subunits have several reported effects on the biophysical properties of HVA VGCCs, including the increase of inactivation rate and the maximum current density (Dolphin, 2003), and hyperpolarisation of the mid-point potential for steady-state inactivation of HVA VGCCs (Cantí *et al*., 2005; Catterall *et al*., 2005). The α2δ-induced increase in maximum current density is believed to be caused by α2δ-associated increase in expression and decrease in protein turnover of Ca_V1 and Ca_V2 channels (Cantí *et al*., 2005; Bernstein and Jones, 2007). Although the precise underlying mechanisms for these effects remain unclear, studies suggest that the MIDAS motif plays an essential role in α2δ function (Cantí *et al*., 2005). Mutations in the MIDAS motif significantly reduce the ability of α2δ-1 (Hoppa *et al*., 2012) and α2δ-2 (Cantí *et al*., 2005) subunits to increase Ca^{2+} currents in heterologous expression systems, and lead to intracellular retention of α2δ-2 and its complexes with $Ca_V\alpha1$ (Cantí *et al*., 2005). Studies also suggest that α2δ subunits may interact with the exofacial loops of the α1 pore-forming subunit, with supporting evidence showing the α2 subunit of α2δ-1 binding to domain III of the $Ca_V1.1$ channel (Gurnett *et al*., 1997). Moreover, investigation into the trafficking of α2δ subunits alone revealed interactions with other cellular trafficking proteins; however, these

are yet to be identified (Cantí *et al*., 2005; Davies et al., 2010; Tran-Van-Minh and Dolphin, 2010).

α2δ subunits as drug targets for hyperexcitability diseases

The α2δ subunits are key therapeutic targets for gabapentinoids, a class of widely prescribed drugs that includes gabapentin, its advanced form pregabalin (Lyrica), and the more recent mirogabalin. Gabapentinoids exhibit a high binding affinity for the α2δ-1 and α2δ-2 subunits and are commonly used in the treatment of hyperexcitability disorders such as epilepsy and chronic pain. They are classified as anticonvulsants and antiepileptic agents, and function by inhibiting excessive neuronal firing during seizures (Calandre *et al*., 2016). Additionally, they are used in the management of neuropathic pain, diabetic neuropathy, fibromyalgia, and restless leg syndrome (Deng *et al*., 2019). The binding of gabapentinoids is facilitated by the RRR gabapentin binding motif in the α2δ-1 and α2δ-2 subunits. In vitro studies have demonstrated that although gabapentin does not acutely affect the functional Ca_V complexes at the plasma membrane, it interferes with the trafficking of newly synthesised α2δ subunits and the Rab11a-dependent recycling of α2δ and Ca_V complexes (Hendrich *et al*., 2008; Bauer *et al*., 2009; Domon *et al*., 2023). This interference results in reduced α2δ protein levels at the plasma membrane, decreasing Ca^{2+} currents (Hendrich *et al*., 2008), and therefore reducing excitatory neurotransmission following gabapentin treatment, which likely explains their therapeutic mechanism of action.

In addition to gabapentinoids, thrombospondin (TSP) proteins, particularly TSP-1, TSP-2, and TSP-4, have been identified as ligands for the α2δ-1 subunit, playing a key role in forming excitatory synapses and contributing to neuronal sensitisation (Risher *et al*., 2018). This interaction has been linked to neuropathic pain, with gabapentin shown to inhibit the process. Animal studies have shown that nerve injuries lead to increased levels of α2δ-1 in the DRGs 2and spinal cord neurons, causing heightened synaptic activity (Luo *et al*., 2001; Boroujerdi *et al*., 2011). TSP-4, in particular, has been found to promote central sensitisation and neuropathic pain through direct interaction with α2δ-1 (Li *et al*., 2014; Pan *et al*., 2015). Moreover, TSP-4 was found to reduce gabapentin binding to α2δ-1, which may influence its effectiveness (Lana *et al*., 2016). Overall, the TSP-4/α2δ-1 interaction presents a potential target for new treatments for neuropathic pain.

1.3.3.4 T-type VGCCs modulation by auxiliary subunits

Several studies show a modest increase in Ca_V3 VGCCs expression associated with α2δ subunits (Dolphin *et al*., 1999; Dubel *et al*., 2004); however, Ca_V3 channels do not require any known auxiliary subunits for correct expression, trafficking, or physiological function. Recent studies have identified various modulators, including the actin binding protein kelch-like 1 (KLHL1) (Aromolaran *et al*., 2010), calnexin (Proft *et al*., 2017) and the stac adaptor protein 1 (Stac1) (Rzhepetskyy *et al*., 2016a). An important study by Cottrell *et al*. (2018) described a member of the α2δ protein family, CACHD1 (cache domain containing 1), as a Ca_V3 channel modulator. CACHD1 showed regulatory effects on T-type currents similar to those observed in α2δ subunits and HVA VGCCs, suggesting that it may act as an auxiliary subunit for Ca_V3 LVA VGCCs.

1.3.4 VGCCs and the α2δ subunits in disease

VGCCs are involved in numerous physiological functions and their dysfunctions are associated with a variety of diseases. It is therefore not surprising that their auxiliary α2δ subunits have been associated with many of these diseases as well. Tables 1.3 and 1.4 summarise HVA and LVA VGCC-associated diseases, and Table 1.5 summarises α2δ-associated diseases.

Ca_V3 LVA VGCCs are of particular interest in this project, and while they seem to be associated with a considerable number of diseases, pharmacological targeting has been mainly limited to absence seizure treatment. Sections 1.4.2 and 1.4.3 further describe the role of Ca_V3 VGCCs in hyperexcitability diseases, namely in neuropathic pain, and their potential as drug targets.

Table 1.3 Diseases associated with HVA VGCCs.

Calcium Channel	Disease	Reference
Ca_V1 (L-type)		
$Ca_V1.1$	Hypokalemic periodic paralysis	Jurkat-Rott *et al*., 1994
	Malignant hyperthermia subtype 5	Yarotskyy and Dirksen, 2013
$Ca_V1.2$	Autism	Bader *et al*., 2011
	Timothy syndrome	Barrett and Tsien, 2008
$Ca_V1.3$	Autism spectrum disorders	Azizan *et al*., 2013
	Bradycardia	Baig *et al*., 2011
	Congenital deafness	Baig *et al*., 2011
	Parkinson's disease	Zamponi *et al*., 2015
$Ca_V1.4$	Congenital stationary night blindness type 2	Hoda *et al*., 2005
Ca_V2 (P, Q, N, R-type)		
$Ca_V2.1$	Familial hemiplegic migraine	Tottene *et al*., 2009
	Neuropathic pain	Zamponi *et al*., 2015
$Ca_V2.2$	Myoclonus-dystonia	Groen *et al*., 2015
	Developmental and epileptic encephalopathies	Helbig *et al.*, 2019
$Ca_V2.3$	Parkinson's disease	Benkert *et al*., 2019

Table 1.4 Diseases associated with LVA VGCCs.

Calcium Channel	Disease	Reference
Ca_V3 (T-type)		
$Ca_V3.1$	Absence epilepsy	Ernst *et al*., 2009
	Autosomal dominant cerebellar ataxia	Coutelier *et al*., 2015
	Bradycardia	Mangoni *et al*., 2006
	Cerebellar ataxia	Kimura *et al*., 2017
	Parkinson's disease	Chandrasekaran and Bonchev, 2013
	Spontaneous absence seizures	Song *et al*., 2004
$Ca_V3.2$	Absence epilepsy	Powell *et al*., 2009
	Amyotrophic lateral sclerosis	Rzhepetskyy *et al*., 2016b
	Autism spectrum disorder	Splawski *et al*., 2006
	Cardiac hypertrophy	David *et al*., 2010
	Chronic pain	Reynders *et al*., 2015
	Diabetic neuropathy	Duzhyy *et al*., 2015
	Idiopathic generalised epilepsy	Heron *et al*., 2007
	Irritable bowel syndrome	Marger *et al*., 2011
	Nerve injury (chronic pain)	Jagodic *et al*., 2008
	Primary aldosteronism	Daniil *et al*., 2016
$Ca_V3.3$	Hemiplegic migraine	Maksemous *et al*., 2022
	Schizophrenia	Gulsuner *et al*., 2013
	Sporadic early onset Alzheimer's disease	Antonell *et al*., 2013

Table 1.5 Diseases associated with α2δ auxiliary subunits.

α2δ subunit	Disease	Reference
α2δ-1	Autism	Iossifov *et al*., 2014
	Brugada syndrome	Burashnikov *et al*., 2010
	Epilepsy	Mefford *et al*., 2011
	Short QT syndrome	Templin *et al*., 2011
	West syndrome	Hino-Fukuyo *et al*., 2015
α2δ-2	Epilepsy	Valence *et al*., 2019 Edvardson *et al*., 2013 Pippucci *et al*., 2013
	Schizophrenia	Rodríguez-López et al., 2018
α2δ-3	Autism	Guo *et al*., 2018 Redin *et al*., 2017
	Central pain processing	Neely *et al*., 2010
α2δ-4	Bipolar disorders	Van Den Bossche *et al*., 2012
	Inherited retinal dystrophy	Huang *et al*., 2015
	Night blindness	Ba-Abbad *et al*., 2016
	Retinitis pigmentosa	Cheng *et al*., 2021

1.4 Ca_V3 (T-type) VGCCs

Ca_V3 LVA VGCCs are discussed in more detail in the following sections.

The Ca_V3 channel family comprises $Ca_V3.1$, $Ca_V3.2$ and $Ca_V3.3$ channels, which are encoded by the *CACNA1G* (Perez-Reyes *et al*., 1998), *CACNA1H* (Cribbs *et al*., 1998) and *CACNA1I* (Lee *et al*., 1999) genes, respectively. Similarly to HVA VGCCs, LVA channels consist of a single α1 pore forming subunit (α1G – $Ca_V3.1$, α1H – $Ca_V3.2$, α1I – $Ca_V3.3$) that contains four homologous domains (I-IV) each made of six transmembrane segments (S1-6) as shown in Figure 1.1. Unlike HVA VGCCs, Ca_V3 channels do not require auxiliary subunits to assemble and function correctly. Studies showed that while co-expression of Ca_V3 channels with α2δ subunits increased T-type current density, they did not form protein complexes (Dolphin *et al*., 1999; Dubel *et al*., 2004), further supporting the consensus that Ca_V3 channels do not require α2δ, β or γ auxiliary subunits to function.

1.4.1 Physiological roles of Ca_V3 VGCCs

Ca_V3 VGCCs belong to the LVA VGCCs group due to their biophysical properties (summarised in Table 1.2). Ca_V3 channels are widely expressed in the nervous (Perez-Reyes, 2003), neuroendocrine and cardiovascular systems where they have a variety of functions, including the control of vascular tone (Kuo *et al*., 2014), pacemaking (Mesirca *et al*., 2014), and hormone release. In the central nervous system, Ca_V3 channels play a key role in the regulation of neuronal excitability (Cain and Snutch, 2010b ; Cheong and Shin, 2013) mainly due to their hyperpolarised range of activation and inactivation. A much smaller depolarisation is required for activation in comparison to Ca_V1 and Ca_V2 channel families, and only a brief membrane hyperpolarisation is sufficient to recover Ca_V3 channels from partial inactivation and facilitate membrane depolarisation and neuronal firing. The fast recovery of Ca_V3 channels from inactivation allows the generation of Ca^{2+} spikes during hyperpolarisation which in turn leads to rebound burst firing (Figure 1.4B; Beurrier *et al*., 1999; Cain and Snutch, 2010a). While most of Ca_V3 channels are inactive at or near resting membrane potentials of neurons, a small fraction of Ca_V3 channels remains open allowing a passive influx of Ca^{2+}. This overlap between activation and inactivation potentials of Ca_V3 channels creates a window current which allows the generation of low frequency oscillations in thalamic neurons (Figure 1.4C; Williams *et al*., 1997; Cain and Snutch, 2010a), further contributing to neuronal excitability regulation (Dreyfus *et al*., 2010). Another way Ca_V3 channels regulate neuronal excitability is the

formation of functional protein complexes with calcium- and voltage-activated potassium channels, allowing them to function at lower membrane potentials (Weiss and Zamponi, 2020).

Based on the distribution of Ca_V3 channels in cortical neurons of rat brain, T-type currents may be responsible or contribute to a variety of neuronal activities (McKay *et al*., 2006). In addition to regulating neuronal excitability, Ca_V3 channels have been linked to hormone secretion (Carabelli *et al*., 2007) and neurotransmitter release (Jacus *et al*., 2012). Moreover, Ca_V3 channels have been shown to play roles in the function of cardiovascular system (Hansen, 2015), as well as being important in sleep-wake cycles ($Ca_V3.1$) (Uebele *et al*., 2009), in relaxation of cerebral arteries ($Ca_V3.2$) (Harraz *et al*., 2014) and in smooth muscle contraction in cerebral arteries in cooperation with $Ca_V1.2$ (Harraz *et al*., 2015).

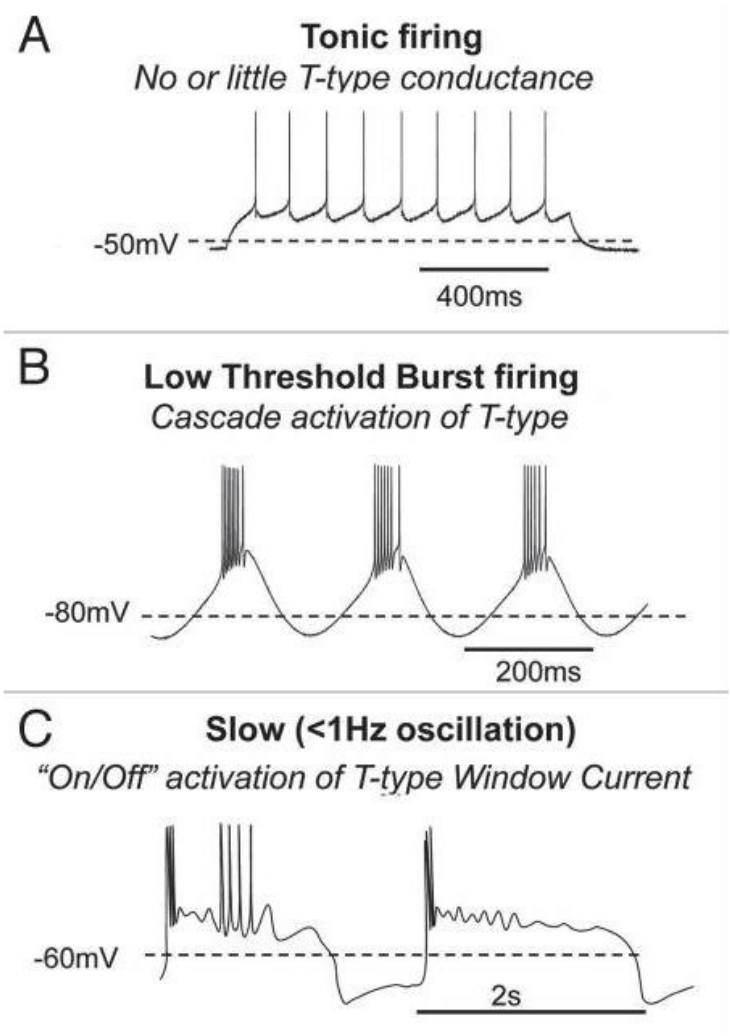

Figure 1.4 Alteration of neuronal firing patterns by Ca_V3 channel activity. Recordings from reticular thalamic (A, B) and thalamic lateral geniculate (C) neurons displaying altered firing properties depending on the level of T-type currents. **(A)** Neurons with a depolarised membrane potential (inactivated Ca_V3 channels) or neurons with low expression of Ca_V3 channels are more likely to fire single or tonic action potentials. Ca_V3 channels will conduct Ca^{2+} during single or tonic action potentials if the firing occurs from a sufficiently hyperpolarised membrane potential and if the expression density of Ca_V3 channels is too low to induce burst firing. **(B)** Burst firing occurs if the expression of Ca_V3 channels is high and the neuron is held at a hyperpolarised membrane potential to ensure Ca_V3 channels are not activated. **(C)** Slow oscillations (< 1 Hz) occur because of bistability of particular neurons depending on whether the T-type window current is "on" or "off", however it is also highly dependent on leak potassium and the non-specific cationic conductance. (From: Cain and Snutch, 2010a).

1.4.2 Ca_V3 VGCCs in neuropathic pain

Neuropathic pain is estimated to affect approximately 7-10% of the global population (International Association for the Study of Pain, IASP), and has various causes, including physical injury, inflammation, or chronic diseases. The most common neuropathic pain symptoms are associated with the disturbances in sensitisation mechanisms and abnormal neuronal firing along the primary nociceptive pathways of the somatosensory system, in particular the peripheral nociceptive Aβ, Aδ, and C nerve fibres (also called nociceptors) (Colloca *et al*., 2017; Finnerup *et al*., 2021). The nociceptive signals are processed in several brain regions, including the thalamus, hypothalamus, midbrain, somatosensory cortices, prefrontal cortex, and cingulum (Apkarian *et al*., 2012). Notably, the activity of anterior cingulate cortex was shown to be upregulated in animal models of pain (Ning *et al*., 2013), suggesting that it plays a key role in persistent neuropathic pain (Wei *et al*., 2002; Xu *et al*., 2008). Neuropathic pain is associated with the sensitisation of nociceptive neurons in the dorsal horn (Ji *et al*., 2003), but to fully comprehend the underlying mechanisms of neuropathic pain, it is important to understand the nociceptive sensory pathway and the involvement of various ion channels (Figure 1.5), such as TRP channels, acid-sensing ion channels (ASIC), hyperpolarisation-activated cyclic nucleotide-gated channels (HCNs), voltage-gated sodium (Na_V), potassium (K_V), and calcium (Ca_V) channels (Finnerup *et al*., 2021) which are often altered in disease states, leading to an imbalance of electrophysiological responses (Rangel-Galván *et al*., 2023).

Ca_V3 VGCCs have been shown to play an important role in the initiation and maintenance of neuropathic pain. Ca_V3 channels can regulate the release of pain mediators, while their biophysical properties facilitate the regulation of neuronal excitability (Zamponi *et al*., 2015), thereby contributing to nociceptive signalling. Ca_V3 VGCCs are expressed in key regions associated with pain processing, including the dorsal root ganglia and dorsal horn. Among the Ca_V3 channel isoforms involved in pain processing, $Ca_V3.2$ is the predominant isoform involved in pain modulation (Zamponi *et al*., 2009). $Ca_V3.2$ contributes to the excitation of primary afferent fibres, synaptic transmission, and overall pain processing (Weiss and Zamponi 2019; Harding and Zamponi 2022). Understanding the role of Ca_V3 VGCCs provides valuable insights into the mechanisms and potential therapeutic targets for the treatment of neuropathic pain.

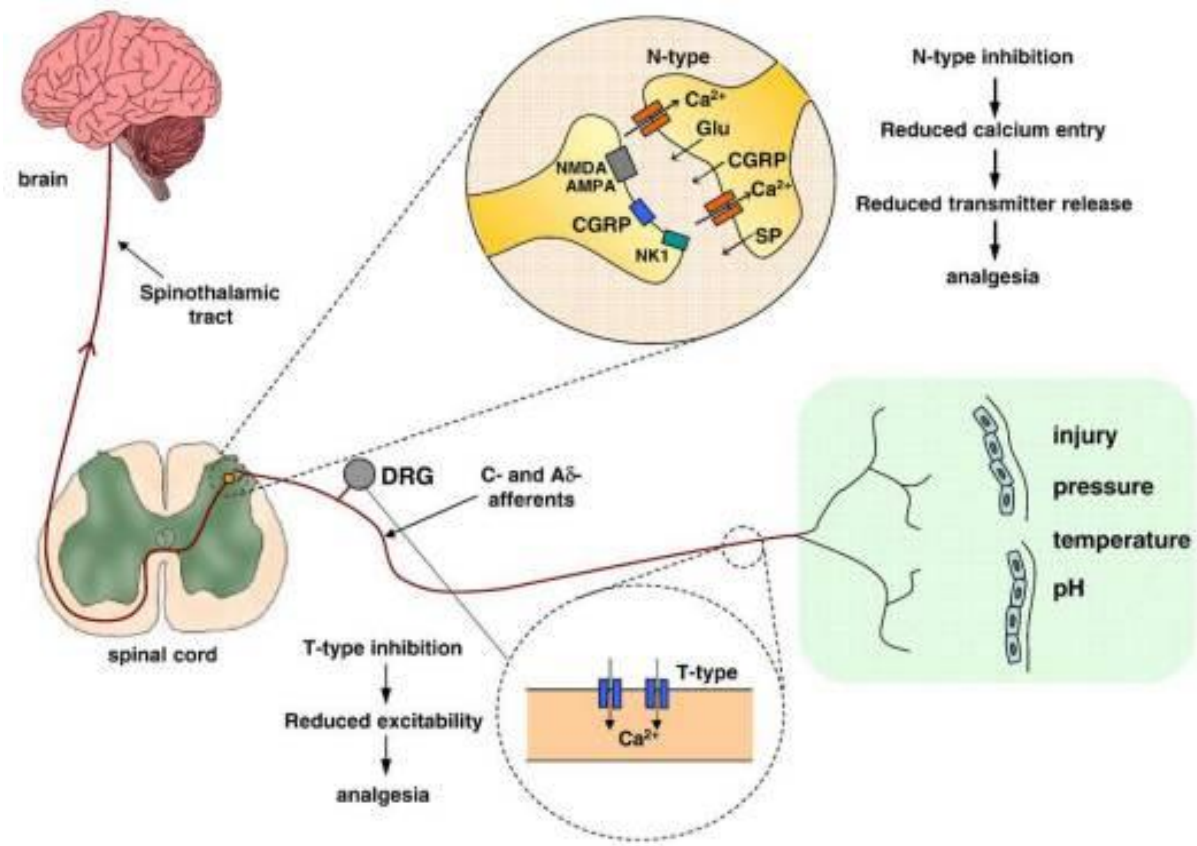

Figure 1.5 N-type and T-type VGCCs in the primary afferent signalling pathway. LVA VGCCs are primarily localised more upstream in the pathway and are thought to be both involved in generating sensory potentials out near free nerve endings, as well as being present in dorsal root ganglion (DRG) cell bodies where they likely contribute to the generation and frequency of action potentials. Action potentials carried along DRG cell axons (mainly C and Aδ afferents) trigger the opening of pre-synaptic $Ca_V2.2$ VGCCs which in turn initiate the release of nociceptive transmitters such as glutamate, substance P and CGRP onto spinal interneurons and projection neurons. (From: Zamponi *et al*., 2009).

1.4.3 Ca_V3 VGCCs as drug targets for neuropathic pain

Numerous studies highlight the involvement of Ca_V3 VGCCs in the pathogenesis of neuropathic pain, particularly $Ca_V3.2$, where its elevated expression in the peripheral nociceptive nerve fibres (nociceptors) has been associated with neuropathic pain development (Bourinet *et al*., 2016). In a spared nerve injury animal model, increased $Ca_V3.2$ expression in the excitatory neurons in the dorsal horn resulted in thermal hyperalgesia and allodynia, while silencing $Ca_V3.2$ appeared to reduce neuropathic pain (Zhi *et al*., 2022). Furthermore, increased expression of $Ca_V3.2$, but not $Ca_V3.1$ or $Ca_V3.3$, resulted in mechanical allodynia in a partial sciatic nerve ligation-induced animal model of neuropathic pain (Feng *et al*., 2019), and in a spinal cord injury model, the activity of Ca_V3 VGCCs appeared to be responsible for the hyperexcitability state of nociceptors (Lauzadis *et al*., 2020). Moreover, following nerve injury, Ca_V3 VGCCs can upregulate the function and expression of pain mediators, such as glutamate and substance P, in the spinal dorsal horn, contributing to neuropathic pain (Ghazisaeidi *et al*., 2023).

Current treatments for neuropathic pain offer symptomatic relief but can take long time to show any analgesic effects. Furthermore, many of these treatments have limited efficacy (approx. 50% maximum) and can cause serious side effects (Rangel-Galván *et al*., 2023), underscoring the need for novel therapeutic strategies. Several studies hypothesise that Ca_V3 VGCCs modulators, channel blockers in particular, could provide neuropathic pain relief. Several compounds (Figure 1.6), including mibefradil, ethosuximide (ETX), TTA-A2 and Z944 can block the activity of Ca_V3 VGCCs; however, some of them lack specificity. Many studies consistently report an upregulation of Ca_V3 VGCCs in neuropathic pain conditions, and therefore the development of neuropathic pain treatment has been focused on more specific Ca_V3 channel blockers.

ETX, known for its antiepileptic properties and as a Ca_V3 channel blocker, showed analgesic effects in several chronic pain models; however, clinical trials in humans revealed that ETX not only failed to reduce overall pain, it also caused a high number of adverse side effects, and consequentially had to be withdrawn (Kerckhove *et al*., 2018). In another approach, alleviation of neuropathic pain was achieved by modulating Ca_V3 VGCCs with a blocker (NNC 55-0396) and subsequently inhibiting the neuronal activity of anterior cingulate cortex in a chronic constriction injury rat model (Shen *et al*., 2015). Additionally, in a varicella-zoster virus infection mice model, an upregulation of $Ca_V3.2$ in dorsal root ganglion led to increased

mechanical and thermal sensitivity, which were alleviated by the treatment with (2T/S)-6-PNG inhibitor (Gaifullina *et al*., 2019). Novel prenylated flavonoids have shown potential to alleviate neuropathic and visceral pain by inhibiting $Ca_V3.2$ and $Ca_V3.3$ activity (Rangel-Galván *et al*., 2021; Nguyen et al., 2019). Moreover, a study by Cai *et al*. (2020) reported that a 5bk compound could reverse mechanical sensitivity associated with Ca_V3 VGCCs independently from the opioid receptors in a paclitaxel and spinal nerve ligation-induced models of pain, providing a potential non-addictive treatment for neuropathic pain.

While these molecules show promise for the treatment of neuropathic pain in animal models, many of them still lack specificity or show poor efficacy. Consequently, there is a pressing need for more targeted and specialised therapy for Ca_V3 VGCC-associated neuropathic pain. Another approach to managing Ca_V3 channel-associated neuropathic pain involves targeting their modulators, such as the α2δ and β auxiliary subunits for HVA VGCCs, as highlighted in section 1.3.3.3. However, Ca_V3 VGCCs do not require any known auxiliary subunits to function. Despite this, the study conducted by Cottrell *et al.* (2018) describing CACHD1 as a modulator of Ca_V3 VGCCs, and the similarities between CACHD1 and α2δ subunits suggest that CACHD1 could represent a potential drug target. Therefore, the subsequent sections discuss CACHD1 protein in more detail.

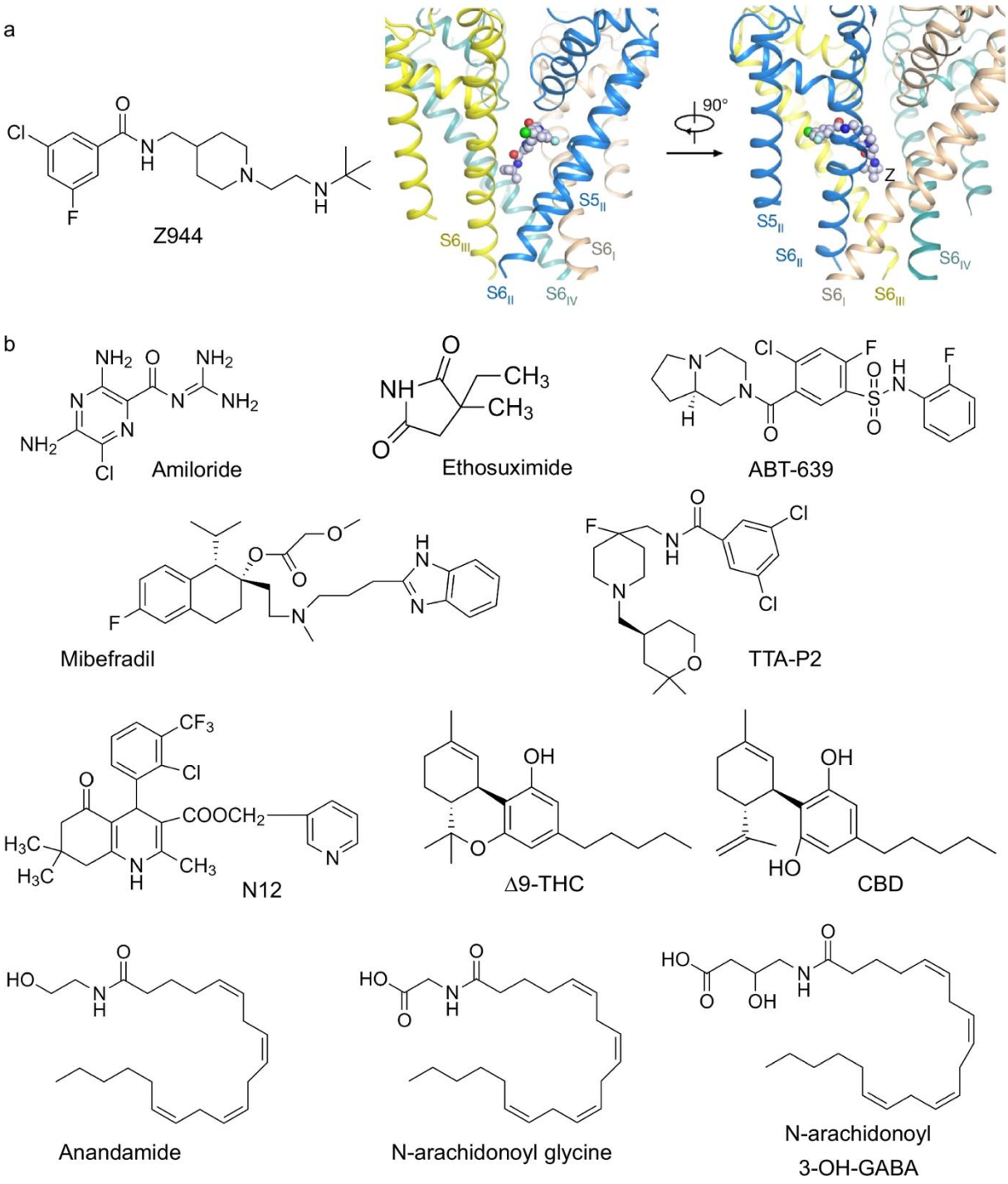

Figure 1.6 Known inhibitors of Ca_V3 channels with analgesic properties. (a) Left: structure of the high affinity and selectivity Ca_V3 channel inhibitor Z944. Right: Z944 shown within the binding pocket of $Ca_V3.1$. **(b)** Structures of commonly utilised Ca_V3 channel inhibitors, with varying degrees of affinity and selectivity. Many of these compounds mediate analgesia in preclinical pain models. (From: Harding and Zamponi 2022).

1.5 CACHD1 as an α2δ-like protein

CACHD1 is encoded by the cache (Ca^{2+} channel and chemotaxis receptor) domain containing 1 gene located on chromosome 1 (1p31.3) and represents a highly conserved protein across various organisms, including vertebrates, fish, and insects. CACHD1 orthologues were identified in numerous species, included but not limited to *Homo sapiens*, *Drosophila melanogaster*, *Caenorhabditis elegans*, *Bos taurus*, *Danio rerio*, and *Xenopus laevis* as shown in Figure 1.7. CACHD1 was first cloned by Nagase *et al*. (2000) and identified to be related to α2δ auxiliary subunits by Whittaker and Hynes (2002) using bioinformatics approach. Despite relatively low gene homology (13-16%) and protein identity (<21%) with α2δ subunits, there are key structural similarities between CACHD1 and α2δ subunits that support the classification of CACHD1 as a member of the α2δ protein family.

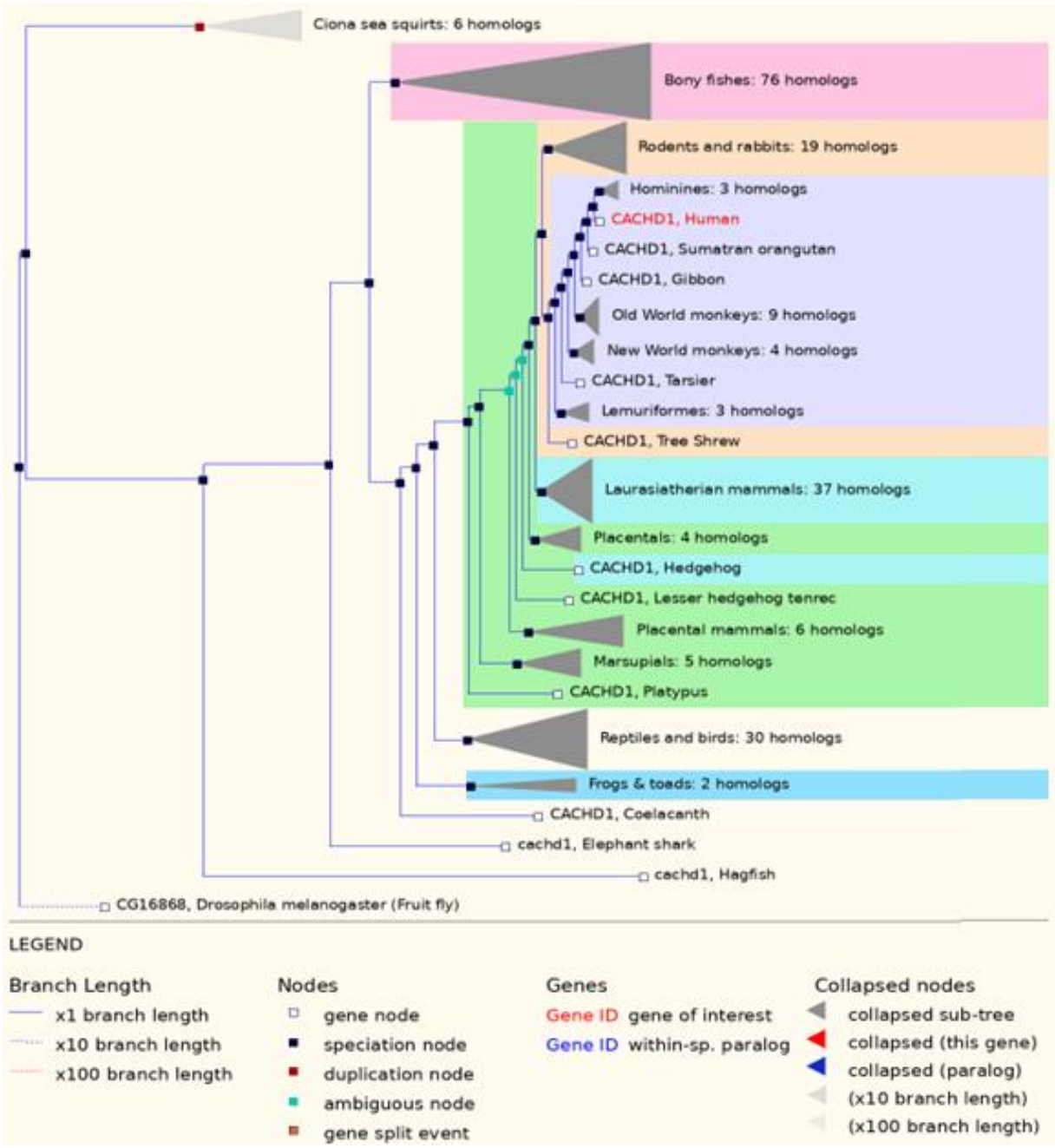

Figure 1.7 Phylogenetic tree showing CACHD1 gene in various species. (Generated using Ensembl; ENSG00000158966).

1.5.1 Structure of CACHD1

Structural studies show that while the sequence homology of CACHD1 and α2δ subunits may be limited, there are structural similarities in terms of protein motifs and their arrangement (Figure 1.8). These structural features include a von Willebrand Factor A domain (VWA), chemosensory-like cache domains and a N-terminal signal sequence (Cottrell *et al*., 2018; Stephens and Cottrell, 2019). However, there are also several important differences between CACHD1 and α2δ subunits. α2δ subunits have multiple glycosylation sites, a fully conserved metal ion-dependent adhesion site (MIDAS) motif (DxSxS), a RRR gabapentin binding motif (α2δ-1 and α2δ-2) or RNR variant motif (α2δ-3 ad α2δ-4) (Wang *et al*., 1999; Marais et al., 2001; Chen *et al*., 2023), and are also reported to be glycophosphatidylinositol (GPI)-anchored proteins (Davies *et al*., 2010). On the other hand, CACHD1 is predicted to have seven potential N-glycosylation sites (Dahimene *et al*., 2018), a variant MIDAS motif (DxGxS), a RSR variant gabapentin binding motif, and a single transmembrane domain with a large intracellular C-terminal tail containing putative tyrosine and dileucine internalisation motifs (Whittaker and Hynes, 2002; Cottrell *et al*., 2018; Stephens and Cottrell, 2019). A recent report by Gumerov *et al*. (2022) has described an additional amino acid binding motif, YRWYD, located within cache domains of CACHD1 and α2δ where gabapentinoids may also bind. In CACHD1, this binding motif is located entirely within the dCache2 domain, unlike in α2δ where the N-terminal (YRW) and C-terminal (YD) parts of the motif straddle the VWA domain.

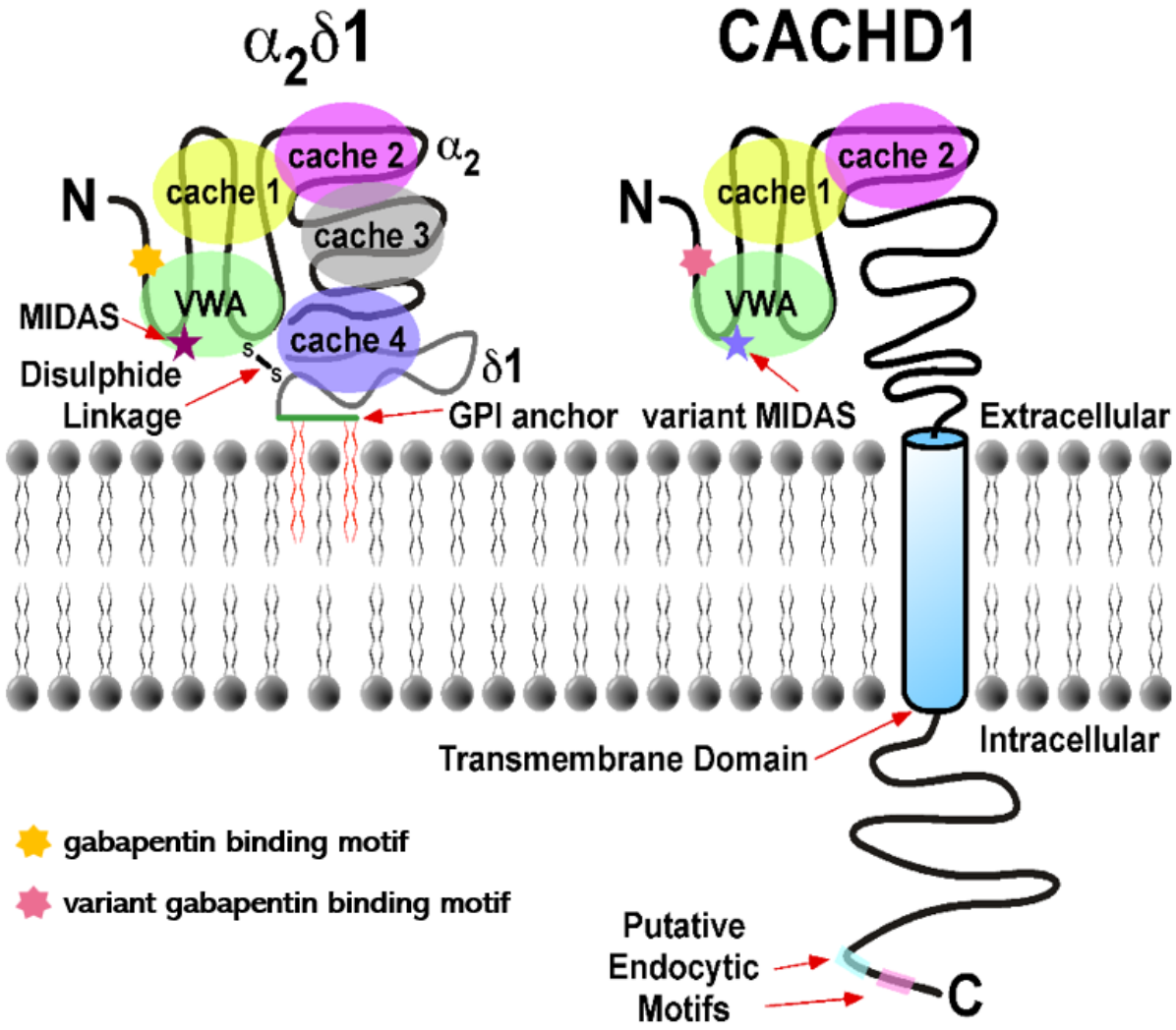

Figure 1.8 Schematic comparison of the major structural domains and motifs of human α2δ-1 and CACHD1 proteins. (Adapted from: Stephens and Cottrell, 2019).

1.5.1.1 Cache domains

Chemoreceptors commonly found in bacteria and archaea are important in recognising extracellular signalling molecules involved in various cellular pathways (Parkison *et al*., 2015; Ortega *et al*., 2017). These chemoreceptors typically contain cache domains that serve as their sensory modules. In bacteria, cache domains bind various ligands, including amino acids, organic acids, sugars, and nucleotides, which then initiate downstream signalling pathways (Ortega *et al*., 2017; Matilla *et al*., 2022). Cache domains are rarely present in eukaryotic proteins; however, they are found in the VGCC α2δ protein family that includes α2δ-1, α2δ-2, α2δ-3, α2δ-4 and CACHD1 proteins. Initial studies reported that α2δ subunits contained a single cache domain, which was later revised to two cache domains (Uniprot P54289). Subsequent crystallographic studies by Wu *et al*. (2016) revealed that α2δ subunits contain four individual cache domains. On the other hand, as a relatively unstudied protein with limited research, CACHD1 is predicted to contain two individual cache domains (Whittaker and Hynes, 2002; Cottrell *et al*., 2018; Stephens and Cottrell., 2019). However, recent study by Gumerov *et al*. (2022) introduced new organisation of the cache domains within α2δ and CACHD1 proteins. This study proposes that both α2δ and CACHD1 contain two double cache domains (termed dCache1 and dCache2) instead of the previously assumed four individual domains (Figure 1.9A-C). Figure 1.5C shows the proposed organisation of α2δ and CACHD1 structural features, where the VWA domain is inserted into the first dCache1 domain, followed by the second dCache2 domain containing an insertion. Moreover, the overlay of 3D protein structures of CACHD1 and α2δ-1 (Figure 1.9D-E) underscores the structural similarities between these proteins, further supporting the classification of CACHD1 as a member of the α2δ protein family.

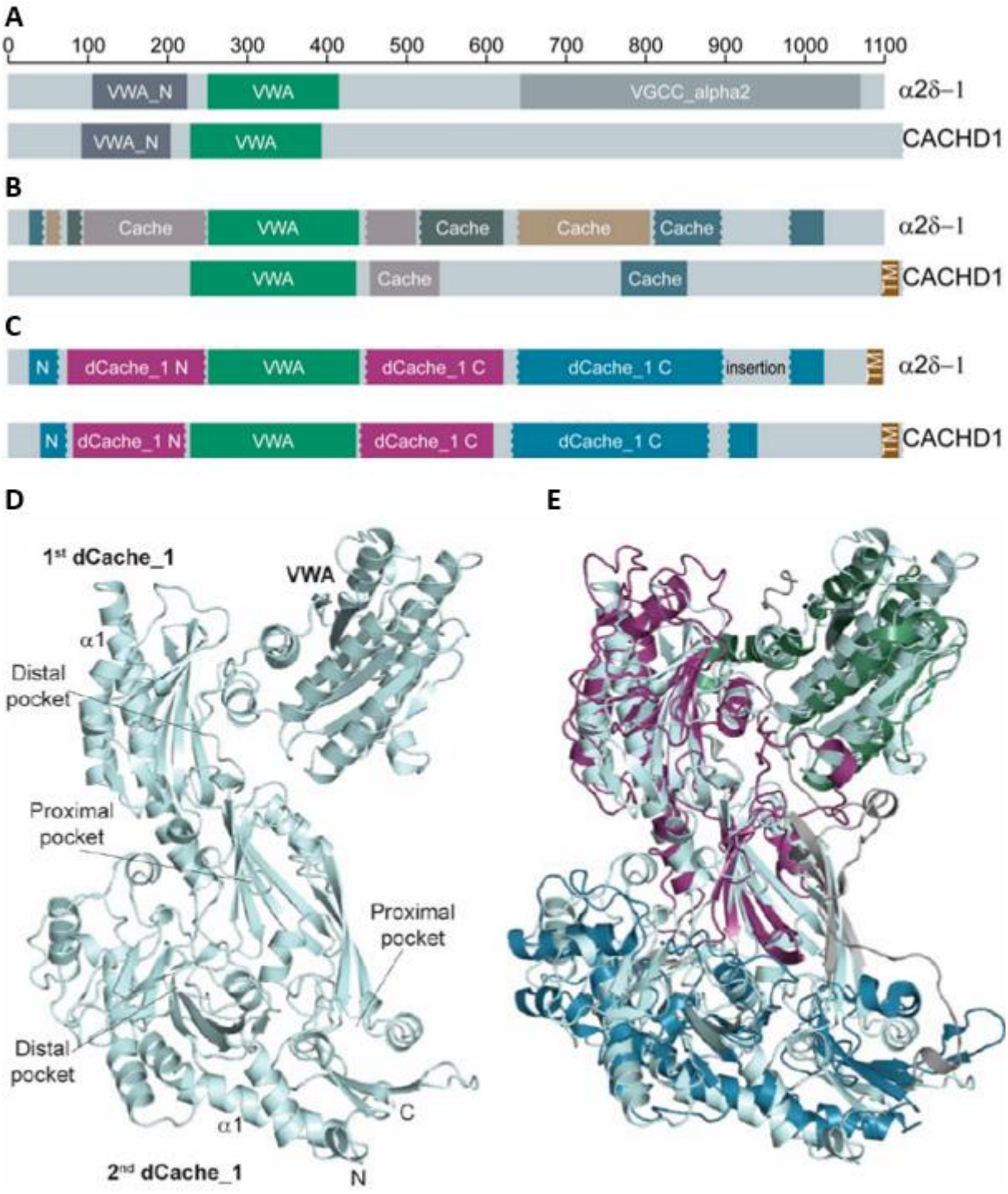

Figure 1.9 Structural comparison of α2δ-1 and CACHD1. (A) α2δ-1 and CACHD1 structural domains recognised by Pfam database and **(B)** experimental studies. **(C)** Newly proposed domain organisation for α2δ-1 and CACHD1 showing two dCache domains instead of previously assumed individual four and two cache domains for α2δ-1 and CACHD1 respectively. **(D)** 3D structure of CACHD1 modelled by AlphaFold. **(E)** Overlay of human CACHD1 and rabbit α2δ-1 proteins showing structural similarities. (Adapted from: Gumerov *et al*., 2022).

1.5.1.2 Metal ion dependent adhesion site (MIDAS) motif

The MIDAS motif is a conserved structural motif found in several transmembrane proteins involved in cell adhesion and signalling. These proteins include, but are not limited to integrins (Brown *et al*., 2018) and cadherins (Higgins *et al*., 2000), where the MIDAS motif coordinates divalent cations like magnesium (Mg^{2+}), calcium (Ca^{2+}), and manganese (Mn^{2+}), playing a crucial role in ligand recognition and binding (Valdramidou *et al*., 2008; Zhang and Chen, 2012). CACHD1 and α2δ subunits share a common VWA domain that contains a MIDAS motif, and while α2δ subunits contain a MIDAS motif with fully conserved key residues (DxSxS), CACHD1 contains a variant MIDAS motif (DxGxS) with a glycine residue in place of the serine residue shown to be critical in α2δ subunits (Briot *et al*., 2018). A fully conserved MIDAS motif is not required for metal ion binding (Whittaker and Hynes, 2002); however, it was shown to be functionally important for VGCCs trafficking and synaptic function (Cantí *et al*., 2005; Hoppa *et al*., 2012; Cassidy *et al*., 2014). Previous studies show that mutations in the key MIDAS residues result in disruption of α2δ-1-$Ca_V2.2$ interaction (Dahimene *et al*., 2018), impairment of α2δ-1 trafficking to cell surface (Cassidy *et al*., 2014), and an ablation of Ca_V1 and Ca_V2 current increases normally seen in wild type α2δ-1 and α2δ-2 (Cantí *et al*., 2005; Hoppa *et al*., 2012; Cassidy *et al*., 2014).

1.5.1.3 Transmembrane domain

CACHD1 is classed as type I transmembrane protein due to its N-terminal signal peptide and an intracellular C-terminal domain (Sharma and Schiller, 2019). Many transmembrane proteins utilise their cytoplasmic endocytic motifs to facilitate endocytosis and subsequent post-endocytic sorting within the cell (Sharma and Schiller, 2019). Although α2δ subunits are generally considered transmembrane proteins, there has been some debate regarding their membrane topology, with some studies suggesting that α2δ subunits could be GPI-anchored instead (Davies *et al*., 2010), therefore lacking a cytoplasmic tail and endocytic motifs. On the other hand, CACHD1 possesses a transmembrane domain and a long intracellular C-terminal tail (Cottrell *et al*., 2018). Therefore, it is possible that CACHD1 and α2δ utilise different molecular mechanisms for endocytosis at the cell surface and subsequent intracellular processing.

1.5.2 Expression of CACHD1

A study by Cottrell *et al*. (2018) showed that CACHD1 is widely expressed in the mammalian central nervous system. In rat tissue, CACHD1 transcripts were highly expressed in thalamus,

hippocampus, and cerebellum, showing unique expression pattern in comparison to α2δ-1 subunits that were mostly expressed in cortex, superior cervical ganglia, and hippocampus (Figure 1.10). Furthermore, immunocytochemistry of adult human brain showed CACHD1 protein was abundantly expressed in hippocampus, cortical regions, and thalamus (Figure 1.11), showing similar distribution to Ca_V3 channels, in particular $Ca_V3.1$, in the central nervous system (Talley *et al*., 1999). In terms of neuronal expression, CACHD1 was shown to be strongly expressed on the surface of cell soma, axon and the dendrites including dendritic spines of primary hippocampal neurons (Figure 1.12; Ablinger *et al*., 2022).

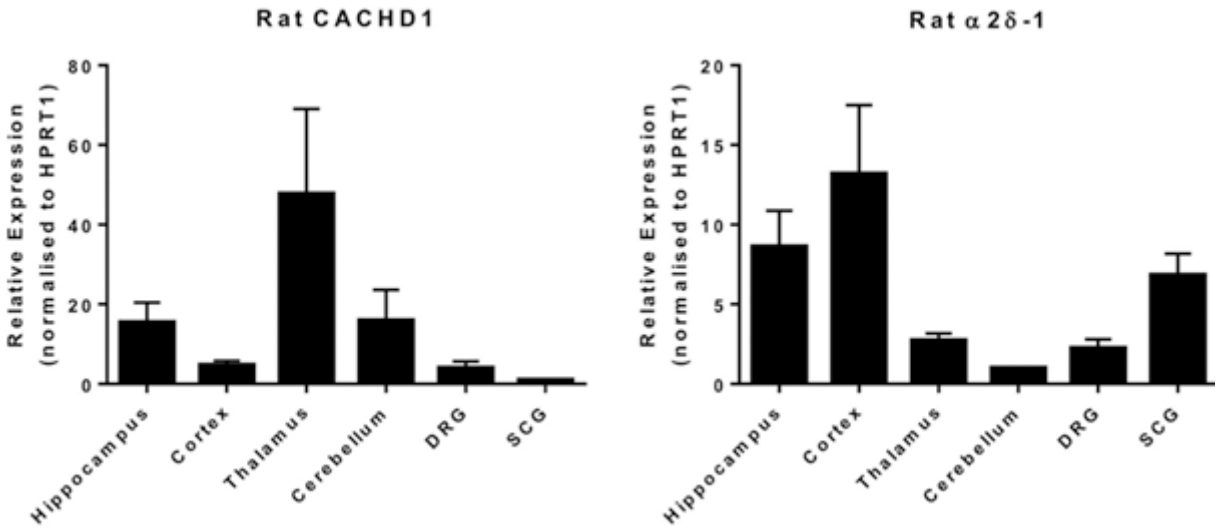

Figure 1.10 Relative expression profile of CACHD1 and α2δ-1 mRNA in rat tissue determined using SYBR green real-time quantitative PCR. HPRT1 was used as the housekeeping gene. DRG, Dorsal root ganglion; SCG superior cervical ganglion. (From: Cottrell *et al*., 2018).

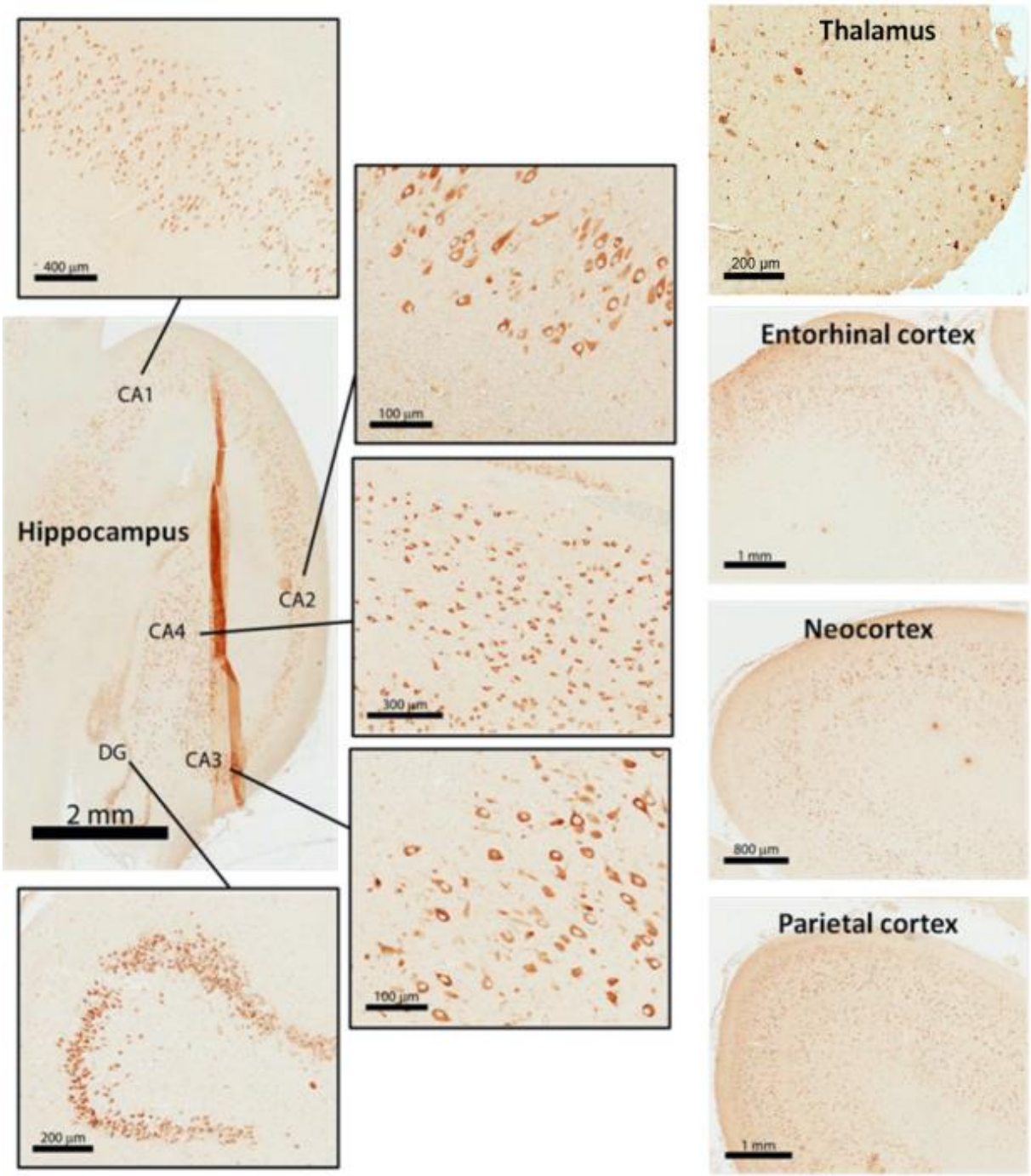

Figure 1.11 CACHD1 protein expression in human brain. Immunocytochemistry of adult human brain using rabbit anti-CACHD1 primary antibody with peroxidase anti-rabbit secondary antibody with DAB stain (brown). CA1-4, Cornu ammonis 1-4; DG, dentate gyrus. (From: Cottrell *et al*., 2018).

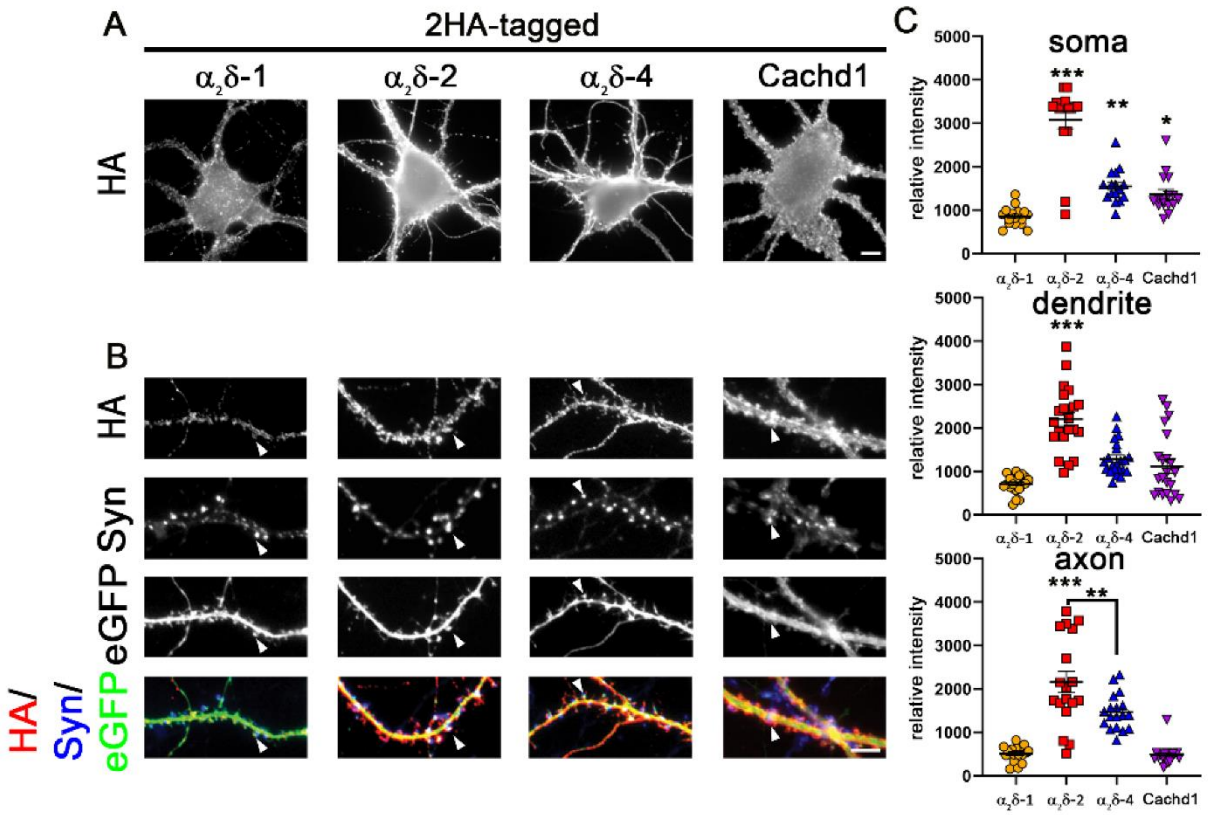

Figure 1.12 CACHD1 can be expressed on the somato-dendritic and axonal surface. (A) Live cell surface staining of wildtype primary hippocampal neurons overexpressing soluble eGFP together with HA-tagged constructs of α2δ subunits or CACHD1. The somatic expression pattern of the anti-HA labelling revealed that all α2δ subunits and CACHD1 can be expressed on the neuronal surface. **(B)** Anti-HA and synapsin immunofluorescent labelling revealed that all α2δ and CACHD1 show synaptic and dendritic membrane targeting (white arrowheads). **(C)** Quantification of the average HA fluorescent intensities illustrated that the surface expression of α2δ-1 was reduced compared to those of the other subunits. α2δ-2 expression in soma, dendrites, and axons was higher compared to α2δ-1, α2δ-4, and CACHD1. (From: Ablinger *et al*., 2022).

1.5.3 CACHD1 as a modulator of VGCCs

As CACHD1 is a novel modulator of VGCCs, the number of studies describing its full potential as VGCC modulator is currently limited and therefore it is of great importance to gain the understanding of the mechanisms of how CACHD1 modulates Ca_V3 and other VGCCs. The main findings to date show that CACHD1 modulates Ca_V3 and $Ca_V2.2$ channels (Cottrell *et al*., 2018; Dahimene *et al*., 2018, respectively).

CACHD1 showed modulation of Ca_V3 channels by increasing the i) peak current density with a corresponding increase in maximal conductance for $Ca_V3.1$ (Figure 1.13), ii) channel open probability for $Ca_V3.1$, iii) calcium current levels for $Ca_V3.2$ and $Ca_V3.3$ (Figure 1.14); while also promoting $Ca_V3.1$ cell surface localisation as well as formation of CACHD1-$Ca_V3.1$ protein complexes in heterologous expression system and native neurons (Figure 1.15), as opposed to α2δ-1 which showed no effect on T-type calcium currents under the same conditions (Cottrell *et al*., 2018; Stephens and Cottrell, 2019). While α2δ-1 showed no effect on Ca_V3 family calcium channels (Cottrell *et al*. 2018), it plays a similar role for Ca_V1 and Ca_V2 channels (Dolphin, 2012).

Furthermore, CACHD1 may act as a modulator for $Ca_V2.2$. While human CACHD1 did not result in significant increase of human $Ca_V2.2$ currents (Soubrane *et al*., 2012), zebrafish and rat Cachd1 showed significant increase in rat $Ca_V2.2$ currents, while promoting $Ca_V2.2$ cell surface expression by reducing endocytosis (Dahimene *et al*., 2018). However, while a significant increase in $Ca_V2.2$ currents caused by Cachd1 was observed, this was not as profound as for α2δ-1 modulated current increase (Figure 1.16A-B). Dahimene *et al*. (2018) suggests that Cachd1 may compete with α2δ-1 for the same structural motif. However, mutagenesis of the $Ca_V2.2$ D122 interaction site did not affect Cachd1 modulated $Ca_V2.2$ current increase (Figure 1.16B), suggesting that Cachd1 may utilise different domains to interact with $Ca_V2.2$, perhaps its cache domains. Moreover, Cachd1 did not modulate $Ca_V2.1$ (Figure 1.16C) (Dahimene *et al.*, 2018), showing that α2δ subunits and Cachd1 may modulate VGGCs utilising different modes of action.

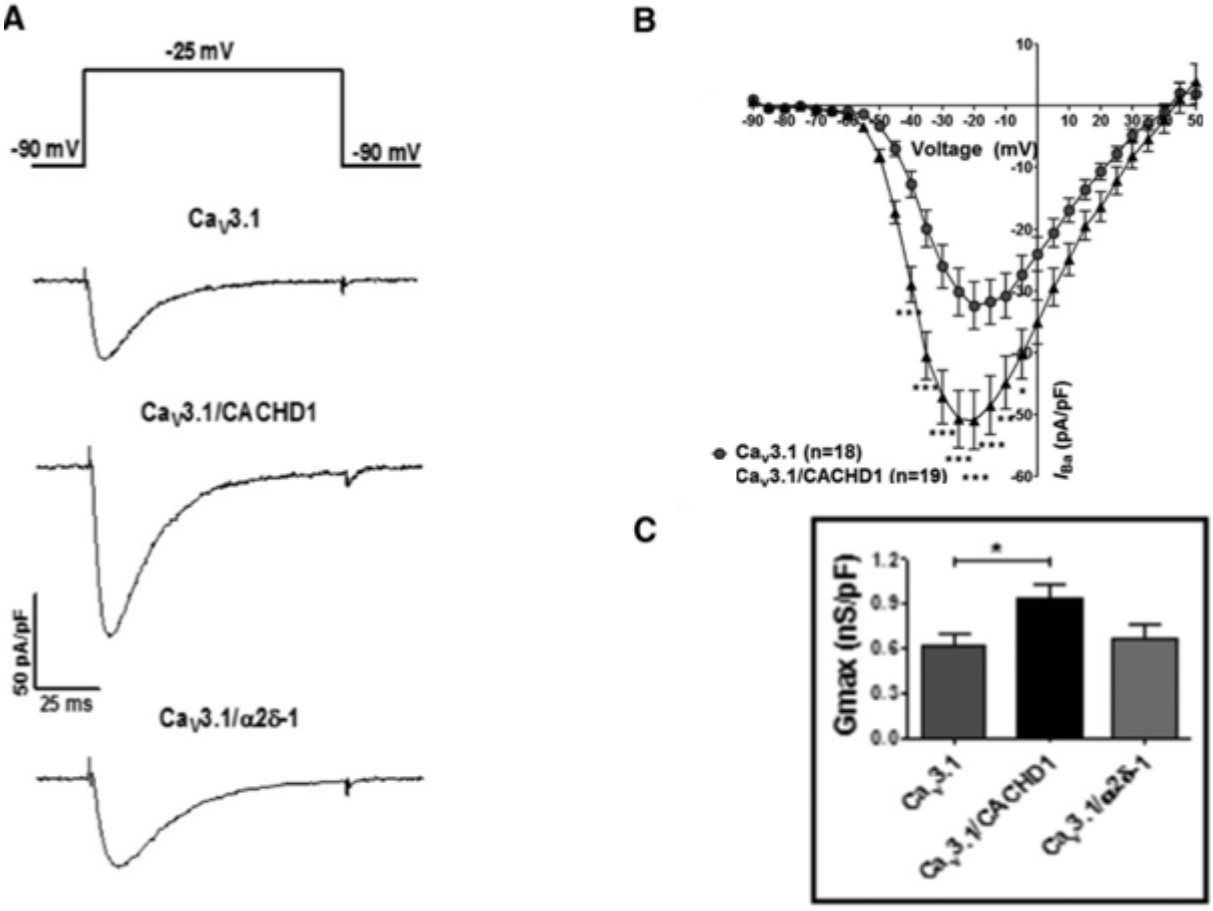

Figure 1.13 Effects of CACHD1 on Ca$_V$3.1channels. (A) CACHD1 significantly increased current density while α2δ-1 had no significant effect as shown by representative current density traces at -25 mV, and **(B)** *I-V* relationship for Ca$_V$3.1, holding potential -90 mV. **(C)** CACHD1, but not α2δ-1 significantly increased maximal conductance. (From: Cottrell *et al*., 2018).

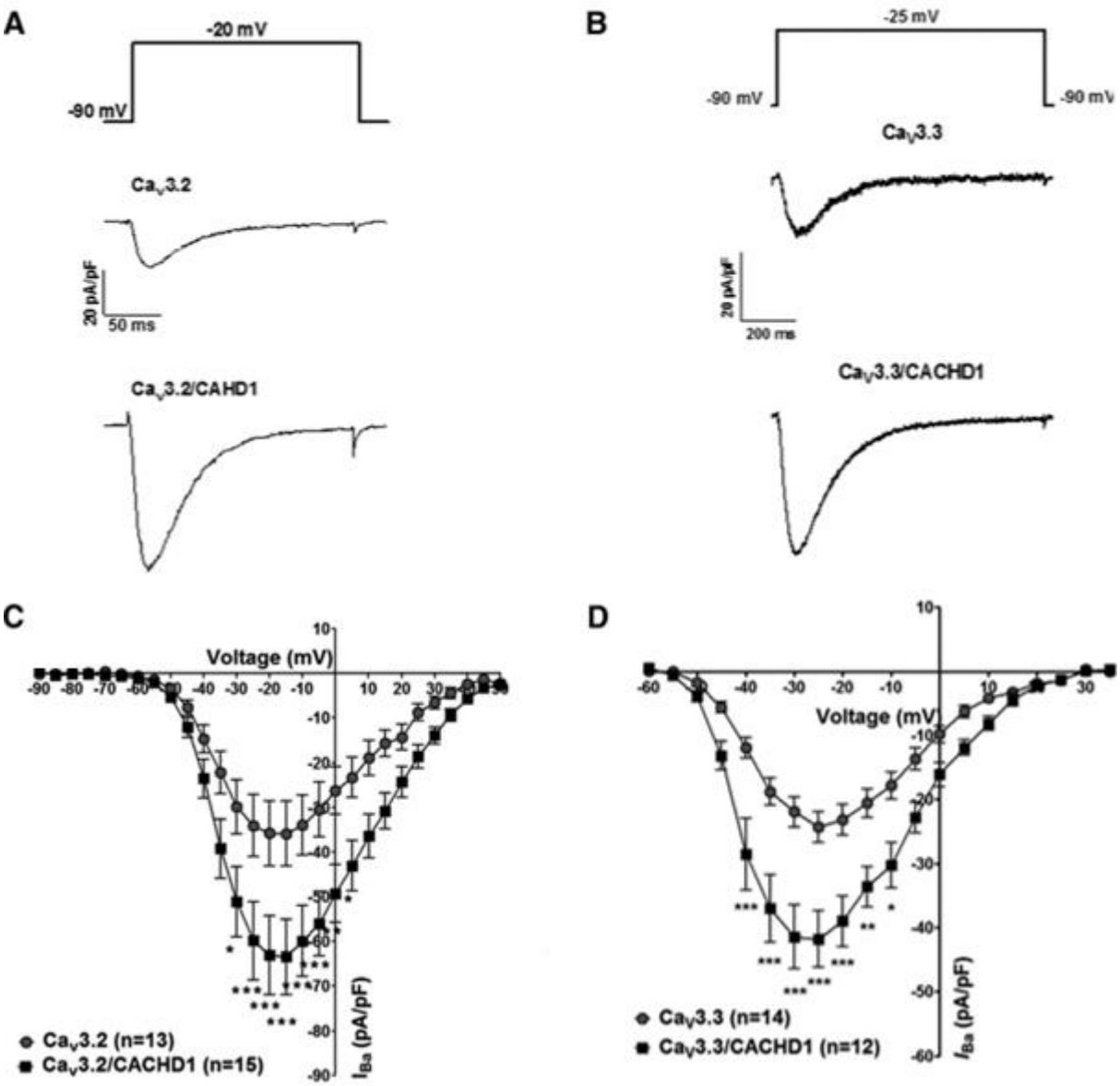

Figure 1.14 Effects of CACHD1 on Ca$_V$3.2 and Ca$_V$3.3 channels. CACHD1 significantly increased current density for Ca$_V$3.2 **(A)** and Ca$_V$3.3 **(B)** as shown by representative traces at -20 mV and -25 mV, and **(C, D)** *I-V* relationships, holding potential -90 mV. (From: Cottrell *et al*., 2018).

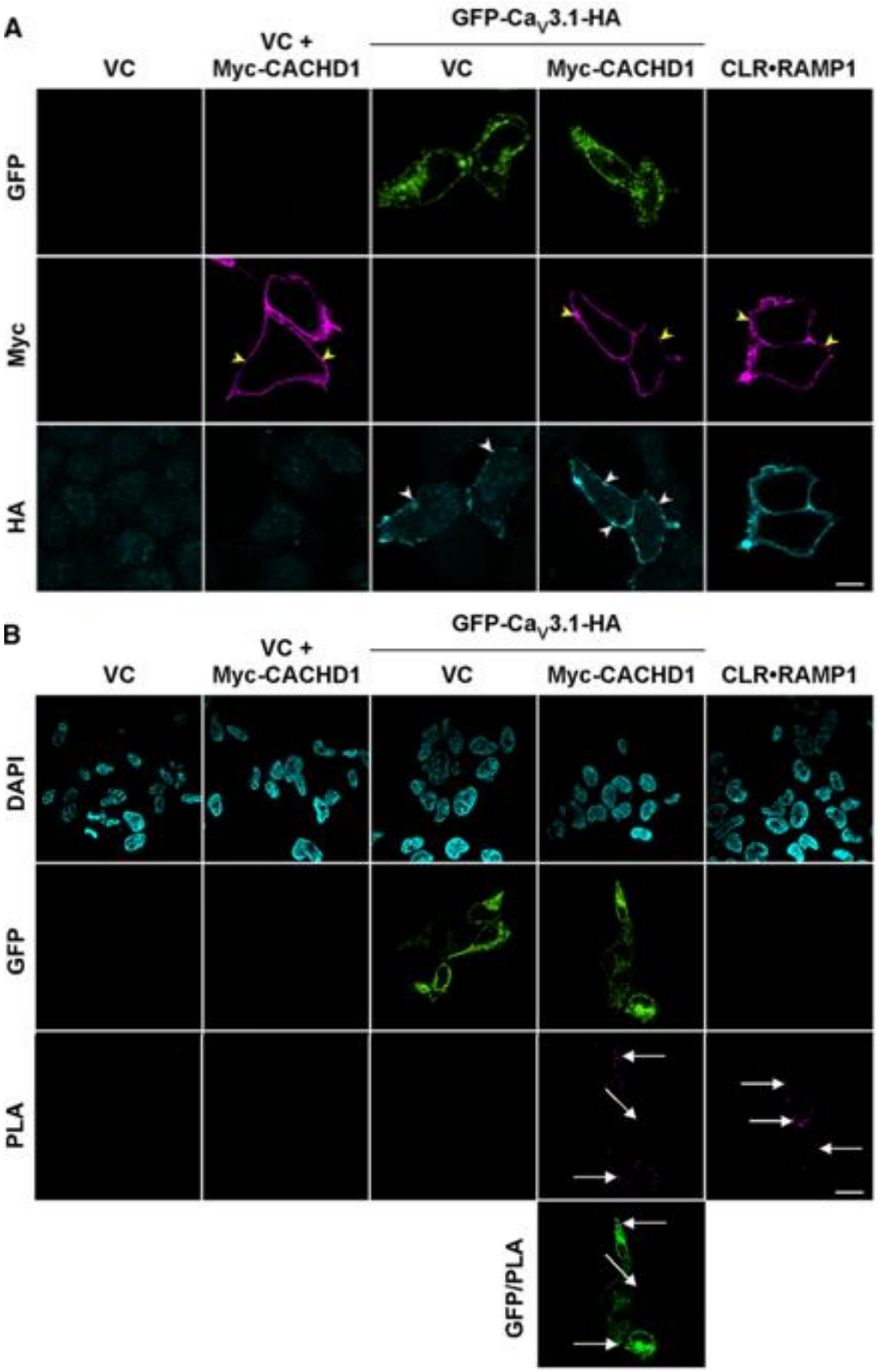

Figure 1.15 Ca$_V$3.1 and CACHD1 are expressed in close proximity at the cell surface. HEK cells were transiently transfected with empty vector (VC), VC + Myc-CACHD1, VC + GFP-Ca$_V$3.1-HA, Myc-CACHD1 + GFP-Ca$_V$3.1-HA, or CLR-RAMP1 (positive control), and live cells were labelled with antibodies to HA and Myc, washed, and fixed with 4% PFA. **(A)** Cells were then incubated with appropriate secondary antibodies and immunoreactive proteins were visualised by confocal microscopy. GFP-Ca$_V$3.1-HA and Myc-CACHD1 are both expressed on cell surface as indicated by the detection of HA (white arrows) and Myc (yellow arrows) fluorescent signals. (Scale bar 10 µm). **(B)** PLA confirmed GFP-Ca$_V$3.1-HA and CACHD1 co-localisation and Ca$_V$3.1/CACHD1 complex formation (arrows) at the cell surface. (Scale bar 20 µm). (From: Cottrell *et al*., 2018).

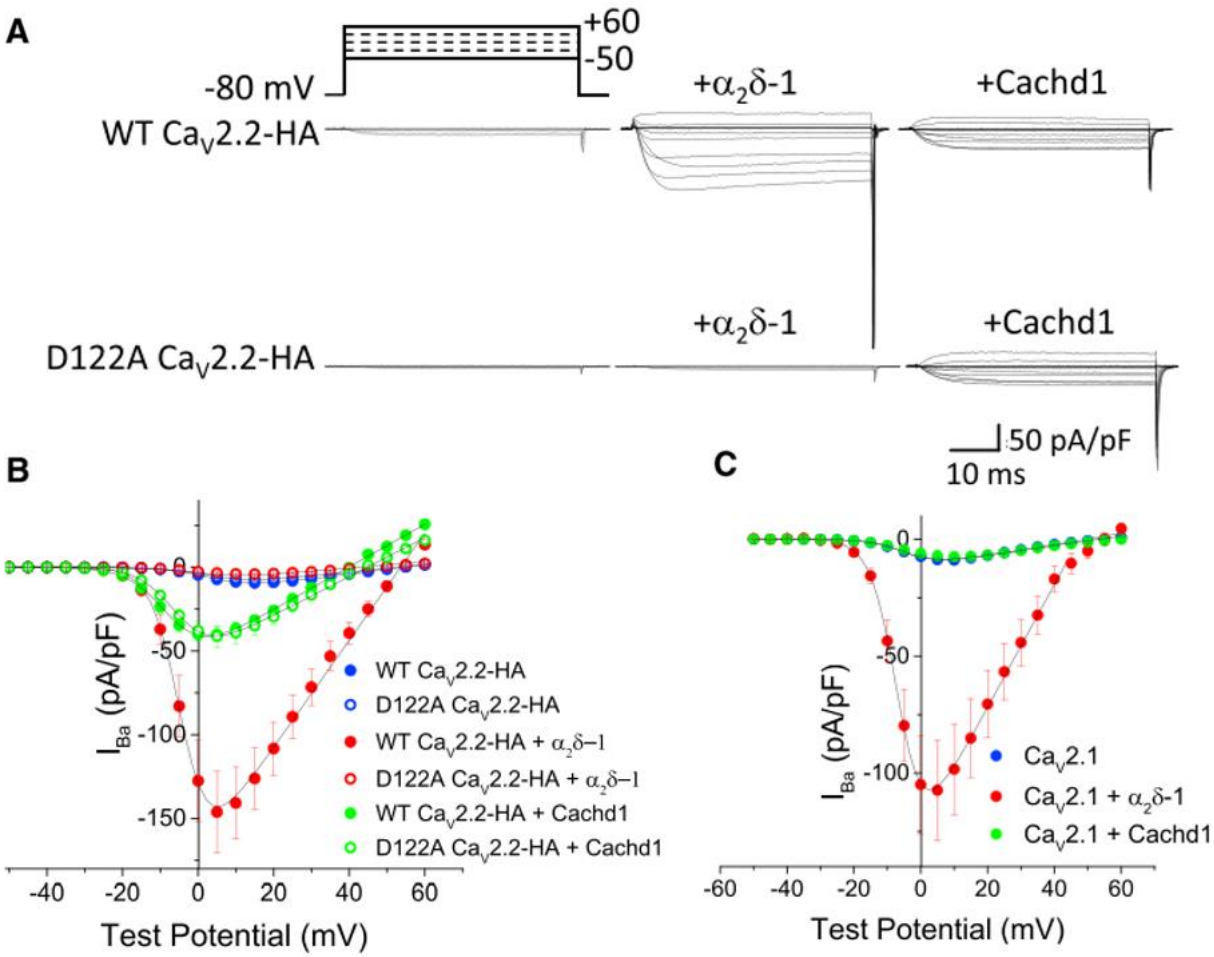

Figure 1.16 D122A mutation of $Ca_V2.2$ abolishes $Ca_V2.2$ current enhancement by α2δ-1 but not CACHD1. (A) Example $Ca_V2.2$-WT and $Ca_V2.2$-D122A current traces co-expressed with β1b only, or with either α2δ-1 or rCACHD1. **(B)** *I-V* relationships (mean±SEM) for the conditions shown in (A). α2δ-1 significantly increased $Ca_V2.2$ currents. CACHD1 also significantly increased $Ca_V2.2$ currents; however, the increase was not as profound as observed for α2δ-1. Mutagenesis of $Ca_V2.2$ D122 interaction site to Ala abolished α2δ-1-mediated $Ca_V2.2$ current increase but had no effect on CACHD1-mediated $Ca_V2.2$ current increase, suggesting that α2δ-1 and CACHD1 use different modes of action for $Ca_V2.2$ modulation. **(C)** CACHD1, unlike α2δ-1, did not modulate $Ca_V2.1$ VGCCs. (From: Dahimine *et al*., 2018).

1.5.4 CACHD1: A potential drug target?

Results from Cottrell *et al*. (2018) showed that CACHD1 plays a role in the modulation of Ca_V3 channels and increases neuronal T-type currents, which in turn promote an increase in action potential firing frequency resulting in increased neuronal excitability, suggesting that CACHD1 may play a role in the management of hyperexcitability diseases such as pain and epilepsy. Furthermore, recent studies link CACHD1 to malignant peripheral nerve sheath tumours in a BL1391 cell line established from a primary tumour, where a *YAP1-CACHD1* in-frame fusion resulted in a mutant protein (1325aa, 1-188 YAP1 + 88-1224 CACHD1) (Tolomeo *et al*., 2020). CACHD1 was also identified as a substrate for β-site amyloid precursor protein (APP) cleaving enzyme 1 (BACE1) protease (Hemming *et al*., 2009; Njavro *et al*., 2019) and for γ-secretase/presenilin complex (Güner and Lichtenthaler, 2020) involved in the generation of pathogenic amyloid-β peptide in Alzheimer's disease, and proposed as a novel biomarker for non-alcoholic steatohepatitis-associated liver preneoplastic and neoplastic lesions due to its elevated expression levels (Kakehashi *et al*., 2021). Modulation of CACHD1 gene expression was also found in patients with type 1 diabetes (Rassi *et al*., 2008). Moreover, study by Tian *et al*., (2021) reported that Cachd1-deficient mice exhibit hearing and balance defects associated with the disturbance of Ca^{2+} homeostasis presumably caused by the loss of Cachd1 regulatory effects on VGCC activity.

Cachd1 is also widely expressed in mouse DRG (Ray *et al*., 2018), which play a critical role in the nociceptive signalling pathway. Moreover, human brain atlas database shows CACHD1 co-expression with $Ca_V3.2$ channels that act as key mediators of neuropathic and inflammatory pain (García-Caballero *et al*., 2014). This evidence further implicates CACHD1 as a potential therapeutic target for pain. It is also worth noting that while the exact biological function and relationship of CACHD1 to different diseases are not yet fully understood, CACHD1 may have multiple functions in the nervous system and therefore represents a potential target for novel treatments for diseases associated with CACHD1 and VGCCs modulated by CACHD1.

1.6 Project aims

α2δ subunits are widely studied because of their interaction with different VGCCs. CACHD1 shares structural and functional similarities with the α2δ subunits, acting as a modulator/auxiliary subunit of Ca_V3 LVA VGCCs, therefore it is of great interest to gain deeper understanding of CACHD1 mechanisms of action. The aims of this project were to characterise the role of different structural motifs in CACHD1.

- The first aim of this project was to characterise the role of the MIDAS motif in CACHD1 expression and function as modulator of Ca_V3 VGCCs. This aim is addressed in Chapters 3 and 4.

- The second aim was to investigate the endocytic pathway and post-endocytic sorting pathway used by CACHD1, as well as to characterise the roles of the tyrosine internalisation motif, transmembrane domain, and the intracellular C-terminal tail in CACHD1 on its expression and trafficking, as addressed in Chapter 5.

- The third aim of this project was to clone and purify a soluble form of CACHD1 for future ligand binding studies, and this aim is addressed in Chapter 6.

2. MATERIALS AND METHODS

2.1 Secondary cell culture

2.1.1 Cell lines

Table 2.1 List of cell lines.

Cell line	Species	Tissue	Medium	Source
293T tsA201	human	embryonic kidney	DMEM, 10% (v:v) FBS, D-glucose (4.5 g/L), glutaMAX™-I, SP	ECACC
293 Flp-In™ T-REx™			DMEM, 10% (v:v) FBS, D-glucose (4.5 g/L), glutaMAX™-I, SP, zeocin (100 µg/ml), blasticidin (5 µg/ml)	Invitrogen
293 Flp-In™ T-REx™ pcDNA5/FRT-CACHD1			DMEM, 10% (v:v) FBS, D-glucose (4.5 g/L), glutaMAX™-I, SP, hygromycin B (50 µg/ml), blasticidin (5 µg/ml)	generated in this study
293 Flp-In™ T-REx™ pcDNA5/FRT-CACHD1-AAA-MIDAS			DMEM, 10% (v:v) FBS, D-glucose (4.5 g/L), glutaMAX™-I, SP, hygromycin B (50 µg/ml), blasticidin (5 µg/ml)	
293 Flp-In™ T-REx™ pcDNA5/FRT-CACHD1-G236S-MIDAS			DMEM, 10% (v:v) FBS, D-glucose (4.5 g/L), glutaMAX™-I, SP, hygromycin B (50 µg/ml), blasticidin (5 µg/ml)	
Lenti-X™ 293T			DMEM, 10% (v:v) FBS, D-glucose (4.5 g/L), glutaMAX™-I, SP	Clontech Laboratories
293 Flp-In™ T-REx™ pLenti6.3-TetO-CACHD1			DMEM, 10% (v:v) FBS, D-glucose (4.5 g/L), glutaMAX™-I, SP, G418 (200 µg/ml)	

293 Flp-In™ T-REx™ pLenti6.3-TetO-CACHD1-AAA-MIDAS			DMEM, 10% (v:v) FBS, D-glucose (4.5 g/L), glutaMAX™-I, SP, G418 (200 μg/ml)	
293 Flp-In™ T-REx™ pcDNA5/FRT-TO-CACHD1-G236S-MIDAS			DMEM, 10% (v:v) FBS, D-glucose (4.5 g/L), glutaMAX™-I, SP, hygromycin B (50 μg/ml), blasticidin (5 μg/ml)	
293 Flp-In™ T-REx™ pcDNA5/FRT-NSS-Myc-CACHD1-trunc-Avi-GG-12His			DMEM, 10% (v:v) FBS, D-glucose (4.5 g/L), glutaMAX™-I, SP, hygromycin B (50 μg/ml), blasticidin (5 μg/ml)	
293 Flp-In™ T-REx™ pcDNA5/FRT-Igκ-Myc-CACHD1-trunc-Avi-GG-12His			DMEM, 10% (v:v) FBS, D-glucose (4.5 g/L), glutaMAX™-I, SP, hygromycin B (50 μg/ml), blasticidin (5 μg/ml)	

DMEM – Dulbecco's modified eagle's serum; FBS – foetal bovine serum; SP – sodium pyruvate. (ECACC – the European Collection of Authenticated Cell Cultures).

2.1.2 Tissue culture

All cell lines were cultured in an appropriate medium (Table 2.1) in a T75 culture flask and maintained in a humidified atmosphere at 37°C, 5% CO_2. Cells were regularly tested for mycoplasma infection using a DNA staining method. This method uses DAPI (4'6-diamidino-2-phenylindole) nuclear stain that binds to adenine-thymine-rich regions in DNA (DAPI fluorescence increases approx. 20-fold when DAPI is bound to double-stranded DNA), and therefore detects mycoplasma double-stranded plasmid DNA.

Briefly, cells were plated on coverslips coated with poly-D-lysine (section 2.3.2) and incubated in antibiotic-free medium at 37°C, 5% CO_2, for 72 h. Cells were then washed, fixed with 4% paraformaldehyde (PFA), and mounted on microscope slides using DAPI mounting medium (Duolink (Sigma) or Vectashield (Vector Laboratories)).

2.1.3 Cell passaging and cell counting

Sub-confluent cells were first washed with Dulbecco's phosphate buffered saline (DPBS, 3.3 mM KCl, 170 mM NaCl, 2.8 mM Na_2HPO_4, 10.6 mM H_2PO_4) without $CaCl_2$ and $MgCl_2$ (DPBS-CM; Invitrogen). Cells were then detached using an appropriate volume of 1x trypsin-ethylenediaminetetraacetic acid (trypsin-EDTA) solution (Sigma) and incubated at 37°C, 5% CO_2 for 2-3 min. Detachment of cells was checked, and culture medium was added to inactivate trypsin-EDTA. The suspended cells were collected by centrifugation at 100 *g* for 5 min, and the culture medium was then discarded. The cell pellet was resuspended in fresh culture medium and passaged in 1:5 - 1:10 ratio to make a fresh culture.

Trypsin is a proteolytic enzyme that cleaves adhesion proteins involved in cell-cell and cell matrix interaction, specifically at the lysine and arginine residues (unless the upstream amino acid is proline) on their C-terminal. EDTA is used as a divalent cation chelator that binds Ca^{2+} and Mg^{2+} into a hexadentate, weakening cell-cell adhesion and enhancing trypsin activity.

To count cells, 100 µl of the remaining cell suspension was diluted 1:10 in culture medium, and 10-15 µl of the diluted cell suspension were added between the cover glass and haemocytometer. Cells in all four outer squares were counted and the total number was divided by four to obtain a mean number of cells/square. To obtain the number of cells/ml, the mean number was multiplied by 10^4 (haemocytometer dilution factor) and by 10 (dilution factor). A desired number of cells were used for subsequent experiments.

2.1.4 Cryopreservation and cell recovery

For all cell lines, sub-confluent cells were detached and resuspended as described above. Cell suspension was then centrifuged at 100 *g* for 5 min to collect cells. Culture medium was discarded, and cell pellet was resuspended in a freezing solution (90% culture medium, 10% dimethyl sulphoxide (DMSO)). The mixture was then aliquoted into cryotubes at 1 ml each (five tubes per T75 cell culture flask), and frozen slowly using a polystyrene box at -80°C before being transferred to liquid nitrogen storage.

To recover cells from liquid nitrogen, cells were thawed quickly in a 37°C water bath. Thawed cells were added to 9 ml of warm fresh culture medium and gently mixed. Cells were collected by centrifugation at 100 *g* for 5 min. After centrifugation, the medium containing freezing mix was discarded and cells were resuspended in 10 ml of fresh culture medium. Resuspended

cells were then seeded in a T75 culture flask and allowed to recover to 80-95% confluency before use, changing medium every 2-3 days.

2.1.5 Transient transfection

Cells were plated at an appropriate density ($6x10^5$ in 12-well plate, $2x10^6$ in 6-well plate) and incubated in an appropriate culture medium (Table 2.1) at 37°C, 5% CO_2, overnight. After overnight incubation and 30 min prior transfection, culture medium was replaced with fresh medium without antibiotics (0.8 ml/well in 12-well plate, 1.5 ml/well in 6-well plate). To prepare the transfection mix, Opti-MEM® medium (Invitrogen) (200 µl for 12-well plate, 500 µl for 6-well plate) and appropriate amount of DNA were added to a sterile microcentrifuge tube. For co-transfection of multiple vectors, vector sizes were used to calculate the molar ratio. Polyethyleneimine (PEI) was used for transient transfection at a 3:1 (transfection reagent : DNA (µg)) ratio. Transfection mix was incubated at room temperature for 15-20 min before adding to cells. Cells with the transfection mix were incubated at 37°C, 5% CO_2, for 4-6 h. Culture medium was then replaced with fresh medium and cells were incubated for further 48 h before analysis. For biotinylation assay, cells were detached as described in section 2.1.3 and transferred to poly-D-lysine (20 µg/ml) coated 100 mm cell culture dishes.

Little is known about how PEI-DNA complexes are processed and transported from cytoplasm to the nucleus (Bieber *et al*., 2002), but most agree PEI works via the so called "proton sponge". PEI is a cationic polymer that binds to DNA, forming positively charged polyplexes that electrostatically interact with the external cell membrane. The polyplexes are then internalised through endocytosis. During the intracellular trafficking process, PEI attraction of protons ("proton sponge") combined with an acidification of the endosomes by the endosomal ATPases (influx of chloride ions) result in lower pH (Remy *et al*., 1998), increased ionic strength and osmotic swelling, disturbing the endosome, and eventually releasing the polyplexes into the cytoplasm (Sabin *et al*., 2022). Once the polyplexes reach the nucleus, PEI binds to and stabilises spontaneously formed holes or defects in the nuclear membrane causing decomplexation of the polyplexes and release of DNA into the nucleus, while PEI remains bound to the nuclear membrane, never entering the nucleus (Sabin *et al*., 2022).

2.1.6 Stable cell line generation: Flp-In™ system

The Flp-In™ system was used to generate stable cell lines (Table 2.1). This system uses pOG44 vector for the expression of Flp recombinase which allows a Flp recombinase-mediated

integration of the gene of interest into the genome of HEK293 Flp-In™ T-REx™ cells. An expression vector containing a FRT site and a hygromycin resistance gene, in this case pcDNA5/FRT, is used to integrate the gene of interest into the genome by DNA recombination at the FRT site.

Briefly, HEK293 Flp-In™ T-REx™ cells were plated at a density of $2x10^6$ cells/well in a 6-well plate (3 wells for each cell line to be generated) and incubated in an appropriate culture medium (Table 2.1) at 37°C, 5% CO_2, overnight. After overnight incubation and 30 min prior transfection, culture medium was replaced with 1.5 ml/well of fresh medium without antibiotics. For each well, transfection mix was prepared by adding 500 µl of Opti-MEM®, 9:1 DNA ratio of pOG44 : FRT vector containing a gene of interest (3 µg of DNA in total), and 8 µl of Lipofectamine 2000 reagent (Invitrogen) into a sterile microcentrifuge tube. Transfection mix was incubated at room temperature for 15-20 min before adding to cells. Cells with the transfection mix were incubated at 37°C, 5% CO_2, for 24 h. This was followed by medium change (no antibiotics) and incubation for further 48 h. After the incubation period, appropriate cells were detached as described in section 2.1.3, added to a centrifuge tube, and collected at 100*g* for 5 min. Cells were then resuspended in an appropriate volume of culture medium containing hygromycin B (Table 2.1), split into four 100 mm dishes at approximately 25% confluency, and incubated at 37°C, 5% CO_2. To allow the selection of stably transfected cells, hygromycin B was used at 50-100 µg/ml. Whilst undergoing hygromycin selection, cells were incubated at 37°C, 5% CO_2, for 2-3 weeks, changing medium every 2-3 days.

Following hygromycin B selection and when multiple colonies of cells were observed, cells were detached and collected as described in section 2.1.3. Cell pellet was then resuspended in 1 ml of fresh medium containing antibiotics and added to one well of a 12-well plate. When cells reached 90-95% confluency, they were detached and transferred to a 6-well plate, T25 flask and then T75 flask. Once confluent, cells were detached and frozen according to section 2.1.4.

2.1.7 Stable cell line generation: Viral transduction

293 Lenti-X™ cells were plated at a density of $2x10^6$ cells/well in a 6-well plate (1 well for each cell line to be generated) and incubated in an appropriate culture medium (Table 2.1) at 37°C, 5% CO_2, overnight. After overnight incubation and 30-60 min prior transfection, culture medium was replaced with 1.5 ml/well of fresh medium without antibiotics. For each well,

transfection mix was prepared by adding 500 µl of Opti-MEM®, 4:1 PEI:DNA ratio, and 5 µg of DNA into a sterile microcentrifuge tube. Molar ratio of vectors was calculated, and each vector made up the following parts of the final 5 µg – 1 part pMD2.5 (VSV-G), 1 part pCMV-dR8.74, 2 parts pLenti6.3 vector containing a gene of interest. Transfection mix was incubated at room temperature for 20 min before adding to cells. Cells with the transfection mix were incubated at 37°C, 5% CO_2, for 6 h. Following incubation, medium containing the transfection mix was replaced with DMEM (D-glucose (4.5 g/L), glutaMAX™-I, SP) containing 2% (v:v) FBS, and cells were incubated at 37°C, 5% CO_2, for 48 h. After 48 h incubation, medium from transfected cells containing lentivirus with a gene of interest was collected, centrifuged at 100 *g* for 5 min to remove cell debris, and filtered through a 0.45 µm filter. Filtered media containing lentivirus was then diluted 1:10 in DMEM containing 10% FBS and 8 µg/ml polybrene (cationic polymer used to neutralise the charge repulsion between the lentivirus and cell membrane, increasing infection efficiency), and stored at -80°C until needed.

A day prior to viral transduction, HEK293 Flp-In™ T-REx™ cells were plated at a density of $1x10^4$ cells/well in a 24-well plate and incubated at 37°C, 5% CO_2, overnight. Once the cells were ready for transduction, 200 µl of the viral dilution was mixed with 200 µl of DMEM (10% FBS, 8 µg/ml polybrene), and added to cells. Cells were incubated with the viral dilution at 37°C, 5% CO_2, for 24 h. After 24 h incubation, the viral dilution was removed, fresh DMEM (10% FBS) was added to the cells, and cells were incubated at 37°C, 5% CO_2, for further 48 h. After 48 h, transduced cells were detached as described in section 2.1.3, resuspended in 2 ml of culture medium containing G418 antibiotic, and plated in 1 well of a 6-well plate (25% final confluency). To allow the selection of stably expressing cells, G418 was used at 400 µg/ml. Whilst undergoing G418 selection, cells were incubated at 37°C, 5% CO_2, for 3-4 weeks, changing medium every 2-3 days.

Following G418 selection and when cells reached 95-100% confluency, cells were detached, collected, and counted as described in section 2.1.3. Cells were then plated at a density of 1 cell/ml in a 100 mm cell culture dish or 0.5 cell/well in a 96-well plate to allow for monoclonal selection. Leftover cells were resuspended and frozen as described in section 2.1.4, obtaining polyclonal cell lines.

Single cells were grown in culture medium containing G418 until colonies started forming. Single clones were then picked and allowed to grow confluent in a 12-well followed by a 6-

well plate at which point each clone was tested by immunocytochemistry and western blotting. Once the expression of gene of interest was confirmed, cells were moved to a T75 flask and allowed to grow. Once confluent, cells were detached and frozen according to section 2.1.4.

2.2 Biochemistry

2.2.1 Antibodies

Table 2.2 List of primary antibodies used for Western blotting.

Primary antibodies				
Target	**Species**	**Type (clone)**	**Dilution**	**Source (cat. no.)**
HA	mouse	monoclonal (15B12)	1:5000	BioLegend (901502)
c-Myc	rabbit	polyclonal	1:5000	Sigma (C3956)
	mouse	monoclonal (9E10)	1:5000	Sigma (M4439)
6-His	rabbit	polyclonal	1:5000	Sigma (SAB4301134)
β-actin	mouse	monoclonal (AC-15)	1:20000	Sigma (A5441)
TFR	mouse	monoclonal (H68.4)	1:1000	Invitrogen (136800)

All antibodies were stored in glycerol (1:1) at -20°C.

Table 2.3 List of secondary antibodies used for Western blotting.

Secondary antibodies				
Antibody	**Conjugate**	**Type**	**Dilution**	**Source (cat. no.)**
Donkey-anti-rabbit IgG (H+L)	HRP	polyclonal	1:10000	Jackson ImmunoResearch (711-035-152)
Donkey anti-mouse IgG (H+L)	HRP	polyclonal	1:10000	Jackson ImmunoResearch (715-035-151)
Goat anti-mouse IgG	HRP	polyclonal	1:10000	Jackson ImmunoResearch (115-035-166)

HRP – horseradish peroxidase. All antibodies were stored in glycerol (1:1) at -20°C.

2.2.2 Buffers and solutions

Table 2.4 List of buffers and solutions used for western blotting.

Buffer	Composition	Purpose
Lysis buffer (pH 7.4)	50 mM Tris/HCl 0.1% Triton-X-100	Cell lysis
RIPA buffer (pH 7.4)	50 mM Tris/HCl 150 mM NaCl 10 mM NaF 10 mM NaP_2O_7 0.1 mM Na_3VO_4 1 mM EGTA 0.5% NP-40 1 mM $MgCl_2$	
10% Sodium dodecyl sulphate (SDS)	10% (w:v) SDS 100% (v:v) ddH_2O	SDS-PAGE electrophoresis
5x Loading buffer (LB)	50% (v:v) Glycerol 10% (w:v) SDS 0.25 M Tris/HCl (pH 6.8) 0.0125% (w:v) Bromophenol blue 23% (v:v) β-mercaptoethanol	
1x Running buffer (pH 8.3)	25 mM Trizma® base 250 mM Glycine 1% (v:v) 10% SDS	
1x Transfer buffer (pH 8.3)	48 mM Trizma® base 39 mM Glycine 1.29 mM SDS 10% (v:v) Methanol	Protein transfer onto Polyvinylidene difluoride (PVDF) membrane
1x Phosphate buffered saline (PBS)	137 mM NaCl 2.7 mM KCl 8.1 mM Na_2HPO_4 1.8 mM KH_2PO_4	Protein detection
1x PBS-Tween® 20 (PBST)	0.1% (v:v) Tween® 20 99.9% (v:v) 1X PBS	
5% milk blocking buffer	5% (w:v) Milk powder 100% (v:v) 1X PBS	

2.2.3 Protein extraction

Cell lysis was performed using 50 mM Tris/HCl 0.1% Triton-X 100 lysis buffer. Briefly, working on ice throughout the whole process, cells were washed 3x with DPBS with $CaCl_2$ and $MgCl_2$ (DPBS+CM; Invitrogen) to ensure removal of all media containing serum before adding lysis buffer. Cells were agitated for 30 min at 4°C, followed by harvesting cells using a cell scraper. Cell suspension was then transferred to a microcentrifuge tube and centrifuged at 12,000 *g*, 20 min, at 4°C, to pellet insoluble material. Supernatant was transferred to separate chilled microcentrifuge tube and protein concentration for each sample was determined using a protein quantification assay described in section 2.2.5.

2.2.4 Cell surface biotinylation

48 h post transfection, working on ice throughout the whole process, cells were washed 3x with cold DPBS+CM to ensure removal of all media containing serum. Cells were then incubated in 3 ml of EZ-Link™ sulfo-NHS-SS-Biotin (0.3 mg/ml in DPBS+CM; Thermo Fisher Scientific) and gently agitated for 1 h at 4°C. Following incubation, cells were washed 3x with cold DPBS+CM, lysed with RIPA buffer (1 ml/dish, 30 min, 4°C; Table 4), and harvested using a cell scraper. After cell lysis and removal of insoluble material by centrifugation (12,000 *g*, 20 min, 4°C), whole lysate samples (100 µl) were collected for further analysis.

To capture biotinylated proteins, high capacity NeutrAvidin agarose beads (20 µl/tube; Thermo Fisher Scientific) were added and incubated on a rotator at 4°C, overnight. NeutrAvidin agarose beads were then collected by centrifugation and washed with RIPA buffer (3x, 12,000 *g*, 1 min, 4°C). After the last wash, beads were resuspended in 20 µl of 2x loading buffer (diluted 5x LB; Table 2.4) and stored at -20°C.

2.2.5 Protein quantification

Bicinchoninic acid (BCA) assay was performed to determine the concentration of total protein in each sample. To prepare the protein standards, 0, 2, 4, 6, 8 or 10 µl of bovine serum albumin (BSA, 1 mg/ml) were added to a 96-well plate in duplicates, and 2 µl of each sample in triplicates. Distilled deionised water (ddH_2O) was then added to a total volume of 10 µl. 200 µl of BCA reagent A and B mix (50:1 ratio) were added to each well, and the plate was incubated at 37°C for 30 min before read at 562 nm using the SoftMaxPro5.4.6 software and SPECTRAmax 340PC Molecular devices plate reader.

The principle of BCA assay is the formation of purple coloured solution when proteins reduce Cu^{2+} to Cu^{1+} in an alkaline solution during a biuret reaction (Wiechelman *et al*., 1988). The cuprous cation is then detected by bicinchoninic acid.

2.2.6 Affinity column chromatography

The purification procedure is shown in Figure 2.1. All buffers (Table 2.5) and protein samples were filtered through a 0.2 µm filter before purification, and flow rate of 1 ml/min was used throughout the whole process. Briefly, PureCube Ni-NTA (nickel-nitrilotriacetic acid) agarose (Cube Biotech) column was equilibrated with 20 column volumes of binding buffer. Protein sample was added to the column and flow-through was collected. Column was then washed with wash buffer and absorbance at 280 nm was measured. Protein of interest was eluted with 10 ml of elution buffer and analysed using western blot (section 2.2.10) and Coomassie staining (section 2.2.9).

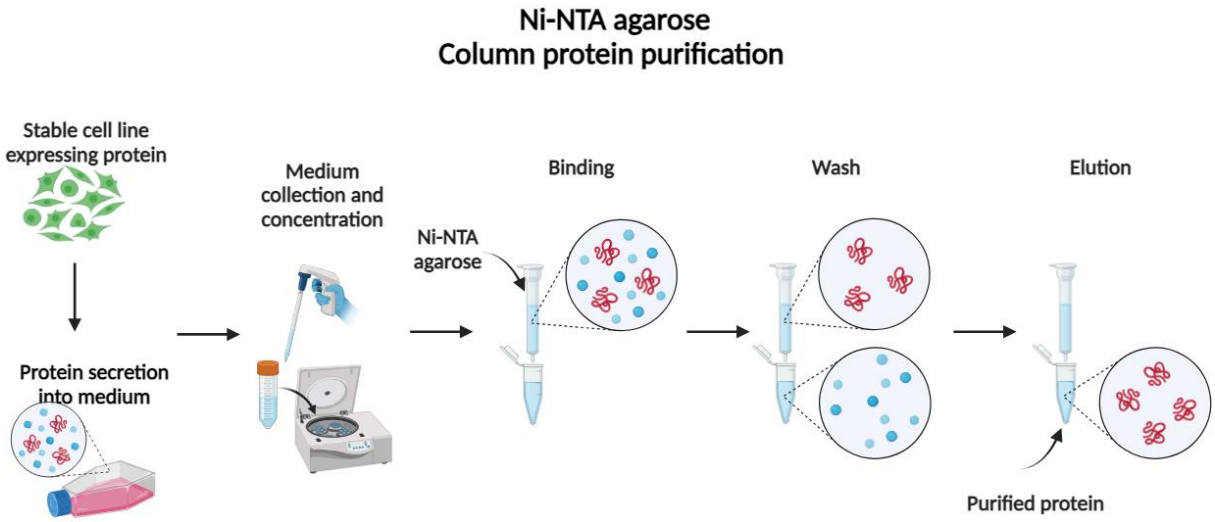

Figure 2.1 Protein purification method using Ni-NTA agarose column. Cells expressing His-tagged protein were plated and allowed to attach overnight, followed by media change to Opti-MEM®. Cells were allowed to grow for 72-96 h, collecting media containing secreted proteins every 48 h. Collected media was concentrated and resuspended in binding buffer (20 mM Tris/HCl, 5 mM imidazole, pH 8.0). Ni-NTA agarose column was equilibrated with binding buffer, followed by protein binding at a 1 ml/min flow rate. Column was then washed with wash buffer (20 mM Tris/HCl, 20 mM imidazole, pH 8.0) and absorbance (280 nm) was measured until no protein was present in the flow-through. His-tagged proteins were eluted with elution buffer (20 mM Tris/HCl, 300 mM imidazole, pH 8.0) and stored at -80°C until analysis. (Made in Biorender.com).

Table 2.5 List of buffers and solutions used for protein purification.

Buffer	Composition	Purpose
Binding buffer (pH 8.0)	20 mM Tris/HCl 5 mM Imidazole	Column equilibration Protein binding
Wash buffer (pH 8.0)	20 mM Tris/HCl 20 mM Imidazole	Column wash
Elution buffer (pH 8.0)	20 mM Tris/HCl 300 mM Imidazole	Protein elution

2.2.7 Protein sample preparation

Protein samples for western blot analysis were prepared by adding 5x loading buffer to cell lysates containing 30 µg of protein at a 1:4 (v:v) ratio and stored at -20°C until needed. Before analysis, samples were boiled at 95-100°C for 5 min and briefly centrifuged.

2.2.8 Protein separation

Proteins were separated on SDS-PAGE gel using the Mini-PROTEAN® Tetra System (BioRad). 1.5 mm 3% stacking, and 7% and 9% resolving gels were used, and their composition is shown in Table 2.6. To prepare a gel, short and spacer glass plates were cleaned with ddH_2O and acetone and placed in a stand. Resolving gel was poured between the glass plates and covered with 200 µl of water-saturated butan-2-ol to exclude air. Once the gel had set, it was rinsed with ddH_2O to remove the butan-2-ol. Stacking gel was then poured on top, a 1.5 mm wide 10-well comb was inserted between the glass plates, and gel was allowed to set. Once the gel had set, it was removed from the stand, placed in the gel holder of the Mini-PROTEAN® Tetra System and submerged in 1x running buffer. The comb was carefully removed, and each well was flushed with 1x running buffer to remove excess non-polymerised acrylamide.

Table 2.6 Composition of SDS-PAGE gels.

Ingredient	Stacking gel	Resolving gel	
	3%	7%	9%
ddH_2O	1.92 ml	5.55 ml	5.05 ml
40% (w:v) Acrylamide/Bis solution 37.5:1	380 µl	1.75 ml	2.25 ml
500 mM Tris/HCl (pH 6.8)	2.5 ml	-	
1.5 M Tris/HCl (pH 8.8)	-	2.5 ml	
10% (w:v) SDS	100 µl	100 µl	
10% (w:v) ammonium persulphate (APS)	100 µl	100 µl	
N,N,N',N'-Tetramethylethylenediamine	7.5 µl	2.5 µl	

Stacking gel – 5 ml/gel; Resolving gel – 10ml/gel.

Protein samples were loaded onto the gel, together with a protein marker (Precision Plus Protein™; BioRad). Proteins were separated according to their size by SDS-PAGE electrophoresis under constant current (20 mA/gel for 30 min, increased to 25-30 mA/gel for 2-2.5 h) until the loading dye ran off the bottom of the gel. Gels were then used for western blotting and Coomassie staining.

2.2.9 Coomassie staining

Coomassie staining was used to detect all proteins in lysate samples. Following SDS-PAGE electrophoresis, gels were removed from glass plates, placed in Coomassie stain (50% (v:v) methanol, 10% (v:v) glacial acetic acid, 0.1% (w:v) Coomassie Brilliant Blue powder, 39.9% (v:v) ddH_2O) and incubated on a rocking platform at room temperature, overnight. Stained gels were placed in a de-staining solution (50% (v:v) methanol, 10% (v:v) glacial acetic acid, 40% (v:v) ddH_2O) at room temperature for 4 h (changing solution every hour) and overnight, followed by re-hydration in ddH_2O and imaging using white light.

2.2.10 Electrophoretic transfer

Following SDS-PAGE electrophoresis, wet electrophoretic transfer was performed to transfer proteins from the gel onto polyvinylidene difluoride (PVDF) membrane (Immobilon®-P, Sigma), using the Mini Trans-Blot system (BioRad). PVDF membrane was activated with 100% methanol for 15 s, agitated in ddH_2O for 1 min and then placed in 1x transfer buffer for at least 10 min. Gels were removed from glass plates, placed in a 1x transfer buffer, and allowed to equilibrate for approx. 10 min. Following equilibration, fibre pad and extra thick blotting paper soaked in 1x transfer buffer were added onto the transfer cassette. PVDF membrane was placed on top of the blotting paper, and a gel was placed onto the membrane. Gel was then covered with another blotting paper and a fibre pad, and the transfer cassette was closed, and placed in the transfer tank filled with pre-chilled 1x transfer buffer. Cooling unit was filled with dry ice to prevent overheating and was replaced every 15-20 min. Proteins were transferred onto PVDF membrane under constant current (1 A) for 1 h.

2.2.11 Immunoblotting

Following protein transfer, PVDF membrane was placed in 1x PBS for 5 min. PVDF membrane was then blocked with 5% milk blocking buffer on a rocking platform at room temperature for 1 h. After blocking period, blocking buffer was replaced with 10 ml of fresh blocking buffer containing appropriate primary antibodies (Table 2.2) and PVDF membrane was incubated on a rocking platform at 4°C overnight. Following overnight incubation, PVDF membrane was washed with 1x PBST (6x 5 min) and incubated in 10 ml of fresh blocking buffer containing appropriate secondary antibodies (Table 2.3) on a rocking platform at room temperature for 1 h. This was followed by another wash step with 1x PBST (6x 5 min) before imaging.

2.2.12 Imaging

After immunoblotting, blots were imaged using the ImageQuant™ LAS 4000 mini detection system for HRP-linked secondary antibodies activated by enhanced chemiluminescence (ECL) solution (BioRad).

2.2.13 Densitometry – protein quantification

Densitometry was used to determine the signal density for proteins detected by western blot. To ensure reliability of this method, protein amount, antibody dilutions, and gel and blot conditions were optimised and kept the same for each set of experiments.

Blot images that showed protein saturation, wavy, streak or smear patterns, or band ghosting, were excluded from quantitative comparison. For each individual experiment, multiple images were taken in 10-30 s increments and once protein bands became overexposed, imaging was stopped, and the overexposed image was discarded, keeping only viable blot images. ImageQuant TL (v8.1.0.0; Cytiva) was used to create protein lanes, detect protein bands of interest, and remove background from the blots to obtain protein-only signal density. Briefly, for each sample lane, the signal form the protein of interest band was normalised to the corresponding β-actin (loading control) protein band signal by dividing the protein data by loading control data, resulting in a sample/control ratio. This process was repeated for at least two separate images of the same blot captured at 10-60 s intervals (technical repeats), and an average of the sample/control ratios was obtained, representing one biological repeat for each sample. Raw data was then analysed using an appropriate statistical test.

2.3 Immunocytochemistry

2.3.1 Antibodies

Table 2.7 List of primary antibodies used for ICC.

Primary antibodies				
Target	**Species**	**Type (clone)**	**Dilution**	**Source (cat. no.)**
c-Myc	rabbit	polyclonal	1:500	Sigma (C3956)
	mouse	monoclonal (9E10)	1:500	Sigma (M4439)
HA	mouse	monoclonal (15B12)	1:500	BioLegend (901502)

All antibodies were stored in glycerol (1:1) at -20°C.

Table 2.8 List of secondary antibodies used for ICC.

Secondary antibodies				
Antibody	**Conjugate**	**Type**	**Dilution**	**Source (cat. no.)**
Donkey anti-mouse IgG (H+L)	Alexa Fluor ™ 546	polyclonal	1:1000	Invitrogen (A10036)
Donkey anti-mouse IgG (H+L)	Alexa Fluor ™ 647	polyclonal	1:1000	Invitrogen (A31571)
Donkey anti-rabbit IgG (H+L)	Alexa Fluor ™ 555	polyclonal	1:1000	Invitrogen (A31572)
Donkey anti-rabbit IgG (H+L)	Alexa Fluor ™ 488	polyclonal	1:1000	Invitrogen (A21206)

All antibodies were stored in glycerol (1:1) at -20°C.

2.3.2 Cell seeding

Glass coverslips were coated with poly-D-lysine (20 µg/ml) for 10 min, rinsed 3x with ddH_2O to remove any excess poly-D-lysine and placed in a 12-well plate. Following transient transfection (section 2.1.5), cells were detached (section 2.1.3), and plated at $1x10^5$/ml density. Cells were allowed to grow for further 48 h at 37°C, 5% CO_2. This was followed by detection using appropriate antibodies (Table 2.7 and 2.8).

2.3.3 Fixation method

Coverslips with transfected cells were washed 3x 5 min with DPBS+CM and incubated in 100 mM PBS containing 4% (w:v) paraformaldehyde (PFA) at room temperature for 20 min. Cells were then washed with blocking solution (1x PBS, 2% normal horse serum (NHS), 0.1% saponin), 3x 5 min, at room temperature.

2.3.4 Live cell labelling

Cells on coverslips were washed, 3x 5 min, with DPBS+CM, followed by addition of appropriate primary antibody (Table 2.7) in DMEM 0.1% BSA and incubation in a humidity chamber at 4°C for 1 h. After incubation period, cells were fixed at 4°C and incubated in appropriate antibody according to the methods described in sections 2.3.3 and 2.3.5.

2.3.5 Fixed cell labelling

Cells on coverslips were fixed according to the method described in section 2.3.3. Appropriate primary antibody (Table 2.7) in blocking solution was added (50 µl/coverslip) and cells were

incubated in a humidity chamber at room temperature for 1 h. This was followed by washing, 3x 5 min, with blocking solution and incubation in appropriate secondary antibody (Table 2.8) in blocking solution (50 µl/coverslip) in a humidity chamber at room temperature for 1 h. After incubation period, cells were washed, 3x 5 min, with blocking solution and rinsed 3x with DPBS+CM. Coverslips were then mounted on microscope slides using mounting medium with DAPI nuclear stain (section 2.1.2).

2.3.6 Imaging

Cells were observed and imaged using epifluorescence and confocal microscopy. For epifluorescence microscopy, EVOS imaging system and x10, x20 and x40 objectives were used. For confocal microscopy, Nikon Eclipse Ti laser-scanning microscope and a 100x/1.45 Oil DIC N2 objective were used. Images were taken at 2x zoom with 5 sections at 0.5µm intervals. Images were processed using the NIS-Elements AR software and Adobe Photoshop.

2.4 Molecular biology

2.4.1 Primers

Table 2.9 List of primers used for construct generation and colony PCR screening.

Primer	Sequence	T_M
bGHrev	5’-AGAAGGCACAGTCGAGGC-3’	59.1°C
CMVfwd	5’-CGCAAATGGGCGGTAGGCGTG-3’	76.9°C
hCACHD1-ATG-fwd	5’-TAATAAAAGCTTCCACCATGGCCCGCCAGCCGGA GGAAGAGGAGACGGCCG-3’	92.6°C
hCACHD1-Myc-fwd	5’-GAGCAGAAGCTGATTAGTGAAGAAGACCTGGAA GCCGACTTCTCCATCCTG-3’	85.4°C
hCACHD1:247-229rev	5'-GACCACATCCAAGTAACGG -3'	60.5°C
CACHD1:2406-2426fwd	5’-GGGCATTGACTTCACACTCAG-3’	64.7°C
CACHD1:3016-3035fwd	5’-GTGCTGGATTGTGAATGGTG-3’	64.1°C
CACHD1:Y1197A	5’-CAGAAAGTGATCATGGTGCCAGCAC CATGAGCCCACAG-3’	86.2°C
CACHD1:Y1197F	5’-CAGAAAGTGATCATGGTTTCAGCAC CATGAGCCCACAG-3’	83.1°C
CACHD1-Avi-GG-rev	5’-CCCGCCCTCGTGCCACTCGATCTTCTGGGCCTCG AAGATGTCGTTCAGGCCAGGGGCGCTTTTAATCATGT-3’	97.0°C
CACHD1-12His-ApaI-rev	5’-TATATAGGGCCCCTAATGGTGATGGTGATGGTGAT GGTGATGGTGATGGTGCCCGCCCTCGTGCCACTCGAT-3’	95.7°C
CACHD1-TM-ApaI-rev	5’-TATATAGGGCCCTTAAATCTGGTGGC GGTAGGCATA-3’	77.0°C
HindIII-KS-Igκ-Myc	5’-TATATAAAGCTTCCACCATGGAGACAGACACACTCCT GCTATGGGTACTGCTGCTCTGGGTTCCAGGTTCCACTGG TGACGAGCAGAAGCTGATTAGTGAAGAAGACCTG-3’	93.9°C

Primers were stored at -20°C.

2.4.2 Plasmids

Table 2.10 List of plasmids.

Plasmid vector	Resistance (prokaryotic/eukaryotic)	Source
pOG44	ampicillin/none	Invitrogen
pcDNA3-HE3-rCa_V3.1	ampicillin/hygromycin B	Dr. E. Perez-Reyes*
pcDNA5/FRT-rCa_V3.1	ampicillin/hygromycin B	generated in this study
pcDNA5/FRT-HA-rCa_V3.1	ampicillin/hygromycin B	
pcDNA5/FRT	ampicillin/hygromycin B	Dr. G.S. Cottrell
pcDNA5/FRT-Myc-CACHD1	ampicillin/hygromycin B	
pcDNA5/FRT-Myc-CACHD1-AAA-MIDAS	ampicillin/hygromycin B	
pcDNA5/FRT-Myc-CACHD1-G236S-MIDAS	ampicillin/hygromycin B	
pcDNA5/FRT/TO	ampicillin/hygromycin B	
pcDNA5/FRT/TO-Myc-CACHD1	ampicillin/hygromycin B	generated in this study
pcDNA5/FRT/TO-Myc-CACHD1-AAA-MIDAS	ampicillin/hygromycin B	
pcDNA5/FRT/TO-Myc-CACHD1-G236S-MIDAS	ampicillin/hygromycin B	
pcDNA5/FRT-Myc-CACHD1-Y1197A	ampicillin/hygromycin B	
pcDNA5/FRT-Myc-CACHD1-Y1197F	ampicillin/hygromycin B	

pcDNA5/FRT-NSS-Myc-CACHD1-trunc-Avi-GG-12-His	ampicillin/hygromycin B	generated in this study
pcDNA5/FRT- Igκ-Myc-CACHD1-trunc-Avi-GG-12-His	ampicillin/hygromycin B	
pcDNA5/FRT-Myc-CACHD1-trunc-TMD	ampicillin/hygromycin B	
pLenti6.3	ampicillin/blasticidin	Invitrogen
pLenti6.3-TO-Myc-CACHD1	ampicillin/blasticidin	generated in this study
pLenti6.3-TO-Myc-CACHD1-AAA-MIDAS	ampicillin/blasticidin	
pLenti6.3-TO-Myc-CACHD1-G236S-MIDAS	ampicillin/blasticidin	
pLenti6.3-Neo-TO	ampicillin/G418	
pLenti6.3-Neo-TO-Myc-CACHD1	ampicillin/G418	
pLenti6.3-Neo-TO-Myc-CACHD1-AAA-MIDAS	ampicillin/G418	
pLenti6.3-Neo-TO-Myc-CACHD1-G236S-MIDAS	ampicillin/G418	
pLenti6.3-Neo	ampicillin/G418	Dr. G.S. Cottrell

Purified plasmids were stored at -20°C (long-term) or 4°C (short-term). * University of Virginia.

2.4.3 Restriction enzymes and buffers

Table 2.11 List of restriction enzymes and buffers used for DNA cloning.

Enzyme	Cut site	Units/ µl	Incubation (°C)	Source (cat. no.)	Optimal buffer	Source (cat. no.)
Afl II	C/TTAAG	20	37°C	NEB (R0520L)	10x rCutSmart™	NEB (B7204S)
Age I-HF	A/CCGGT	20		NEB (R3552S)		
Apa I	GGGCC/C	50	25°C	NEB (R0114L)		
Apa LI	G/TGCAC	10	37°C	NEB (R0507S)		
Bam HI-HF	G/GATCC	20	37°C	NEB (R3136S)		
Cla I	AT/CGAT	10	37°C	NEB (R0197S)		
Eco RV-HF	GAT/ATC	20		NEB (R3195S)		
Hind III-HF	A/AGCTT	20		NEB (R3104S)		
Mfe I-HF	C/AATTG	20		NEB (R3589S)		
Nhe I	G/CTAGC	20		NEB (R3131S)		
Nsi I-HF	ATGCA/T	20		NEB (R3127S)		
Sex AI	A/CCWGGT	5		NEB (R0605S)		
Sna BI	TAC/GTA	5		NEB (R0130S)		
Not I	GC/GGCCGG	10		NEB (R0189S)	10x NEBuffer™ 3.1	NEB (B6003S)
-	-	-	-	-	10x NEBuffer™ 2.1	NEB (B7202S)
100x BSA		10mg /ml	-	NEB (B9001S)	-	-

All buffers and enzymes were stored at -20°C. *IUPAC (International Union of Pure and Applied Chemistry) single letter codes used to designate more than one nucleotide: R – A or G, Y – C or T, W – A or T.

2.4.4 Bacteria

Table 2.12 List of competent bacterial cells.

Strain	Genotype	Source
GM2163	F$^-$ *dam-13:Tn9(Cam^R) dcm-6 ara-14 his*G4 *leu*B6 *thi-1 lac*Y1 *gal*K2 *gal*T22 *gln*V44 *hsd*R2 *xly*A5 *mtl-1 rps*L 136(Str ^{R}) *rtb*D1 *ton*A31 *tsx78 mcr*A *mcr*B1	NEB
Mach1	F$^-$ ϕ80(*lac*Z)ΔM15 Δ*lac*X74 *hsd*R(r_K^-, m_K^+) Δ*rec*A1398 *end*A1 *ton*A	Invitrogen
Stbl3	F$^-$ *mcr*B *mrr hsd*S20(r_B^-, m_B^-) *rec*A13 *sup*E44 *ara*-14 *gal*K2 *lac*Y1 *pro*A2 *rps*A2 *rps*L20(Str^R) *xyl*-5 λ$^-$ *leu mtl*-1	Invitrogen

All bacterial cells were stored at -80°C prior to use.

2.4.5 Competent bacterial cells preparation – Inoue method

Chemically competent bacterial cells were prepared by using the Inoue method (Inoue *et al*., 1990). Mach1 or Stbl3 bacteria were streaked on antibiotic-free super optimal broth (SOB) agar (20% (w:v) tryptone, 5% (w:v) yeast extract, 8.5 mM NaCl, 2.5 mM KCl, 10 mM $MgCl_2$, 1.5% (w:v) agar bacteriological) plates and incubated at 37°C, overnight. The next evening, 200 ml of antibiotic-free SOB medium (20% (w:v) tryptone, 5% (w:v) yeast extract, 8.5 mM NaCl, 2.5 mM KCl, 10 mM $MgCl_2$) was inoculated with 5 different clones and grown at room temperature, 200-250 rpm, overnight. Following incubation, optical density at 600 nm (OD_{600}) was measured using a UV-Vis spectrophotometer (fresh SOB medium used as a blank). Once the OD_{600} value reached 0.5-0.6, bacterial pellet was collected by centrifugation at 3000 *g* (10 min, 4°C), resuspended in 30 ml of transformation buffer (TB; Table 13), and incubated on ice for 10 min. This was followed by centrifugation at 3000 *g* (10 min, 4°C) to collect bacterial pellet and resuspension in 20 ml of TB + DMSO mix (93% TB, 7% DMSO). Competent bacteria were then aliquoted at 250 µl and flash-frozen in liquid nitrogen before storing at -80°C.

TB was prepared by dissolving KCl, $CaCl_2{\cdot}2H_2O$ and PIPES (piperazine-1,2-bis[2-ethanesulforic acid]; in milli-Q pure H2O, pH 6.7, filter sterilised) in 800 ml of ddH_2O and pH was adjusted to 6.7 with KOH. $MnCl_2{\cdot}4H_2O$ was dissolved in 100 ml of ddH_2O, and gradually added to the mixture. Drop in pH is expected after the addition of $MnCl_2{\cdot}4H_2O$ and should not be adjusted back to 6.7 as this will precipitate a yellow/brown hydroxide. TB was filter sterilised through a pre-washed 0.20 µm filter and stored at 4°C.

Table 2.13 List of reagents used for preparation of transformation buffer.

Reagent	Volume	Final concentration
PIPES (0.5 M)	20 ml	10 mM
$CaCl_2 \cdot 2H_2O$	2.20 g	15 mM
KCl	18.65 g	250 mM
$MnCl_2 \cdot 4H_2O$	10.88 g	55 mM
ddH_2O	up to 1 L	-

2.4.6 Polymerase Chain Reaction (PCR)

Table 2.14 PCR components.

Reagent	Source (cat. no.)	Volume	Final concentration
5x Q5 reaction buffer	NEB (B9027)	10 µl	1x
dNTPs (10 mM each)	Qiagen (1005631) or NEB (N0447)	1 µl	0.2 mM
Q5 DNA polymerase (2 U/µl)	NEB (M0491)	0.5 µl	0.02 U/µl
Forward primer (10 µM)	Sigma	2 µl	0.4 µM
Reverse primer (10 µM)	Sigma	2 µl	0.4 µM
ddH_2O	-	32.5-34.0 µl	-
Template	-	0.5-2.0 µl	-

Total volume of 50 µl/reaction.

Table 2.15 Cycling condition for PCR.

Temperature	Time	Step	Cycles
98°C	5 min	initial denaturation	1
98°C	30 s	denaturation	25-35
55°C	30 s	annealing	
72°C	1 min	elongation	
72°C	10 min	final elongation	1
12°C	∞	hold	hold

2.4.7 DNA cloning

DNA cloning was used to insert genes of interest into expression vectors. Workflow of DNA cloning is shown in Figure 2.2.

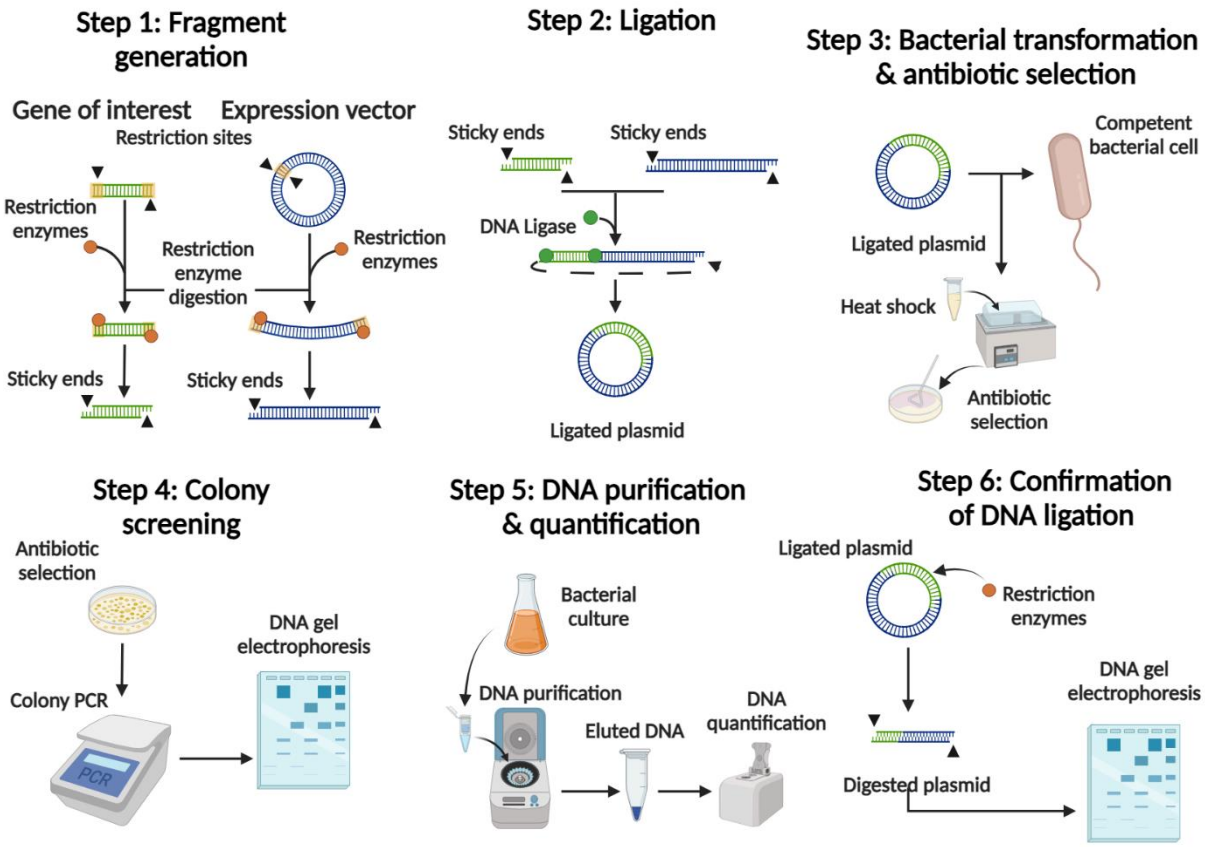

Figure 2.2 DNA cloning method. Plasmid vectors and PRC products were digested with restriction enzymes, and DNA fragments containing appropriate restriction sites on each end were extracted. These DNA fragments were then ligated using a T4 DNA ligase for at least 4 h at 14°C, followed by bacterial transformation where the full construct was inserted into competent bacteria using a heat shock at 42°C. Following bacterial transformation, bacteria were plated on SOB agar plates containing appropriate antibiotics and incubated for 16-24 h at 28°C or 37°C depending on the cell line, allowing antibiotic selection of successfully transformed bacterial cells. Colony PCR was used to screen single clones, and positive clones were used to inoculate 200 ml of SOB media to prepare a bacterial culture from which the final plasmid DNA construct was purified. Accurateness of DNA ligation and any mutagenesis performed was confirmed by restriction digest and DNA sequencing. (Made in Biorender.com).

2.4.8 Restriction digest

Appropriate restriction enzymes were determined using NEBcutter V2.0, Mendelgen.com and Serial Cloner 2.6 software. Digestion reactions were set up by adding restriction enzymes, DNA, appropriate buffer and ddH_2O up to 20 µl, and incubating at required temperature (Table 2.11).

For cloning experiments, digestion reactions were incubated overnight, whilst for diagnostic purposes reactions were incubated for 1-2 h.

2.4.9 Agarose gel electrophoresis

Agarose gel electrophoresis was used to separate DNA fragments in the range 100 bp - 10 kbp. Depending on the expected fragment size, 0.8-2% (w:v) agarose gels were made with 1x tris-acetate EDTA (TAE) buffer. Gels were prepared by dissolving an appropriate amount of agarose in 1x TAE buffer (50 ml/gel) using a microwave, until the solution became clear. The solution was allowed to cool down to approx. 50°C before adding SYBR® Safe DNA gel stain (1:25,000; Thermo Fisher Scientific) to allow visualisation of DNA under UV and blue light. The solution was poured into a gel casting tray, making sure to remove any bubbles. Appropriate comb was used to create sample wells. Once the gel had set, it was placed in the electrophoresis tank together with the casting tray and submerged in 1x TAE, ensuring the wells were fully covered. Samples were prepared by adding 6x loading dye (NEB, B7025) to a final concentration of 1x to the desired DNA concentration. 1kb or 100bp DNA marker (NEB, N0468S and N3231S) and samples were loaded into wells and DNA fragments were separated under constant voltage (70-80 V, 1-1.5 h). DNA separation was checked using a Dark Reader® Transilluminator (Clare Chemical Research) before imaging with U:GENIUS3 system and U:GENIUS 3.0.7.0 software (Syngene). For DNA cloning purposes, only Dark Reader® Transilluminator was used to visualise DNA fragments to avoid DNA damage by UV light.

2.4.10 DNA extraction

DNA fragments of interest were extracted from agarose gel using the QIAquick gel extraction kit (Qiagen, 28704) following manufacturer's guidelines. Briefly, DNA fragment of interest was cut out of agarose gel, placed in a 1.5 ml tube, and weighed. Appropriate volume of QG buffer (1:3 ratio of gel (mg) : buffer volume (µl)) was added to the tube, and gel was melted in a water bath (50°C, 5-7 min). Once melted, the mixture was poured into a spin column and centrifuged (17,000 *g*, 30-60 s) to allow DNA binding to the silica membrane inside the spin

column. This was followed by wash steps with QG and PE (containing ethanol) buffers, and elution of DNA with ddH_2O.

2.4.11 DNA ligation

Extracted DNA fragments were ligated to generate plasmid vector of interest. For each experiment, two reactions were set up - one containing vector DNA fragment only which served as a negative control and second one containing vector and insert DNA fragments. Ligation reactions were incubated at 14°C for at least 4 h or overnight. Components for ligation reaction are shown in Table 2.16.

Table 2.16 Components used for DNA ligation.

Component	Source (cat. no.)	Vector	Vector + insert
10x Ligation buffer	NEB (B0202S)	0.5 µl	0.5 µl
Vector	-	0.5 µl	0.5 µl
Insert	-	-	2 µl
ddH_2O	-	3.75 µl	1.75 µl
T4 DNA ligase	NEB (M0202M)	0.25 µl	0.25 µl

5 µl total volume/reaction.

2.4.12 Bacterial transformation

Competent bacterial cells (Table 2.12) were thawed slowly on ice for 30 min. Once thawed, 50 µl were aliquoted into pre-cooled sterile tubes and ligation reactions were added, gently mixed, and incubated on ice for further 30 min (plasmid DNA binds to cell surface). Following incubation period, cells were heat shocked at 42°C for 38 s (increases permeability of the cell wall allowing DNA entry into the bacterial cell), and placed immediately back on ice for 5 min. 950 µl of super optimal broth with catabolite repression (SOC) medium (20% (w:v) tryptone, 5% (w:v) yeast extract, 8.5 mM NaCl, 2.5 mM KCl, 10 mM $MgCl_2$, 20 mM glucose) were added and cells were allowed to recover at an appropriate temperature for 1 h to obtain optimal transformation efficiency. Cells were then collected by centrifugation at 3500 *g* for 3 min or until pellet formed. Supernatant was discarded (poured out) and cells were resuspended in remaining supernatant and plated on SOB agar plates containing appropriate antibiotic (100

µg/ml ampicillin or 50 µg/ml kanamycin). Plates were then incubated at an appropriate temperature for 16-24 h.

2.4.13 Colony PCR

Colony PCR was used for screening of bacterial colonies to verify the presence of DNA insert in the plasmid construct. Colony template was prepared by adding a colony to 10µl of ddH_2O and mixed. PCR reactions were set up (Table 2.17) and placed in a thermal cycler (BioRad MJMini) with cycling conditions as shown in Table 2.18.

Table 2.17 Colony PCR components.

Reagent	Source (cat. no.)	Volume	Final concentration
10x PCR buffer	Qiagen (1005479)	2 µl	1x
dNTPs (10 mM)	Qiagen (1005631)	0.4 µl	0.2 mM
Taq enzyme (5 U/µl)	Qiagen (201203)	0.1 µl	0.025 U/µl
Forward primer (10 µM)	Sigma	1 µl	0.5 µM
Reverse primer (10 µM)	Sigma	1 µl	0.5 µM
ddH_2O	-	13.5 µl	-
Template	-	2 µl	-

Total volume of 20 µl/reaction. PCR master mix excluding colony template was prepared and aliquoted at 18 µl/reaction.

Table 2.18 Cycling condition for colony PCR.

Temperature	Time	Step	Cycles
95°C	5 min	initial denaturation	1
95°C	30 s	denaturation	35
55°C	30 s	annealing	
68°C	1 min	elongation	
68°C	10 min	final elongation	1
12°C	∞	hold	hold

2.4.14 Bacterial culture

Bacterial glycerol stocks or bacterial colonies from SOB agar plates were used to inoculate an appropriate volume (5 ml for miniprep, 200 ml for maxiprep) of SOB medium. Inoculated medium was incubated at an appropriate temperature, 200-250 rpm for up to 16 h.

2.4.15 Plasmid purification

Plasmid DNA was purified using the QIAprep spin miniprep kit (Qiagen, 27115) or Plasmid maxi kit (Qiagen, 12162) following manufacturer's guidelines.

For QIAprep spin miniprep kit, bacterial culture was centrifuged at 6800 *g* (5 min, room temperature). Bacterial pellet was resuspended in buffer P1 and lysed with buffer P2. The mixture was incubated at room temperature for 2 min before adding buffer P3. The mixture was then centrifuged at 17,900 *g* for 10 min to separate cell bodies and supernatant containing plasmid DNA. After centrifugation, supernatant was transferred to a spin column and centrifuged to allow DNA binding to the silica membrane inside the spin column. This was followed by wash steps with buffer PB, buffer PE (containing ethanol), and elution of DNA with ddH_2O.

For Plasmid maxi kit, similar protocol was followed. Briefly, bacterial pellet was collected by centrifugation at 6800 *g* (20 min, 4°C), resuspended in buffer P1, and lysed with buffer P2 for 5 min at room temperature. After cell lysis, neutralisation buffer N3 was added and the mixture was incubated at room temperature for 10 min, followed by brief centrifugation to

remove cell debris, and filtration into a clean 50 ml tube. Buffer ER was added to the filtered lysate and the mixture was incubated on ice for 30 min. Meanwhile, filter column was equilibrated with QBT buffer. After 30 min, lysate mixture was added to the filter column and filtered by gravity flow, allowing binding of DNA to the membrane inside the column. This was followed by wash step 2x with buffer QC, and elution of DNA with buffer QN into a clean tube. DNA was then precipitated with isopropanol, centrifuged at 15,000 *g* (30 min, 4°C) and supernatant was discarded. Endotoxin free ethanol was added to DNA pellet and centrifuged for further 10 min. Supernatant was discarded and DNA pellet was air dried for approx. 5-10 min before resuspending in an appropriate volume of ddH_2O. The mixture was then centrifuged at 17,900 *g* (10 min) and supernatant containing DNA was transferred to a sterile tube.

2.4.16 DNA quantification

Purified plasmid DNA was quantified using NanoDrop 2000 UV-Vis spectrophotometer (Thermo Fisher Scientific). Briefly, 2 µl of plasmid DNA were added onto the measurement surface. DNA concentration was measured, and the purity of plasmid DNA was assessed by measuring the 260/280 and 260/230 absorbance ratios. Values of ~1.8 (DNA) for 260/280 ratio, and 1.8-2.2 for 260/230 ratio were accepted as 'pure' for DNA.

2.5 Electrophysiology

2.5.1 Electrical properties of a cell

Electrical signals are fundamental for nervous system function, and understanding the electrical properties of cells is important to determine how electrical signals spread along the plasma membrane. These electrical properties depend on the physical properties of the plasma membrane. All eukaryotic cells have a thin lipid bilayer that acts as an insulating barrier separating the charged particles in the extracellular fluid from those present in the cytoplasm, thus behaving as a combined capacitor and resistor.

In general, a capacitor consists of two conducting plates separated by an insulating barrier. Similarly, the lipid barrier is made up of two layers of lipid molecules, where the hydrophilic heads act as conducting plates, and the hydrophobic tails congregated together act as an insulating barrier. The ability of plasma membrane to store charge or membrane capacitance (C_M, [F]) is inversely proportional to the distance between the two lipid layers of the lipid bilayer, and directly proportional to the cell size (larger cell = larger plasma membrane = more charge is stored).

Membrane resistance (R_M [Ω]) prevents the flow of ions through plasma membrane according to their concentration gradients. At a resting state, more negatively charged ions are present in the cytoplasm compared to the extracellular fluid, resulting in a negative resting membrane potential (V_m) and a separation of charge across the membrane. This charge separation results in a driving force (voltage *V* [V]), allowing the movement of charge (current *I* [A]) across the membrane through ion channels.

The movement of charge (current *I* [A]) in excitable cells is dependent on voltage *V* [V] as the driving force, conductance *G* [S] of ions through ion channels, and membrane resistance *R* [Ω]. Ohm's law relates these properties together as:

$$\boldsymbol{V = I \times R} \qquad \text{or} \qquad \boldsymbol{V = I / G}$$

As such, the plasma membrane can be modelled as a resistor-capacitor (RC) circuit (Figure2.3), where the capacitor and resistors are in parallel. The ion channels act as both conductors and resistors, while the plasma membrane acts as a capacitor.

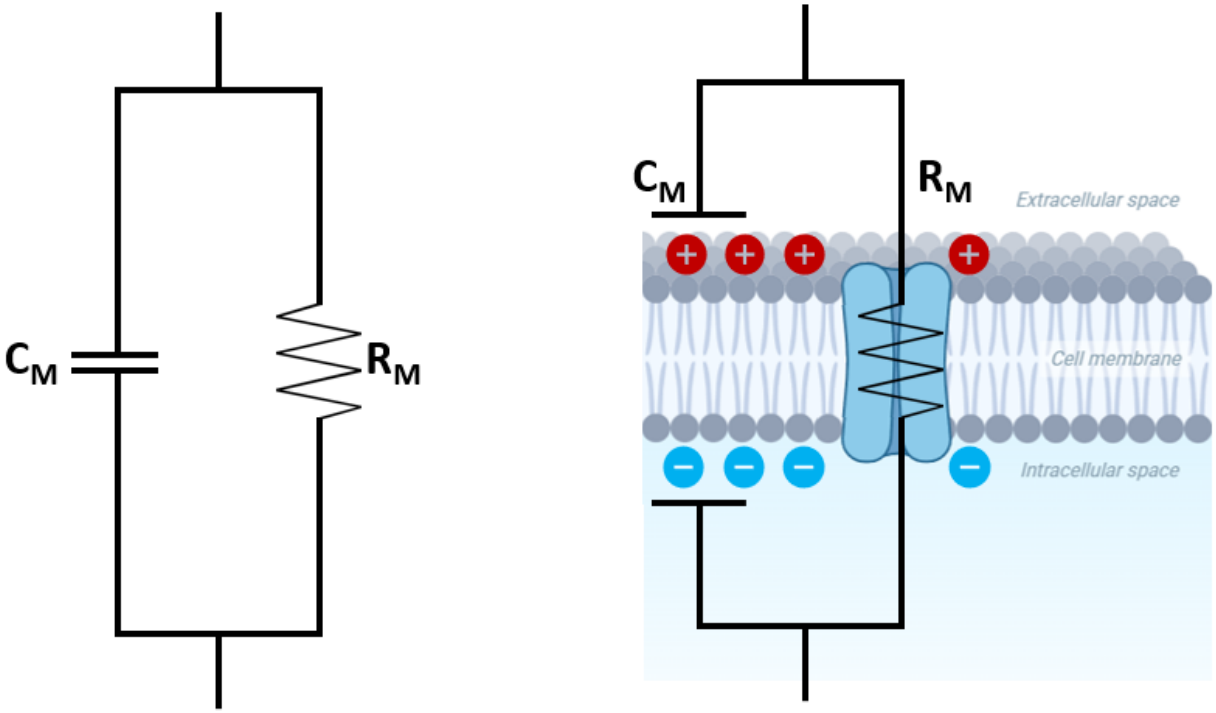

Figure 2.3 Schematic of the electrical properties of a plasma membrane. Membrane capacitance (C_M) and membrane resistance (R_M) are in parallel to each other. Ion channels (K^+, Cl^-, Ca^{2+}, Na^+) act as conductors and resistors, while the plasma membrane acts as a capacitor.

2.5.2 Whole-cell patch clamp: methodology

The patch-clamp electrophysiology technique is the most common method used to study the electrical properties of excitable cells and the function of ion channels. It allows the control of voltage across the plasma membrane and measurement of current flow across it (voltage clamp), or control of current and measurement of changes in potential across the membrane (current clamp). The first voltage-clamp experiments on a squid giant axon were conducted by Alan Hodgkin and Andrew Huxley (1952). Based on this work, the patch-clamp technique was developed by Bert Sakmann and Erwin Neher in 1976, and further improved in 1981 by using a glass electrode with low resistance and larger diameter tip (Hamill *et al*., 1981). From this breakthrough several different recording configurations were established as shown in Figure 2.4.

Briefly, a recording electrode inside a pipette filled with intracellular solution (ICS) is submerged in extracellular solution (ECS), resulting in closed pipette-bath-amplifier circuit where the voltage between the reference and recording electrodes should be 0 mV. A rectangular current stimulus (termed 'test pulse') that allows the monitoring of pipette resistance (R_{pip}, [MΩ]) is injected and the amplifier's offset voltage is adjusted to 0 mV. Prior to approaching a cell, positive pressure is applied to the pipette to prevent cell debris or tissue from obstructing the pipette tip. The pipette is then lowered onto a cell, and once the pipette comes in contact with cell membrane, pipette resistance increases while current amplitude decreases. Positive pressure is released, and mild suction is applied to form a high-resistance seal (giga-seal [GΩ]), further increasing pipette resistance. At this point, a negative command voltage that matches the expected potential (~ -70 mV, depending on cell type) is applied to the recording electrode, resulting in a cell-attached configuration. From this configuration, different steps can be taken to achieve a whole-cell, inside-out or outside-out configurations (Figure 2.4). During this project, the whole-cell configuration was used.

Once a tight seal is formed, sharp suction is applied to rupture cell membrane under the pipette tip, allowing the ICS and cytoplasm contents to exchange. When the cell membrane is ruptured, membrane components can obstruct the current flow from recording electrode to the cell, resulting in a so-called access resistance (R_a). The sum of initial R_{pip} and R_a is referred to as series resistance (R_s), which is an important experimental parameter that indicates the quality of the pipette-cell membrane seal. Generally, R_s above 20 MΩ indicates a poorly ruptured membrane. During whole-cell configuration, the pipette and cell become 'one', and

the current flow across the cell membrane in response to voltage change can be measured using the voltage-clamp technique. In theory, as the potential (voltage) becomes more positive, the cell is depolarised and voltage-gated ion channels open, allowing more current flow through the cell membrane.

As described in section 2.5.1, the cell membrane behaves as a capacitor and stores charge. This charge can become visible in the form of artefactual transient currents during the cell-attached and whole-cell configurations, at the start and end of the test pulse. These 'fast' capacitive currents can be corrected using the amplifier's capacitance compensation option; the level of compensation is proportional to the surface area of the cell membrane, thus indicating cell size.

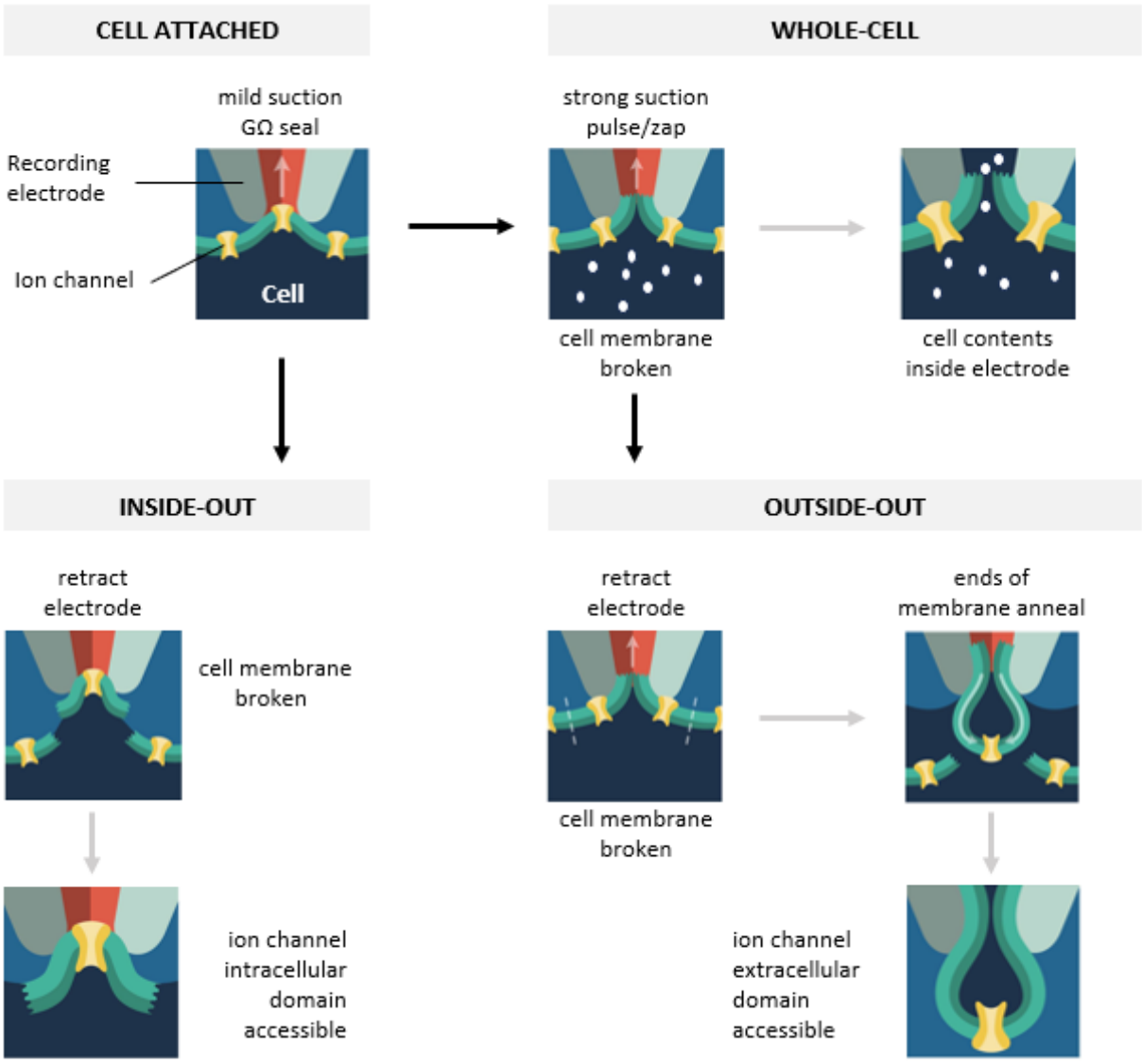

Figure 2.4 Patch-clamp recording methods. Cell-attached: recording electrode is attached to cell membrane and mild suction is applied to gain a tight seal (GΩ). **Whole-cell:** strong suction pulse and/or zap is applied to rupture the cell membrane and gain access to the cytoplasm. **Outside-out:** in the whole-cell configuration, recording electrode is retracted, resulting in two pieces of cell membrane that anneal and form a small vesicle with the extracellular side facing the bath solution. **Inside-out:** in the cell-attached configuration, recording electrode is retracted, resulting in a membrane patch that is separated from the rest of the membrane. The intracellular side is facing the bath solution, giving access to the intracellular domain of ion channels. (Adapted from: Neuroscience: Canadian 1st Edition, Chapter 3.1, eCampusOntario Pressbooks).

2.5.3 Whole-cell voltage clamp: Experimental approach

Fire-polished borosilicate glass capillaries with internal filaments (O.D. 1.2 mm, I.D. 0.68 mm; WPI, USA, 1B120F-4, lot no.: 2605333) were used to fabricate patch clamp pipettes using a horizontal puller (Intracel, model P-1000, Sutter Instrument, USA). A pre-set program consisting of several heat and pull steps was used to produce two fine-tip pipettes. All pipettes were used on the day they were made. Patch clamp pipettes were backfilled with ICS (Table 2.22) and upon entering the ECS (Table 2.22) in the 'bath' mode, the pipette resistance ranged from 1.8-2.8 MΩ.

The electrophysiology 'rig' set-up is shown in Figure 3. Cells were observed using an upright microscope (Olympus) with a 40x/0.80W LUMPlan FL N objective (Olympus, Japan), and X-Cite Series 120 Q (Lumen Dynamics) light source at a wavelength of 470 nm was used to detect fluorescent cells expressing $Ca_V3.1$ channel. A silver-chloride pellet was used as a grounding electrode in a petri dish with ECS, and a micromanipulator (Scientifica, UK) was used to move the head-stage (Scientifica, UK) holding a patch pipette. Data were acquired using Clampex 11.2 software using a MultiClamp 700B amplifier and Digidata 1550B (Axon Instruments, USA). MultiClamp 700B software was used for pipette offset, capacitance compensation and formation of the whole-cell configuration, and Clampex 11.2 software was used to record currents. A sampling rate of 30 kHz was used to accurately capture rapid changes in T-type currents, while a filtering frequency of 10 kHz was used to effectively remove high-frequency noise, ensuring a clear and accurate recording of T-type currents.

Table 2.19 Solutions used for whole-cell patch clamp electrophysiology.

Intracellular solution (ICS)		Extracellular solution (ECS)	
Component	**Final concentration (mM)**	**Component**	**Final concentration (mM)**
CsCl	135	$BaCl_2$	10
EGTA	10	$(C_2H_5)_4N^+Cl^-$	130
Mg-ATP	4	HEPES	10
Na_3GTP	0.3	-	-
HEPES	10	-	-

Solution pH was adjusted to 7.3 (ICS) and 7.4 (ECS) with CsOH. Freezing-point depression test (The Advanced™ Micro Osmometer, model 3300) was used to measure and obtain the correct osmolarity (ICS ~300mOsm, ECS ~300-310mOsm). Solutions were stored at -20°C (ICS) and 4°C (ECS). **ICS:** CsCl blocks K+ currents, EGTA stabilises intracellular concentration of free Ca^{2+} ions, Mg-ATP provides energy for the Na^+/K^+ ATPase that maintains sodium-potassium gradients across the membrane. **ECS:** $BaCl_2$ is a charge carrier that passes through VGCCs and produces larger currents compared to Ca^{2+}, $(C_2H_5)_4N^+Cl^-$ (TEA-Cl) blocks voltage-gated K^+ channels. HEPES maintains physiological pH.

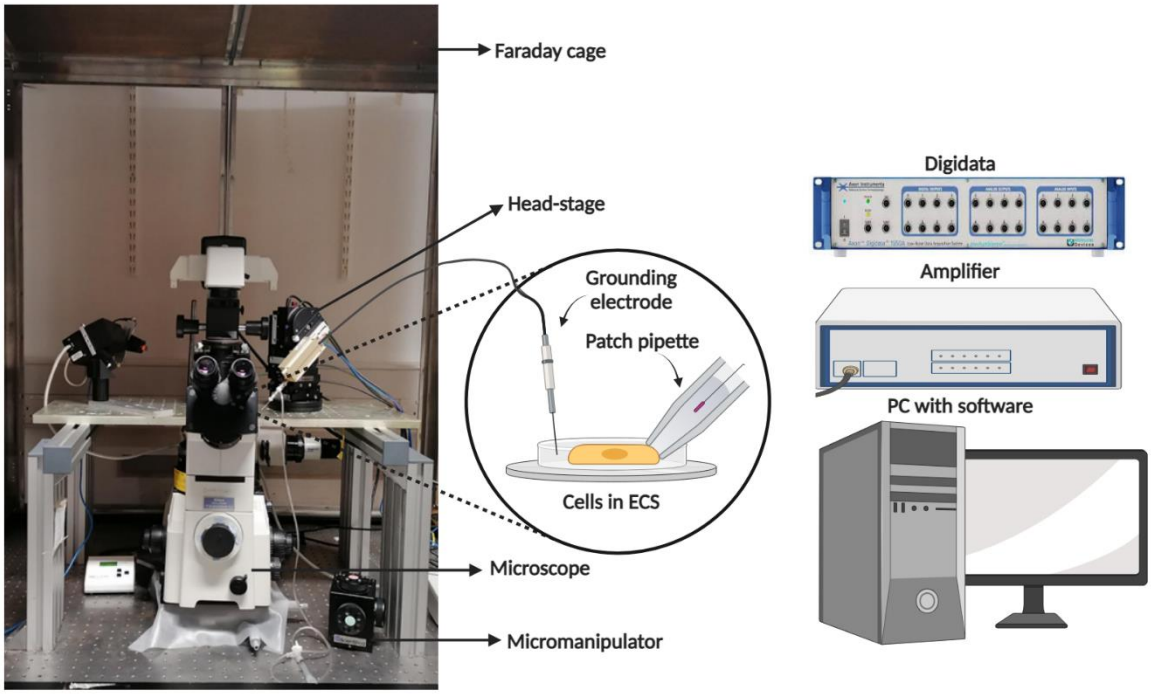

Figure 2.5 Electrophysiology rig set-up. (Made in Biorender.com).

Briefly, cells were transfected as described in section 2.1.5 and allowed to grow for 48 h. 30-60 min before experiments, cells were detached (section 2.1.3), plated on poly-D-lysine coated coverslips, and incubated at 37°C, 5% CO_2, for 30-60 min to allow cells to settle and attach while remaining rounded. Cells were then kept in culture medium at room temperature for the duration of the experiment. Whole-cell voltage clamp electrophysiology was performed at room temperature. Cells on coverslip were placed in an ECS bath and used for recording for no longer than 1 h. Only cells with fluorescent signal as a marker for successful transfection of $Ca_V3.1$ Ca^{2+} channel were recorded from. Before lowering a pre-filled pipette into ECS, slight positive pressure was applied (~0.2 ml air) to stop any debris from entering the pipette. Whilst in the 'bath' mode (command holding voltage 0 mV), the pipette was lowered into ECS and used to approach a cell until a 'dimple' in the cell membrane was observed. At this point, positive pressure was released, and slight negative pressure was applied. The mode was changed to 'patch' (command holding voltage -70 mV), allowing the establishment of a high-resistance seal ('giga-seal') between the pipette and cell. Once a stable giga-seal was established, more negative pressure was applied to 'break in' and establish a whole-cell configuration. Using MultiClamp 700B the mode was changed to 'whole cell' and capacitance compensation was adjusted using the 'auto' function. A voltage clamp recording was taken using appropriate protocols (detailed in Chapter 4). Data were collected from at least three separate transfections. R_s was compensated for during seal formation with no additional correction performed during recording.

2.5.4 Whole-cell voltage clamp: Data analysis

Leak-subtracted (P/4 leak subtraction, opposite to waveform) voltage-clamp data were analysed in Clampfit11.2. Maximal current amplitudes were measured for each voltage step and normalised to cell capacitance (pF), resulting in current-voltage-capacitance data (pA/pF). These data were fitted with a modified Boltzmann equation, as follows:

$$\mathbf{I = G_{max}\,(V - V_{rev}) \,/\, [1 + exp\,[-(V - V_{1/2}) \,/\, \mathit{k}]]}$$

G_{max} is the maximal conductance (nS/pF), V is voltage, V_{rev} is reversal potential, $V_{1/2}$ is the midpoint of activation or the voltage at which 50% of the channels are open, and *k* is the slope factor (Stephens *et al*., 2000).

Following curve fitting with Boltzmann equation, current-voltage-capacitance (pA/pF), G_{max}, V_{rev}, $V_{1/2}$, and slope factor *k* data were checked for normal distribution using Shapiro-Wilks

normality test. Normally distributed data were analysed using two-way ANOVA with Bonferroni *post hoc* test or two-tailed unpaired Student's *t* test as appropriate and as stated in text. If data was not normally distributed, non-parametric tests (e.g. Kruskal-Wallis and Welch's test) could be used.

All data were shown as mean ± standard error of the mean (SEM), and only data with coefficient of determination (R^2) > 0.9 were used. Data outside two standard deviations (SD) were considered outliers and were excluded from the analysis.

2.6 Bioinformatics and statistics

2.6.1 Primer design for PCR

All primers were designed manually, using Primer3, Clustal Omega and Mendelgen.com software programs/websites, using plasmid DNA constructs as templates. Where possible, primers were designed based on the following criteria – 18-21 bases long, GC content 40-60%, GC clamp, no runs of same base, no secondary structure, no primer dimer.

2.6.2 Statistical analysis

GraphPad Prism was used for statistical analysis. Raw data was analysed using an appropriate statistical test (stated in text or figure legend) and graphs were drawn with mean and SEM. SEM was used to indicate the precision/reliability of the sample mean, as opposed to SD which would show the variability of individual data points around the mean of a dataset. $p < 0.05$ was considered significant throughout and values of $p < 0.01$, $p < 0.005$, and $p < 0.001$ are specified where appropriate.

All data were checked for normal distribution using Shapiro-Wilks normality test. Normally distributed data were analysed using two-tailed unpaired Student's *t* test (two groups, one variable), two-way ANOVA (two groups, two variables), or one-way ANOVA (three or more groups, one variable). Data that were not normally distributed were analysed using non-parametric tests, including Kruskal-Wallis test (three or more groups, one variable) and Welch's test (two groups, unequal group sample sizes).

3. THE ROLE OF MIDAS MOTIF IN EXPRESSION AND TRAFFICKING OF CACHD1 PROTEIN IN A HETEROLOGOUS EXPRESSION SYSTEM

3.1 Introduction

The MIDAS motif is a conserved structural motif found in several transmembrane proteins involved in cell adhesion and signalling. These proteins include, but are not limited to integrins (Brown *et al*., 2018) and cadherins (Higgins *et al*., 2000), where the MIDAS motif coordinates divalent cations like magnesium (Mg^{2+}), calcium (Ca^{2+}), and manganese (Mn^{2+}), playing a crucial role in ligand recognition and binding (Valdramidou *et al*., 2008; Zhang and Chen, 2012).

Of particular interest to this project are the α2δ subunits, which are well-known modulators of HVA VGCCs, and contain a fully conserved MIDAS motif (DxSxS) within their VWA domain (Cantí *et al*., 2005). In α2δ subunits, the MIDAS motif is involved in protein-protein interactions essential for HVA VGCCs regulation. CACHD1 was identified as a member of the α2δ family by Whittaker and Hynes (2002) using bioinformatics approach, leading to identification of CACHD1 as a modulator of Ca_V3 LVA VGCCs by Cottrell *et al*. (2018). Similarly to α2δ subunits, CACHD1 also contains a MIDAS motif within its VWA domain; however, unlike the fully conserved MIDAS motif observed in α2δ subunits, CACHD1 contains a variant MIDAS motif (D^{234}xGxS), where the second key serine residue in α2δ subunits is replaced by glycine in CACHD1 (Cottrell *et al*., 2018; UniProt, Q5VU97). While a fully conserved α2δ-1 MIDAS motif is not required for metal ion binding (Whittaker and Hynes, 2002), it is functionally important for HVA VGCCs trafficking and synaptic function (Cantí *et al*., 2005; Hoppa *et al*., 2012; Cassidy *et al*., 2014). Previous studies showed that mutations in the three key residues of α2δ-1 MIDAS motif, either through single amino acid substitution (D112A) or mutagenesis of all three key residues (D112A, G114A, S116A, termed AAA), resulted in disruption of α2δ-1-$Ca_V2.2$ interaction (Dahimene *et al*., 2018) and impairment of α2δ-1 trafficking to cell surface (Cassidy *et al*., 2014).

Given the role of MIDAS motif in α2δ subunit trafficking and interaction with HVA VGCCs, an in-depth investigation into the role of the variant MIDAS motif in CACHD1 is important. In this chapter, the effects of MIDAS motif key residue mutagenesis on CACHD1 protein expression and trafficking in a heterologous expression system are outlined.

3.2 Objective

CACHD1 is considered a member of the α2δ protein family (Cottrell *et al*., 2018), and it is therefore of importance to determine the functional effects of the key residues in the variant CACHD1 MIDAS motif (D^{234}xGxS). Previous studies showed that mutations in the MIDAS motif of α2δ subunit, in particular the three key residues (DxSxS), resulted in reduced trafficking of the subunits to cell surface (Cassidy *et al*., 2014). Due to the structural similarities of α2δ and CACHD1, it is therefore of interest to mutate the three key residues in the variant MIDAS motif (DxGxS) of CACHD1 (Cottrell *et al*., 2018).

- The first objective of this chapter was to characterise CACHD1 wild-type expression and localisation in a heterologous expression system.

- The second objective was to investigate the effects of mutating the three key residues in MIDAS motif on the expression and localisation of CACHD1 in a heterologous expression system.

Hypothesis: Mutagenesis of the three key residues, D^{234}xGxS, within the variant MIDAS motif of CACHD1 will disrupt CACHD1 trafficking to cell surface.

This hypothesis is based on the results shown for α2δ subunits where mutagenesis of the key residues in MIDAS motif of α2δ subunits to alanine resulted in reduced cell surface expression of α2δ-1 (Cassidy *et al*., 2014), and on preliminary data produced by Ince (MSc thesis, 2018).

3.3 Experimental approach

3.3.1 Optimisation of protein expression and detection

Protein expression and detection methods, including transfection, western blot and immunocytochemistry used throughout this project required several optimisation steps to determine optimal experimental conditions.

To obtain efficient expression of Myc-CACHD1 proteins, transient transfection was performed as described in section 2.1.5. Several conditions were simultaneously compared in a 12-well plate, including varying DNA amounts (1-5 μg), DNA:PEI ratios (1:2, 1:3, 1:4), and cell densities (5-10x10^5 cells/well; 12-well plate). For the purposes of this project, the following transfection conditions were determined as optimal: 3 μg (12-well plate) and 6 μg (6-well plate) of DNA, 1:3 DNA:PEI ratio, and 6x10^5 (12-well plate) and 2x10^5 (6-well plate) cells/well cell densities.

To optimise western blot conditions, the binding of primary and secondary antibodies, as well as chemiluminescence of secondary HRP-conjugated antibodies were tested using a dot blot. Briefly, nitrocellulose membrane was spotted with 2 μl of primary antibodies and allowed to air dry. The membrane was then blocked with 5% milk, incubated with secondary antibodies (1:10000), and imaged. The dot blot results (Figure 3.1) showed successful binding of primary and secondary antibodies, while also confirming the chemiluminescence of secondary antibodies. Next, the optimal antibody dilutions were determined by running 30 μg of protein samples on a SDS-PAGE gel and immunoblotting with different antibody dilutions. The following antibody dilutions were determined as optimal for the purposes of this project: rabbit anti-Myc 1:5000, mouse anti-HA 1:5000, rabbit anti-6-His 1:5000, mouse anti-β-actin 1:20000, mouse anti-TFR 1:1000.

To optimise immunocytochemistry conditions, different antibody dilutions (1:200 - 1:1000) were compared. For the purposes of this project, it was determined that the optimal dilutions for primary and secondary antibodies were 1:500 and 1:1000, respectively.

Figure 3.1 Dot blot analysis of primary and secondary antibody binding and chemiluminescence. 2 µl of rabbit anti-Myc, rabbit anti-6His, mouse anti-β-actin and mouse anti-TFR (transferrin receptor) were spotted on a nitrocellulose membrane and allowed to air dry. Blots were blocked for 1 h with 5% milk, followed by incubation with horseradish peroxidase (HRP)-linked secondary antibodies for 1 h at room temperature. Blots were then washed 6x 5 min with 1X PBST before imaging. **(A)** Incubation with donkey anti-rabbit HRP-linked secondary antibody showed successful binding of rabbit primary antibodies and donkey anti-rabbit secondary antibodies. **(B)** Incubation with donkey anti-mouse HRP-linked secondary antibody showed successful binding of mouse primary antibodies and donkey anti-mouse secondary antibodies. Chemiluminescence of both secondary antibodies was confirmed.

3.3.2 Characterisation of Myc-CACHD1 expression in a heterologous expression system

Human CACHD1 was previously N-terminally tagged by inserting a Myc tag (EQKLISEEDL) after the natural signal peptide and between the Ala^{35} and Glu^{36} residues by Ince (MSc thesis, 2018). The first step in the current study was the characterisation of expression and sub-cellular localisation of CACHD1 in the absence of $Ca_V3.1$ in HEK293 tsA201 cells.

HEK293T tsA201 cells were plated at a $2x10^6$ cells/well density in a 6-well plate and transiently transfected with 6 µg of pcDNA5/FRT-Myc-CACHD1-wt or pcDNA5/FRT (vector control) as described in section 2.1.5. Subsequently, transfected cells were seeded onto poly-D-lysine coated coverslips ($1x10^5$ cells/well, 12-well plate) for immunocytochemistry, while the remaining cells were allowed to grow in the 6-well plate for western blot analysis. Cells were cultured at 37°C, 5% CO_2, for 48 h before analysis. To investigate sub-cellular localisation, cells on coverslips were labelled live and fixed (section 2.3.4 and 2.3.5) with rabbit and mouse anti-Myc antibodies, respectively. Live cell labelling allowed the detection of proteins located exclusively at the cell surface. To confirm molecular mass of CACHD1 protein, transfected cells were lysed and extracted proteins were analysed by western blotting as described in section 2.2.11, using rabbit anti-Myc (1:5000) and mouse anti-β-actin (1:20000) antibodies. Cell surface expression of CACHD1 was further investigated by the cell surface biotinylation method as detailed in section 2.2.4.

3.3.3 Mutagenesis of the variant MIDAS motif in Myc-CACHD1

Considering the structural similarities between α2δ and CACHD1, including the presence of a MIDAS motif within the VWA domains of both proteins, it is of interest to investigate the effects of mutating the key residues of the variant MIDAS motif in CACHD1 on its expression and trafficking.

In a preliminary study conducted by Ince (MSc thesis, 2018), two Myc-CACHD1 MIDAS motif mutants were generated; the specific amino acid mutagenesis is illustrated in Figure 3.2. The first CACHD1 MIDAS mutant was created by mutating the three key residues (aspartic acid, glycine, serine) to alanine (D234A, G236A, S238A; AxAxA, termed AAA mutation/mutant), containing the same mutation that was previously studied in α2δ subunits. Interestingly, the AAA mutation showed varied effects in different α2δ subunits, and while it reduced cell surface expression in α2δ-1 (Cassidy *et al*., 2014), it had no significant effects on the total protein expression or trafficking of α2δ-2 to cell surface (Cantí *et al*., 2005). The second

CACHD1 MIDAS mutant was generated by mutating a single residue, glycine, to serine (G236S), thereby generating a CACHD1 protein containing a MIDAS motif with three key residues identical to those found in α2δ subunits.

A two-step Q5 DNA polymerase PCR approach was used to generate both CACHD1 MIDAS mutants. Initially, forward primers containing the mutations were used in the first PCR reaction, generating PCR fragments that were then used as megaprimers in the subsequent PCR reaction. The PCR products were digested with *Nhe* I + *Cla* I restriction enzymes, and pcDNA5/FRT-Myc-CACHD1 construct was digested with *Not* I + *Cla* I and with *Nhe* I + *Not* I restriction enzymes. A 3-way ligation was then used to ligate all fragments together, resulting in the final constructs pcDNA5/FRT-Myc-CACHD1-AAA and pcDNA5/FRT-Myc-CACHD1-G236S.

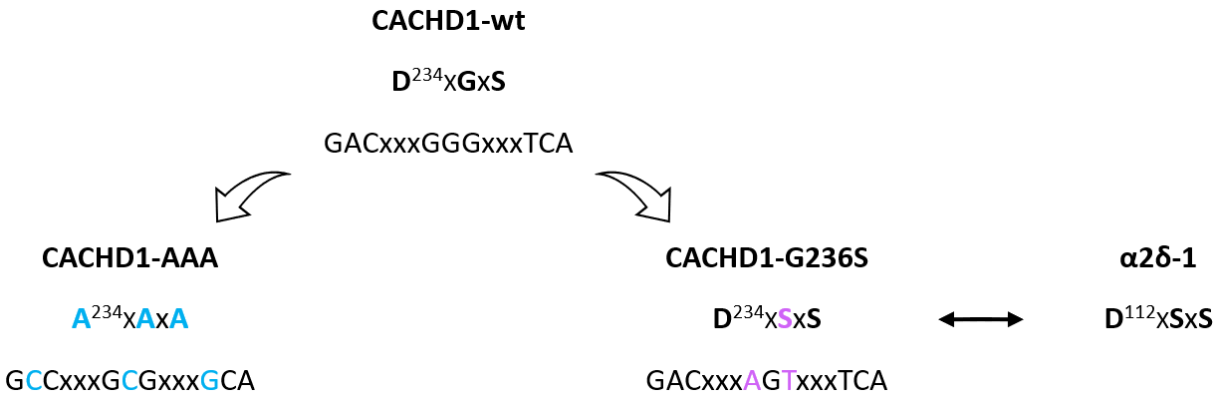

Figure 3.2 Amino acid modifications of the key MIDAS motif residues in CACHD1 by site-directed mutagenesis. Q5 DNA polymerase PCR method was used to generate two CACHD1 MIDAS motif mutants. For the first mutant termed CACHD1-AAA, the three key residues within the MIDAS motif were mutated to alanine (D234A, G236A, S238A), resulting in a CACHD1 mutant containing a mutation previously studied in α2δ subunits. The second mutant termed CACHD1-G236S was generated by mutagenesis of single residue (G^{236}) to serine, resulting in a CACHD1 mutant containing MIDAS motif with key residues identical to those found in α2δ MIDAS motifs (DxSxS).

3.3.4 Characterisation of MIDAS motif mutants in a transient expression system

To investigate the effects of MIDAS motif mutagenesis on the expression, sub-cellular localisation, and molecular mass of Myc-tagged CACHD1-wt, CACHD1-AAA and CACHD1-G236S, several techniques, including western blotting, densitometry, and immunocytochemistry were employed.

HEK293T tsA201 cells were plated, transiently transfected with pcDNA5/FRT-Myc-CACHD1-wt, pcDNA5/FRT-Myc-CACHD1-AAA, pcDNA5/FRT-Myc-CACHD1-G236S or pcDNA5/FRT (vector control), and expression and sub-cellular localisation were analysed by western blotting and immunocytochemistry as described in section 3.3.2.

3.3.5 Analysis of CACHD1 expression levels in heterologous expression systems

To determine any effects of MIDAS motif mutagenesis on CACHD1 expression levels, densitometry analysis of appropriate immunoblots was conducted as described in section 2.2.13. For each sample lane, the signal of CACHD1 protein band was normalised to the corresponding β-actin (loading control) protein band signal, resulting in a sample/control ratio. This process was repeated for at least two separate images of the same blot captured at 10-60 s intervals (technical repeats), and an average of the sample/control ratios was obtained, representing one biological repeat for each sample (e.g. Myc-CACHD1-wt, Myc-CACHD1-AAA and Myc-CACHD1-G236S). The raw data were statistically analysed by one-way ANOVA with Tukey's *post hoc* test. The data were then normalised to CACHD1-wt, where CACHD1-wt expression was considered as 100%, and representative graphs with mean $\pm$ SEM were plotted using GraphPad Prism. Significant changes were indicated at $p < 0.05$.

Upon statistical analysis of densitometry data for transiently expressed CACHD1 MIDAS motif mutants, notable differences in expression levels between CACHD1-wt and both MIDAS motif mutants were observed. The underlying cause for this observation remains unclear; however, the process of transient transfection poses number of potential challenges, and any results should be interpreted with caution. The inherent variability of transient transfection can affect the consistency and reliability of protein expression, potentially confounding the results. To address any challenges related to transient transfection efficiency, stable cell lines were generated to provide a more robust and consistent system for studying protein expression levels. Stable cell lines expressing Myc-CACHD1-wt, Myc-CACHD1-AAA and Myc-CACHD1-G236S were generated using the Flp-In™ system, following the protocol detailed in section

2.1.6. Co-transfection of pOG44 and pcDNA5/FRT-Myc-CACHD1-wt, pcDNA5/FRT-Myc-CACHD1-AAA or pcDNA5/FRT-Myc-CACHD1-G236S into HEK293 Flp-In™ T-REx™ cells facilitated Flp recombinase-mediated integration of the CACHD1 genes into the genome of HEK293 Flp-In™ T-REx™ cells, allowing selection of positive clones with 100 µg/ml of hygromycin B in DMEM 10% FBS cell culture medium. The resulting stable cell lines were maintained with 50 µg/ml of hygromycin B. Subsequently, the analysis process outlined for transiently transfected cells was repeated for stably expressing cell lines to further understand the effects of MIDAS motif mutagenesis on CACHD1 expression levels.

3.4 Results

3.4.1 Myc-CACHD1 is expressed in transiently transfected HEK293 tsA201 cells

Sub-cellular localisation of Myc-tagged CACHD1 in transiently transfected HEK293 tsA201 cells was determined by immunocytochemistry, using rabbit anti-Myc antibody for live cell labelling (section 2.3.4), and mouse anti-Myc antibody for fixed cell labelling (section 2.3.5). Live cell labelling allowed the detection of proteins located exclusively at the cell surface, while fixed cell labelling allowed the visualisation of protein expression throughout the cell. As shown in Figure 3.3A, no immunoreactive signals were detected for vector control. Immunoreactive Myc-CACHD1 was expressed on cell surface, with some expression in intracellular vesicles. It is important to note that visual identification of staining in intracellular compartments can be subjective and does not provide a quantitative measurement. The fluorescence intensity in different cellular compartments could be quantified using an image analysis software.

Western blot analysis was used to determine the molecular mass of Myc-tagged CACHD1 protein expressed in transiently transfected HEK293 tsA201 cells. In Figure 3.3B, immunolabelling with rabbit anti-Myc antibody showed immunoreactive Myc-CACHD1-wt present in cell lysates. The expected molecular mass of CACHD1 was 142 kDa (UniProt, Q5VU97), and Myc-CACHD1-wt was detected at ~150-170 kDa, suggesting that CACHD1 might undergo post-translational modifications, such as glycosylation. CACHD1 is known to have up to seven glycosylation sites (Dahimene *et al.*, 2018), therefore the 150 kDa protein band could be un-glycosylated CACHD1, while the 170 kDa protein band could be fully glycosylated CACHD1 protein.

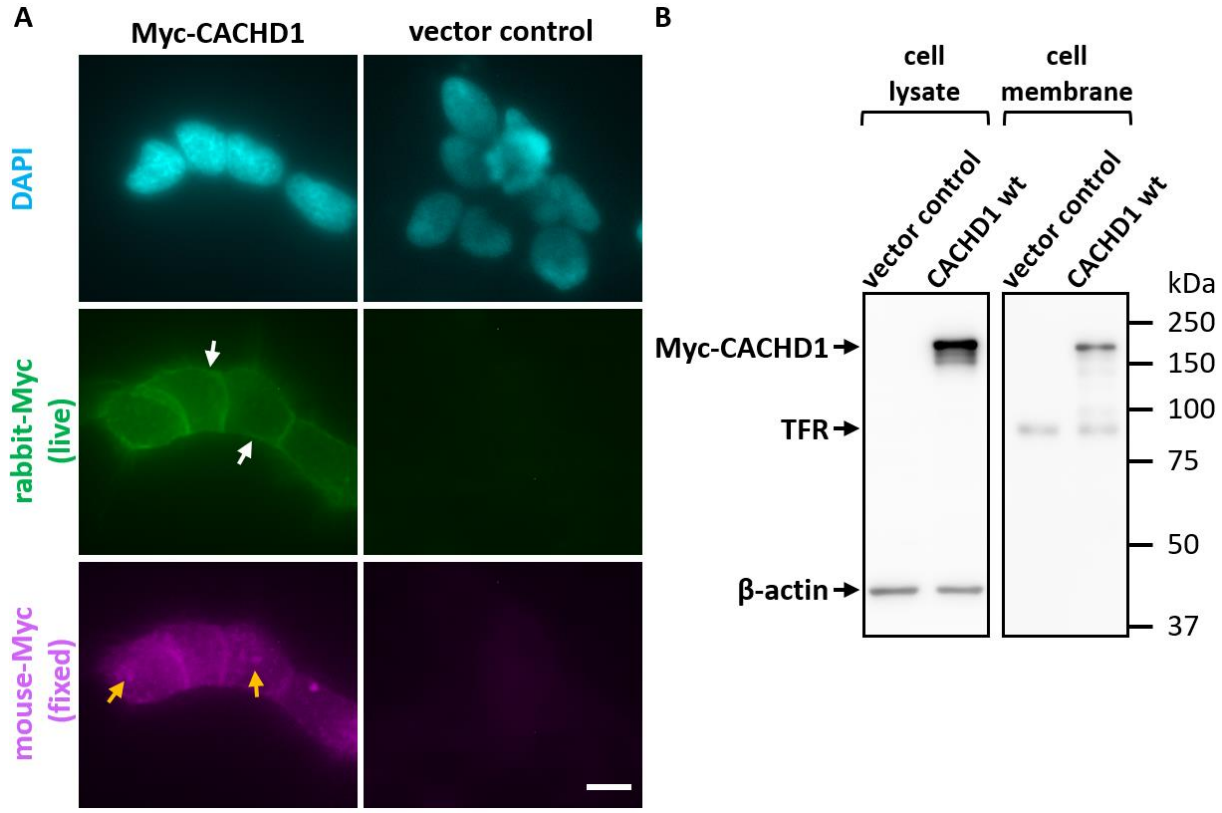

Figure 3.3 Characterisation of Myc-CACHD1-wt expression and sub-cellular localisation using western blotting and ICC. HEK293T tsA201 cells were transiently transfected with Myc-CACHD1-wt or empty vector (control), and expression was analysed by western blotting and ICC. **(A)** Transfected cells were labelled live with rabbit anti-Myc antibody, fixed with 4% PFA, and labelled with mouse anti-Myc antibody. Myc-CACHD1-wt was detected with rabbit and mouse anti-Myc antibodies, showing some expression in intracellular compartments (yellow arrows), but mostly on cell surface (white arrows). **(B)** Cells were incubated with EZ-LinkTM sulfo-NHS-SS-Biotin (0.3 mg/ml in DPBS+CM) at 4°C to label cell surface proteins. Cells were then lysed with RIPA buffer and whole-cell lysate samples were collected. Biotinylated proteins were captured by NeutrAvidin agarose beads at 4°C overnight. Proteins were then separated by SDS-PAGE and blots were incubated with rabbit anti-Myc antibody. Immunoreactive Myc-CACHD1 was detected in cells transfected with Myc-CACHD1 only, confirming antibody specificity. Myc-CACHD1-wt was detected at 150-170 kDa in whole-cell lysates, and at approx. 170 kDa in membrane samples. Signals for β-actin and TFR (transferrin receptor; loading controls) were present in both cell types. (Epifluorescence microscopy; Scale bar 10 µm, n=3).

3.4.2 Amino acid substitution mutations in the MIDAS motif of CACHD1 protein affect CACHD1 protein expression levels in HEK293 cells

The effects of amino acid mutagenesis of three key residues in the MIDAS motif of CACHD1 were determined by western blotting and densitometry. Immunoreactive Myc-CACHD1-wt, Myc-CACHD1-AAA and Myc-CACHD1-G236S were detected at 150-170 kDa by rabbit anti-Myc antibody (Figure 3.4A and 3.5A), showing that the AAA and G236S mutations did not change the molecular mass of CACHD1 protein. In transiently transfected cells, the total protein expression levels of the Myc-CACHD1-AAA and Myc-CACHD1-G236S mutants were significantly lower in comparison to Myc-CACHD1-wt, where the protein levels of Myc-CACHD1-AAA and Myc-CACHD1-G236S mutants were reduced to 7.1±1.1% and 13.6±4.1% (mean±SEM), respectively (Figure 3.4B). In stable cell lines, while the Myc-CACHD1-G236S mutant was expressed at similar levels compared to Myc-CACHD1-wt, 93.3±4.2% (mean±SEM), the Myc-CACHD1-AAA mutant remained significantly reduced at 21.6±6.8% and 22.3±6.2% (mean±SEM) compared to Myc-CACHD1-wt and Myc-CAHD1-G236S mutant, respectively (Figure 3.5B). The exact reason for the observed difference in Myc-CACHD1-G236S expression levels in transiently and stably expressing HEK293 cells is unknown; however, as highlighted in section 3.3.5, it could be due to many different factors, including transfection efficiency, cell confluency, integration into cells, and protein stability.

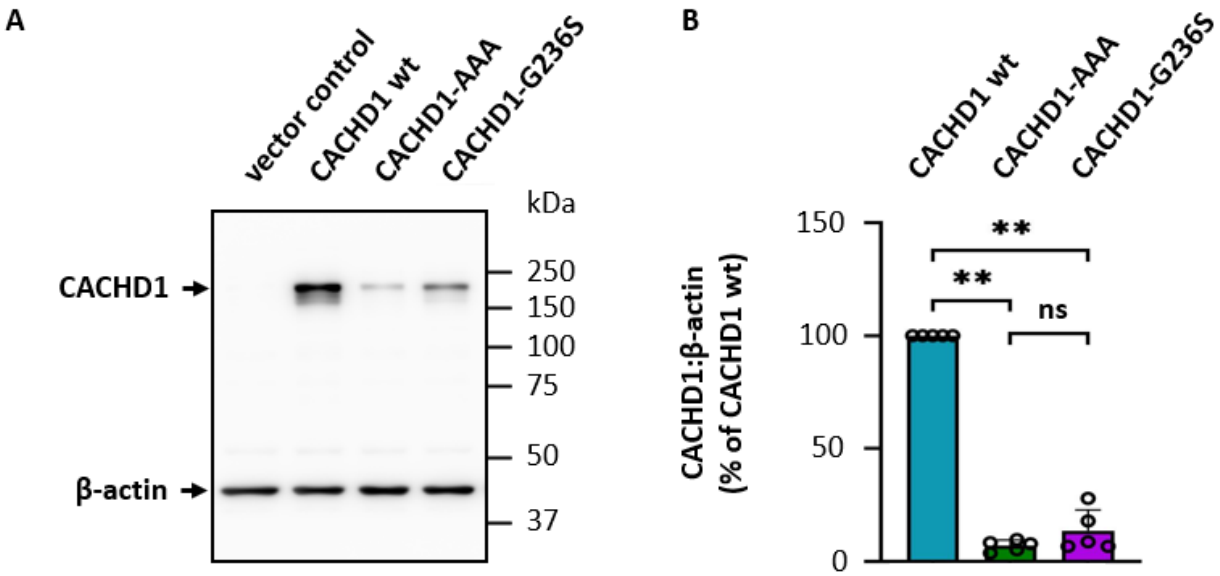

Figure 3.4 Analysis of expression of Myc-CACHD1-wt, Myc-CACHD1-AAA and Myc-CACHD1-G236S in transiently transfected HEK293T tsA201 cells by western blotting. (A) Expression of Myc-CACHD1-wt, Myc-CACHD1-AAA and Myc-CACHD1-G236S in transiently transfected HEK293T tsA201 cells was determined by western blotting. Cells were lysed, proteins separated by SDS-PAGE and blots incubated with rabbit anti-Myc and mouse anti-β-actin (loading control) antibodies. Immunoreactive Myc-CACHD1-wt, Myc-CACHD1-AAA and Myc-CACHD1-G236S proteins were detected at 150-170kDa, which corresponded with the predicted size of CACHD1 protein. Signals for β-actin were present in all cell types. **(B)** Densitometry was performed on viable blots and raw data was analysed by one-way ANOVA with Tukey's *post hoc* test. Results showed that Myc-CACHD1-AAA and Myc-CACHD1-G236S were expressed at significantly lower levels compared to Myc-CACHD1-wt, 7.1±1.1% and 13.6±4.1%, respectively (mean±SEM). (n=5, $^{**}p < 0.01$, ns – non-significant).

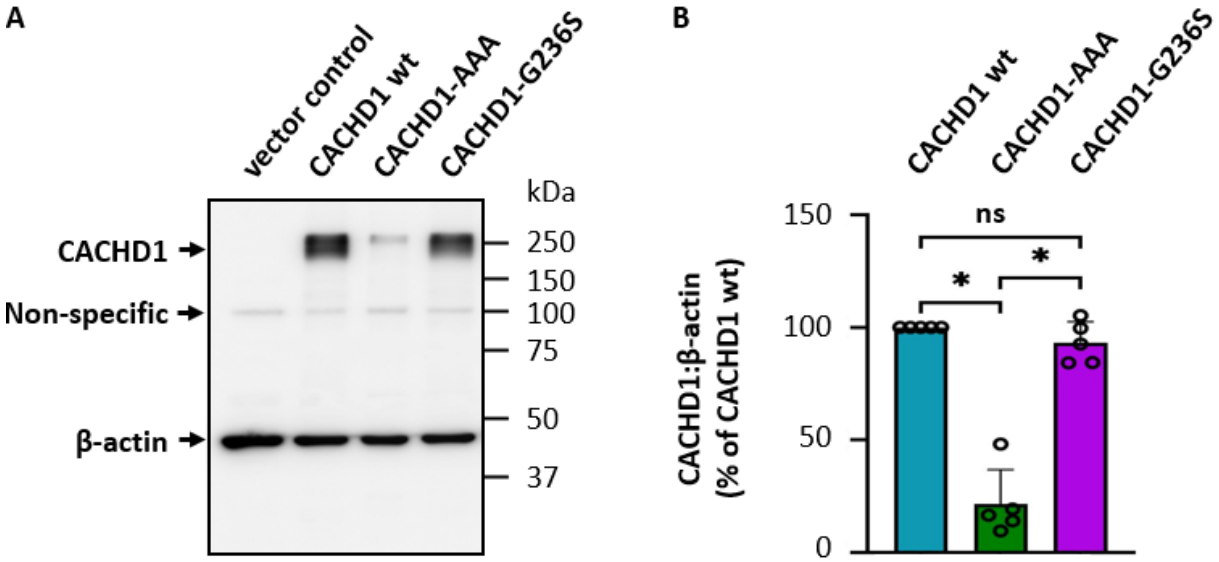

Figure 3.5 Analysis of expression of Myc-CACHD1-wt, Myc-CACHD1-AAA and Myc-CACHD1-G236S in stably expressing HEK293 cells by western blotting. (A) Expression of Myc-CACHD1-wt, Myc-CACHD1-AAA and Myc-CACHD1-G236S in stable HEK293 cells was determined by western blotting. Cells were lysed, proteins separated by SDS-PAGE and blots incubated with rabbit anti-Myc and mouse anti-β-actin (loading control) antibodies. Immunoreactive Myc-CACHD1-wt, Myc-CACHD1-AAA and Myc-CACHD1-G236S proteins were detected at 150-170 kDa. Signals for β-actin were present in all cell types. **(B)** Densitometry was performed on viable blots and raw data was analysed by one-way ANOVA with Tukey's *post hoc* test. Results showed that Myc-CACHD1-AAA was consistently expressed at significantly lower levels in comparison to Myc-CACHD1-wt (21.3±6.8%, mean±SEM) and Myc-CACHD1-G236S (22.3±6.2%, mean±SEM), while Myc-CACHD1-G236S was expressed at similar levels to Myc-CACHD1-wt (93.3±4.2%, mean±SEM). (n=5, *p <0.05, ns – non-significant).

3.4.3 The AAA mutation in the MIDAS motif of CACHD1 protein abolishes CACHD1 protein trafficking to cell surface in stable HEK293 cells

Sub-cellular localisation of Myc-tagged CACHD1-wt and MIDAS mutants was determined by immunocytochemistry, using live and fixed cell labelling with rabbit and mouse anti-Myc antibodies, respectively (Figure 3.6). Live cell labelling showed immunoreactive Myc-CACHD1-wt and Myc-CACHD1-G236S mutant expressed on cell surface, while the Myc-CACHD1-AAA mutant could not be detected on cell surface, suggesting that the AAA mutation affected trafficking of the final protein. Fixed cell labelling showed immunoreactive Myc-CACHD1-wt, Myc-CACHD1-G236S and Myc-CACHD1-AAA expressed in intracellular compartments. The same expression pattern was observed in transiently (data not shown) and stably expressing HEK293 cells.

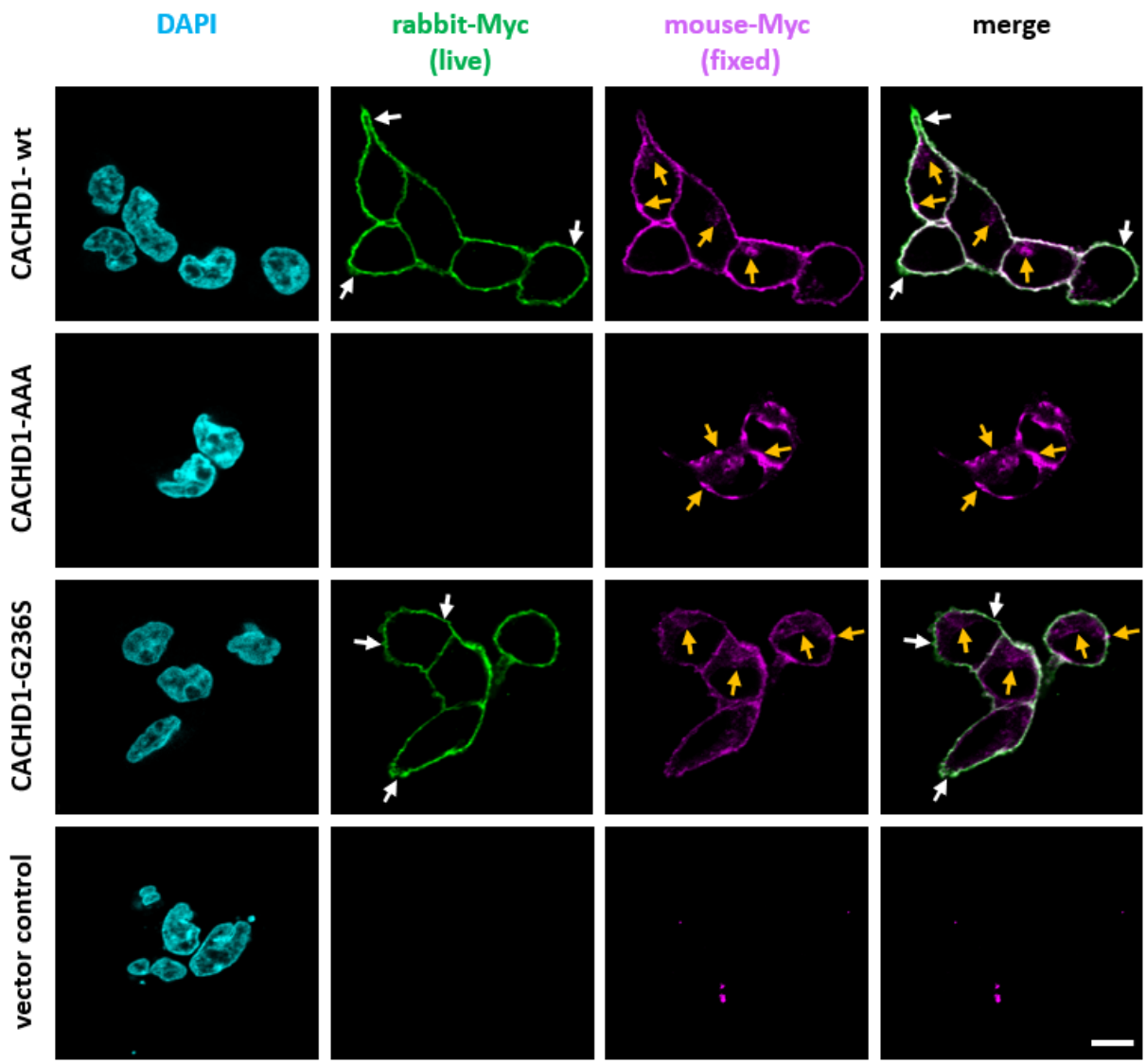

Figure 3.6 Analysis of expression and sub-cellular localisation of Myc-CACHD1-wt, Myc-CACHD1-AAA and Myc-CACHD1-G236S in stable HEK293 cells by immunofluorescence. Stable HEK293 cells expressing Myc-tagged CACHD1-wt, CACHD1-AAA and CACHD1-G236S were labelled live with rabbit anti-Myc antibody, fixed with 4% PFA, and labelled with mouse anti-Myc antibody. Myc-CACHD1-wt and Myc-CACHD1-G236S were detected at the cell surface (white arrows) by live cell staining, and in intracellular compartments (yellow arrows) by staining of permeabilised cells. Myc-CACHD1-AAA could not be detected at the cell surface and was only detected in intracellular compartments. (Scale bar 10 µm, n=5).

3.5 Discussion

α2δ subunits are well-known and characterised modulators of HVA VGCCs. Previous studies have shown the importance of an intact MIDAS motif within the VWA domain of α2δ subunits in their expression and trafficking in heterologous expression systems (Cantí *et al*., 2005; Hoppa *et al*., 2012; Cassidy *et al*., 2014). The classification of CACHD1 protein as a member of the α2δ protein family (Whittaker and Hynes, 2002), its characterisation as a modulator of LVA VGCCs, and structural similarities between α2δ subunits and CACHD1 (Cottrell *et al*., 2018) underscore the significance of understanding whether the MIDAS motif of CACHD1 protein functions similarly to the MIDAS motif present in α2δ subunits. It is important to note that the CACHD1 protein contains a variant MIDAS motif (DxGxS), where the second key residue is glycine instead of the serine typically observed in α2δ subunits (DxSxS; Whittaker and Hynes, 2002). This chapter investigated the variant MIDAS motif by mutating key residues within the motif, aiming to understand its role in CACHD1 expression and localisation in heterologous expression systems. It is important to note that, here, CACHD1 was studied in the absence of $Ca_V3.1$ expression.

3.5.1 Characterisation of CACHD1 protein expression in a heterologous expression system

As a first step, the expression and sub-cellular localisation of Myc-tagged CACHD1 were characterised in a transient expression system. Through a series of experiments, it was shown that Myc-CACHD1 was successfully expressed in transiently transfected HEK293 tsA201 cells, showing localisation in intracellular compartments and at the cell membrane which corresponds with the findings reported by Ince (MSc thesis, 2018). Detection of CACHD1 at the cell membrane by live cell immunolabelling indicates that CACHD1 may interact with the extracellular environment and other membrane proteins (Chataigner *et al*., 2020). CACHD1, unlike α2δ subunits which are generally accepted to be GPI-anchored (Davies *et al*., 2010), is predicted to be a type-I transmembrane protein, and the sub-cellular localisation observed during the current study supports the classification of CACHD1 as a transmembrane protein.

Western blot analysis revealed that Myc-CACHD1 molecular mass ranged between ~150-170 kDa. The predicted molecular mass of CACHD1 is 142 kDa (UniProt, Q5VU97), therefore the varying molecular mass could indicate that CACHD1 undergoes post-translational modifications, in particular glycosylation, as CACHD1 was previously shown to have up to

seven glycosylation sites (Dahimene *et al*., 2018). The addition of sugar molecules to specific amino acid residues within the protein can increase its molecular mass by approx. 2.5 kDa per site (Kornfeld and Kornfeld, 1985); therefore, the presence of multiple protein bands could indicate differentially glycosylated forms of the CACHD1 protein, with the lower molecular mass protein band representing a non-glycosylated form of CACHD1, and the higher molecular mass protein bands representing partially or fully glycosylated forms of CACHD1. Additionally, the 170 kDa protein band appears to be notably stronger in intensity compared to the lower molecular mass protein bands, therefore indicating that fully glycosylated CACHD1 may be the most abundant form of CACHD1 in the samples collected from HEK293 tsA201 cells. Moreover, protein stability, protein folding, levels of glycosylation and cellular localisation can affect the half-life of a protein, resulting in faster protein turnover (synthesis ⇔ degradation) (Watanabe *et al*., 2004; Lee *et al*., 2023), which could also explain the detection of lower molecular mass CACHD1 proteins. Furthermore, cell surface biotinylation analysis showed that the 170 kDa protein band was the membrane associated CACHD1, consistent with the suggestion that a fully glycosylated form of CACHD1 is trafficked to cell surface where it interacts with the extracellular environment, including other proteins such as LVA VGCCs (Cottrell *et al*., 2018).

3.5.2 MIDAS motif within the VWA domain of CACHD1 is important for protein expression and trafficking

The preliminary study conducted by Ince (MSc thesis, 2018) explored the impact of amino acid substitution within the MIDAS motif on CACHD1 expression and trafficking in a transient expression system and showed that mutating the second key residue to serine had no effect on CACHD1 trafficking to cell membrane, but it significantly reduced the total CACHD1 protein expression levels. On the other hand, mutagenesis of all three key residues to alanine not only reduced total CACHD1 expression levels but also impaired trafficking to cell surface. This chapter aimed to confirm the results presented by Ince (MSc thesis, 2018) and deepen the understanding of the role of the variant MIDAS motif in CACHD1 protein.

CACHD1 is classified as a member of the α2δ protein family, therefore it is important to consider previous investigations into α2δ subunits and their MIDAS motif as a foundation for the current study. Amino acid substitutions in the key residues of α2δ MIDAS motif, in particular the AAA mutation where all three key residues (aspartic acid, serine, serine; DxSxS) were mutated to alanine (AxAxA), showed varied effects on different α2δ subunits. While the

AAA mutation reduced cell surface expression in α2δ-1 (Cassidy *et al*., 2014), it had no significant effects on the total protein expression or trafficking of α2δ-2 in tsA201 or Cos-7 cells (Cantí *et al*., 2005). Similarly to α2δ-1, the AAA mutation in CACHD1 impaired its trafficking and expression at the cell membrane. Furthermore, the AAA mutation significantly reduced total CACHD1 protein expression levels in both transiently and stably expressing HEK293 cells, corresponding with preliminary results reported by Ince (MSc thesis, 2018). The exact reasons for these observations remain unknown, but one could speculate that the mutagenesis of all three key residues causes conformational changes in CACHD1 protein structure, leading to protein misfolding. Protein misfolding could interrupt CACHD1 interaction with trafficking proteins, explaining why it was not detected at the cell membrane. Moreover, misfolded proteins are often recognised and degraded by intracellular mechanisms to prevent accumulation of potentially toxic protein aggregates, which could explain the low expression levels of CACHD1-AAA. Furthermore, the AAA mutation could disrupt CACHD1 interaction with other cellular proteins that may be required for its trafficking, explaining the disrupted trafficking of CACHD1 to cell surface.

It is important to note that the second key MIDAS residue of CACHD1, glycine (G^{236}), is not fully conserved in comparison to the typical MIDAS motif containing serine, which is present in approx. 46% of the proteins that have a MIDAS motif within their VWA domain (Whittaker and Hynes, 2002). However, it is yet to be established whether the key residues of the variant MIDAS motif found in CACHD1, DxGxS, are equally as important for the functionality of the motif as in other proteins, especially α2δ subunits. To further understand the role of the glycine residue, it was mutated to serine, generating a CACHD1 protein with a fully conserved MIDAS motif as found in α2δ subunits. The G236S mutation had no observable effects on the trafficking and cell surface expression of CACHD1; however, similarly to the AAA mutation, it significantly reduced total CACHD1 protein levels in transiently expressing HEK293 cells, corresponding with the findings shown by Ince (MSc thesis, 2018). Interestingly, in stably expressing HEK293 cells, the G236S mutation had no significant effect on total CACHD1 protein levels and was comparable to wild-type CACHD1. The exact reason for the difference in expression levels between transiently and stably expressing cells remains unknown; however, many different factors could be the cause, including DNA preparation, transfection efficiency, cell confluency, integration into cells, and protein stability. In transiently transfected cells, the integration and folding of the G236S mutant protein could be affected,

resulting in a misfolded protein that is degraded by intracellular degradation mechanisms and could pose as a possible explanation for low levels of CACHD1-G236S detected in transiently expressing HEK293 cells.

Previous studies investigating the MIDAS motif in other proteins showed that the key MIDAS residues may bind Ca^{2+}, Mn^{2+} or Mg^{2+} ions, causing conformational changes within the VWA domain and subsequently promote protein function. Cantí *et al*. (2005) hypothesised that, in α2δ subunits, the key MIDAS motif residues bind Ca^{2+}/Mg^{2+} when the concentration of divalent cations is high in the endoplasmic reticulum, causing conformational changes in α2δ that allow correct folding and subsequent trafficking of the $Ca_V\alpha1$ complex to cell membrane. Interestingly, the mutagenesis of all three key residues to alanine (DxSxS ⇔ AxAxA) showed no effect on α2δ-2 protein folding or trafficking when expressed alone; however, it reduced cell surface expression of its complexes with the pore-forming $Ca_V\alpha1$ and $Ca_V2.2$ subunits (Cantí *et al*., 2005). In integrin β1 subunit, mutation of the first key residue, aspartic acid (D^{130}), to alanine within the MIDAS motif disrupted Mn^{2+} and Mg^{2+} ion binding, leading to inhibition of conformational changes within the VWA domain and subsequent ligand binding (Mould *et al*., 2002; Valdramidou *et al*., 2008). Furthermore, studies showed that an intact MIDAS motif is required for correct folding of α4β7 integrins and the binding of Mn^{2+} and Mg^{2+} ions (de Château *et al*., 2001; Chen *et al*., 2003; Yu *et al*., 2012). These studies support the theory that the loss of membrane expression in CACHD1-AAA mutant may be due to the inhibition of metal ion binding to MIDAS motif residues and interruption of subsequent conformational changes that stabilise the protein and promote its cell surface expression. In contrast, the mutagenesis of second key residue to serine (G236S) did not appear to affect the trafficking of CACHD1, suggesting that CACHD1 can function in a similar way whether it contains a variant or a fully conserved MIDAS motif within its VWA domain. This theory is further supported by the results reported by Cantí *et al*. (2005) showing the serine residue in α2δ subunits to be important for metal ion binding that leads to correct protein processing.

3.5.3 Conclusion

The results presented in this chapter emphasise the criticality of key residues within the MIDAS motif of CACHD1. Mutagenesis of all three key residues to alanine disrupted protein trafficking and caused pronounced decrease in expression levels. Conversely, mutating only the second key residue to serine had minimal impact on total protein expression and trafficking to the cell surface, suggesting that the variant MIDAS motif in CACHD1 functions

similarly to the fully conserved MIDAS motif found in α2δ subunits. Although the G236S mutation showed no significant effects on CACHD1 trafficking and expression, it raises the question about its effects on the modulation of Ca_V3 VGCCs by CACHD1 (Cottrell *et al*., 2018). The effects of MIDAS motif mutagenesis on CACHD1 as a subunit of Ca_V3 VGCCs are further investigated in Chapter 4.

3.6 Future work

Although the findings in this chapter show the importance of key residues within the MIDAS motif of CACHD1, further investigation into the significance of individual residues is required. Site-directed mutagenesis of single key residues, one at a time, could provide insights into the importance of each key amino acid residue in CACHD1 expression, trafficking, and function. Additionally, mutagenesis of the key residues to more conserved residues instead of alanine (e.g. D234E and S238T) could provide deeper understanding into the importance of individual amino acid residues within the MIDAS motif. Using fluorescence microscopy to further investigate the sub-cellular co-localisation of CACHD1-wt and its MIDAS motif mutants with other proteins, in particular trafficking proteins, could deepen the understanding of the underlying mechanisms behind the disrupted trafficking of CACHD1-AAA to cell surface. This investigation could reveal whether the disruption is caused by protein misfolding and subsequent degradation or due to the mutation disrupting CACHD1 binding to its associated trafficking proteins that facilitate its trafficking to cell membrane. Furthermore, structural analysis with X-ray crystallography or cryo-EM could provide insights into how mutations in the MIDAS motif alter CACHD1 protein structure and interaction with other proteins or ligands.

In this study, heterologous expression systems were used to study CACHD1. While they are useful for an initial exploration of protein expression, trafficking and localisation, the findings may not fully translate to native physiological conditions. Therefore, it is important to further investigate the effects of MIDAS motif mutagenesis in native expression systems, such as SH5YSY neuronal cell line or native neurons. Additionally, by using a native expression system, questions related to the physiological relevance of the findings can be addressed better. Combination of data from both heterologous and native expression systems can provide a more comprehensive understanding into the role of the MIDAS motif in CACHD1 function, cellular physiology, and disease pathology.

4. EFFECTS OF MIDAS MOTIF MUTAGENESIS ON CACHD1 FUNCTION AS A MODULATOR OF $Ca_V3.1$, T-TYPE CALCIUM CHANNEL

4.1 Introduction

Chapter 3 highlighted the importance of key residues within the MIDAS motif of CACHD1 (D^{234}HGAS) on protein expression and trafficking. Through various experiments, it was shown that mutating all three key residues to alanine (DxGxS to AxAxA) led to a disruption in CACHD1 trafficking to cell surface, coupled with a significant decrease in protein expression levels. On the other hand, mutating only the second key residue to serine (G236S) had minimal impact on CACHD1 trafficking or protein expression levels. These findings suggested the possibility that the variant MIDAS motif in CACHD1 functions similarly to the fully conserved MIDAS motif (DxSxS) found in α2δ subunits. However, despite the lack of significant effects on CACHD1 trafficking and expression resulting from the G236S mutation, questions arise about its modulatory effects on Ca_V3 VGCCs.

As CACHD1 is a relatively novel modulator of Ca_V3 VGCCs, the number of studies describing its full potential is limited and therefore it is of great importance to gain the understanding of the mechanisms of how CACHD1 modulates Ca_V3 VGCCs. The main findings to date show that CACHD1 modulates Ca_V3 channels by increasing the i) peak current density with a corresponding increase in maximal conductance for $Ca_V3.1$, ii) channel open probability for $Ca_V3.1$, iii) T-type calcium current levels for $Ca_V3.2$ and $Ca_V3.3$; while also promoting $Ca_V3.1$ cell surface localisation as well as formation of CACHD1-$Ca_V3.1$ protein complexes in heterologous expression system and native neurons (Cottrell *et al*., 2018; Stephens and Cottrell, 2019). Moreover, α2δ-1 showed no effect on Ca_V3 calcium channels (Cottrell *et al*., 2018), but it plays a similar role for Ca_V1 and Ca_V2 channels (Dolphin, 2012).

Previous studies showed that mutagenesis of the three key residues of α2δ-1 MIDAS motif, either through single amino acid substitution (D112A) or mutagenesis of all three key residues (D112A, G114A, S116A, termed AAA), results in the ablation of Ca_V1 and Ca_V2 current increase normally seen in wild-type α2δ-1 (Cantí *et al*., 2005; Hoppa *et al*., 2012; Cassidy *et al*., 2014). Furthermore, the AAA mutation in α2δ-2 was reported to prevent α2δ-2-mediated increase in $Ca_V2.2$ current density (Cantí *et al*., 2005; Hoppa *et al*., 2012). Therefore, this chapter further investigates the effects of MIDAS motif mutagenesis on CACHD1 function as a modulator of Ca_V3 VGCCs, $Ca_V3.1$ in particular.

4.2 Objective

Previous studies have shown that mutations in the MIDAS motif of α2δ subunit, particularly the key residues (DxSxS), led to the abolishment of α2δ-1 and α2δ-2-associated increases in current of Ca_V1 and Ca_V2 channels (Cantí *et al*., 2005; Hoppa *et al*., 2012; Cassidy *et al*., 2014). CACHD1, unlike α2δ subunits, has been identified and described as a modulator of Ca_V3 VGCCs (Cottrell *et al*., 2018), it is therefore of interest to understand whether CACHD1 and α2δ subunits use similar mechanisms to modulate the biophysical properties of VGCCs, and how mutagenesis of the variant MIDAS motif in CACHD1 affects its function as a modulator of Ca_V3 VGCCs.

Considering the variation in expression levels of CACHD1-wt, CACHD1-AAA, and CACHD1-G236S reported in Chapter 3, it is important to understand whether any effects on CACHD1-associated $Ca_V3.1$ T-type current increase caused by the MIDAS motif mutagenesis stem from the mutations themselves rather than the difference in expression levels.

- The first objective of this chapter was to generate inducible stable cell lines expressing CACHD1-wt, CACHD1-AAA, or CACHD1-G236S, where expression levels can be regulated by an inducing agent.

- The second objective was to tag rat $Ca_V3.1$ ($rCa_V3.1$) with a HA epitope tag and characterise $rCa_V3.1$ expression in a heterologous expression system.

- The final objective was to investigate the impact of mutating the three key residues in MIDAS motif on CACHD1 modulatory effects on $rCa_V3.1$ in the inducible CACHD1 stable cell lines using patch clamp electrophysiology.

Hypothesis: Mutagenesis of the three key residues, D^{234}xGxS, within the variant MIDAS motif of CACHD1 will reduce CACHD1-mediated current increase of $rCa_V3.1$.

This hypothesis is based on the results shown for α2δ subunits where mutagenesis of the key residues in MIDAS motif of α2δ-1 and α2δ -2 subunits to alanine resulted in ablation of α2δ-1 and α2δ-2-associated current increase of Ca_V1 and Ca_V2 channels (Cantí *et al*., 2005; Hoppa *et al*., 2012; Cassidy *et al*., 2014).

4.3 Experimental approach

Given the varying expression levels of CACHD1-wt, CACHD1-AAA and CACHD1-G236S mutants reported in Chapter 3, it is important to standardise their expression and achieve similar protein expression levels. The standardisation of expression levels will allow the understanding of CACHD1 functional effects on $Ca_V3.1$ T-type currents associated with MIDAS motif mutagenesis independently of any effects caused by the varying protein expression levels. To achieve equal protein expression of CACHD1-wt, CACHD1-AAA and CACHD1-G236S mutants, a tetracycline-ON (TetON) regulatory system that requires tetracycline to induce gene expression was used. Addition of tetracycline causes conformational changes in the reverse tetracycline transactivator (rtTA) which is comprised of the tetracycline repressor (TetR) and the VP16 transactivation domain (Gossen and Bujard, 1992). These conformational changes enable rtTA binding to the tetracycline operator (TetO), initiating the transcription of the gene of interest (Gossen and Bujard, 1992).

4.3.1 Generation and characterisation of inducible CACHD1-wt, CACHD1-AAA, and CACHD1-G236S stable HEK293 cell lines

The generation of stable HEK293 Flp-In™ T-REx™ cell lines where the expression of CACHD1 can be regulated with tetracycline consisted of two main steps: i) the addition of TetO and ii) generation of stable cell lines using viral transduction method.

4.3.1.1 Addition of a tetracycline operator to regulate protein expression

The process of adding a TetO to Myc-CACHD1-wt, Myc-CACHD1-AAA and Myc-CACHD1-G236S constructs consisted of three steps.

1) TetO was inserted into the existing pcDNA5/FRT-Myc-CACHD1-wt/AAA/G236S constructs using *Hind* III and *Apa* I restriction enzymes (Figure 4.1).

2) The TetO-Myc-CACHD1-wt/AAA/G236S were transferred into a lentiviral vector that would facilitate stable CACHD1 expression through lentiviral transduction. In this case, pLenti6.3-neo was used because it contains the necessary elements for packaging lentiviral particles, including the lentiviral genome backbone, a CMV promoter to drive gene expression, and long terminal repeats (LTRs) required for integration into the host genome. Due to limited restriction sites available, this transfer required two steps. TetO-Myc-CACHD1-wt/AAA/G236S

were first inserted into pLenti6.3-blast using *Sna* BI and *Bam* HI restriction sites as shown in Figure 4.2.

3) Using *Mfe* I and *Sex* AI restriction sites, TetO-Myc-CACHD1-wt/AAA/G236S were inserted into pLenti6.3-neo plasmid (Figure 4.3) which contains the G418 resistance gene. However, prior to this step, pLenti6.3-neo plasmid had to be demethylated as the *Sex* AI restriction site is sensitive to methylation by the DNA methyltransferase enzyme (Dcm). To obtain non-methylated pLenti6.3-neo plasmid DNA, GM2163 competent bacterial cells were transformed with pLenti6.3-neo. *E. coli* (GM2163) lack the Dcm enzyme and therefore transformation into these cells prior to cloning results in a non-methylated DNA construct, avoiding cloning issues related to DNA methylation along the line, such as low restriction enzyme digestion efficiency (Marinus and Løbner-Olesen, 2014). The non-methylated pLenti6.3-neo plasmid DNA was then obtained according to protocols outlined in sections 2.4.14 and 2.4.15.

When working with lentiviral vectors, Mach1 competent bacterial cell were used for transformation at 28°C to slow down their growth rate. This reduces the chance of homologous recombination which is particularly important for lentiviral vectors containing LTRs. Following Mach1 bacterial transformation, the final pLenti6.3-neo-TO-Myc-CACHD1-wt/AAA/G236S plasmid DNA was transformed into Stbl3 competent cells for propagation and prepared according to sections 2.4.14 and 2.4.15. Stbl3 competent cells have mutations in the *rec*A gene which reduces homologous recombination, helping to maintain the stability of DNA constructs and prevent rearrangements during bacterial transformation.

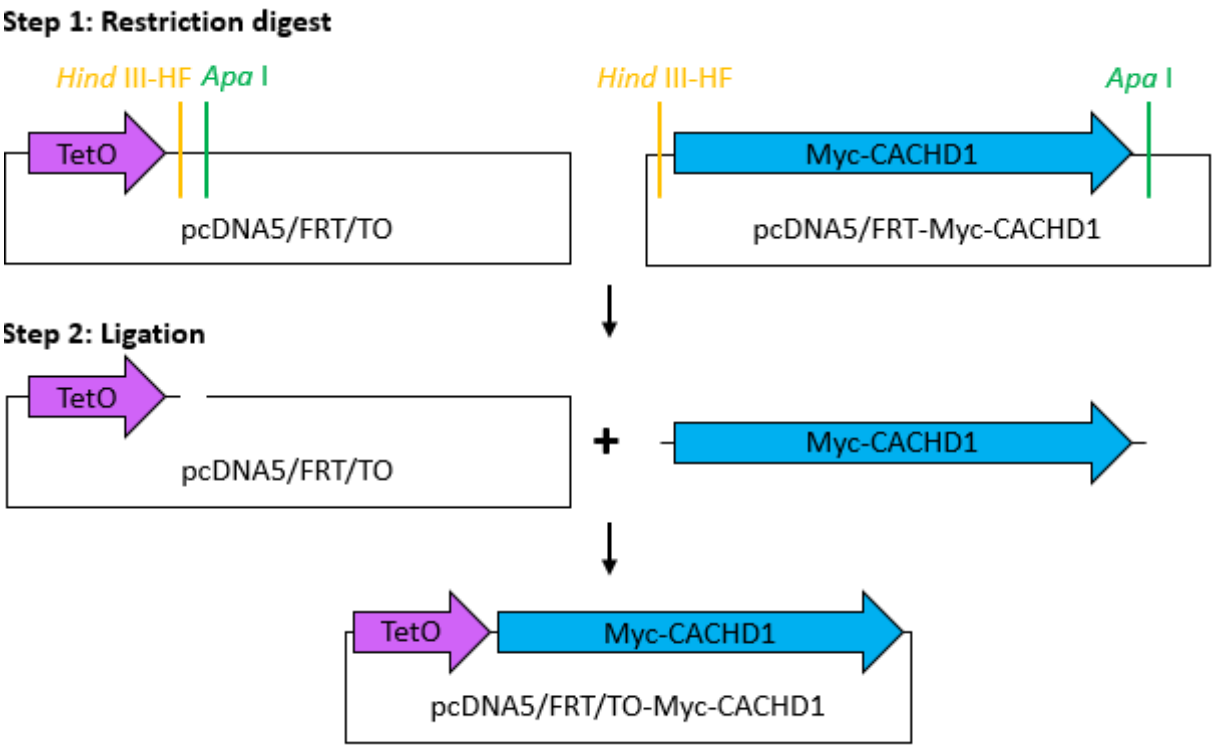

Figure 4.1 Cloning procedure for the addition of TetO to Myc-CACHD1-wt/AAA/G236S. pcDNA5/FRT/TO and pcDNA5/FRT-Myc-CACHD1-wt/AAA/G236S were digested with *Hind* III-HF and *Apa* I to introduce single-stranded overhangs. The final pcDNA5/FRT/TO-Myc-CACHD1-wt/AAA/G236S constructs were generated by a 2-way ligation with T4 DNA ligase.

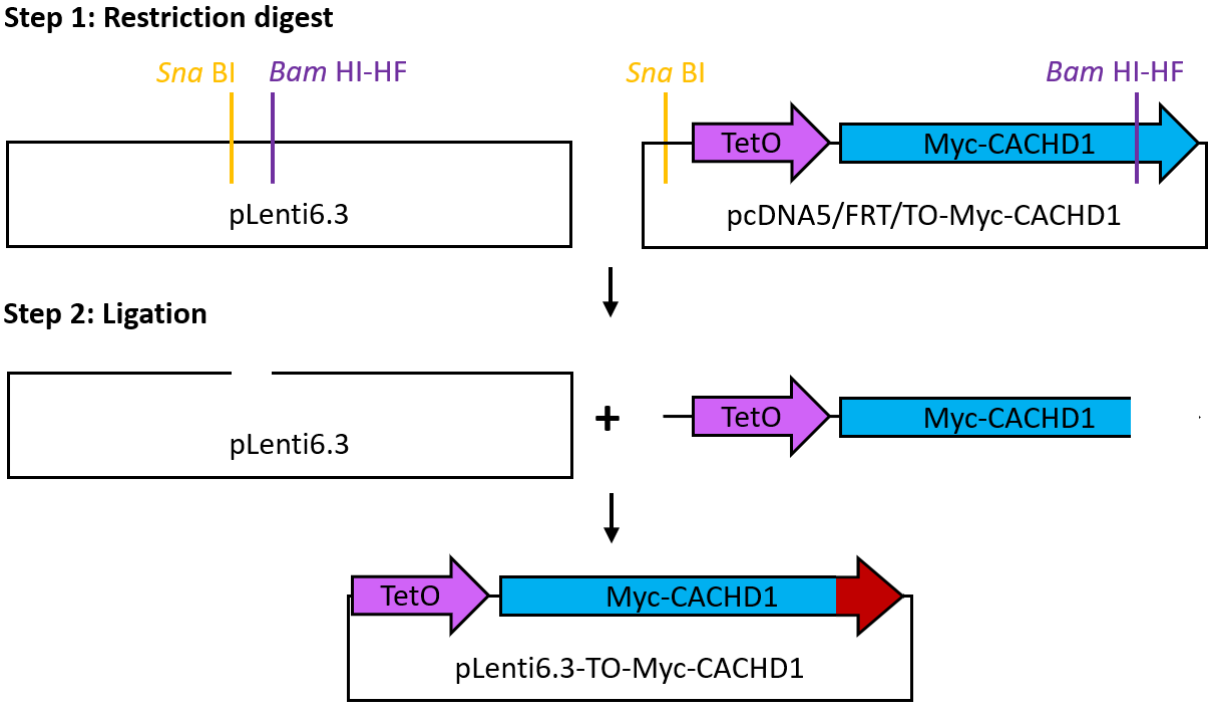

Figure 4.2 Cloning procedure for the insertion of TO-Myc-CACHD1-wt/AAA/G236S into pLenti6.3. pLenti6.3 and pcDNA5/FRT/TO-Myc-CACHD1-wt/AAA/G236S were digested with *Sna* BI and *Bam* HI-HF to introduce single-stranded overhangs. The final pLenti6.3-TO-Myc-CACHD1-wt/AAA/G236S constructs were generated by a 2-way ligation with T4 DNA ligase.

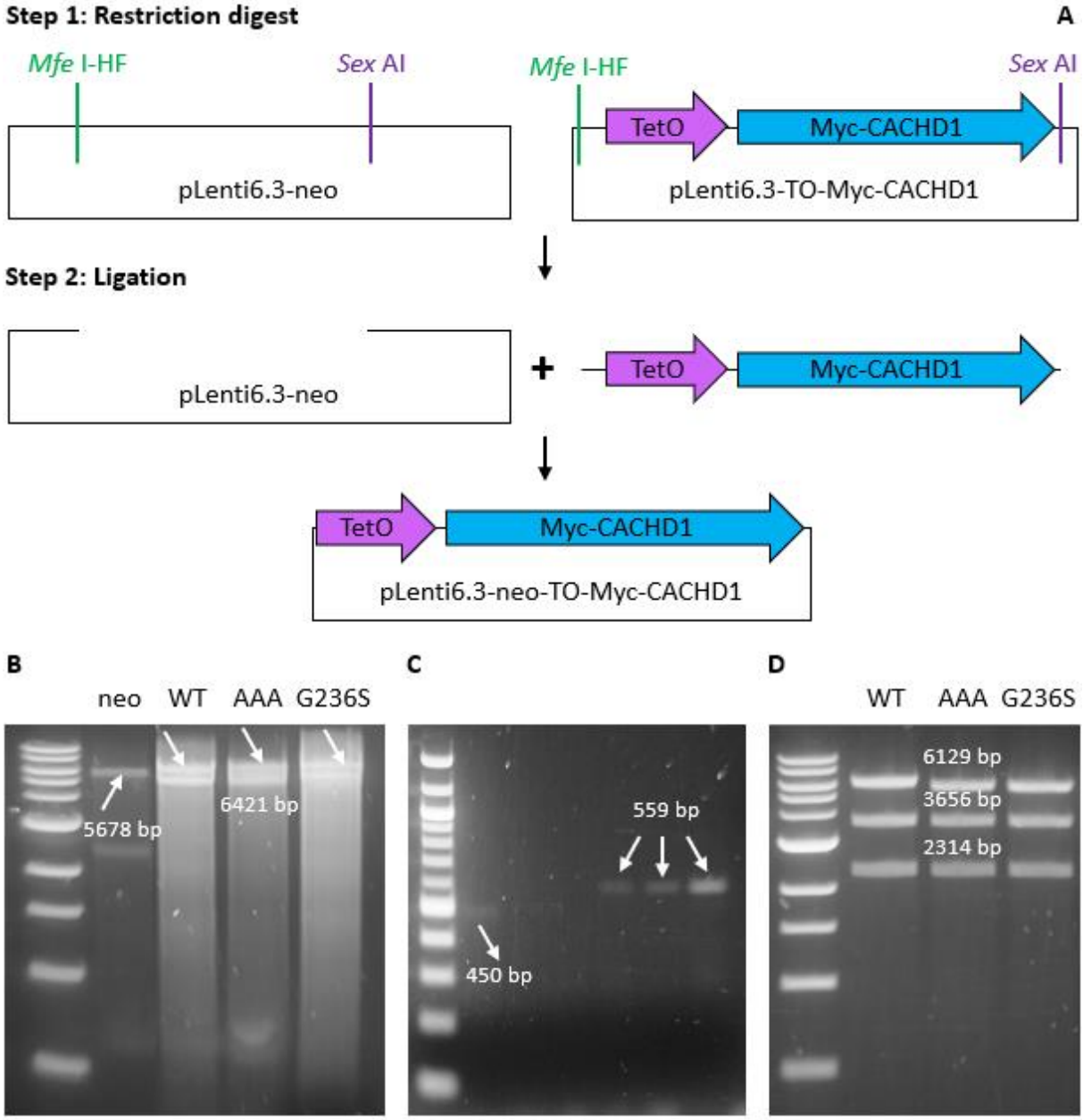

Figure 4.3 Cloning procedure for generation of pLenti6.3-neo-TO-Myc-CACHD1-wt/AAA/G236S. pLenti6.3 was demethylated using GM2163 competent bacterial cells. **(A, B)** pLenti6.3-neo and pLenti6.3-TO-Myc-CACHD1-wt/AAA/G236S were digested with *Mfe* I-HF and *Sex* AI to produce 5678 bp and 6421 bp DNA fragments with single-stranded overhangs, respectively. The final pLenti6.3-neo-TO-Myc-CACHD1-wt/AAA/G236S constructs were generated by a 2-way ligation with T4 DNA ligase. **(C)** Positive colony PCR with CMV fwd and hCACHD1:247-229rev primers (450 bp fragment for pLenti6.3-TO-Myc-CACHD1-wt, control; 559 bp fragment for pLenti6.3-neo-TO-CACHD1-wt/AAA/G236S), **(D)** and restriction digest of final product with *Afl* II showed expected DNA fragments, suggesting successful insertion of TetO-Myc-CACHD1-wt/AAA/G236S into pLenti6.3-neo. (B: 0.8% agarose gel, 1 kb DNA ladder, NEB; C: 2% agarose gel, 100 bp DNA ladder, NEB; D: 1% agarose gel, 1 kb DNA adder, NEB).

4.3.1.2 Stable cell line generation and characterisation

HEK293 Flp-In™ T-REx™ stable cell lines expressing CACHD1, and the MIDAS mutants were generated by viral transduction, following the protocol outlined in section 2.1.7. Following antibiotic selection, monoclonal CACHD1-wt, CACHD1-AAA and CACHD1-G236S clones were picked, and their expression and sub-cellular localisation were assessed by western blotting and immunocytochemistry.

Stable HEK293 cells in a 12-well plate were treated with 1 µg/ml of tetracycline or plain culture medium (negative control), followed by overnight incubation at 37°C, 5% CO_2. Some cells were seeded onto poly-D-lysine coated coverslips ($1x10^5$ cells/well, 12-well plate) for immunocytochemistry, while the remaining cells were lysed and extracted proteins were analysed by western blotting as described in section 2.2.11, using rabbit anti-Myc (1:5000) and mouse anti-β-actin (1:20000) antibodies. To evaluate sub-cellular localisation of Myc-tagged CACHD1-wt, CACHD1-AAA and CACHD1-G236S, cells on coverslips were labelled live and fixed (section 2.3.4 and 2.3.5) with rabbit and mouse anti-Myc antibodies, respectively, followed by imaging using epifluorescence microscopy.

4.3.2 Tagging and characterisation of rCa$_V$3.1 in a heterologous expression system

Untagged rCa$_V$3.1 construct was provided by Dr. Perez-Reyes for the purposes of this project. While a human Ca$_V$3.1 (hCa$_V$3.1) construct was available, there were issues with its detection and usability during initial expression and electrophysiology experiments. rCa$_V$3.1 serves as a suitable alternative to hCaV3.1, as the proteins share approx. 94% amino acid sequence homology (alignment of hCa$_V$3.1 (UniProt, O434497) and rCa$_V$3.1 (UniProt, O54898) amino acid sequences was carried out using Clustal Omega multiple sequence alignment tool; Appendix II, Figure 9.1). While studies comparing hCa$_V$3.1 and rCa$_V$3.1 are limited, studies have compared the human and rat Ca$_V$3 families. Study by Gomora *et al*. (2002) compared human and rat Ca$_V$3 channels, and while they did not specifically use Ca$_V$3.1, the results showed that human and rat Ca$_V$3.3 channels shared similar biophysical properties. Moreover, both human and rat Ca$_V$3 channels showed similar activation thresholds (< -35 mV), with rat Ca$_V$3 currents activated at slightly lower potentials compared to human Ca$_V$3 currents (Hartung *et al*., 2022). These similarities suggest that the functional characteristics, including their biophysical properties, are likely to be conserved between species, supporting the suitability of rCa$_V$3.1 as a model for studying Ca$_V$3.1 modulation throughout this project.

The Q5 DNA polymerase PCR method was used (section 2.4.6) to insert a HA epitope tag (Y2-A10: YPYDVPDYA) after M1 residue of rCa$_V$3.1. Given the poor quality of available anti-rCa$_V$3.1 antibodies, the decision to use an epitope tag was made to ensure reliable detection of rCa$_V$3.1 during biochemical experiments, such as sub-cellular localisation, expression levels and trafficking. The cloning procedure is shown in Figure 4.4. Required DNA fragments were ligated with T4 DNA ligase and Mach 1 bacteria were transformed with ligation reactions. CMV fwd and rCa$_V$3.1:1014-994rev primers were used for screening of positive colonies, resulting in 1154 bp and 1189 bp DNA fragments for pcDNA5/FRT-rCa$_V$3.1 (control) and pcDNA5/FRT-HA-rCa$_V$3.1, respectively. Final constructs were sequenced to confirm successful addition of a HA epitope tag in rCa$_V$3.1.

The expression of HA-rCa$_V$3.1 was then characterised by western blotting and immunocytochemistry. HEK293T tsA201 cells were plated at a 2x10^6 cells/well density in a 6-well plate and transiently transfected with 6 µg of pcDNA5/FRT-HA-rCa$_V$3.1 or pcDNA5/FRT (vector control) as described in section 2.1.5. Subsequently, transfected cells were seeded onto poly-D-lysine coated coverslips (1x10^5 cells/well, 12-well plate) for immunocytochemistry, while the remaining cells were allowed to grow in the 6-well plate for western blot analysis. Cells were cultured at 37°C, 5% CO_2, for 48 h before analysis. To investigate sub-cellular localisation, cells on coverslips were fixed with 4% PFA (section 2.3.3) and labelled with mouse anti-HA antibodies (section 2.3.5). To confirm molecular size of HA-rCa$_V$3.1 protein, transfected cells were lysed and extracted proteins were analysed by western blotting as described in section 2.2.11, using mouse anti-Myc (1:5000) and mouse anti-β-actin (1:20000) antibodies.

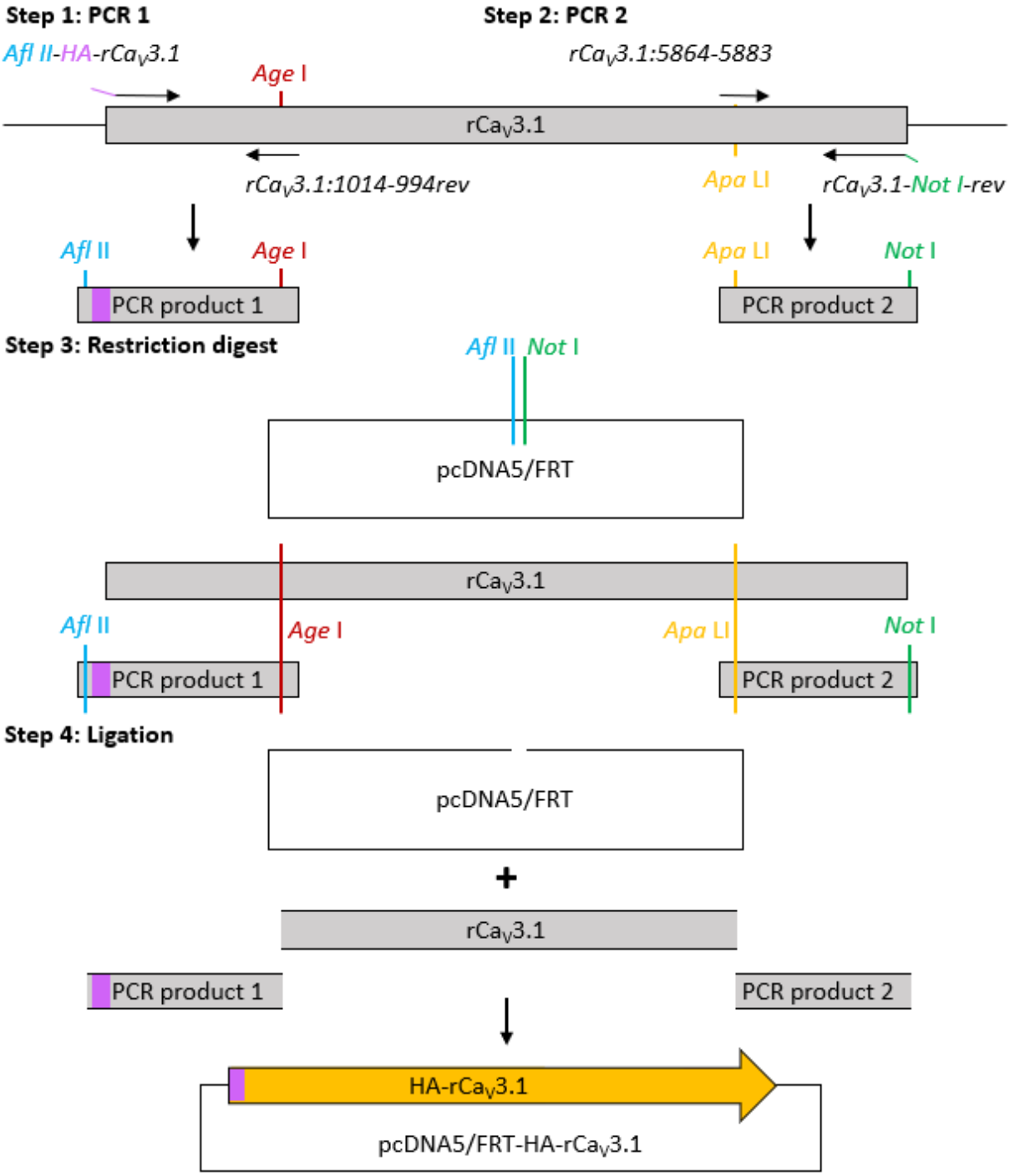

Figure 4.4 Cloning procedure for the addition of HA epitope tag in rCa$_V$3.1. Afl II-HA-rCa$_V$3.1 and rCa$_V$3.1:1014-994rev primers were used to produce 1058 bp rCa$_V$3.1 fragment with *Afl* II and *Age* I restriction sites, and a HA epitope tag sequence following the start codon (ATG) of rCa$_V$3.1 (PCR product 1). rCa$_V$3.1:5864-5883 and rCa$_V$3.1-Not I-rev primers were used to produce 1053 bp rCa$_V$3.1 fragment with *Apa* LI and *Not* I restriction sites (PCR product 2). PCR product 1, PCR product 2, pcDNA3-HE3-rCa$_V$3.1, and pcDNA5/FRT were digested with *Afl* II + *Age* I, *Apa* LI + *Not* I, *Age* I + *Apa* LI, and *Afl* II + *Not* I respectively to introduce single-stranded overhangs. The final pcDNA5/FRT-HA-rCa$_V$3.1 construct was generated by a 4-way ligation with T4 DNA ligase.

4.3.3 Patch-clamp electrophysiology of rCa$_V$3.1 channels

Transient transfection with rCa$_V$3.1 or HA-rCa$_V$3.1 with mVenus was carried out as described in section 2.1.5. The presence of mVenus in cells can be a good indicator of successful transfection and protein expression, while aiding with cell visualisation during patch-clamp electrophysiology experiments. HEK293 tsA201 were used to assess the impact of the addition of HA tag on rCa$_V$3.1 currents, and inducible HEK293 stable cell lines expressing CACHD1-wt, CACHD1-AAA, or CACHD1-G236S were used to assess the effects of MIDAS motif mutagenesis on rCa$_V$3.1 channel biophysical properties.

Inducible stable cell lines expressing CACHD1 were transfected as detailed above, and after 4-6 h incubation period the cells were divided between two separate 30 mm dishes. The day before electrophysiological experiments, culture medium containing 1 µg/µl tetracycline was added to cells in one dish to induce CACHD1 expression, while the cells in the second dish underwent media change without tetracycline induction. This approach was implemented to maintain consistent experimental conditions across both conditions. On the day of the experiment, cells were plated onto coverslips and labelled as A and B to maintain blinding throughout.

Voltage-clamp recordings were obtained as described in Vogl *et al*. (2015; section 2.5) and performed with 10 mM Ba^{2+} as the charge carrier. Ba^{2+} was chosen as a standard charge carrier to measure channel activity due to its high permeability and avoidance of Ca^{2+}-dependent current inactivation processes. rCa$_V$3.1 currents were induced by depolarisation from a holding potential of -90 mV to +60 mV, using 10 mV incremental steps. Ba^{2+} current density (I_{Ba} (pA/pF)) was determined by measuring peak currents at different voltage potentials and dividing by individual cell capacitance values, as measured using Clampfit11.2 (Molecular Devices). Subsequently, current density-voltage data were analysed according to section 2.5.4, and G_{max}, V_{rev}, $V_{1/2}$, and slope factor *k* values were determined to compare any effects on rCa$_V$3.1 channel biophysical properties associated with HA tag addition and CACHD1 MIDAS motif mutagenesis. Liquid junction potential was +8.5 mV and all results are shown uncorrected.

4.4 Results

4.4.1 CACHD1 MIDAS mutants are expressed in stable HEK293 cells, and their expression can be regulated with tetracycline

Western blot analysis was used to confirm the molecular mass, and inducibility and regulation of Myc-tagged CACHD1-wt, CACHD1-AAA and CACHD1-G236S expression by tetracycline in stable HEK293 cells. Figure 4.5A shows immunoreactive Myc-CACHD1 proteins at ~150-170 kDa, which is consistent with findings reported in Chapter 3. Moreover, immunoreactive Myc-tagged CACHD1-wt, CACHD1-AAA and CACHD1-G236S were detected in whole cell lysate samples treated with tetracycline only, indicating that the addition of tetracycline induced gene transcription and subsequent protein expression. These results were further confirmed by immunocytochemistry, where immunofluorescent Myc-tagged CACHD1-wt, CACHD1-AAA and CACHD1-G236S were detected only in cells treated with tetracycline (Figure 4.5B). Furthermore, the sub-cellular localisation of Myc-tagged CACHD1-wt, CACHD1-AAA and CACHD1-G236S in stably expressing HEK293 cells was evaluated using rabbit anti-Myc antibody for live cell labelling (section 2.3.4), and mouse anti-Myc antibody for fixed cell labelling (section 2.3.5). As shown in Figure 4.5B, both CACHD1-wt and CACHD1-G236S were expressed on cell surface and in intracellular compartments, while CACHD1-AAA was detected exclusively in intracellular compartments, aligning with the expression patterns reported in Chapter 3.

Following the selection of CACHD1-wt, CACHD1-AAA and CACHD1-G236S clones that showed similar protein expression levels, cells were treated with 1 µg/ml of tetracycline, and the total expression levels were assessed by densitometry prior to any functional studies. Statistical analysis of total protein expression levels showed that treatment with 1 µg/ml of tetracycline resulted in comparable expression levels of 100.0±0.0%, 138.2±32.8% and 125.8±34.9% for CACHD1-wt, CACHD1-AAA and CACHD1-G236S, respectively, showing no significant differences in total CACHD1 expression (Figure 4.6).

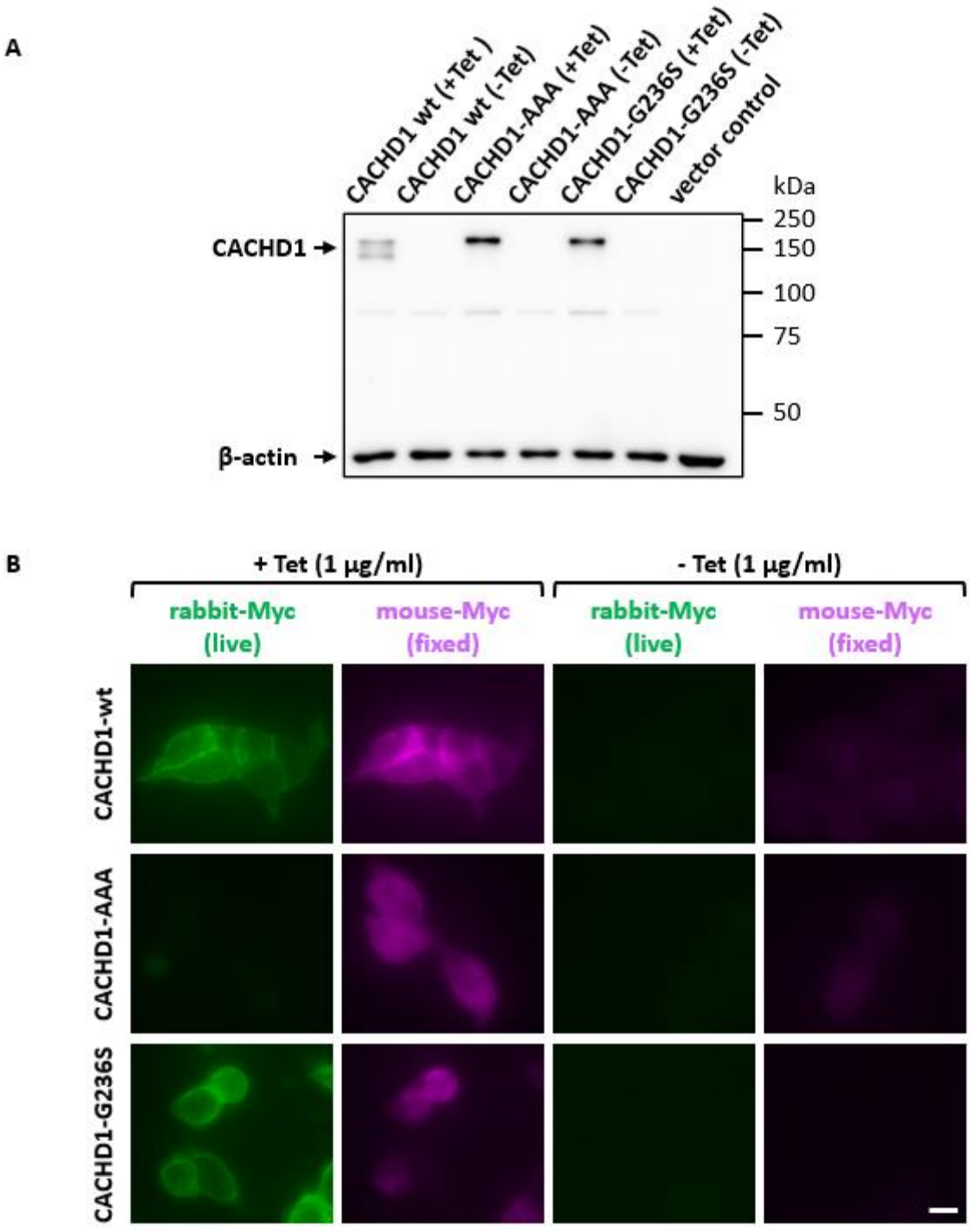

Figure 4.5 Characterisation of Myc-tagged CACHD1-wt and MIDAS mutants expression regulation and sub-cellular localisation using western blotting and ICC. Stably expressing HEK293T cells were treated with 1 µg/ml of tetracycline or culture medium (-ve control), and expression was analysed by western blotting and ICC. **(A)** Cells were lysed and whole-cell lysate samples were collected. Proteins were then separated by SDS-PAGE and blots were incubated with rabbit anti-Myc antibody. Immunoreactive Myc-CACHD1 proteins were detected in cells treated with tetracycline only, confirming inducibility and regulation of CACHD1 expression. Myc-tagged CACHD1-wt, CACHD1-AAA and CACHD1-G236S were detected at 150-170 kDa in whole-cell lysates. Signals for β-actin (loading control) were present in treated and non-treated cells. (9% SDS-PAGE gel, n=3). **(B)** Cells were labelled live with rabbit anti-Myc antibody, fixed with 4% PFA, and labelled with mouse anti-Myc antibody. Myc-tagged CACHD1 proteins were detected with rabbit antibodies, showing expression on cell surface, and with mouse anti-Myc antibodies, showing some expression in intracellular compartments. (Scale bar 10 µm, n=3).

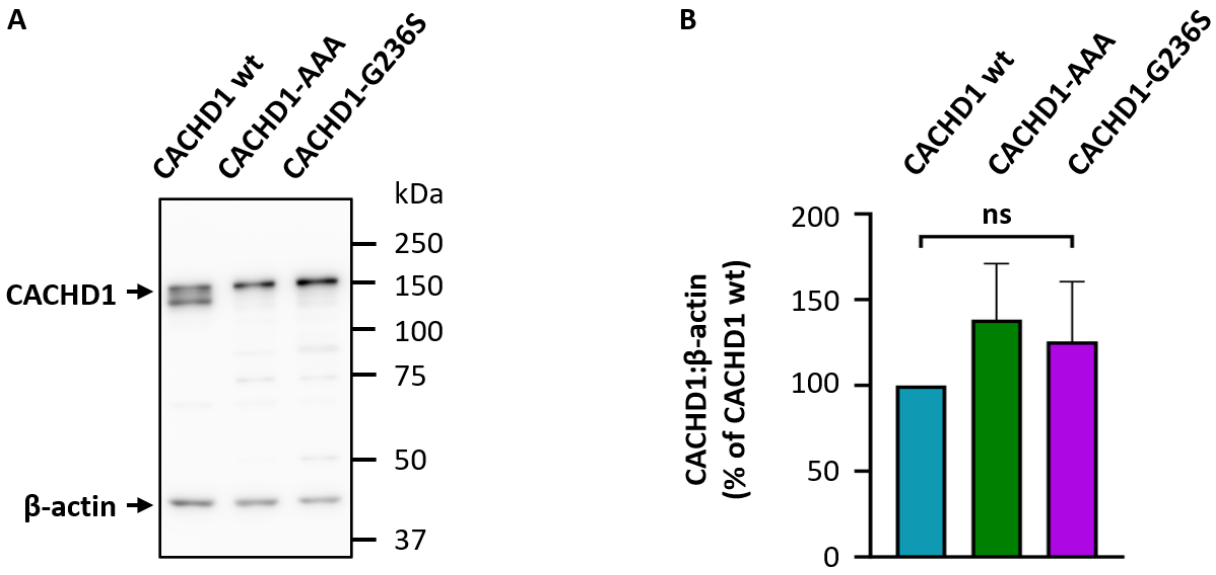

Figure 4.6 Analysis of expression of Myc-CACHD1-wt, Myc-CACHD1-AAA and Myc-CACHD1-G236S in inducible stably expressing HEK293 cells by western blotting. (A) Expression of Myc-CACHD1-wt, Myc-CACHD1-AAA and Myc-CACHD1-G236S in induced stable HEK293 cells was determined by western blotting. Cells were lysed, proteins separated by SDS-PAGE and blots incubated with rabbit anti-Myc and mouse anti-β-actin (loading control) antibodies. Immunoreactive Myc-CACHD1-wt, Myc-CACHD1-AAA and Myc-CACHD1-G236S proteins were detected at 150-170 kDa. Signals for β-actin were present in all cell types. **(B)** Densitometry was performed on viable blots and raw data was analysed by One-way ANOVA with Tukey's post hoc test. Results showed that Myc-CACHD1-wt, Myc-CACHD1-AAA, and Myc-CACHD1-G236S expression induced with 1 µg/ml of tetracycline was consistently at comparable levels (100.0±0.0%, 138.2±32.8%, 125.8±34.9% for CACHD1-wt, CACHD1-AAA and CACHD1-G236S respectively; mean±SEM). (n=8, ns – non-significant).

4.4.2 The HA-tagged rCa$_V$3.1 is expressed in transiently transfected HEK293 tsA201 cells

Western blot analysis was used to confirm the expression and size of HA-tagged rCa$_V$3.1 protein expressed in transiently transfected HEK293 tsA201 cells. In Figure 4.4A, immunolabelling with mouse anti-HA antibody showed immunoreactive HA-rCa$_V$3.1 present in whole-cell lysates. HA-rCa$_V$3.1 was detected at a molecular mass of ~ 300 kDa which corresponds with the predicted molecular mass of rCa$_V$3.1 protein reported by UniProt (>250 kDa with multiple N-glycosylation sites; O54898).

Expression of HA-tagged rCa$_V$3.1 in transiently transfected HEK293 tsA201 cells was further confirmed by immunocytochemistry, using mouse anti-HA antibody for fixed cell labelling (section 2.3.5). As shown in Figure 4.4B, immunoreactive HA-rCa$_V$3.1 was expressed mainly in intracellular compartments. No immunoreactive signals were detected for vector control.

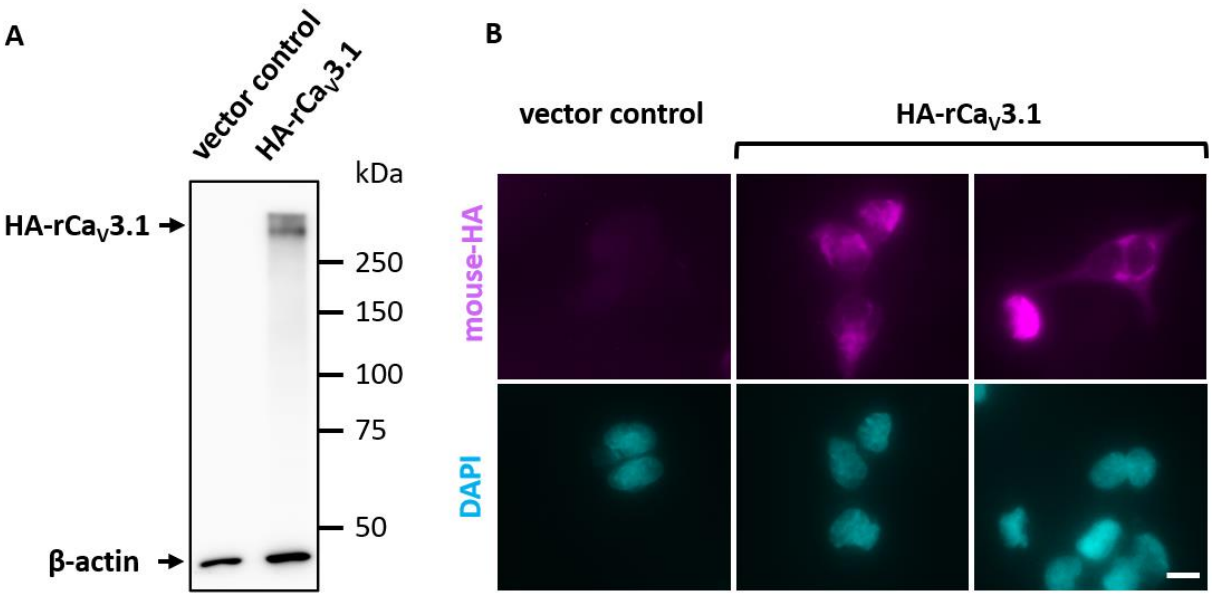

Figure 4.7 Characterisation of HA-rCa$_V$3.1 expression using western blotting and ICC. HEK293T tsA201 cells were transiently transfected with HA-rCa$_V$3.1 or empty vector (control), and expression was analysed by western blotting and ICC. **(A)** Cells were lysed and whole-cell lysate samples were collected. Proteins were then separated by SDS-PAGE and blots were incubated with mouse anti-HA antibody. Immunoreactive HA-rCa$_V$3.1 was detected in cells transfected with HA-rCa$_V$3.1 only, confirming antibody specificity. HA-rCa$_V$3.1 was detected at ~300 kDa in whole-cell lysates. Signals for β-actin (loading controls) were present in both cell types. (9% SDS-PAGE gel, n=2) **(B)** Transfected cells were fixed with 4% PFA and labelled with mouse anti-HA antibody. HA-rCa$_V$3.1 was detected by epifluorescence microscopy showing some expression on cell surface but mostly in intracellular compartments. (Scale bar 10 µm, n=2).

4.4.3 The presence of HA tag appears to have no effect on rCa$_V$3.1 currents

Following co-transfection of rCa$_V$3.1 or HA-rCa$_V$3.1 with mVenus in HEK293 tsA201 cells, voltage-clamp electrophysiology was carried out to investigate the potential impact of adding a HA tag at the N-terminus of rCa$_V$3.1 on the biophysical properties of the channel. Analysis of the modified Boltzmann curve fitting to current-voltage relationships showed that the addition of HA tag had no significant effect on peak current density (Figure 4.8A). Representative Ba^{2+} current density traces following depolarisation from -90 mV to -20 mV are shown in Figure 4.8B. Moreover, the addition of HA tag did not cause changes in conductance (G_{max}), midpoint activation ($V_{1/2}$), reversal potential (V_{rev}), or slope factor *k* of rCa$_V$3.1, as shown in Figure 4.8C-F and summarised in Table 4.1.

Table 4.1 Effects of HA-tag addition on biophysical properties of rCa$_V$3.1

Cell line		n	G_{max} (pS/pF)	V_{rev} (mV)	$V_{1/2}$ (mV)	Slope *k* (mV)
HEK293 tsA201	rCa$_V$3.1	10	970 ± 140	46.8 ± 1.6	-35.4 ± 1.2	4.7 ± 0.3
	HA-rCa$_V$3.1	7	920 ± 150	50 ± 2.7	-34.5 ± 3.0	4.6 ± 0.3

In all cases, comparisons were performed in culture-matched experiments, and data was collected from a minimum of three separate transfections. All data were normally distributed (Shapiro-Wilk test, $p > 0.05$; mean ± SEM; two-tailed unpaired Student's *t* test; *$p < 0.05$).

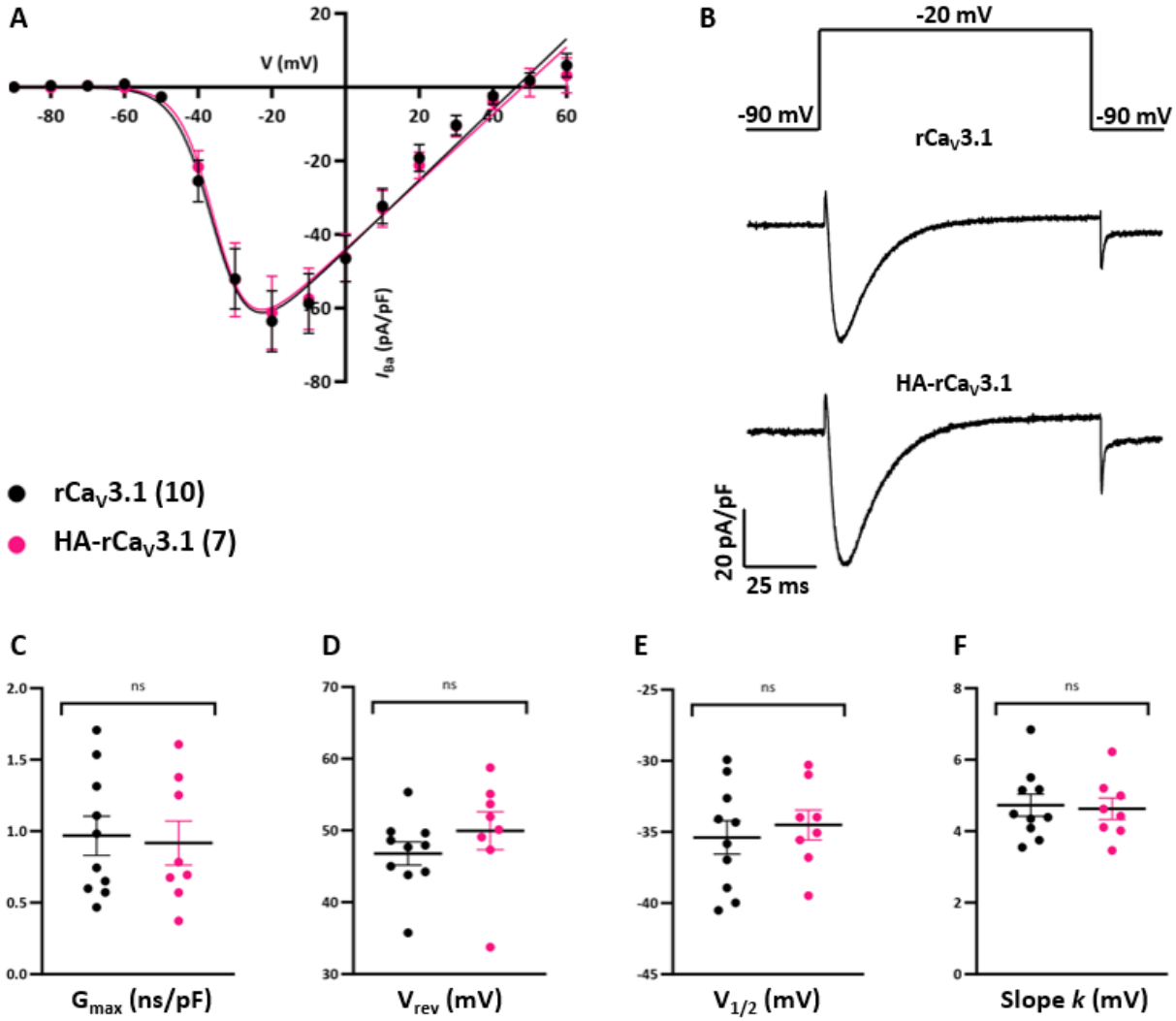

Figure 4.8 Effects of HA tag addition on rCa$_V$3.1 channel. Addition of HA tag had no effect on current density as shown by **(A)** I-V relationships (holding potential -90 mV; $p > 0.05$; two-way ANOVA with Bonferroni *post hoc* test; curve fitted with modified Boltzmann) and **(B)** representative current density traces at -20 mV. Addition of HA tag had no effect on **(C)** maximal conductance (G_{max}), **(D)** reversal potential (V_{rev}), **(E)** midpoint activation ($V_{1/2}$), or **(F)** slope factor *k* ($p > 0.05$; two-tailed unpaired Student's *t* test; rCa$_V$3.1, n = 10; HA-rCa$_V$3.1, n = 7).

4.4.4 Effects of MIDAS motif mutagenesis on CACHD1 modulation of rCa$_V$3.1

During this study, the effects of CACHD1 MIDAS motif mutagenesis on rCa$_V$3.1 currents were determined by voltage patch-clamp electrophysiology. Stable CACHD1-wt/AAA/G236S HEK293 Flp-In™ T-REx™ cells were transfected with rCa$_V$3.1 + mVenus, and comparison was made between non-induced cells that served as control, and cells where CACHD1 expression was induced and regulated with 1 µg/ml of tetracycline, considered as the "treatment" group within each respective cell line. Consequently, any observed effects on rCa$_V$3.1 biophysical properties associated with CACHD1-wt, CACHD1-AAA or CACHD1-G236S were assessed within their corresponding cell lines, rather than across the different cell lines to limit unnecessary variation. For example, the effects of CACHD1-wt on rCa$_V$3.1 channel properties were evaluated within the HEK293 CACHD1-wt inducible cell line, while the effects of CACHD1-AAA and CACHD1-G236S were evaluated within their respective inducible cell lines.

Following co-transfection of rCa$_V$3.1 with mVenus in inducible CACHD1 stable cells, voltage-clamp electrophysiology was carried out to investigate the impact of MIDAS motif mutagenesis on CACHD1 function as a modulator of Ca$_V$3.1 channels, and the results are summarised in Table 4.2. Furthermore, the effects of CACHD1 MIDAS mutants on rCa$_V$3.1 currents at a range of voltage steps are summarised in Table 4.3.

Subsequently, power calculations on G_{max} data (α = o.o5, power = 0.8) were carried out in SPSS for each cell line to determine the optimal sample size (Appendix II, Figures 9.2-4), which confirmed that the obtained *n* numbers were sufficient.

Table 4.2 Effects of CACHD1 MIDAS mutants on biophysical properties of rCa$_V$3.1

Cell line			n	G_{max} (pS/pF)	V_{rev} (mV)	$V_{1/2}$ (mV)	Slope *k* (mV)
CACHD1-wt	-Tet	rCa$_V$3.1	22	980 ± 100	54.9 ± 1.6	-36.2 ± 1.1	4.5 ± 0.2
	+Tet	rCa$_V$3.1+CACHD1-wt	18	1430 ± 120**	51.0 ± 1.4	-38.8 ± 1.7	4.2 ± 0.2
CACHD1-AAA	-Tet	rCa$_V$3.1	13	820 ± 120	51.5 ± 0.7	-35.2 ± 1.3	4.2 ± 0.2
	+Tet	rCa$_V$3.1+CACHD1-AAA	14	510 ± 60*	49.1 ± 2.3	-33.5 ± 1.4	4.8 ± 0.5
CACHD1-G236S	-Tet	rCa$_V$3.1	10	390 ± 60	52.0 ± 1.9	-35.2 ± 2.0	5.0 ± 0.3
	+Tet	rCa$_V$3.1+CACHD1-G236S	15	580 ± 50*	48.0 ± 2.6	-37.9 ± 1.6	4.5 ± 0.3

In all cases, comparisons were performed in culture-matched experiments, and data was collected from a minimum of three separate transfections. All data were normally distributed (Shapiro-Wilk test, $p > 0.05$; mean ± SEM; two-tailed unpaired Student's *t* test; * $p < 0.05$, ** $p < 0.01$).

Table 4.3 Comparison of the effects of CACHD1 MIDAS mutants on rCa$_V$3.1 currents at a range of voltage steps.

Voltage step (mV)	rCa$_V$3.1 +/- CACHD1-wt	rCa$_V$3.1 +/- CACHD1-AAA	rCa$_V$3.1 +/- CACHD1-G236S
-90	ns	ns	ns
-80	ns	ns	ns
-70	ns	ns	ns
-60	ns	ns	ns
-50	ns	ns	ns
-40	ns	ns	ns
-30	**	****	***
-20	**	****	***
-10	**	***	*
0	*	**	ns
10	ns	ns	ns
20	ns	ns	ns
30	ns	ns	ns
40	ns	ns	ns
50	ns	ns	ns
60	ns	ns	ns

Two-way ANOVA with Bonferroni *post hoc* test; * $p < 0.05$, ** $p < 0.01$, *** $p < 0.005$, **** $p < 0.001$.

4.4.4.1 Wild-type CACHD1 protein increases rCa$_V$3.1 currents

Depolarisation of cells co-expressing rCa$_V$3.1 and CACHD1-wt from holding potential of -90 mV to +60 mV resulted in an increase in peak current density by approx. 1.36-fold compared to cells expressing rCa$_V$3.1 alone. Ba^{2+} current density was significantly higher at depolarisation steps ranging from -30 mV to 0 mV, with a peak Ba^{2+} current density at -20 mV significantly increased from -73.4 $\pm$ 8.0 pA/pF to -99.4 $\pm$ 7.5 pA/pF (Figure 4.9A; $p < 0.01$, two-way ANOVA with Bonferroni *post hoc* test). Representative Ba^{2+} current density traces following depolarisation from -90 mV to -20 mV are shown in Figure 4.9B. Moreover, CACHD1-wt significantly increased rCa$_V$3.1 G_{max} from 980 $\pm$ 100 pS/pF to 1430 $\pm$ 120 pS/pF ($p < 0.01$, two-tailed unpaired Student's *t* test) but had no significant effect on midpoint activation ($V_{1/2}$), reversal potential (V_{rev}), or slope factor *k* of rCa$_V$3.1, as shown in Figure 4.9C-F and summarised in Table 4.2.

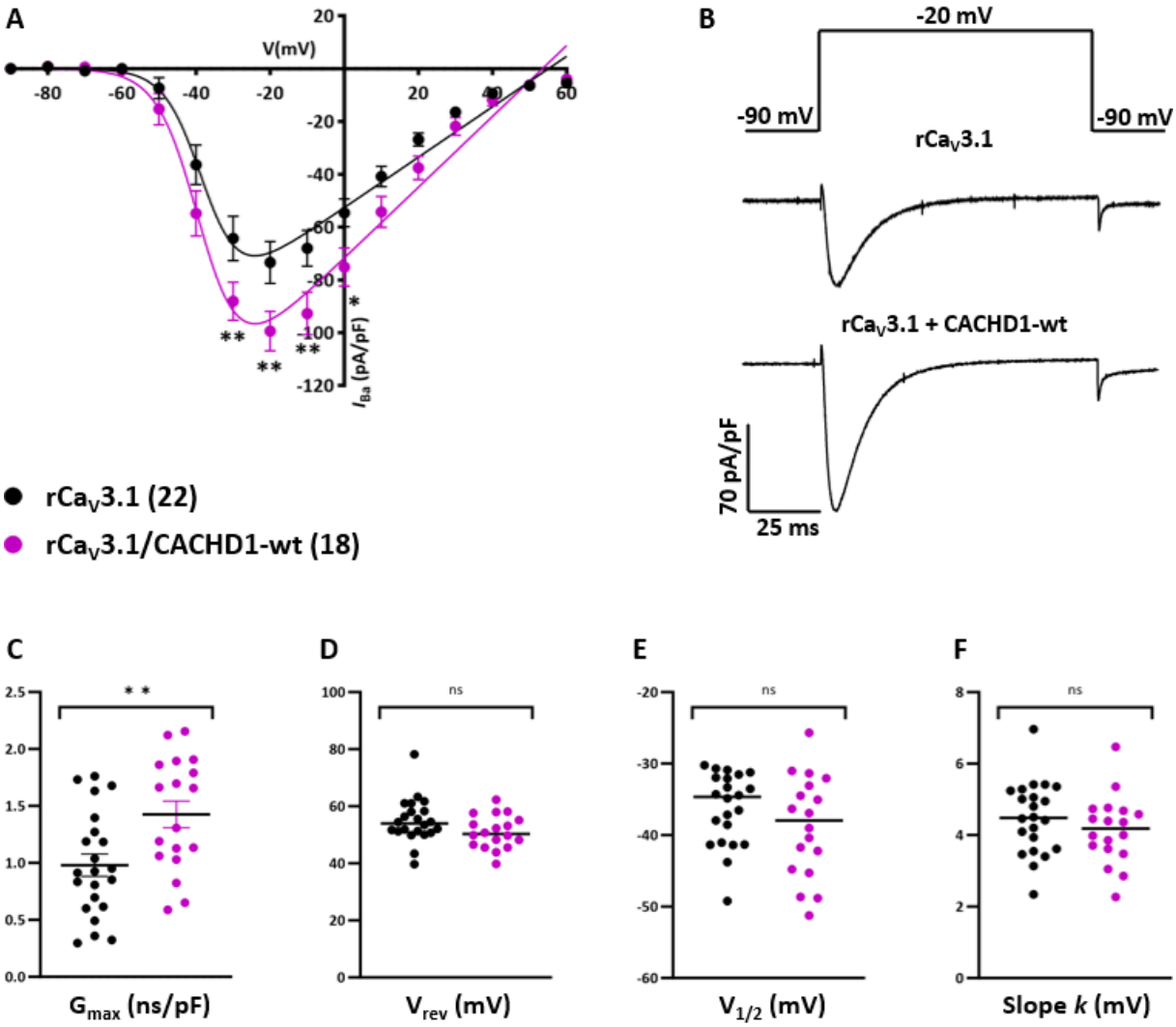

Figure 4.9 Effects of CACHD1-wt on rCa$_V$3.1 channels. CACHD1-wt significantly increased peak current density 1.36-fold as shown by **(A)** I-V relationships (holding potential -90 mV; **p* < 0.05, ***p* < 0.01; two-way ANOVA with Bonferroni *post hoc* test; curve fitted with modified Boltzmann) and **(B)** representative current density traces at -20 mV. CACHD1-wt significantly increased **(C)** maximal conductance (G_{max}) but had no effect on **(D)** reversal potential (V_{rev}), **(E)** midpoint activation ($V_{1/2}$), or **(F)** slope factor *k* (***p* < 0.01, ns – non-significant; two-tailed unpaired Student's *t* test; rCa$_V$3.1, n = 22; rCa$_V$3.1+CACHD1-wt, n = 18).

4.4.4.2 The AAA mutation in CACHD1 MIDAS motif prevents CACHD1-mediated rCa$_V$3.1 current increase, and further decreases rCa$_V$3.1 currents

Depolarisation of cells co-expressing rCa$_V$3.1 and CACHD1-AAA from holding potential of -90 mV to +60 mV showed that CACHD1-AAA MIDAS mutant abolished the CACHD1-associated rCa$_V$3.1 current increase shown in section 4.4.4.1, and further decreased rCa$_V$3.1 currents by 0.55-fold compared to rCa$_V$3.1 alone. Ba^{2+} current density was significantly lower at depolarisation steps ranging from -30 mV to 0 mV, with a peak Ba^{2+} current density at -20 mV significantly decreased from -59.2 $\pm$ 9.5 pA/pF to -32.4 $\pm$ 4.6 pA/pF (Figure 4.10A; $p < 0.0001$, two-way ANOVA with Bonferroni *post hoc* test). Representative Ba^{2+} current density traces following depolarisation from -90 mV to -20 mV are shown in Figure 4.10B. Moreover, CACHD1-AAA significantly decreased rCa$_V$3.1 G_{max} from 820 $\pm$ 120 pS/pF to 510 $\pm$ 60 pS/pF ($p < 0.05$, two-tailed unpaired Student's *t* test) but similarly to CACHD1-wt it had no significant effect on midpoint activation ($V_{1/2}$), reversal potential (V_{rev}), or slope factor *k* of rCa$_V$3.1, as shown in Figure 4.10C-F and summarised in Table 4.2. CACHD1-AAA-associated decrease in rCa$_V$3.1 T-type currents and G_{max} were caused by the mutagenesis of the key residues to alanine, and not due to any significant differences in expression levels.

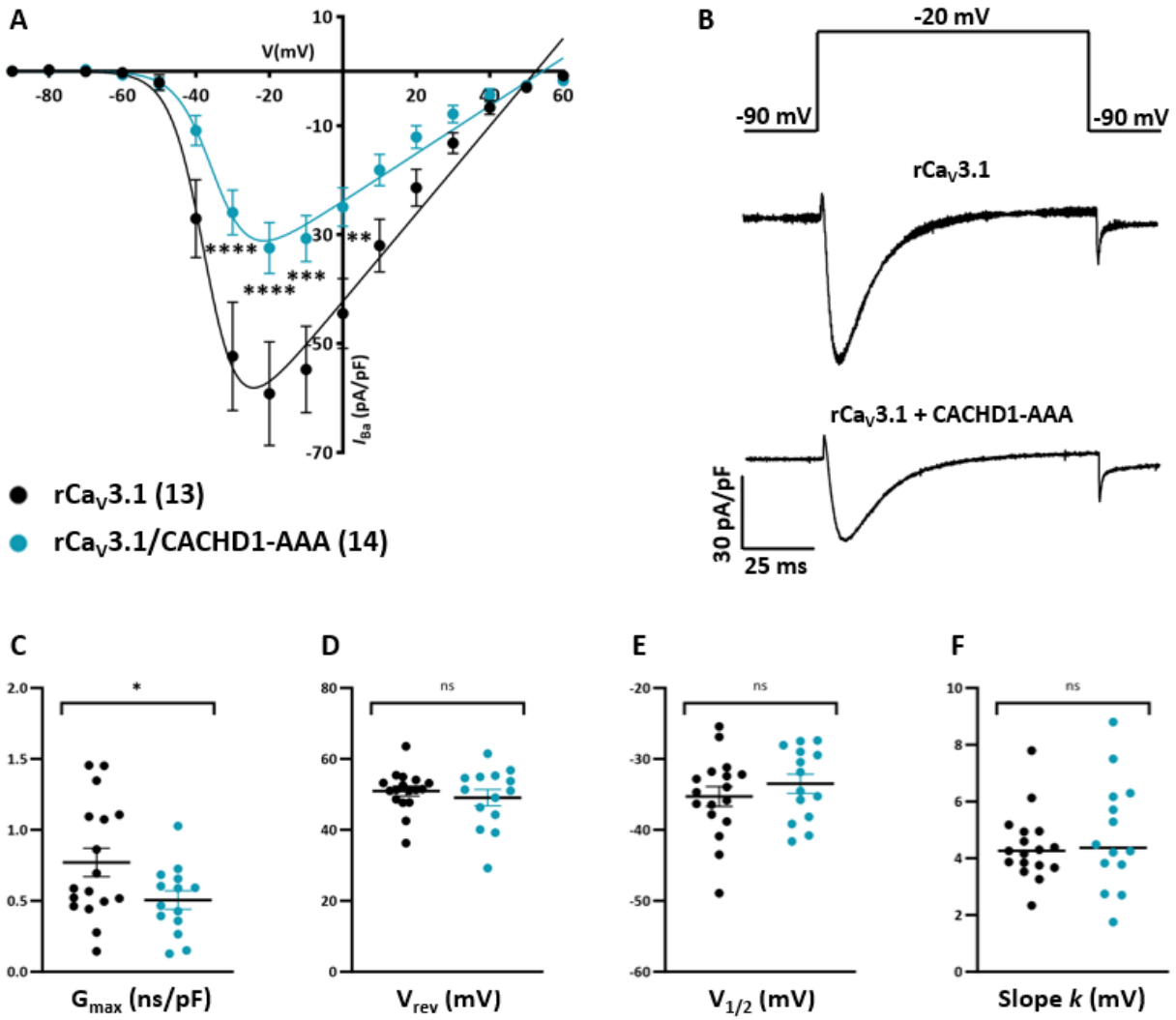

Figure 4.10 Effects of CACHD1-AAA MIDAS mutant on rCa$_V$3.1 channels. CACHD1-AAA abolished rCa$_V$3.1 current increase seen for CACHD1-wt, and significantly decreased peak current density 0.55-fold as shown by **(A)** I-V relationships (holding potential -90 mV; $^{**}p < 0.01$, $^{***}p < 0.001$, $^{****}p < 0.0001$; two-way ANOVA with Bonferroni *post hoc* test; curve fitted with modified Boltzmann) and **(B)** representative current density traces at -20 mV. CACHD1-AAA significantly decreased **(C)** maximal conductance (G_{max}) but had no effect on **(D)** reversal potential (V_{rev}), **(E)** midpoint activation ($V_{1/2}$), or **(F)** slope factor *k* ($^{*}p < 0.05$, ns – non-significant; two-tailed unpaired Student's *t* test; rCa$_V$3.1, n = 13; rCa$_V$3.1+CACHD1-wt, n = 14).

4.4.4.3 The G236S mutation in CACHD1 MIDAS motif increases rCa$_V$3.1 currents

Depolarisation of cells co-expressing rCa$_V$3.1 and CACHD1-G236S from holding potential of -90 mV to +60 mV resulted in an increase in peak current density by approx. 1.49-fold compared to cells expressing rCa$_V$3.1 alone. Ba^{2+} current density was significantly higher at depolarisation steps ranging from -30 mV to -10 mV, with a peak Ba^{2+} current density at -20 mV significantly increased from -25.8 $\pm$ 4.1 pA/pF to -38.9 $\pm$ 2.9 pA/pF (Figure 4.11A; $p < 0.001$, two-way ANOVA with Bonferroni *post hoc* test). Representative Ba^{2+} current density traces following depolarisation from -90 mV to -20 mV are shown in Figure 4.11B. Moreover, similarly to CACHD1-wt, CACHD1-G236S significantly increased rCa$_V$3.1 G_{max} from 390 $\pm$ 60 pS/pF to 580 $\pm$ 50 pS/pF ($p < 0.05$, two-tailed unpaired Student's *t* test) but had no significant effect on midpoint activation ($V_{1/2}$), reversal potential (V_{rev}), or slope factor *k* of rCa$_V$3.1, as shown in Figure 4.11C-F and summarised in Table 4.2. CACHD1-G236S-associated increase in rCa$_V$3.1 T-type currents and G_{max} were caused by the mutagenesis of the second key residue (G^{236}) to serine, and not due to any significant differences in expression levels.

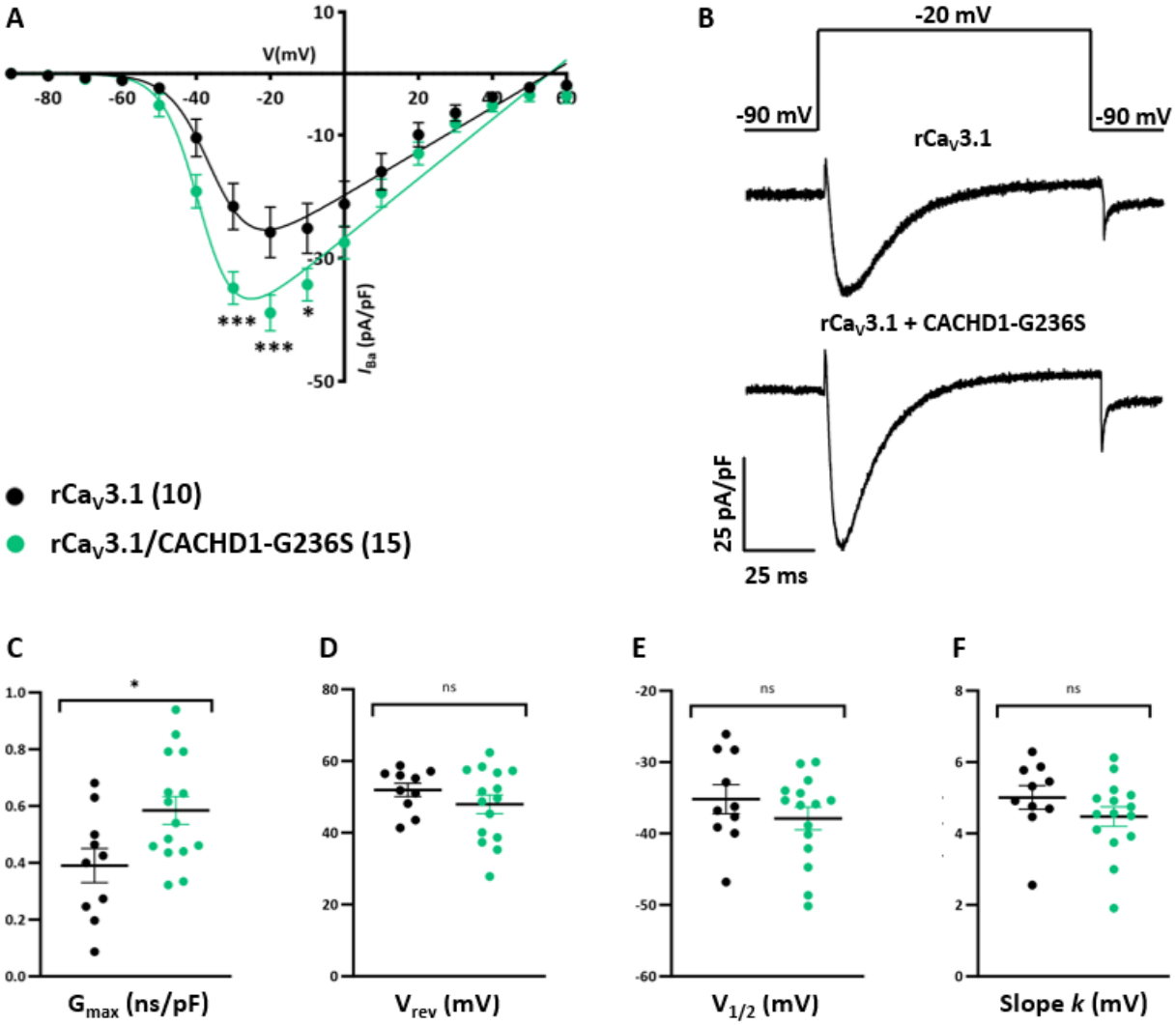

Figure 4.11 Effects of CACHD1-G236S MIDAS mutant on rCa$_V$3.1 channels. CACHD1-G236S significantly increased peak current density 1.49-fold as shown by **(A)** I-V relationships (holding potential -90 mV; *$p < 0.05$, ***$p < 0.001$; two-way ANOVA with Bonferroni *post hoc* test; curve fitted with modified Boltzmann) and **(B)** representative current density traces at -20 mV. CACHD1-G236S significantly increased **(C)** maximal conductance (G_{max}) but had no effect on **(D)** reversal potential (V_{rev}), **(E)** midpoint activation ($V_{1/2}$), or **(F)** slope factor *k* (*$p < 0.05$, ns – non-significant; two-tailed unpaired Student's *t* test; rCa$_V$3.1, n = 10; rCa$_V$3.1+CACHD1-wt, n = 15).

4.5 Discussion

α2δ subunits are well characterised modulators of HVA VGCCs. Several studies have demonstrated the MIDAS motif within their VWA domain has an important role in the function of α2δ as VGCC modulators (Cantí *et al*., 2005; Hoppa *et al*., 2012; Cassidy *et al*., 2014). CACHD1 has been classified as a member of the α2δ protein family by Whittaker and Hynes (2002), and its role as a modulator of LVA VGCCs has been described by Cottrell *et al*. (2018), showing an increase in $Ca_V3.1$-3 current densities accompanied with corresponding increases in conductance (G_{max}), as well as increased expression of $Ca_V3.1$ channels at the cell surface when co-expressed with CACHD1. Up until the study by Cottrell *et al*. (2018), there have been no known auxiliary subunits associated with the correct function of LVA VGCCs, and therefore it is important to understand what mechanisms are involved in CACHD1-associated modulation of LVA VGCCs.

In this chapter, the role of the variant MIDAS motif (DxGxS) within CACHD1 was investigated by mutating the key residues, aiming to determine whether the variant MIDAS motif has a similar role to the fully conserved MIDAS motif (DxSxS) found in α2δ subunits. Voltage patch-clamp electrophysiology was used to assess the functional effects of the mutagenesis on $rCa_V3.1$ biophysical properties, shedding light on the involvement of the variant MIDAS motif in CACHD1 modulation of LVA VGCCs.

4.5.1 TetON regulatory system is an efficient way to regulate CACHD1 protein expression levels

Building on results from Chapter 3 showing that mutagenesis of all three key residues to alanine resulted in a significant reduction in expression levels accompanied by disruption in CACHD1-AAA trafficking to cell surface, the first objective of this chapter was to normalise the expression levels of CACHD1-wt, CACHD1-AAA and CACHD1-G236S. To ensure comparable expression levels, a TetON expression system was used, enabling the investigation of MIDAS motif mutagenesis effects on $rCa_V3.1$ independently from any effects that may have been caused by the varying expression levels, especially for the CACHD1-AAA mutant.

This study demonstrated the effective regulation of CACHD1 expression levels in HEK293 cells using the TetON system, validated by western blotting and immunocytochemistry experiments which confirmed tetracycline-induced gene transcription and subsequent CACHD1 protein expression. Through a series of experiments, it was shown that Myc-tagged

CACHD1-wt, CACHD1-AAA and CACHD1-G236S were expressed only in the presence of tetracycline. Moreover, the selected clones showed similar expression levels of CACHD1-wt, CACHD1-AAA and CACHD1-G236S when treated with 1 µg/ml of tetracycline, indicating successful regulation of expression. Western blot analysis further confirmed CACHD1-wt, CACHD1-AAA and CACHD1-G236S molecular mass, ranging between 150-170 kDa, showing consistency throughout the project and with the molecular mass reported by Cottrell *et al*. (2018) and Dahimine *et al*. (2018). Additionally, assessment of sub-cellular localisation of Myc-tagged CACHD1-wt, CACHD1-AAA and CACHD1-G236S confirmed findings from Chapter 3, showing consistent expression patterns with CACHD1-wt and CACHD1-G236S present both at the cell surface and in intracellular vesicles, while CACHD1-AAA was detected exclusively in intracellular vesicles.

4.5.2 Characterisation of HA-tagged rCa$_V$3.1 protein in a heterologous expression system

The second objective of this chapter was the tagging of rCa$_V$3.1 with a HA epitope tag, aiming to facilitate better detection during expression, protein-protein interaction, and functional studies. However, the addition of an epitope tag to a protein, particularly in a complex membrane protein like rCa$_V$3.1, could interfere with protein folding, assembly, or interaction with other proteins. Such interference could lead to alterations in the biophysical properties of the rCa$_V$3.1 channel complex. Therefore, it was important to characterise and validate that any effects on rCa$_V$3.1 biophysical properties were associated with CACHD1 rather than the HA tag. Voltage patch-clamp recordings of untagged and HA-tagged rCa$_V$3.1 were carried out in culture matched experiments, and statistical analysis revealed that the HA tag had no significant impact on rCa$_V$3.1 biophysical properties, indicating that the tag itself did not interfere with channel function. Additionally, assessment of HA-rCa$_V$3.1 expression and sub-cellular localisation in transiently transfected HEK293 tsA201 cells showed rCa$_V$3.1 localisation predominantly in intracellular compartments. HA-rCa$_V$3.1 molecular mass of approx. 300 kDa was confirmed by western blotting, corresponding with Ca$_V$3.1-HA molecular mass reported by Cottrell *et al*. (2018). Several studies have used various tags to investigate the biophysical and biochemical properties of Ca$_V$3 VGCCs. For example, study by Cottrell *et al*. (2018) used a GFP and HA-tagged Ca$_V$3.1 (GFP-Ca$_V$3.1-HA), while study by Dubel *et al*. (2004) showed that adding a N-terminal GFP tag, or HA and FLAG epitope tags between the S1 and S2 transmembrane segments of Ca$_V$3.1-3 had no significant effects on channel properties. A

review by Maue (2007) further summarised the use of epitope tags to study ion channels, showing that HA tag is one of the most widely used tag that can be inserted at the N- or C-terminus, as well as within the coding region of a channel protein without significantly affecting its properties in biochemical and functional studies (Poteser *et al*., 2006). In this study, the HA tag was inserted at the N-terminus following the start codon of $rCa_V3.1$ and showed no significant effects on biophysical properties of $rCa_V3.1$ channel, corresponding with results from other studies (Dubel *et al*., 2004; Poteser *et al*., 2006). These findings combined with the results outlined in this chapter validate the reliability of the HA epitope tag for detecting $rCa_V3.1$ in biochemical experiments, including trafficking, expression, and protein-protein interaction studies.

4.5.3 Variant MIDAS motif within the VWA domain of CACHD1 is important for CACHD1 modulation of $rCa_V3.1$ channel

The study conducted by Cottrell *et al*. (2018) characterised CACHD1 as a modulator of LVA VGCCs, showing significant increase in current density and maximal conductance (G_{max}). This chapter aimed to replicate and expand upon their findings, focusing on the effects of CACHD1 on $rCa_V3.1$ channels. Here, the impact of mutagenesis in the three key residues within the variant MIDAS motif on CACHD1 function as $rCa_V3.1$ modulator were investigated to deepen the understanding of what mechanisms may be used by CACHD1 for modulation of $Ca_V3.1$ channels. As highlighted in Chapter 3, CACHD1 contains a variant MIDAS motif (DxGxS) within its VWA domain, where the second key residue is glycine instead of the serine typically found in α2δ subunits. The similarities between CACHD1 and α2δ subunits, and the characterisation of CACHD1 as a modulator of LVA VGCCs underscore the significance of understanding whether CACHD1 and α2δ subunits utilise similar modulation mechanisms, namely their MIDAS motif. Previous studies of α2δ subunits and their MIDAS motif provided the foundation for the current study, showing that amino acid substitutions in the key residues of α2δ MIDAS motif, in particular the AAA mutation where all three key residues were mutated to alanine, resulted in ablation of Ca_V1 and Ca_V2 current increases normally associated with wild type α2δ -1 and α2δ-2 subunits (Cantí *et al*., 2005; Hoppa *et al*., 2012; Cassidy *et al*., 2014). Cantí *et al*. (2005) also reported that α2δ-2-AAA mutant showed no stimulation of channel complexes co-expressed with their auxiliary subunits (e.g. $Ca_V2.2/\beta_{1b}$, $Ca_V1.2$ or $Ca_V2.1/\beta4$). Moreover, α2δ-2-AAA further reduced the current density compared to $Ca_V2.2/\beta_{1b}$ alone (Cantí *et al*., 2005).

Additionally, previous studies investigating the effects of MIDAS motif mutagenesis on other proteins showed that the key residues (DxSxS) are essential for Mn^{2+} and Mg^{2+} ion binding required for correct folding of α4β7 integrins (de Château *et al*., 2001; Chen *et al*., 2003; Yu *et al*., 2012), and ligand binding in integrin β1 subunit (Mould *et al*., 2002; Valdramidou *et al*., 2008). In addition to the effects on protein folding, MIDAS motif has been shown to be important for the physiological function of other proteins. Mutations in the MIDAS motif of β2 integrin (D^{134}LSYS) resulted in nonfunctional β2 integrins Mac-1 and LFA-1, leading to leukocyte adhesion deficiency (Hogg *et al*., 1999). Study by Valdramidou *et al*. (2008) showed that mutations of the MIDAS motif (D^{130}xSxS) present in the βI domain of integrin α2β1 completely blocked collagen binding to α2β1, while highlighting the importance of an intact MIDAS motif for the interaction between αI and βI domains of α2β1. Moreover, mutation of the D^{130} residue to alanine (D130A) resulted in nonfunctional integrins (Valdramidou *et al*., 2008). In addition to integrins, a recent study by Sacharok et al., (2023) reported that *Kingella kingae* bacteria require an intact MIDAS motif for bacterial adherence, showing that mutating the key residues to alanine (D^{90}xSxS ⇔ AxAxA) led to significant disruption in binding to epithelial cells and extracellular matrix proteins.

In this study, the effects of CACHD1 MIDAS motif mutants (CACHD1-AAA and CACHD1-G236S) on rCa_V3.1 currents were investigated, aiming to understand CACHD1 modulatory mechanisms. Cottrell *et al*. (2018) reported that α2δ-1 had no significant effects on Ca_V3.1 currents or any other biophysical properties of the channels; however, while it appears that CACHD1 and α2δ subunits may not modulate the same VGCCs, they likely share common interaction mechanisms with their respective VGCCs. The MIDAS motif appears to play an equally important role in CACHD1 as previously reported for α2δ, as supported by the results presented in this chapter. Here, CACHD1-wt was found to significantly increase rCa_V3.1 current density by 1.36-fold compared to rCa_V3.1 alone, while also increasing maximal conductance (G_{max}). These results correspond with the findings reported by Cottrell *et al*. (2018) where CACHD1-wt significantly increased Ca_V3.1 currents and G_{max}. Next, the CACHD1-AAA, similarly to α2δ-2-AAA, abolished the observed rCa_V3.1 current increase induced by CACHD1-wt, and even further reduced rCa_V3.1 current density by 0.55-fold compared to rCa_V3.1 alone, while also reducing G_{max}. These results mirror the effects seen for α2δ-2, where the α2δ-2-AAA significantly reduced current density compared to $Ca_V2.2/\beta_{1b}$ alone (Cantí *et al.*, 2005). On another hand, CACHD1-G236S did not disrupt CACHD1 modulatory function.

CACHD1-G236S resulted in rCa$_V$3.1 current density and G_{max} increase (1.49-fold) similar to CACHD1-wt (1.36-fold), showing that the G^{236} residue can be substituted for serine without affecting CACHD1 modulation of rCa$_V$3.1. Both CACHD1-wt and CACHD1-G236S resulted in a significant increase in rCa$_V$3.1 currents in cells treated with tetracycline in comparison to rCa$_V$3.1 expressed in non-induced cells, further confirming CACHD1 as a modulator of Ca$_V$3.1 channels as previously reported by Cottrell *et al*. (2018) and Stephens and Cottrell (2019). The observed increase could be caused by more Ba^{2+} entering the cell because the same number of channels allowed more ions through. Additionally, the significant difference observed for rCa$_V$3.1 currents in the presence of CACHD1 further confirms successful regulation of CACHD1 expression using the TetON system. These results also indicate that CACHD1 variant MIDAS motif functions similarly to the fully conserved MIDAS motif found in α2δ subunits.

A plausible hypothesis, based on the ability of CACHD1 to promote Ca$_V$3.1 cell surface expression (Cottrell *et al*., 2018), is that the higher current density associated with CACHD1-wt and CACHD1-G236S may result from an increased number of rCa$_V$3.1 channels present at the cell surface. This hypothesis is supported by previous findings suggesting that α2δ-mediated current increase may be linked to enhanced forward trafficking of VGCCs complexes to cell surface (Barclay *et al*., 2001; Hendrich *et al*., 2008). On the other hand, further investigation into the effects of CACHD1 on single-channel conductance could provide additional insights and confirm this theory, as previous work on α2δ subunits showed that α2δ-1 and α2δ-2 subunits have no effects on single-channel conductance (Barclay *et al*., 2001; Hendrich *et al*., 2008). These studies suggest that α2δ-associated current increases are due to enhanced forward trafficking of Ca$_V$1 and Ca$_V$2 channels to cell surface (Barclay *et al*., 2001; Hendrich *et al*., 2008). It is important to consider the possibility that CACHD1 and α2δ subunits function in a similar way, which would indicate that both CACHD1-wt and CACHD1-G236S may contribute to enhanced rCa$_V$3.1 expression at the cell surface, explaining the elevated rCa$_V$3.1 current increase.

4.5.4 Conclusion

In conclusion, this study further emphasised the importance of the variant MIDAS motif in CACHD1 on its function as a modulator of $rCa_V3.1$ channels. Mutagenesis of all three key residues to alanine (CACHD1-AAA) not only abolished the current increase associated with wild-type CACHD1, but further reduced current density and maximal conductance of $rCa_V3.1$, showing similar effects to those reported for $\alpha2\delta$-2-AAA/$Ca_V2.2/\beta_{1b}$ (Cantí *et al.*, 2005). On the other hand, mutating only the second key residue to serine (CACHD1-G236S) resulted in $rCa_V3.1$ current and maximal conductance increase comparable with the increase associated with CACHD1-wt. The findings suggest that the variant MIDAS motif in CACHD1 functions similarly to the fully conserved MIDAS motif found in $\alpha2\delta$ subunits, and CACHD1 and $\alpha2\delta$ subunits may utilise the same mechanisms for modulation of their respective VGCCs.

4.6 Future work

The findings in this chapter show the importance of key residues within the MIDAS motif of CACHD1 on its function as a modulator of $rCa_V3.1$ T-type VGCCs; however, further experiments are required to gain deeper understanding of the mechanisms behind CACHD1 modulatory function. There are several experiments that could be considered, and they are outlined in the following sections.

4.6.1 Single-channel conductance

As previously discussed, investigating the effects of CACHD1 and its MIDAS mutants on single-channel conductance could shed more light on the mechanisms involved in CACHD1 modulation of Ca_V3 channels. If CACHD1-wt or its MIDAS mutants showed no effects on single-channels conductance, it would support the theory that CACHD1-wt and CACHD1-G236S modulate $rCa_V3.1$ current increase by promoting $rCa_V3.1$ expression at the cell surface. This would also further support the hypothesis that CACHD1 and $\alpha2\delta$ subunits may utilise the same mechanisms for modulation of their representative VGCCs.

To measure single-channel conductance, voltage patch-clamp electrophysiology can be used as described in sections 2.5.3 and 4.3.3. However, instead of using whole-cell configuration where the cell membrane is ruptured by applying suction (Figure 2.4), a cell-attached configuration is used instead. In this configuration, the recording electrode is attached to cell membrane, allowing the measurement of Ba^{2+} currents for individual channels without interference from the intracellular environment.

4.6.2 Trafficking and protein interaction studies

It has been shown that CACHD1-wt and $Ca_V3.1$ are in close proximity (Cottrell *et al*., 2018), but it is not known if this is the case for CACHD1-AAA and CACHD1-G236S. The effects caused by the AAA mutation showed significant disruptive effects on CACHD1 function as a modulator of $rCa_V3.1$, while also resulting in reduced protein expression levels and disrupted trafficking to cell surface as shown in Chapter 3. These effects warrant further investigation into the interaction between $rCa_V3.1$ and CACHD1-AAA to determine how these two proteins interact and where the interaction takes place within a cell. There are several experiments that could be considered, including cell surface biotinylation of CACHD1+$rCa_V3.1$ expressing cells that would show how CACHD1-wt and its MIDAS mutants affect the levels of $rCa_V3.1$ channels expressed at the cell surface. Another experiment is a proximity ligation assay (PLA) that could determine where within a cell CACHD1 interacts with $rCa_V3.1$, and whether CACHD1-AAA causes intracellular retention of $rCa_V3.1$, leading to subsequent reduction in $rCa_V3.1$ currents. Furthermore, cell surface PLA could provide insights into CACHD1-$rCa_V3.1$ interactions specifically at the cell surface, while whole cell PLA could detect any interactions occurring inside the cell, including those in various cellular compartments. CACHD1-AAA does not traffic to cell surface, and it significantly reduces $rCa_V3.1$ currents. Whole cell PLA could reveal whether its effects on $rCa_V3.1$ are due to $rCa_V3.1$ intracellular retention resulting from CACHD1-AAA-$rCa_V3.1$ interaction inside the cell. Additionally, investigation of sub-cellular localisation and trafficking of $rCa_V3.1$ in the absence and presence of CACHD1-wt or MIDAS mutants could further deepen our understanding of CACHD1-$Ca_V3.1$ interaction.

4.6.3 Functional studies in native tissues

In this study, heterologous expression systems were used to study CACHD1 modulation of $rCa_V3.1$. As highlighted in Chapter 3, these systems are useful for initial studies, but the findings may not fully translate to native physiological conditions. Therefore, further investigations of the effects associated with MIDAS motif mutagenesis in native expression systems, such as SH5YSY neuronal cell line or native neurons could provide a more comprehensive understanding into the role of the MIDAS motif in CACHD1 function as a Ca_V3 channel modulator.

4.6.4 Animal studies

Furthermore, Prof. Patel has recently provided CACHD1 knockout mice that offer a valuable resource for investigating the role of CACHD1 in cellular and physiological processes, and

disease pathology. Electrophysiological recordings from knockout mice could reveal how CACHD1 deletion affects synaptic transmission and neuronal excitability associated with Ca_V3 VGCCs. Techniques such as patch-clamp or multi-electrode array analysis of brain slices and native neurons could be used to understand the effects of CACHD1 deletion, and the potential effects of reintroducing CACHD1 via transfection in neurons. Reintroduction of CACHD1 into these neurons may help understand if and how transiently transfected CACHD1 can mitigate any inhibitory effects resulting from endogenous CACHD1 deletion.

5. INVESTIGATING THE ROLE OF THE C-TERMINAL TAIL IN THE TRAFFICKING OF THE Ca_V3 CALCIUM CHANNEL AUXILIARY SUBUNIT, CACHD1

5.1 Introduction

The movement of membrane proteins is regulated through various intricate pathways within cells, divided into two basic pathways – endocytosis and exocytosis. The endocytic pathway facilitates the internalisation of cargo from cell surface into intracellular compartments, and the exocytic pathway transports cargo from intracellular compartments to cell surface, ensuring turnover and replenishment of membrane components (Wu *et al*., 2014). Together, these pathways help in maintaining cellular homeostasis and response to extracellular stimuli. Here, the endocytic pathway and its components will be discussed in more detail.

5.1.1 The endocytic pathway

Endocytosis is a fundamental cellular process that governs the entry of macromolecules into cells. For membrane proteins it involves internalisation at the plasma membrane and subsequent post-endocytic processing. Proteins present at the plasma membrane either remain at the membrane or undergo internalisation into coated pits and vesicles (Goldstein *et al*., 1979; Sorkina *et al*., 2005), with numerous studies describing the role of endocytic pathway in this process (Goldstein *et al*., 1979; Marks *et al*., 1996; Bonifacino and Dell'gelica, 1999; Bonifacino and Traub, 2003). Following internalisation, membrane proteins undergo degradation by lysosomes (von Zastrow and Sorkin, 2007) or are recycled back to plasma membrane via process called retro-endocytosis (Deng *et al*., 2001; Pandey *et al*., 2002). Two primary endocytic pathways are usually involved in the internalisation of membrane proteins, namely clathrin-mediated endocytosis, and caveolae-dependent endocytosis.

Clathrin-mediated endocytosis (Figure 5.1) is a well-established internalisation pathway used by many membrane receptors and proteins (Bonifacino and Traub, 2003; Ungewickell and Hinrichsen, 2007; Antonescu *et al*., 2009), and involves the short-sequence signal motifs recognition by adaptor protein-2 (AP-2) that also binds clathrin (Traub, 2003). During clathrin-mediated endocytosis, a clathrin-coated pit is formed by invagination and separation from the plasma membrane, resulting in the formation of a clathrin-coated vesicle. The vesicle then undergoes scission through the mechanochemical activity of the scission GTPase, dynamin

(Sauvonnet *et al*., 2005), which constricts the neck of the vesicle, leading to subsequent detachment from the plasma membrane.

Caveolae-dependent endocytosis (Figure 5.1) is involved in the internalisation of various proteins, for example transforming growth factor-β (TGF-β), integrins, and adenosine receptors (Gines *et al*., 2001; Di Guglielmo *et al*., 2003; Sharma *et al*., 2005). Caveolae, composed of caveolin and cavin proteins, serve as docking sites for intracellular signalling networks (Gines *et al*., 2001; Di Guglielmo *et al*., 2003; Sharma *et al*., 2005). Similarly to clathrin-coated pits, caveolae are created by plasma membrane invagination (Parton, 2018). The functionality of caveolae largely depends on the lipid cluster structure of membrane lipids, particularly cholesterol which promotes caveolae-dependent endocytosis (Choudhury *et al*., 2006). Caveolae-dependent endocytosis, like clathrin-mediated endocytosis, uses dynamin to constrict the neck of the caveolae (Shajahan *et al*., 2004). Even though there is limited similarity between clathrin and caveolae-dependent pathways, the *Src*-dependent phosphorylation of dynamin residues (Y^{231} and Y^{597}) enhances dynamin assembly, which can in turn facilitate both internalisation pathways (Shajahan *et al*., 2004). Additionally, a dynamin-related ATPase, EH-domain-containing protein 2 (EHD2), contributes to membrane fission leading to separation of caveolae from the plasma membrane (Rennick *et al*., 2021).

The plasma membrane contains various types of microdomains, and caveolae are thought to form from specialised microdomains within the plasma membrane with the help of caveolin proteins (Pani and Singh, 2010). These dynamic microdomains, known as lipid rafts, are rich in cholesterol, glycosphingolipids and glycerophospholipids (Anderson, 1998; Kurzchalia and Parton, 1999; Simons and Toomre, 2000). They are thought to originate from regions of the membrane characterised by a liquid-ordered phase consisting mainly of saturated sphingolipids, which floats within a liquid-disordered phase predominantly made up of unsaturated glycerophospholipids that are stabilised by cholesterol (Anderson, 1998; Pike *et al*., 2002). Lipid rafts are involved in many different cellular processes, including cell adhesion, membrane trafficking and signal transduction by facilitating the segregation and sorting of proteins into different cellular compartments (Simons and Toomre, 2000; Pike, 2006; Patel *et al*., 2008). Additionally, lipid rafts are involved in the endocytosis of GPI-anchored proteins, such as α2δ, through the invagination of rafts into endocytic vesicles. These vesicles are then transported to early endosomes and processed through late endosomal pathways, such as the Rab11a-dependent recycling pathway for α2δ subunits (Tran-Van-Minh and Dolphin, 2010).

Furthermore, the presence of raft-like domains in late endosomes indicates that these microdomains may also form from the endocytosis of plasma membrane rafts via both clathrin-dependent and clathrin-independent pathways (Pani and Singh, 2010).

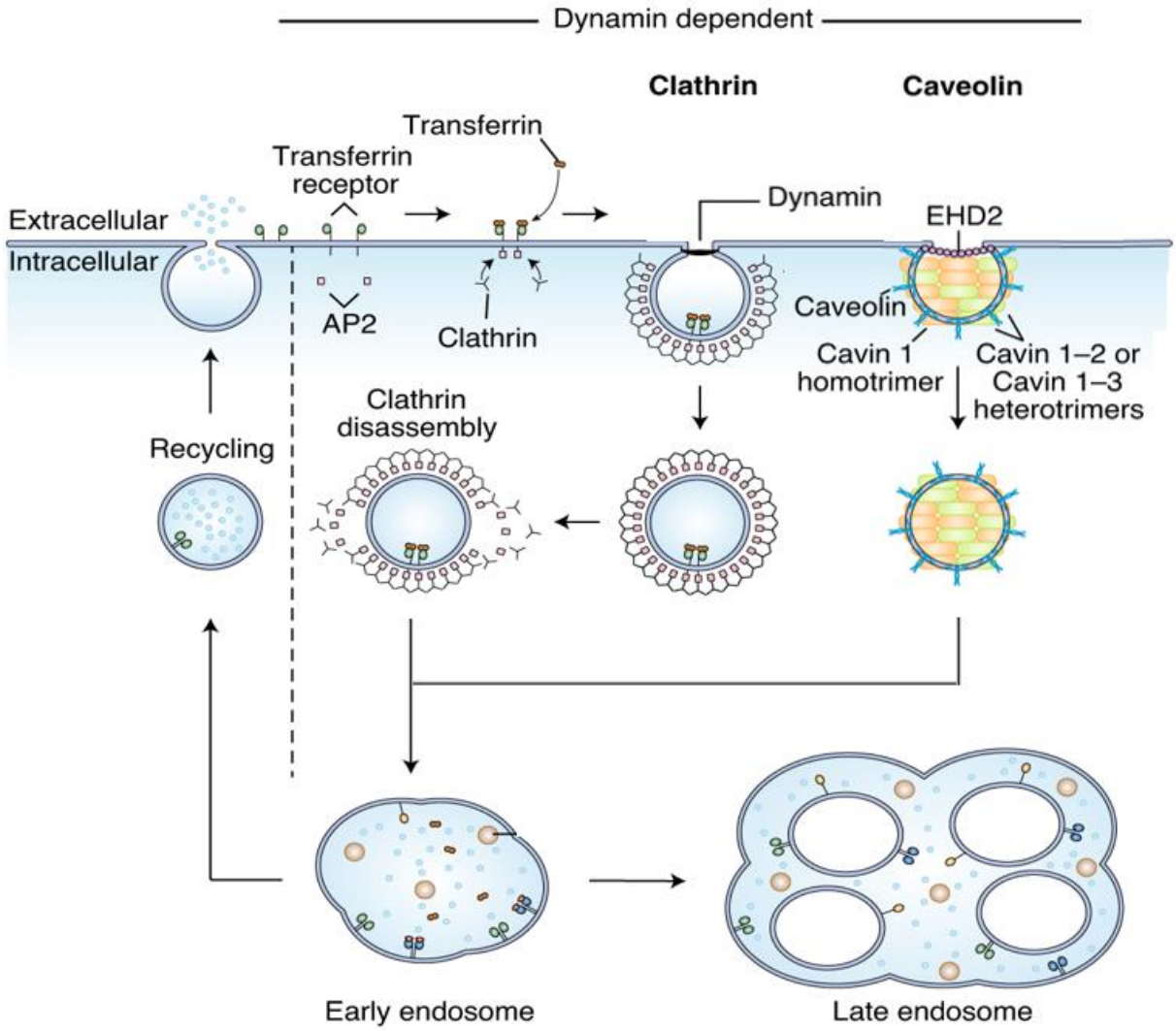

Figure 5.1 Clathrin and caveolae dependent endocytic pathways. Clathrin-mediated endocytosis is driven by the adaptor complex, AP-2, that recruits clathrin to cytosolic receptor domains, initiating the formation of clathrin-coated pit and subsequent clathrin-coated vesicle. Clathrin-coated vesicle undergoes scission by dynamin, leading to detachment from the plasma membrane. Clathin coat is disassembled, and the vesicle is targeted to early endosomes. Formation of caveolae is dependent on caveolin and cavin proteins. Caveolin, a structural protein, coats the caveolae. Cavin 1-3 proteins contribute to oligomerisation of caveolin proteins and facilitate their incorporation into the caveolar membrane, thus improving structural integrity of caveolae. EH-domain-containing protein 2 (EHD2) stabilises and constricts the neck of the caveolae leading to separation of caveolae from the plasma membrane. (Adapted from: Rennick *et al*., 2021).,

5.1.2 Short-sequence signal motifs

Complex trafficking mechanisms, such as the clathrin-mediated and caveolae-dependent endocytosis, are directed by a set of short-signal sequence motifs commonly found in the cytoplasmic domains of membrane proteins. Several studies have demonstrated the importance of the C-terminal domain in mediating internalisation and post-endocytic sorting to intracellular compartments in various membrane proteins, facilitated by the short-signal sequence motifs (Bonifacino and Dell'gelica, 1999; Miranda *et al*., 2001; Brothers *et al*., 2002; Bonifacino and Traub, 2003). These motifs typically consist of short linear sequences of conserved amino acids (Bonifacino and Traub, 2003; Kozik *et al*., 2010), with one to three residues crucial for the motif function, often represented by bulky hydrophobic amino acids. An early study described two major classes of short-signal sequence motifs commonly utilised by membrane proteins for endocytosis and post-endocytic sorting, namely tyrosine and di-leucine based signals (Bonifacino and Dell'gelica, 1999). Here, the tyrosine-based signals are discussed in more detail.

The tyrosine-based signal motifs consist of YXXϕ residues, where Y is the tyrosine residue, X is any amino acid, and ϕ is an amino acid with a large bulky hydrophobic side chain (Pandey, 2009). They are usually located at the C-terminal tail, approximately 6-8 amino acids from the transmembrane domain (Rohrer *et al*., 1996; Bonifacino and Traub, 2003). The YXXϕ motifs direct membrane proteins internalisation and sorting by interacting with adaptor protein complexes AP-1, AP-2, AP-3, and AP-4 (Hirst *et al*., 2001; Bonifacino and Traub, 2003), providing critical trafficking and sorting information. In the YXXϕ signal motif, the Tyr residue serves as the critical residue because of its phenolic hydroxyl group that is required for generation of endocytic and sorting signals (Pandey, 2009). Several studies have demonstrated the importance of YXXϕ signal motifs in protein internalisation; for example, YSGL motif in the chemokine-CXCR3 receptor protein regulates internalisation (Meiser *et al*., 2008) and YKKL motif in the GPCR protease-activated receptor 1 (PAR-1) mediates constitutive internalisation in a clathrin- and dynamin-dependent mechanism (Paing *et al*., 2004).

5.1.3 Rab protein network

The intricate process of transporting proteins between intracellular compartments involves a series of meticulously coordinated steps. Initially, proteins are selected and segregated by adaptor proteins, forming complexes that are encapsulated within a clathrin-coated pits or caveolae. This is followed by dynamin scission that leads to the formation of a transport vesicle that is navigated towards their target compartments or membranes, guided by protein complexes that work in conjunction with Rab GTPases (Yarwood *et al*., 2020). The regulation of these steps is associated with the Rab family of small GTPases, which cycle between active (GTP-loaded) and inactive (GDP-loaded) states (Hutagalung and Novick, 2011; Homma *et al*., 2021), and localise to early, late, and recycling endosomes via their prenylated C-terminal group (Martínez-Morales *et al*., 2022). Approximately 60 Rab proteins have been identified (Hutagalung and Novick, 2011; Homma *et al*., 2021), each playing distinct roles in vesicle formation, translocation, anchoring and fusion during endocytic transport (Figure 5.3; Grant and Donaldson, 2009). Here, the focus is on the role of Rab proteins in protein internalisation and recycling, particularly Rab5 and Rab11.

Rab5, associated with early endosomes (Yuan and Song, 2020), facilitates the internalisation and sorting of various proteins, including many GPCRs, for example, the dopamine D2 receptors (De Vries *et al*., 2019), the cannabinoid receptor 2 (Grimsey *et al*., 2011), and the FFA1 and FFA4 receptors (Qian *et al*., 2014; Flores-Espinoza *et al*., 2020). Proteins within early endosomes can undergo processing via different trafficking pathway. As endosomes mature, Rab5 is replaced by Rab7, a marker for late endosomes, which directs proteins towards degradation pathways within lysosomes (Wartosch *et al*., 2015). However, some endocytic cargo can avoid the degradation pathway through protein recycling to cell surface, resulting from the formation of intermediate vesicles that separate from the endosomes and are directed towards the membrane (Cullen and Steinberg, 2018). The recycling process involves a rapid recycling associated with Rab4 (van der Sluijs *et al*., 1992) or a slow indirect route through recycling endosomes associated with Rab11 (Goldenring, 2015). Rab11, localised at the trans-Golgi network, post-Golgi vesicles, and recycling endosomes, serves as an important intersection between endocytic and exocytic trafficking pathways (Welz *et al*., 2014).

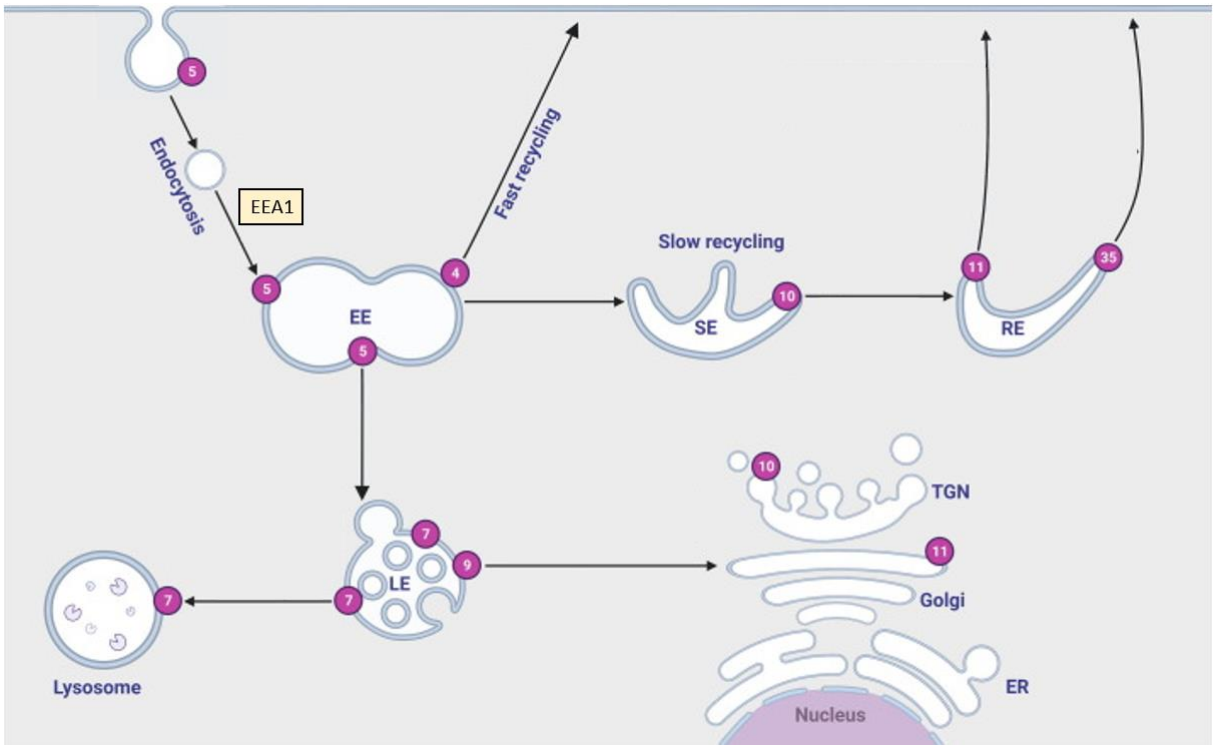

Figure 5.2 Rab GTPases are molecular switches for endocytic trafficking. Rab4 medicates fast endocytic recycling directly from the early endosome to the plasma membrane. Rab5, which is localized to the early endosome, mediates endosomal fusion of clathrin-coated vesicles and the maturation of early endosomes. Rab11 and Rab35 regulate the slow endocytic recycling (that delivers the cargo back to the cell surface) through recycling endosomes. Rab7 modulates the transport from late endosomes to lysosomes. Rab9 functions in the pathway from late endosomes to the Golgi apparatus. Rab10 is localized to sorting endosomes and operates in the route from sorting endosomes to recycling endosomes. EE: early endosome; SE: sorting endosome; RE: recycling endosome; LE: late endosome; TGN: trans-Golgi network; ER: endoplasmic reticulum. (Adapted from: Zhang *et al*., 2022).

5.1.4 CACHD1 and α2δ subunits

CACHD1 is a relatively unstudied protein and current research focuses on its functional effects on LVA VGCCs and its potential role in disease; however, at present, no studies have investigated the trafficking or processing of CACHD1. Given the lack of available data, it is imperative to consider any studies investigating the trafficking of α2δ subunits. An initial study by Tran-Van-Minh and Dolphin (2010) demonstrated constitutive endocytosis and recycling of α2δ-2 to be dependent on Rab11a. This study showed that cell surface localisation of α2δ -2 was increased by recycling through Rab11a-associated endosomes back to plasma membrane, while in the presence of a dominant-negative mutant Rab11a(S25N), which inhibits Rab11a-dependent recycling (Eisfeld *et al*., 2011), the cell surface expression of α2δ-2 was reduced. Subsequent research showed Rab11a-dependent recycling increased α2δ-1 at the cell surface, associated with an increase in forward trafficking of $Ca_V2.2$ VGCCs; by contrast, Rab11a-dependent recycling had no effects on α2δ-3 cell surface expression levels (Meyer and Dolphin, 2021), suggesting that α2δ-3 recycling and cell surface expression are not mediated by the same endosomal recycling pathway. Additionally, while α2δ-1 intracellular levels were reduced in the presence of Rab11a(S25N) mutant, it had no effect on α2δ-3 expression levels (Meyer and Dolphin, 2021), suggesting that blocking of the Rab11a-dependent recycling pathway may result in re-routing of α2δ-1 to degradation pathways. Moreover, considering α2δ subunits are GPI-anchored proteins (Davies *et al*., 2010; Wu *et al*., 2016), these results indicate the possibility of an adaptor protein that bridges the interaction between α2δ subunits and intracellular trafficking pathways. A study by Kadurin *et al*. (2017), investigated LRP1 (low density lipoprotein (LDL) receptor-related protein-1) as a potential linker between α2δ subunits and intracellular trafficking pathways. LRP1 was investigated because of its involvement in forward trafficking of other GPI-anchored proteins, such as prion protein (PrP) (Parkyn *et al*., 2008) and in clathrin-mediated endocytosis (Lillis *et al*., 2008; Fuentealba *et al*., 2010). The results showed that α2δ-1 acts as a ligand for LRP1, and their interaction is modulated by receptor-associated protein (RAP) (Kadurin *et al*., 2017). However, whether α2δ-1 uses clathrin or caveolae-dependent endocytic pathways remains to be determined, as LRP1 has been shown to be recruited to caveolae (Zhang *et al*., 2004) and play role in caveolae (Taylor and Hooper, 2007) and clathrin-mediated endocytosis (Lillis *et al*., 2008; Fuentealba *et al*., 2010).

5.2 Objective

Unlike α2δ subunits, which are GPI-anchored proteins, CACHD1 is predicted to be a transmembrane protein. Transmembrane proteins are often internalised via clathrin-mediated or caveolae-dependent endocytic pathways, utilising tyrosine-based YXXϕ signal motifs for protein internalisation and post-endocytic sorting.

Sequence analysis of CACHD1 revealed the presence of a putative YXXϕ endocytic motif (termed tyrosine internalisation motif, TyrIM) within its intracellular C-terminal tail, (Y^{1197}STM), suggesting a potential role in mediating CACHD1 endocytosis and post-endocytic sorting. This chapter aimed to address several objectives, as outlined below:

- The first objective was to characterise constitutive internalisation of CACHD1.
- The second objective was to determine if CACHD1 uses clathrin-mediated or caveolae-dependent endocytic pathways.
- The third objective was to characterise the interaction of CACHD1 with Rab proteins, specifically Rab5 and Rab11, as well as early endosomal antigen-1 (EEA1), an early endosomal Rab5 effector protein associated with the docking of incoming endocytic vesicles before fusion with early endosomes.
- The fourth objective was to determine if CACHD1 internalisation and processing are facilitated by its putative TyrIM.
- The final objective was to determine the role of the C-terminal tail and the transmembrane domain of CACHD1 in protein internalisation.

5.3 Experimental approach

5.3.1 Endocytosis assay design

A general trafficking assay was designed and optimised during this study based on the requirements for different experiment. Any modifications are described in the appropriate sections. Depending on the experiment, transiently and stably expressing HEK293 cells were used.

HEK293 cells were seeded onto coverslips (1-2x10^5 cell/well density; 12-well plate) and allowed to attach at 37°C 5% CO_2 overnight. The subsequent steps were performed on ice or at 4°C where possible. Cells were washed 3x with DPBS+CM to remove any residual serum, and live-labelled with appropriate primary antibodies in DMEM 0.1% BSA for 1 h. Cells were then washed again with DPBS+CM and incubated at 37°C 5% CO_2 for 0-4 h to allow for protein internalisation. At each timepoint, cells were washed with ice cold DPBS+CM and fixed with 4% PFA at 4°C for 20 min. Following fixation, the protocol for fixed cell labelling outlined in section 2.3.5 was used and all subsequent steps were performed at room temperature. Briefly, cells were washed with a blocking buffer (3x 5 min), incubated with appropriate secondary antibodies, and imaged using epifluorescence (x40 objective) or confocal microscopy (x100 objective).

5.3.2 Constitutive internalisation of CACHD1

HEK293 Flp-In™ T-REx™ cells stably expressing Myc-CACHD1-wt and rabbit anti-Myc primary antibodies were used.

5.3.3 Endocytosis inhibition studies

HEK293 Flp-In™ T-REx™ cells stably expressing Myc-CACHD1-wt were used. Before immunolabelling, cells were pretreated with DMEM 0.1% BSA (control), 400 mM sucrose, 5 mM methyl-β-cyclodextrin (MβCD), or 30 µg/ml nystatin (all diluted in DMEM 0.1% BSA) for 1 h at 37°C. For cholesterol recovery experiments, following treatment, cells were washed with DPBS+CM (3x) to remove all inhibitors. Cells were then allowed to incubate in DMEM 0.1% BSA at 37°C 5% CO_2 for 0-2 h to allow for cholesterol replenishment at the plasma membrane through cholesterol synthesis. The trafficking assay outlined in section 5.3.1 was then carried out, using rabbit anti-Myc primary antibodies.

Sucrose (400 mM) was used as an inhibitor for the clathrin-mediated endocytic pathway. Sucrose is known to disrupt the formation of clathrin-coated pits at the plasma membrane, thus inhibiting the clathrin-mediated endocytosis (Im *et al*., 2011).

MβCD (5 mM) and nystatin (30 μg/ml) were used as inhibitors of the caveolae-dependent endocytic pathway. MβCD and nystatin inhibit caveolae pathway through cholesterol disruption. MβCD strips cholesterol from membrane, while nystatin forms complexes with cholesterol, disrupting the lipid composition and integrity of caveolae (Zhu *et al*., 2010; Harvey and Calaghan, 2014), thus inhibiting the caveolae-dependent endocytosis.

5.3.4 Characterisation of CACHD1 post-endocytic sorting via the Rab protein network

HEK293 Flp-In™ T-REx™ cells stably expressing Myc-CACHD1-wt were used. The cells were further transiently transfected with pEGFP-C1-dRab5 or pEGFP-C1-dRab11 constructs and allowed to grow for 48 h before performing the trafficking assay. Here, the timepoints were changed to 0, 15, 30 and 60 min.

For co-localisation studies with endogenous early endosomal antigen-1 (EEA1), following fixation with 4% PFA, cells were additionally labelled with mouse anti-EEA1 primary antibodies. For co-localisation studies with dRab5 (dog Rab5) and dRab11 (dog Rab11), no additional primary antibodies were used due to their GFP tags.

5.3.5 Determining the role of Tyrosine internalisation motif in CACHD1 trafficking

Sequence analysis of CACHD1 revealed the presence of a putative YXXϕ endocytic motif (termed tyrosine internalisation motif, TyrIM) within its intracellular C-terminal tail, (Y^{1197}STM). Mutations of the Tyr residue to Ala or Phe was shown to increase cell surface expression associated with impaired or slower rate of internalisation of H^+/K^+-ATPase (Courtois-Coutry *et al*., 1997), PAR-1 (Pain *et al*., 2004), and LRP (Li *et al*., 2000) proteins. Here the Tyr1197 residue was mutated to Ala or Phe to determine the role of the YSTM signal motif in CACHD1 internalisation (Figure 5.3).

5.3.5.1 Mutagenesis of TyrIM in CACHD1

A two-step Q5 DNA polymerase PCR approach was used to generate both CACHD1 TyrIM mutants (Figure 5.4). Initially, forward primers containing the mutations were used in the first PCR reaction, generating PCR fragments that were then used as megaprimers in the subsequent PCR reaction. The PCR products and pcDNA5/FRT-Myc-CACHD1 construct were digested with *Nsi* I + *Apa* I restriction enzymes. 2-way ligation was then used to ligate all fragments together, resulting in the final constructs pcDNA5/FRT-Myc-CACHD1-Y1197A and pcDNA5/FRT-Myc-CACHD1-Y1197F.

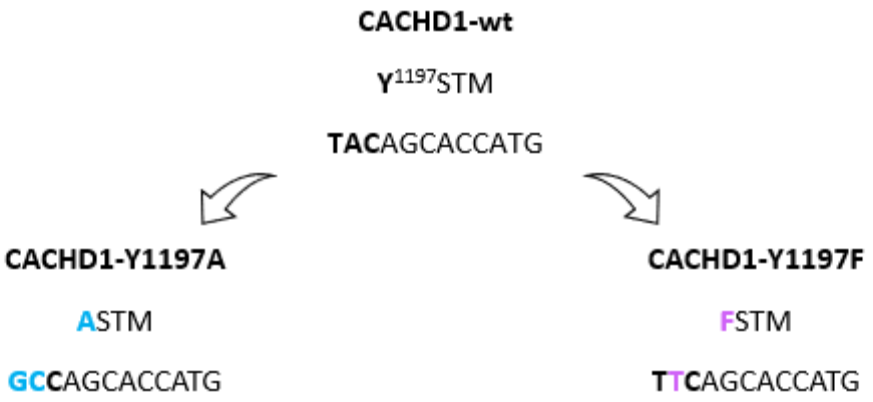

Figure 5.3 Amino acid modifications of the Y1197 residue in the TyrIM motif of CACHD1 by site-directed mutagenesis. Q5 DNA polymerase PCR method was used to generate two CACHD1 TyrIM mutants. For the first mutant termed CACHD1-Y1197A, the Tyr residue was mutated to alanine (Y1197A). For the second mutant termed CACHD1-Y1197F, the Tyr residue was mutated to phenylalanine (Y1197F).

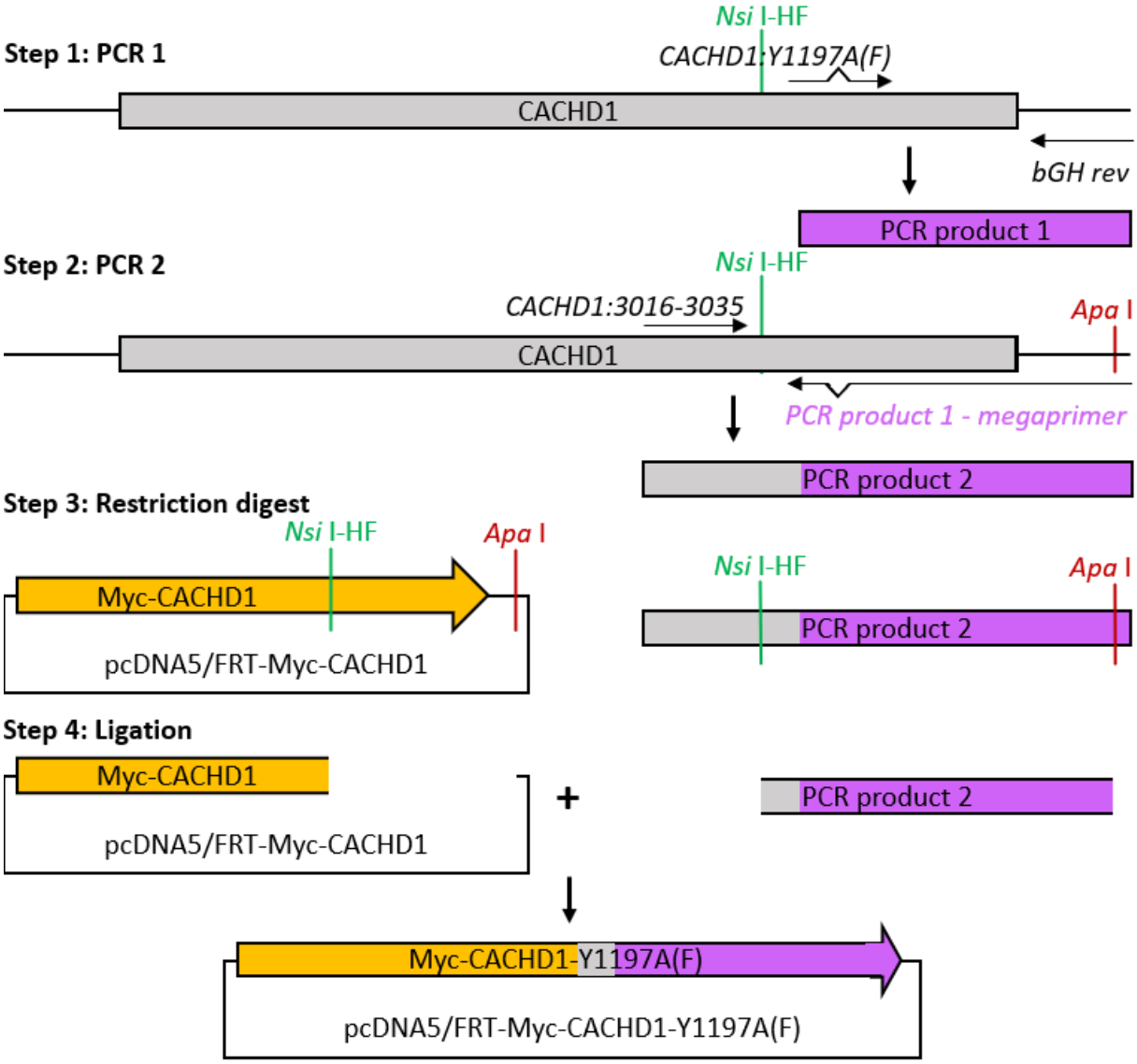

Figure 5.4 Cloning procedure for CACHD1 tyrosine internalisation motif site-directed mutagenesis. A two-step PCR strategy was used to obtain CACHD1 containing a Y1197A/F mutation. First, CACHD1:Y1197A(F) and bGHrev primers were used to generate a PCR fragment containing the Y1197A/F mutation. Second PCR was performed using CACHD1:3016-3035 forward primer and the PCR product as a reverse megaprimer to generate PCR fragment containing the Y1197A/F mutation and *Nsi* I and *Apa* I restriction sites. *Nsi* I-HF and *Apa* I restriction enzymes were used to digest the second PCR product and a pcDNA5/FRT-Myc-CACHD1 construct to introduce single-stranded overhangs (sticky ends) that were ligated with T4 DNA ligase to generate the final pcDNA5/FRT-Myc-CACHD1-Y1197A/F construct.

5.3.5.2 Characterisation of TyrIM mutant expression in HEK293 cells

HEK293 tsA201 were transiently transfected with pcDNA5/FRT (control), pcDNA5/FRT-Myc-CACHD1-wt, pcDNA5/FRT-Myc-CACHD1-Y1197A or pcDNA5/FRT-Myc-CACHD1-Y1197F and allowed to grow for 48 h before analysis.

The expression and sub-cellular localisation were determined using western blotting, densitometry and immunocytochemistry as described in sections 2.2.11, 2.2.13 and 2.3, respectively. To determine the effects of the Y1197A/F mutations on CACHD1 expression at the cell surface, cell surface biotinylation assay, and live and fixed cell labelling were used as described in sections 2.2.4, 2.3.4 and 2.3.5, respectively.

Cell surface and total protein expression levels were determined by densitometry analysis of appropriate immunoblots as described in section 2.2.13. For each sample lane, the signal of CACHD1 protein band was normalised to the corresponding β-actin or TFR (loading controls) protein band signal, resulting in a sample/control ratio. This process was repeated for at least two separate images of the same blot captured at 10-60 s intervals (technical repeats), and an average of the sample/control ratios was obtained, representing one biological repeat for each sample (e.g. Myc-CACHD1-wt, Myc-CACHD1-AAA and Myc-CACHD1-G236S). The cell surface data were then normalised to total expression by dividing the sample/control ratio value for cell surface expression by the sample/control ratio value for total expression levels. The raw data were statistically analysed by one-way ANOVA with Tukey's *post hoc* test (normally distributed) or Kruskal-Wallis test with Dunn's *post hoc* test (not normally distributed). The data were then normalised to CACHD1-wt, where CACHD1-wt expression was considered as 100%, and representative graphs with mean ± SEM were plotted using GraphPad Prism. Significant changes were indicated at $p < 0.05$.

The effects of the Y1197A and Y1197F mutations on CACHD1 constitutive internalisation were then determined using the endocytosis assay outlined in section 5.3.1.

5.3.6 Determining the roles of the transmembrane domain and C-terminal tail in CACHD1 trafficking

Previous studies have shown the importance of the C-terminal tail in mediating internalisation in various membrane proteins, often facilitated by the short-signal sequence motifs (Bonifacino and Dell'gelica, 1999; Miranda *et al*., 2001; Brothers *et al*., 2002; Bonifacino and Traub, 2003). Here, two truncated version of CACHD1 were generated – first mutant where the C-terminal tail only was removed (CACHD1ΔH1122-C1274), and a second mutant where the C-terminal tail and the transmembrane domain were removed (CACHD1ΔV1096-C1274). Avi and 12His tags were added to this mutant for future ligand-binding studies.

5.3.6.1 Mutagenesis of C-terminal tail in CACHD1

To generate the first truncated version of CACHD1, the C-terminal tail was removed by Q5 PCR method (Figure 5.5). A reverse primer was used to introduce a stop codon and an *Apa* I restriction site after the I1131 residue of Myc-CACHD1. The PCR product and pcDNA5/FRT-Myc-CACHD1 construct were digested with *Eco* RV-HF + *Apa* I restriction enzymes. 2-way ligation was then used to ligate all fragments together, resulting in the final pcDNA5/FRT-Myc-CACHD1-TMD construct.

To generate the second truncated version of CACHD1, the C-terminal tail and the transmembrane domain were removed by 2-step Q5 PCR method (Figure 5.6) Reverse primer was used to remove the transmembrane domain and add a stop codon and an Avi tag after the P1105 residue. The second PCR was used to add the 12His tag and introduce an *Apa* I restriction site to PCR1 product. The PCR2 product and pcDNA5/FRT-Myc-CACHD1 construct were digested with *Eco* RV-HF + *Apa* I enzymes. 2-way ligation was then used to ligate all fragments together, resulting in the final pcDNA5/FRT-Myc-CACHD1-trunc-Avi-GG-12His construct.

All final constructs were sequenced to confirm successful truncation of CACHD1 and sequence identity.

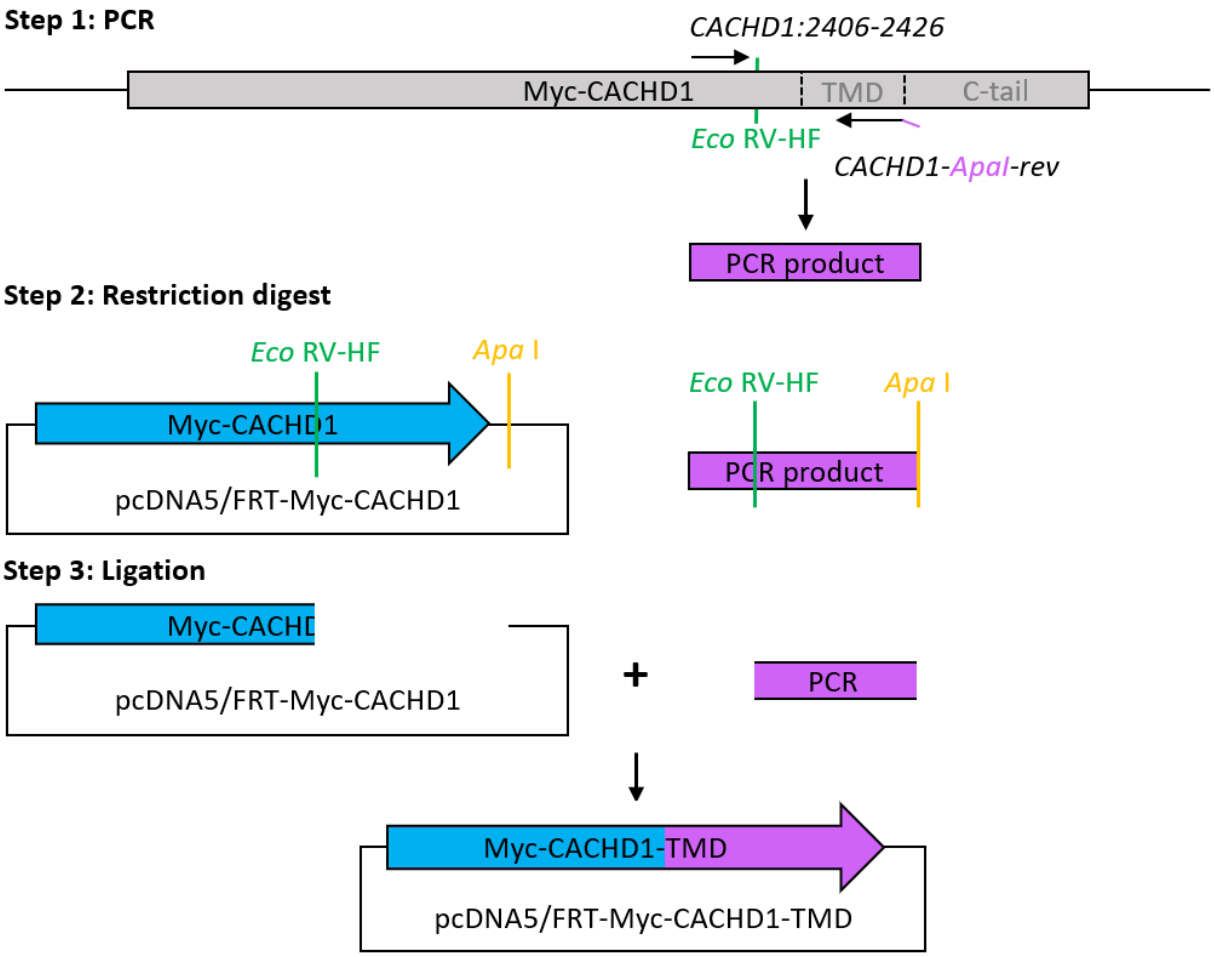

Figure 5.5 Cloning procedure for the generation of a truncated CACHD1 protein without its intracellular C-terminal tail. CACHD1:2406-2426 and CACHD1-ApaI-rev primers were used to introduce and *Apa* I restriction site after the transmembrane domain of CACHD1. The PCR product and pcDNA5/FRT-Myc-CACHD1 were digested with *Eco* RV-HF and *Apa* I restriction enzymes to introduce blunt end at the *Eco* RV site and a single-stranded overhang (sticky end) at the *Apa* I site. DNA fragments were ligated with T4 DNA ligase to generate the final pcDNA5/FRT-Myc-CACHD1-TMD construct. TMD – transmembrane domain.

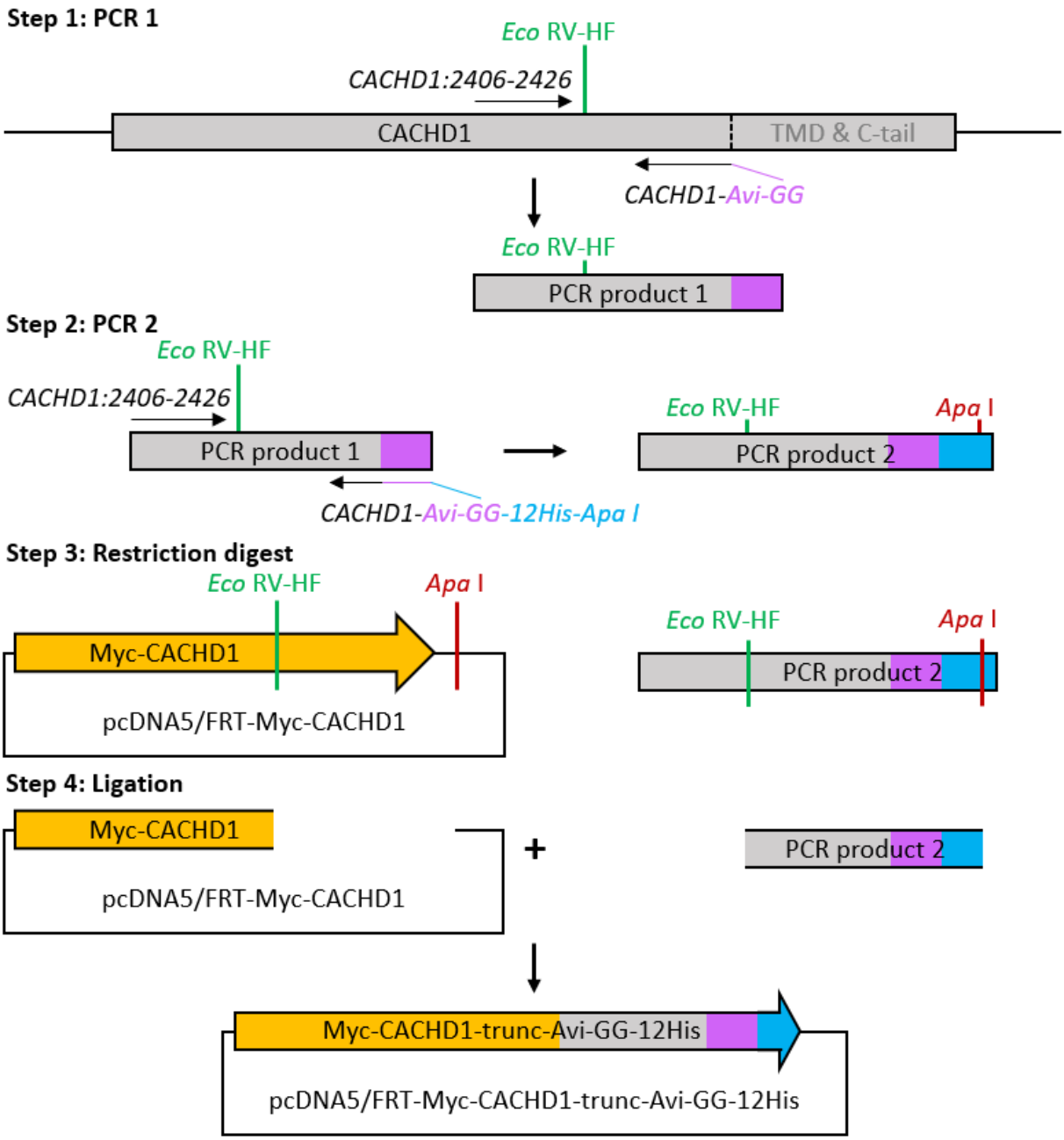

Figure 5.6 Cloning procedure for the generation of a truncated CACHD1 protein without its intracellular C-terminal tail and transmembrane domain. A two-step PCR strategy was used to obtain a truncated CACHD1 without the transmembrane domain and C-terminal tail. Using CACHD1 wild type as a template, CACHD1:2406-2426 and CACHD1-Avi-GG primers were used to truncate CACHD1 and introduce an Avi tag. The PCR product was then used as a template for the second PCR, where CACHD1-Avi-GG-12His-ApaI reverse primer was used to introduce a 12-histidine tag and an *Apa* I restriction site. *Eco* RV-HF and *Apa* I restriction enzymes were used to digest the second PCR product and a pcDNA5/FRT-Myc-CACHD1 construct to introduce blunt end at *Eco* RV site and a single-stranded overhang (sticky end) at the *Apa* I site. The digested fragments were then ligated with T4 DNA ligase to generate the final pcDNA5/FRT-Myc-CACHD1-trunc-Avi-GG-12His construct.

5.3.6.2 Characterisation of truncated CACHD1 variants in HEK293 cells

HEK293 tsA201 were transiently transfected with pcDNA5/FRT (control), pcDNA5/FRT-Myc-CACHD1-wt, pcDNA5/FRT-Myc-CACHD1-TMD or pcDNA5/FRT-Myc-CACHD1-trunc-Avi-GG-12His and allowed to grow for 48 h before analysis.

The expression and sub-cellular localisation were determined using western blotting and immunocytochemistry as described in sections 2.2.11 and 2.3, respectively. To determine the effects of truncation on CACHD1 expression at the cell surface, live and fixed cell labelling with rabbit and mouse anti-Myc antibodies were used as described in sections 2.2.4, 2.3.4 and 2.3.5, respectively. The effects of the truncation on CACHD1 constitutive internalisation were then determined using the endocytosis assay outlined in section 5.3.1.

5.4 Results

5.4.1 CACHD1 constitutively traffics from cell surface to intracellular compartments

To characterise constitutive trafficking of Myc-CACHD1, stably expressing HEK293 cells were live-labelled with rabbit anti-Myc primary antibody. Using live cells enabled specific labelling of proteins present at the cell surface, allowing the observation of protein movement over time. Following incubation at 37°C for 0-4 h, the localisation of immunoreactive Myc-CACHD1 was determined using immunofluorescence and confocal microscopy. As shown in Figure 5.7, initially (0 h timepoint), Myc-CACHD1 was localised exclusively at the cell surface. In contrast, at subsequent 1, 2 and 4 h timepoints, Myc-CACHD1 was detected in intracellular vesicles, indicating Myc-CACHD1 internalisation. Interestingly, at the 4 h timepoint, less CACHD1 appeared to be localised to intracellular vesicles, suggesting the possibility of CACHD1 recycling and transport back to cell surface as part of its constitutive trafficking pathway.

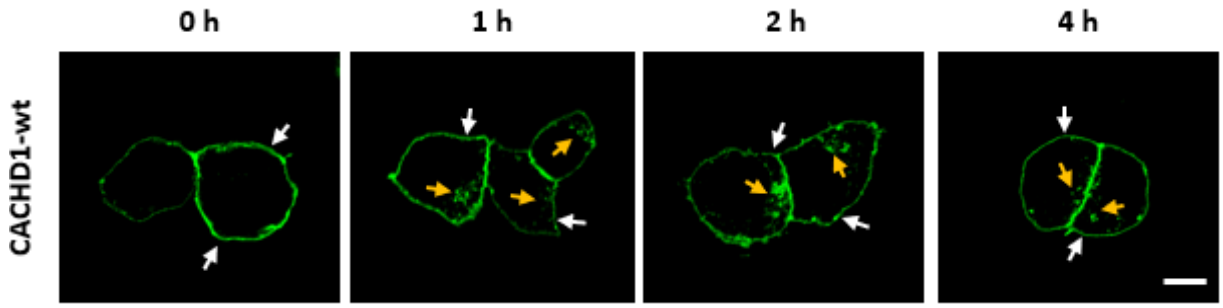

Figure 5.7 Constitutive trafficking of Myc-CACHD1 in stably expressing HEK293 cells. Stable HEK293 cells expressing Myc-CACHD1 were plated on poly-D-lysine coated coverslips and incubated overnight. Cells were labelled live with a rabbit anti-Myc antibody at 4°C, incubated in DMEM 0.1% BSA at 37°C for 0 h, 1 h, 2 h or 4 h, fixed with 4% PFA at 4°C, and labelled with Alexa Fluor™ 488 secondary antibody. Immunoreactive Myc-CACHD1 was detected exclusively at the cell surface at 0 h, and at the cell surface (white arrows) and in intracellular compartments (yellow arrows) at 1, 2 and 4 h, showing CACHD1 internalisation. (Scale bar 10 µm, n = 5).

5.4.2 CACHD1 internalisation is inhibited by MβCD, but can be rescued by cholesterol recovery

The next steps aimed to determine the endocytic pathway utilised by CACHD1. Two main pathways were investigated, specifically the clathrin-mediated and caveoale-dependent endocytosis, by using 400 mM sucrose, 5 mM MβCD, and 30 µg/ml nystatin as inhibitors, respectively. Following treatment with these inhibitors, stably expressing HEK293 cells were live-labelled, and incubated at 37°C for 0-4 h. Untreated cells served as control for CACHD1 constitutive trafficking. The impact of sucrose, MβCD, and nystatin were assessed using confocal microscopy.

Figure 5.8A shows that at 0 h, immunoreactive Myc-CACHD1 was localised exclusively at the cell surface in all cells (untreated and treated). Similar to untreated cells, Myc-CACHD1 underwent endocytosis in cells treated with 400 mM sucrose, as early as 1 h post-treatment, indicating clathrin-independent CACHD1 internalisation. In contrast, 5 mM MβCD inhibited CACHD1 internalisation at 1 and 2 h timepoints. However, by the 4 h timepoint, some internalisation was observed, although less pronounced compared to control and sucrose-treated cells. These results indicate that CACHD1 may utilise the MβCD-sensitive endocytosis pathway.

Subsequent experiments were carried out using nystatin (30 µg/ml), another caveolae pathway inhibitor. Surprisingly, unlike MβCD, nystatin did not inhibit CACHD1 internalisation, showing similar internalisation pattern as observed in untreated cells (Figure 5.8B). These results contradict the effects observed for MβCD; however, the reason for these discrepancies between two different cholesterol depleting agents remains unclear.

Another experiment where the cholesterol levels were allowed to recover post-treatment with 5 mM MβCD was carried out by incubating cells in DMEM 0.1% BSA for 0-2 h, and the effects were assessed by confocal microscopy. Interestingly, even brief cholesterol recovery (1 h) partially reversed the inhibition of CACHD1 internalisation caused by MβCD, with normal levels of CACHD1 internalisation observed after 2 h of cholesterol recovery (Figure 5.9), indicating that CACHD1 endocytosis may primarily rely on cholesterol.

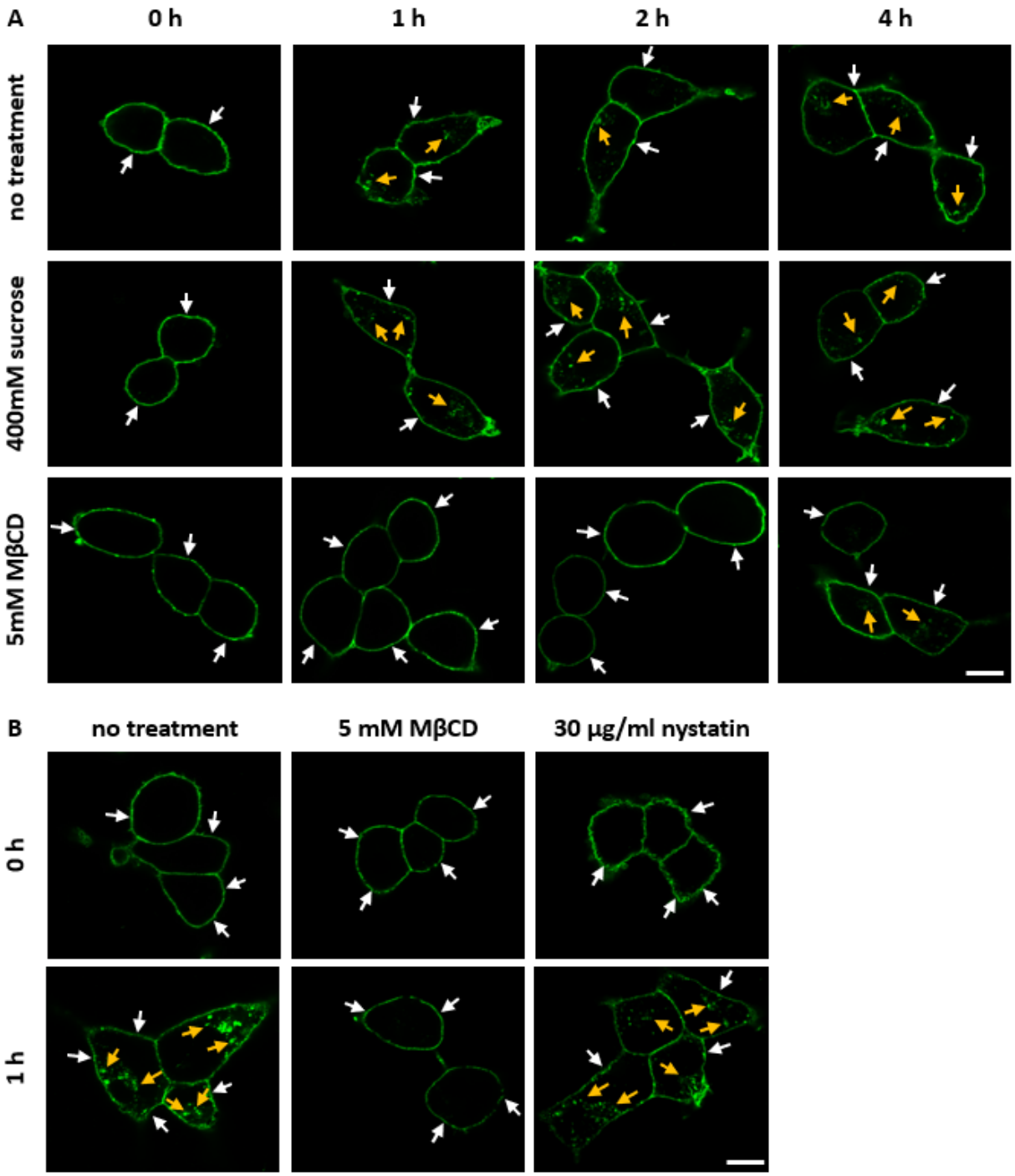

Figure 5.8 Inhibition of clathrin-mediated and caveolae-dependent endocytosis in stable HEK293 cells. Stable HEK293 cells expressing Myc-CACHD1 were plated on poly-D-lysine coated coverslips and incubated overnight. Cells were then treated with 400 mM sucrose, and 5 mM MβCD or 30 µg/ml nystatin (clathrin/caveolae pathway inhibitors, respectively) in DMEM + 0.1% BSA at 37°C for 1 h. Untreated cells were used as control. Cells were labelled live with a rabbit anti-Myc antibody at 4°C, incubated in DMEM 0.1% BSA at 37°C for 0 h, 1 h, 2 h or 4 h, fixed with 4% PFA at 4°C, and labelled with Alexa Fluor ™ 488 secondary antibody. **(A)** Immunoreactive Myc-CACHD1 was detected exclusively at the cell surface (white arrows) in control and treated cells at 0 h. At 1, 2 and 4 h, immunoreactive Myc-CACHD1 was detected in intracellular compartments (yellow arrows) of control cells and cells treated with 400 mM sucrose. Conversely, in cells treated with 5 mM MβCD, Myc-CACHD1 internalisation did not occur until 4 h post-treatment. (Scale bar 10 µm, n = 5). **(B)** Immunoreactive Myc-CACHD1 was detected at the cell surface in all cells at 0 h, and at cell surface and in intracellular compartments in untreated cells and cells treated with 30 µg/ml nystatin at 1 h, while showing no internalisation in cells treated with 5 mM MβCD at 1 h. (Scale bar 10 µm, n = 3).

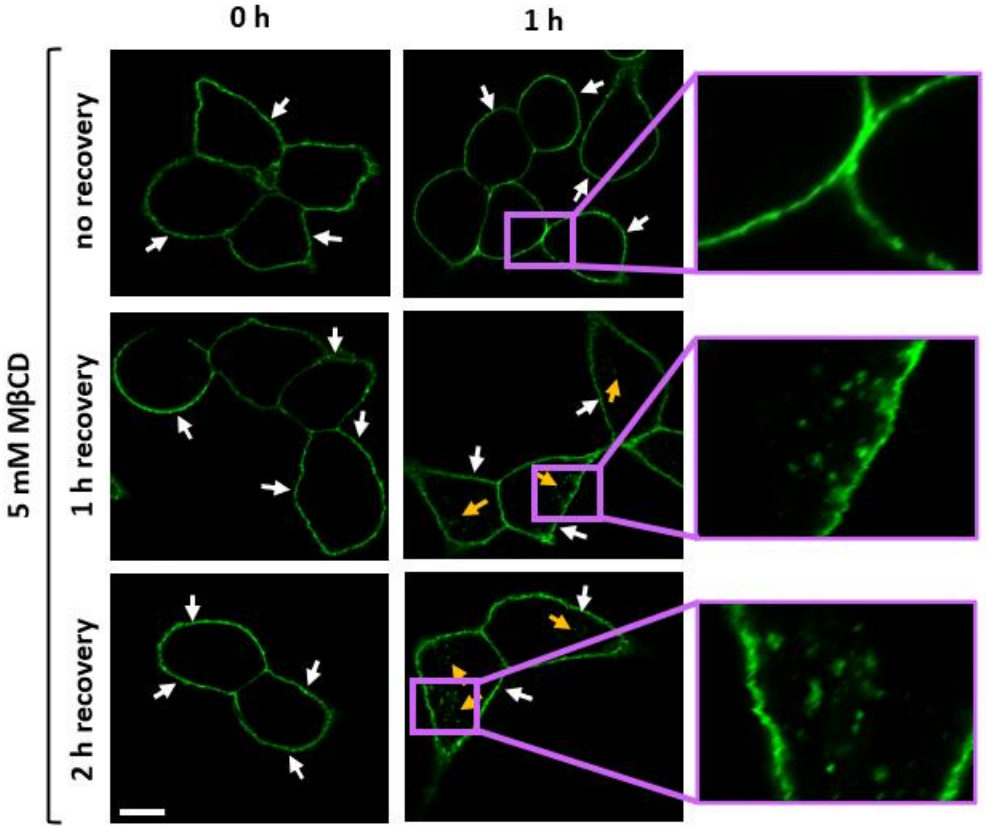

Figure 5.9 Cholesterol recovery reversed MβCD-associated CACHD1 endocytosis inhibition. Stable HEK293 cells expressing Myc-CACHD1 were plated on poly-D-lysine coated coverslips and incubated overnight. Cells were then treated with 5 mM MβCD in DMEM + 0.1% BSA at 37°C for 1 h. Cells were washed with DPBS+CM and cholesterol was allowed to recover in DMEM 0.1% BSA for 0-2 h. Cells without recovery period were used as control. Cells were then labelled live with a rabbit anti-Myc antibody at 4°C, incubated in DMEM 0.1% BSA at 37°C for 0 or 1 h, fixed with 4% PFA at 4°C, and labelled with Alexa Fluor™ 488 secondary antibody. Immunoreactive Myc-CACHD1 was detected exclusively at the cell surface (white arrows) in all cells at 0 h. At 1 h, immunoreactive Myc-CACHD1 was detected in intracellular compartments (yellow arrows) of all cells that underwent cholesterol recovery, while control cells showed no Myc-CACHD1 internalisation. (Scale bar 10 µm, n = 3).

5.4.3 CACHD1 is processed through Rab protein network

In addition to characterisation of endocytic pathway, the endosomal processing of CACHD1 was investigated in stable HEK293 cells. Co-localisation of CACHD1 with endosomes was determined by confocal microscopy.

HEK293 cells expressing Myc-CACHD1 were used to determine CACHD1/EEA1 interaction. Cells were labelled live with rabbit anti-Myc antibody and incubated at 37°C for 0-60 min. After fixation with 4% PFA cell were additionally labelled with mouse anti-EEA1 antibody. Figure 5.10 shows immunoreactive Myc-CACHD1 expressed at the cell surface at 0 h, with subsequent internalisation at 15, 45 and 60 min. Immunoreactive EEA1 was detected inside the cells at all timepoints. Co-localisation of Myc-CACHD1 with EEA1 occurred as early as 15 min post-incubation with anti-Myc antibody.

To determine CACHD1/Rab5 and CACHD1/Rab11 interactions, HEK293 cells stably expressing Myc-CACHD1 were transiently transfected with pEGFP-C1-dRab5 or pEGFP-C1-dRab11 plasmid. Following transfection, cells were labelled live with rabbit anti-Myc antibody and incubated at 37°C for 0-60 min. To note, additional labelling with anti-Rab5 or Rab11 antibodies was not required due to their GFP tags. Figures 5.11-12 show immunoreactive Myc-CACHD1 expressed exclusively at the cell surface at 0 h, and immunofluorescent dRab5 and dRab11 expressed inside the cells at all timepoint. Myc-CACHD1 internalisation was detected at 15, 30 and 60 min, with CACHD1/Rab5 and CACHD1/Rab11 co-localisation evident as early as 15 min post-incubation.

These results indicate CACHD1 internalisation at early timepoints, with its post-endocytic processing mediated through endosomal protein network, particularly involving EEA1, Rab5 and Rab11 that are indicative of early sorting and recycling endosomes.

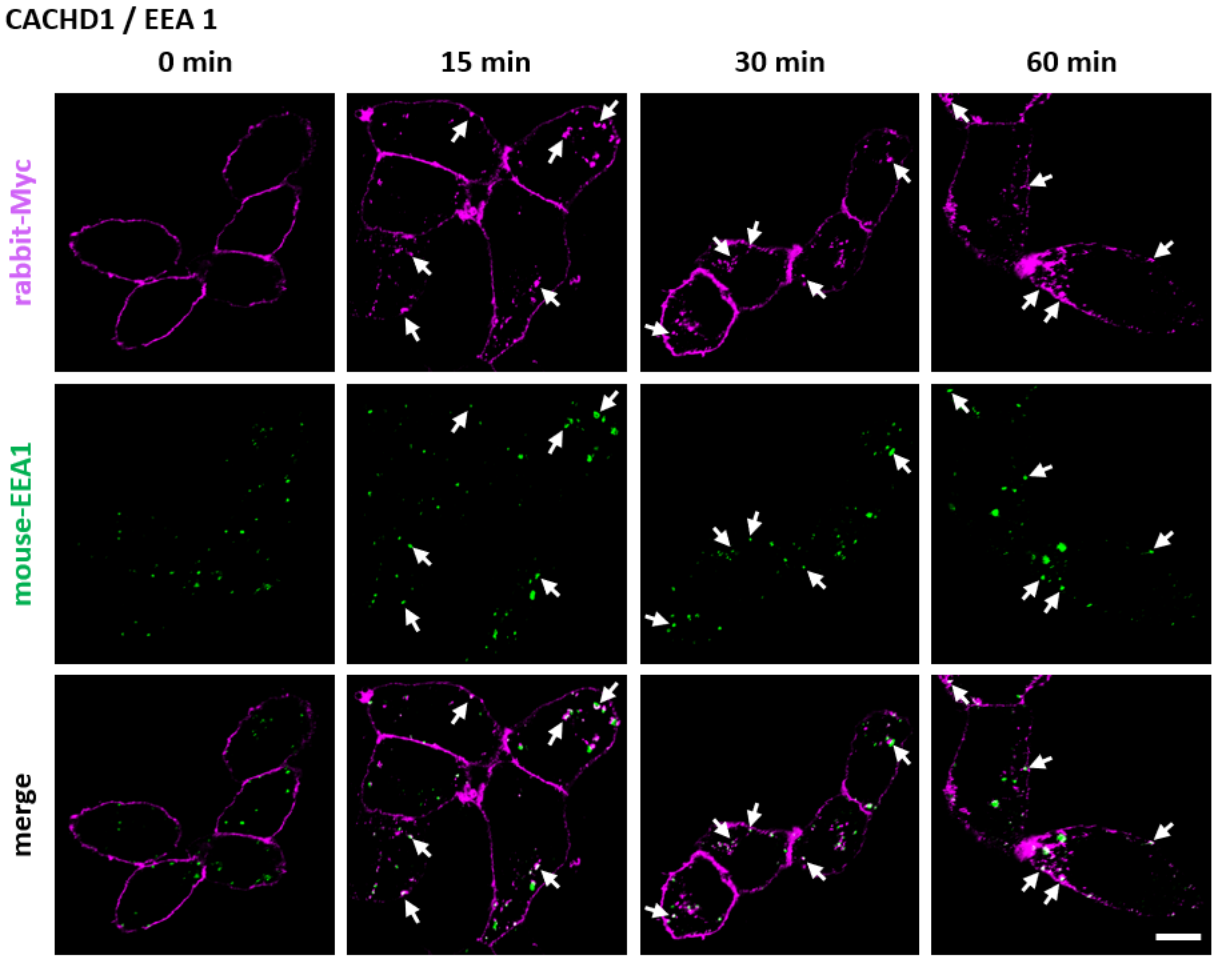

Figure 5.10 CACHD1 localises to EEA1 in stable HEK293 cells. Stable HEK293 cells expressing Myc-CACHD1 were labelled live with rabbit anti-Myc antibody, fixed with 4% PFA, and labelled with mouse anti-EEA1 antibody. Secondary anti-rabbit and anti-mouse Alexa Fluor™ 555 and 647 (respectively) were then used. Immunoreactive Myc-CACHD1 was detected at the cell surface at 0 h, and immunoreactive EEA1 was detected inside cells at all timepoints. Myc-CACHD1 co-localised with EEA1 (white arrows) at the 15, 30 and 60 min timepoints. (Scale bar 10 µm, n = 4).

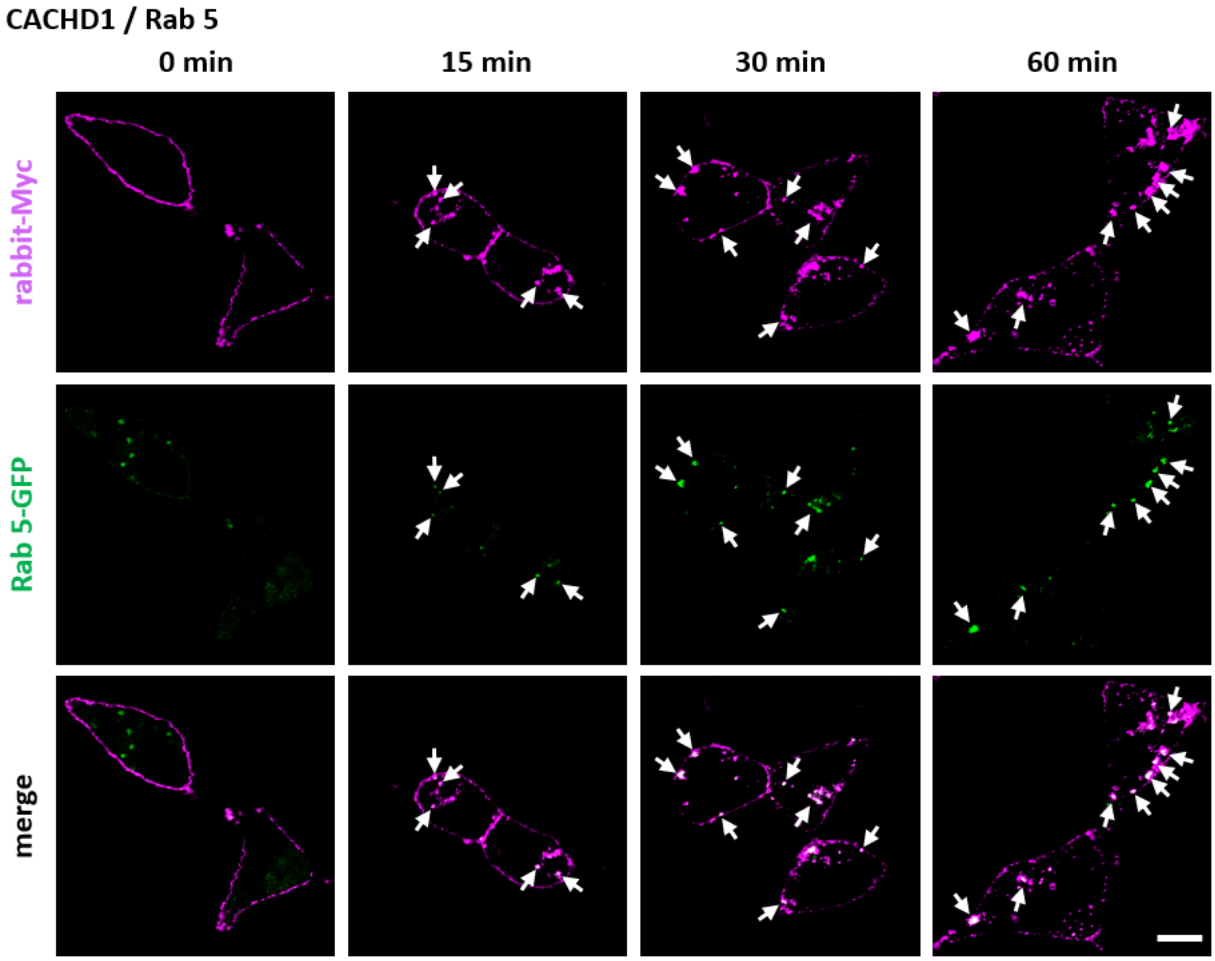

Figure 5.11 CACHD1 localises to dRab5 early sorting endosomes. Stable HEK293 cells expressing Myc-CACHD1 were transiently transfected with pEGFP-C1-dRab5 plasmid and grown for 48 h. Cells were labelled live with rabbit anti-Myc antibody, fixed with 4% PFA, and labelled with anti-rabbit Alexa Fluor™ 555 secondary antibody. Immunoreactive Myc-CACHD1 was detected at the cell surface at 0 h, and EGFP-tagged dRab5 endosomes were detected inside cells at all timepoints. Myc-CACHD1 co-localised with dRab5 (white arrows) at the 15, 30 and 60 min timepoints. (Scale bar 10 µm, n = 4).

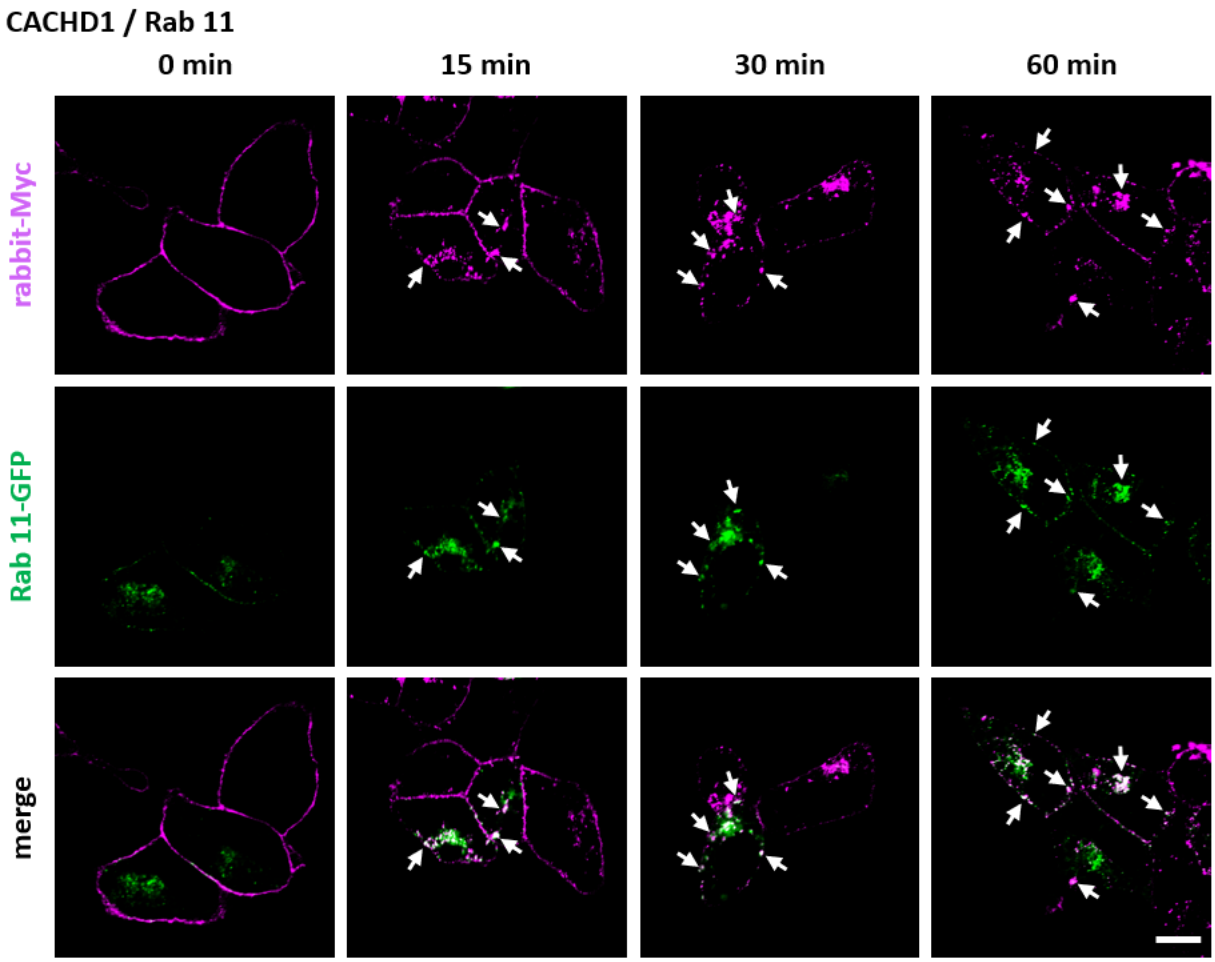

Figure 5.12 CACHD1 localises to dRab11 recycling endosomes. Stable HEK293 cells expressing Myc-CACHD1 were transiently transfected with pEGFP-C1-dRab11 plasmid and grown for 48 h. Cells were labelled live with rabbit anti-Myc antibody, fixed with 4% PFA, and labelled with anti-rabbit Alexa Fluor™ 555 secondary antibody. Immunoreactive Myc-CACHD1 was detected at the cell surface at 0 h, and EGFP-tagged dRab11 endosomes were detected inside cells at all timepoints. Myc-CACHD1 co-localised with dRab11 (white arrows) at the 15, 30 and 60 min timepoints. (Scale bar 10 µm, n = 4).

5.4.4 Amino acid substitution mutations in the TyrIM of CACHD1 have no effect on CACHD1 expression or internalisation at the cell surface

The impact of mutagenesis of the Y^{1197} residue within the TyrIM of CACHD1 was investigated by western blotting and immunocytochemistry techniques. Using western blotting, immunoreactive Myc-CACHD1-wt, Myc-CACHD1-Y1197A, and Myc-CACHD1-Y1197F were detected at 150-170 kDa by rabbit anti-Myc antibody (Figure 5.13A,C), showing that the Y1197A and Y1197F mutations did not alter the molecular mass of final CACHD1 protein in transiently transfected HEK293 tsA201 cells. Cell surface biotinylation assay further confirmed the presence of CACHD1-wt and both TyrIM mutants at the cell surface (Figure 5.13A).

In transiently transfected cells, the total protein expression levels of the Myc-CACHD1-Y1197A and Myc-CACHD1-Y1197F mutants were significantly higher in cell surface and whole-cell lysate samples in comparison to Myc-CACHD1-wt. The cell surface protein levels of Myc-CACHD1-Y1197A and Myc-CACHD1-Y1197F mutants were elevated to 177.6±33.5% and 191.6±22.2% (mean±SEM), respectively (Figure 5.13B). The total protein levels of Myc-CACHD1-Y1197A and Myc-CACHD1-Y1197F mutants were elevated to 135.4±5.4% and 146.8±10.6% (mean±SEM), respectively (Figure 5.13D). Although the TyrIM mutants showed elevated expression, transient transfection efficiency can vary, as previously discussed in chapter 3. While transient transfection is useful for preliminary assessment, stable cell line approach provides a more robust and consistent method, supported by results presented in section 3.4.2.

Sub-cellular localisation of Myc-tagged CACHD1-wt, CACHD1-Y1197A and CACHD1-Y1197F was determined by immunocytochemistry, using live and fixed cell labelling with rabbit and mouse anti-Myc antibodies to determine CACHD1 expression at the cell surface and in intracellular compartments, respectively (Figure 5.14). Live cell labelling of cell surface proteins showed immunoreactive Myc-CACHD1-wt, Myc-CACHD1-Y1197A and Myc-CACHD1-Y1197F expressed at the cell surface, while labelling of permeabilised cells showed immunoreactive Myc-CACHD1-wt, Myc-CACHD1-Y1197A and Myc-CACHD1-Y1197F present in intracellular compartments.

Following characterisation of TyrIM mutants, the effects of Y^{1197} mutagenesis on CACHD1 internalisation at the cell surface were investigated through immunocytochemistry and trafficking assay as described in section 5.3.1. Figure 5.15 shows that neither Y1197A or

Y1197F mutation inhibited CACHD1 internalisation. However, while the CACHD1-Y1197F mutants internalised, the internalisation rate appeared to be slower compared to CACHD1-wt or CACHD1-Y1197A, despite no statistical or quantitative evidence. These results indicate that CACHD1 internalisation may be mediated by its TyrIM; however, more experimentation is required to fully understand the involvement of the TyrIM in CACHD1 endocytosis.

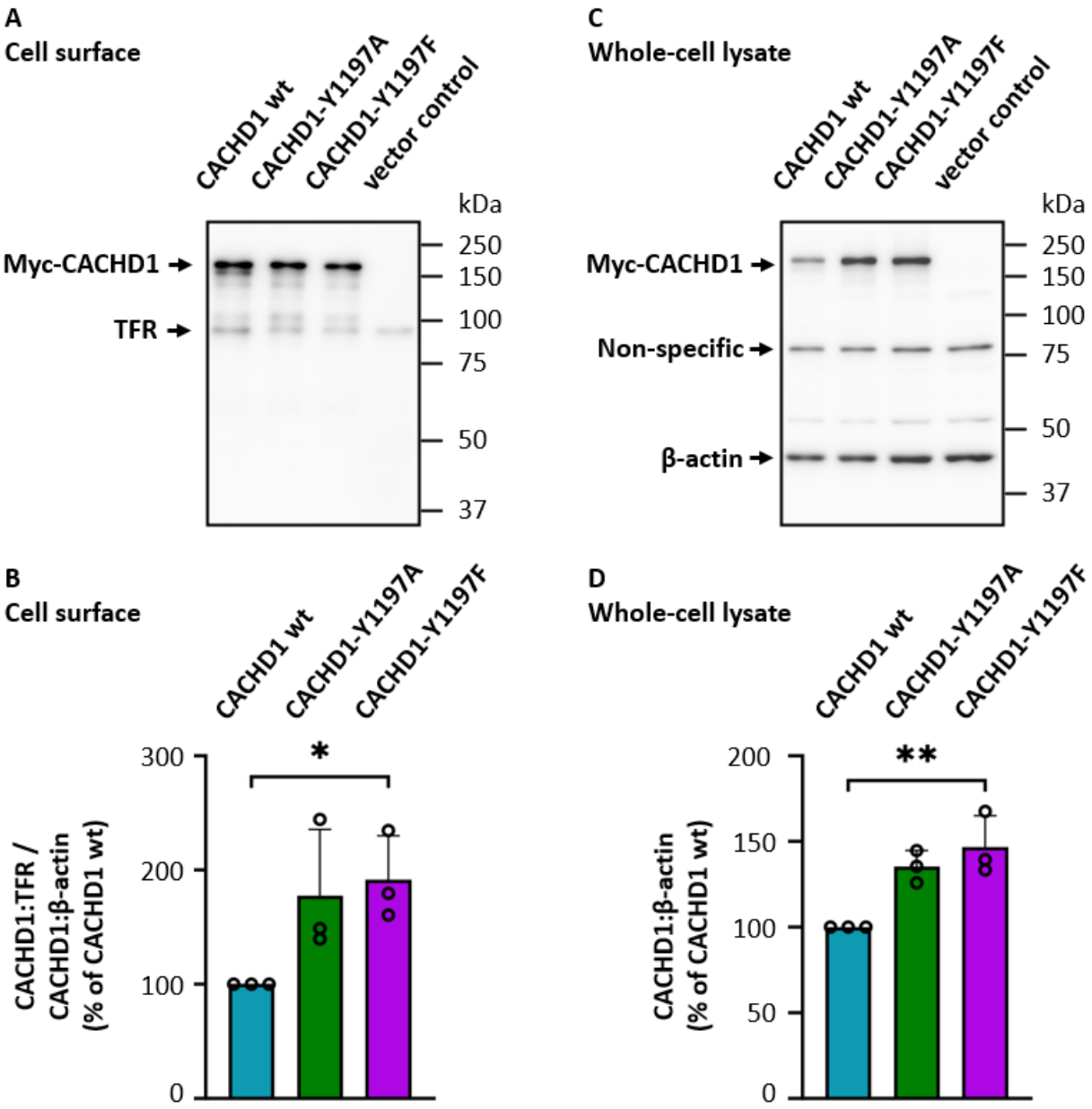

Figure 5.13 Analysis of expression of Myc-CACHD1-wt, Myc-CACHD1-Y1197A and Myc-CACHD1-Y1197F in transiently transfected HEK293T tsA201 cells by western blotting. (A,C) Expression of Myc-CACHD1-wt, Myc-CACHD1-AAA and Myc-CACHD1-G236S in transiently transfected HEK293T tsA201 cells was determined by western blotting. Cells were incubated with EZ-LinkTM sulfo-NHS-SS-Biotin (0.3 mg/ml in DPBS+CM) at 4°C to label cell surface proteins. Cells were then lysed with RIPA buffer and whole-cell lysate samples were collected. Biotinylated proteins were captured by NeutrAvidin agarose beads at 4°C overnight. Proteins were separated by SDS-PAGE and blots were incubated with rabbit anti-Myc, mouse anti-β-actin or mouse anti-TFR (transferrin receptor; loading controls) antibodies. Immunoreactive Myc-CACHD1-wt, Myc-CACHD1-Y1197A and Myc-CACHD1-Y1197F proteins were detected at 150-170kDa at the cell surface (A) and in whole cell lysates (C), which corresponded with the predicted size of CACHD1 protein. Signals for TFR were preset in all cell surface samples (A), and β-actin signals were present in all whole-cell lysate samples (C). Densitometry was performed on viable blots and raw data was analysed by (B) Kruskal-Wallis with Dunn's post hoc test and (D) One-way ANOVA with Tukey's post hoc test. **(B)** Myc-CACHD1-Y1197A and Myc-CACHD1-Y1197F were expressed at significantly higher levels compared to Myc-CACHD1-wt in membrane samples, 177.6±33.5% and 191.6±22.2%, respectively (mean±SEM). (n=3, $*p < 0.05$). **(D)** Myc-CACHD1-Y1197A and Myc-CACHD1-Y1197F were expressed at significantly higher levels compared to Myc-CACHD1-wt in whole-cell lysates, 135.4±5.4% and 146.8±10.6%, respectively (mean±SEM). (n=3, $**p < 0.01$).

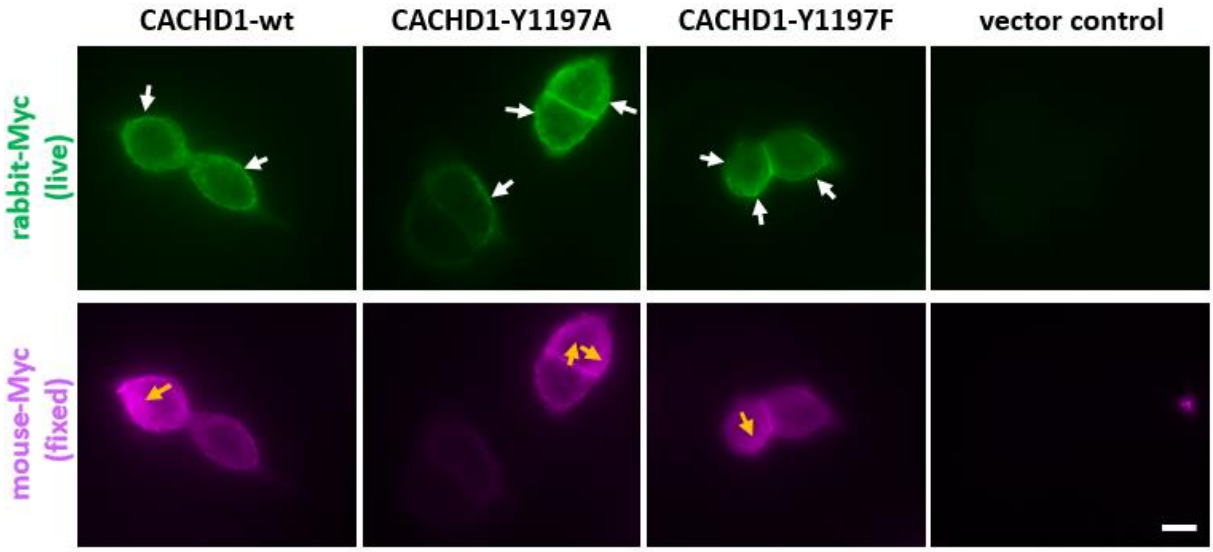

Figure 5.14 Characterisation of expression and sub-cellular localisation of Myc-CACHD1-wt, Myc-CACHD1-Y1197A and Myc-CACHD1-Y1197F in transiently transfected HEK293 tsA201 cells. HEK293 tsA201 cells were transiently transfected with Myc-CACHD1-wt, Myc-CACHD1-Y1197A, Myc-CACHD1-Y1197F or empty vector (control). Transfected cells were labelled live with rabbit anti-Myc antibody, fixed with 4% PFA, and labelled with mouse anti-Myc antibody. Immunoreactive Myc-CACHD1-wt, Myc-CACHD1-Y1197A and Myc-CACHD1-Y1197F were detected with rabbit and mouse anti-Myc antibodies, showing expression at the cell surface (white arrows) and in intracellular compartments (yellow arrows). No immunoreactive signals were detected in control cells. (Scale bar 10 µm, n = 4).

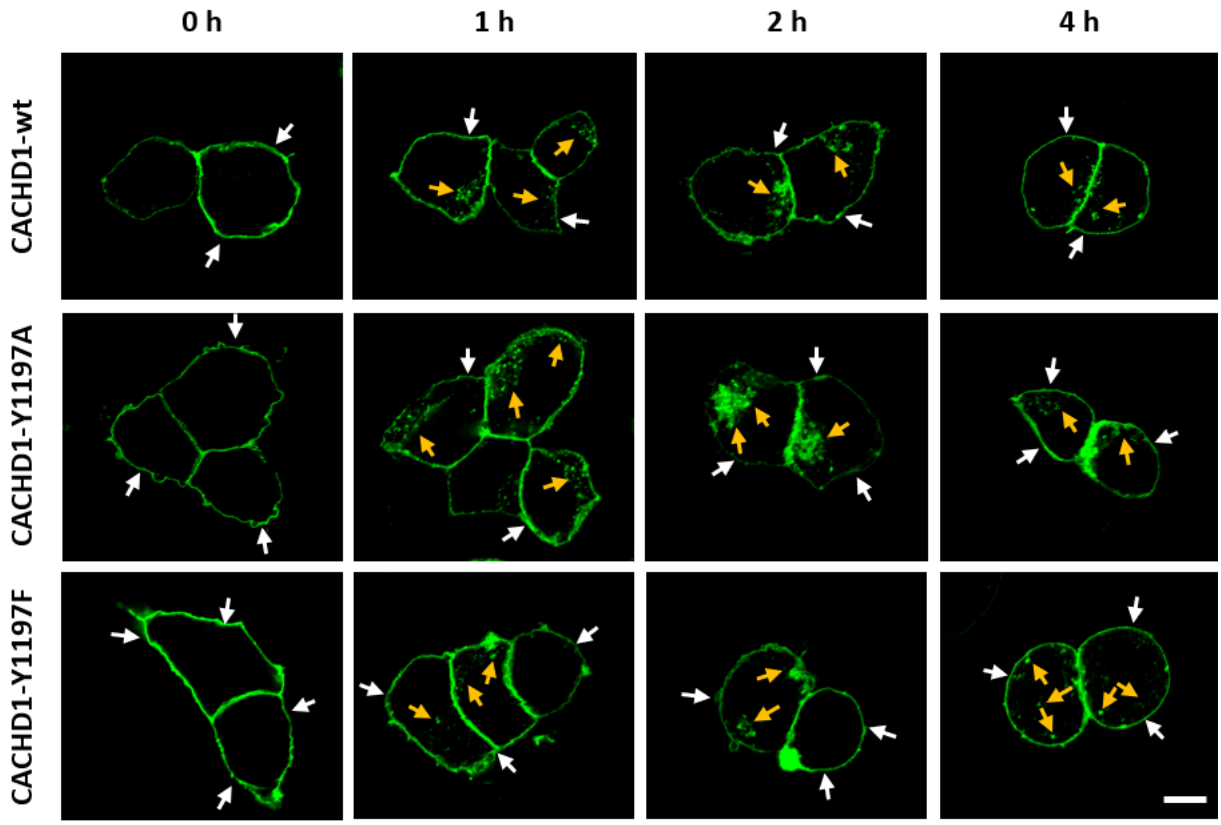

Figure 5.15 Analysis of TyrIM-mediated internalisation of Myc-CACHD1 in transiently transfected HEK293 tsA201 cells. Transiently transfected HEK293 tsA201 cells were labelled live with rabbit anti-Myc antibody at 4°C, incubated in DMEM 0.1% BSA at 37°C for 0 h, 1 h, 2 h or 4 h, fixed with 4% PFA at 4°C, and labelled with Alexa Fluor™ 488 secondary antibody. Immunoreactive Myc-CACHD1-wt, Myc-CACHD1-Y1197A and Myc-CACHD1-Y1197F were detected exclusively at the cell surface at 0 h, and at the cell surface (white arrows) and in intracellular compartments (yellow arrows) at 1, 2 and 4 h, showing CACHD1 internalisation. CACHD1-Y1197F appeared to internalise slower compared to CACHD1-wt and CACHD1-Y1197A. (Scale bar 10 µm, n = 5).

5.4.5 The transmembrane domain and C-terminal tail are important for CACHD1 trafficking to cell surface

Here, the role of the CACHD1 C-terminal tail and transmembrane domain in CACHD1 trafficking was investigated. First, the expression and sub-cellular localisation of Myc-tagged CACHD1-wt, CACHD1-TMD (CACHD1ΔH1122-C1274), and CACHD1-trunc (CACHD1ΔV1096-C1274) were determined by western blotting and immunocytochemistry.

Western blot analysis showed immunoreactive Myc-CACHD1-wt, Myc-CACHD1-TMD and Myc-CACHD1-trunc protein bands at 140-170 kDa in whole-cell lysates, with truncated variants exhibiting 140-150 kDa molecular mass (Figure 5.16B). Additionally, cell surface biotinylation assay confirmed the expression of Myc-CACHD1-wt and Myc-CACHD1-TMD at the cell surface, with molecular mass of 150-170 kDa and 140-150 kDa, respectively (Figure 5.16A). By marked contrast, the CACHD1-trunc was absent in membrane samples (Figure 5.16A). Immunocytochemistry experiments further supported these findings, showing that unlike CACHD1-wt and CACHD1-TMD, the CACHD1-trunc was not expressed at the cell surface (Figure 5.16C). All three CACHD1 variants were detected in intracellular compartments (Figure 5.16C). These observations suggested two potential explanations for the absence of Myc-CACHD1-trunc at the cell surface: i) Myc-CACHD1-trunc protein is not transported to the membrane, or ii) if transported, it lacks the means to anchor to the membrane due to the removal of the transmembrane domain and C-terminal tail, leading to secretion out of the cell. To address these theories, western blot analysis of cell lysates and culture supernatant was carried out. Figure 5.17 shows that Myc-CACHD1-trunc was not present in the culture medium, confirming the first theory that Myc-CACHD1-trunc is not transported to the membrane.

Furthermore, the predicted molecular mass of Myc-CACHD1-TMD and Myc-CACHD1-trunc was 126 kDa (Uniprot); despite the removal of C-terminal tail and transmembrane domain from Myc-CACHD1-trunc, the predicted size is similar to Myc-CACHD1-TMD due to the addition of Avi and 12-His tags for future ligand binding studies. While the predicted molecular mass is 126 kDa, both proteins were detected at 140-150 kDa. This difference in molecular mass is most likely the result of post-translational modifications, such as glycosylation, as CACHD1 is predicted to have up to 7 glycosylation sites (Dahimene *et al*., 2018).

Following characterisation of truncated CACHD1 variants, their effects on CACHD1 internalisation at the cell surface were investigated through immunocytochemistry and trafficking assay as described in section 5.3.1. Figure 5.18 shows that similarly to CACHD1-wt, the CACHD1-TMD variant was internalised. Despite no statistical or quantitative evidence, its internalisation appeared to be slower in comparison to CACHD1-wt, especially visible at the 1 h timepoint.

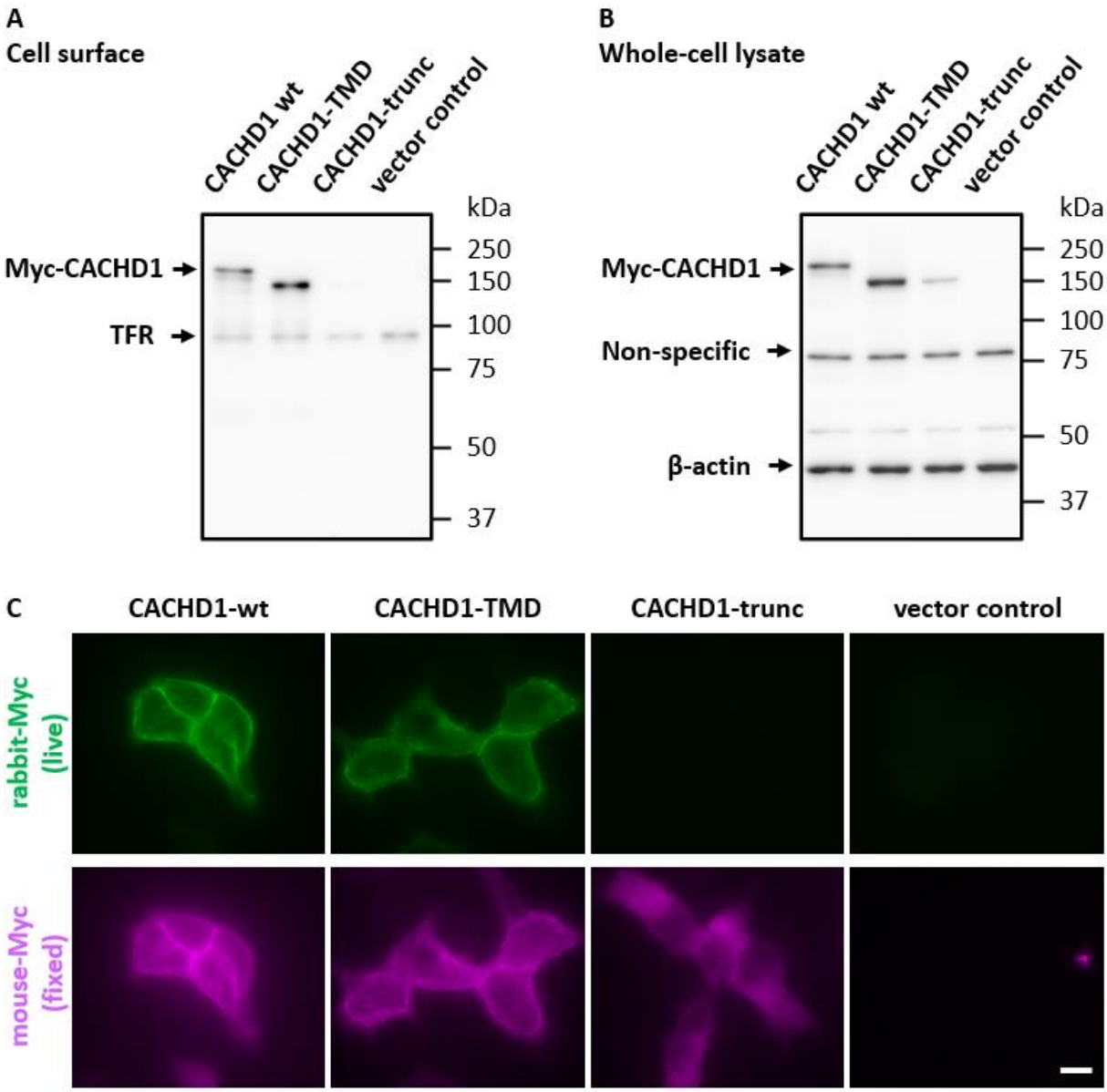

Figure 5.16 Characterisation of expression and sub-cellular localisation of Myc-CACHD1-wt and its truncated variants in transiently transfected HEK293 tsA201 cells. HEK293 tsA201 cells were transiently transfected with Myc-CACHD1-wt, Myc-CACHD1-TMD, Myc-CACHD1-trunc or empty vector (control), and expression was analysed by western blotting, cell surface biotinylation assay and ICC. **(A,B)** Cells were incubated with EZ-LinkTM sulfo-NHS-SS-Biotin (0.3 mg/ml in DPBS+CM) at 4°C to label cell surface proteins. Cells were then lysed with RIPA buffer and whole-cell lysate samples were collected. Biotinylated proteins were captured by NeutrAvidin agarose beads at 4°C overnight. Proteins were separated by SDS-PAGE and blots were incubated with rabbit anti-Myc antibody. Immunoreactive Myc-CACHD1-wt, Myc-CACHD1-Y1197A and Myc-CACHD1-Y1197F were detected in cells transfected with CACHD1 constructs only, confirming antibody specificity. Myc-tagged CACHD1-wt and CACHD1-TMD were detected at 150-170 and 140-150 kDa in whole-cell lysates (B) and in membrane samples (A), while the Myc-CACHD1-trunc was only detected in whole cell lysates (B). Signals for β-actin and TFR (transferrin receptor; loading controls) were present in both cell types. (9% SDS-PAGE gel; n = 4). **(C)** Transfected cells were labelled live with rabbit anti-Myc antibody, fixed with 4% PFA, and labelled with mouse anti-Myc antibody. Immunoreactive Myc-CACHD1-wt, Myc-CACHD1-TMD were detected with rabbit and mouse anti-Myc antibodies, showing expression at the cell surface and in intracellular compartments, while the Myc-CACHD1-trunc was absent at the cell surface. No immunoreactive signals were detected in control cells. (Scale bar 10 µm, n = 4).

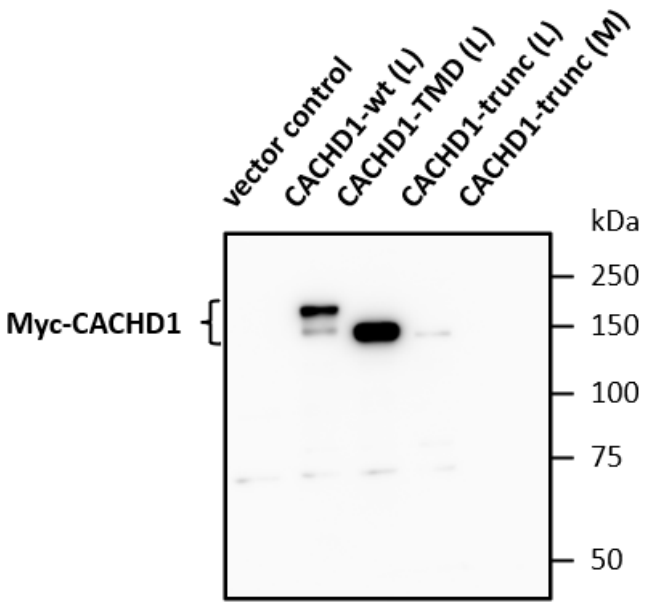

Figure 5.17 Analysis of expression and secretion of Myc-CACHD1-trunc variant by western blotting. HEK293 tsA201 cells were transiently transfected with Myc-CACHD1-wt, Myc-CACHD1-TMD, Myc-CACHD1-trunc, or vector control, and protein expression and secretion were determined by western blotting. Culture supernatant containing secreted proteins was collected and remaining cells were lysed. Proteins were separated by SDS-PAGE and blots incubated with rabbit anti-Myc antibody. Immunoreactive Myc-CACHD1-wt, Myc-CACHD1-TMD and Myc-CACHD1-trunc proteins were detected in cell lysates (L). No Myc-CACHD1-trunc was detected in the culture supernatant (M). (7% SDS-PAGE gel, n=3).

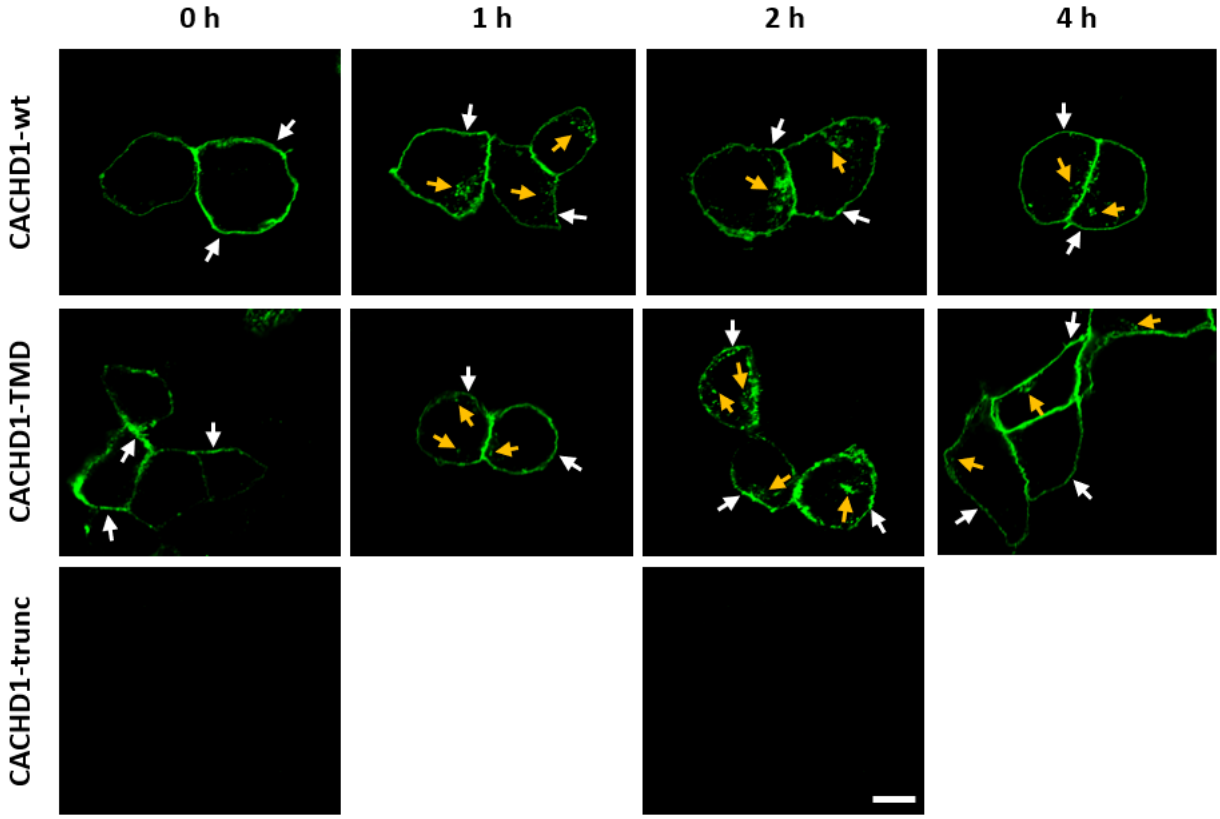

Figure 5.18 Analysis of internalisation of Myc-CACHD1-wt and its truncated variants in transiently transfected HEK293 tsA201 cells. Transiently transfected HEK293 tsA201 cells were labelled live with rabbit anti-Myc antibody at 4°C, incubated in DMEM 0.1% BSA at 37°C for 0 h, 1 h, 2 h or 4 h, fixed with 4% PFA at 4°C, and labelled with Alexa Fluor™ 488 secondary antibody. Immunoreactive Myc-CACHD1-wt and Myc-CACHD1-Y1197A were detected exclusively at the cell surface at 0 h, and at the cell surface (white arrows) and in intracellular compartments (yellow arrows) at 1, 2 and 4 h, showing CACHD1 internalisation. Myc-CACHD1-trunc was not detected. (Scale bar 10 µm, n = 5).

5.5 Discussion

Protein trafficking within cells involves a complex network of molecules that serve various functions in the regulation of protein internalisation and sorting. In this chapter, a series of experiments were conducted to explore the trafficking and processing mechanisms of CACHD1 protein. As CACHD1 is a relatively unstudied protein, this study represents the first investigation into the various mechanisms potentially involved in CACHD1 trafficking.

Initial findings showed that CACHD1 undergoes constitutive internalisation in HEK293 cells, showing internalisation at 1-, 2- and 4-hour timepoints, with an observed decrease in intracellular CACHD1 levels at the 4-hour mark. This observation suggests the possibility of CACHD1 recycling back to the cell surface following endocytosis. Further evidence and discussion on this topic are provided in the following sections.

5.5.1 CACHD1 endocytosis appears to be cholesterol-dependent

The intricate mechanisms responsible for protein endocytosis are commonly studied using pharmacological inhibitors (Iversen *et al*., 2011). In this study, two main endocytic pathways were investigated, namely clathrin-mediated and caveolae-dependent pathways.

Clathrin-mediated endocytosis is important in the internalisation and recycling of many transmembrane proteins (Goh and Sorkin, 2013), facilitated by their interaction with AP-2, which then recruit clathrin to the vesicles (Cocucci *et al*., 2012; Kaksonen and Roux, 2018). Following vesicle formation, scission protein, dynamin, facilitates the separation of the vesicle from plasma membrane (Antonny *et al*., 2016). AP-2 recognises YXXϕ signal motifs in transmembrane proteins (Ohno *et al*., 1995; Kelly *et al*., 2008), and given that CACHD1 contains a YSTM signal motif, the clathrin-mediated pathway was investigated using sucrose as an inhibitor.

The caveolae-dependent pathway, characterised by invaginations of the plasma membrane enriched in cholesterol (Palade, 1953), is another route for protein internalisation. The two main components of caveolae are cholesterol and caveolin proteins. Cholesterol is an important component of caveolae, and normal levels of free cholesterol are essential for maintaining caveolae endocytosis (Lay *et al*., 2006). Caveolin proteins play a structural role in caveolae formation at the plasma membrane (Williams and Lisanti, 2004). Caveolins oligomerise and the oligomers are stabilised by cholesterol binding (Monier *et al*., 1996).

Various proteins, including transforming growth factor-β (TGF-β) (Di Guglielmo *et al*., 2003) and integrins (del Pozo *et al*., 2005), use the caveolae-dependent endocytic pathway. Here, the possibility of CACHD1 internalisation through the caveolae-dependent endocytosis was also examined. Typically, the involvement of caveolae in protein endocytosis is assessed through cholesterol and caveolin dependence, by depletion of cholesterol or knockdown of caveolin-3 expression (Woodman et al., 2002; Balijepalli *et al*., 2006). In this study, the cholesterol depletion method was investigated using the commonly used cholesterol stripping agents, MβCD and nystatin (Vercauteren *et al*., 2010). MβCD and nystatin inhibit caveolae pathway through cholesterol disruption. MβCD strips cholesterol from membrane, while nystatin forms complexes with cholesterol, disrupting the lipid composition and integrity of caveolae (Zhu *et al*., 2010; Harvey and Calaghan, 2014). It was previously shown that cholesterol depletion can induce flattening of caveolae within just a few minutes (Rothberg *et al*., 1992; Hailstones *et al*., 1998).

In this study, out of the three inhibitors tested, only MβCD resulted in the inhibition of CACHD1 internalisation, indicating a potential involvement of caveolae and dependency of CACHD1 endocytosis on cholesterol. Surprisingly, treatment with nystatin showed no effect on CACHD1 internalisation, necessitating further experimentation to understand how CACHD1 utilises the caveolae-dependent pathway. It is important to note, that while MβCD is a cholesterol depleting agent commonly used for the study of endocytosis, it was reported to cause several secondary effects at the membrane, such as reduced number of invaginated caveolae and clathrin-coated pits (Rodal *et al*., 1999), and depolymerisation of the actin cytoskeleton (Mundhara *et al*., 2019). Recovery of cholesterol for 1 hour following treatment with MβCD resulted in partial reversal of MβCD-associated inhibition of CACHD1 internalisation, with a complete restoration of internalisation observed after 2 hours. Similar outcomes were reported for I-transferrin, where inhibition of cholesterol synthesis indicated that the restored I-transferrin internalisation following MβCD treatment was due to cholesterol synthesis in cells (Rodal *et al*., 1999). Moreover, cholesterol recovery with serum-free medium in Jurkat T cells resulted in fluorescence levels comparable to control cells (Mahammad and Parmryd, 2008). The dependence of CACHD1 endocytosis on caveolin proteins could be further assessed through caveolin knockout (KO) experiments, using CRISPR/Cas9 caveolin-1 KO HeLa cell line (Abcam; ab255371). Additionally, several alternative

pathways could be explored to gain further understanding into CACHD1 endocytosis, such as dynamin-dependent or macropinocytosis pathways.

Although the results presented in this chapter suggest that the cholesterol-dependent caveolae endocytic pathway may serve as the primary endocytic pathway for CACHD1, further studies are needed. Nonetheless, these findings represent a step forward towards the characterisation of endocytosis mechanisms used by CACHD1.

5.5.2 CACHD1 localises to Rab5- and Rab11-positive vesicles post-endocytosis, indicative of a recycling pathway

Following endocytosis, proteins undergo sorting and processing through a complex network of intracellular mechanisms, involving Rab proteins associated with various endosomes, each playing distinct role in vesicle formation, translocation, anchoring and fusion during endocytic transport (Grant and Donaldson, 2009). In this study, the involvement of EEA1, Rab5 and Rab11 in the post-endocytic sorting of CACHD1 was investigated.

EEA1, an early endosomal Rab5 effector protein, is associated with the docking of incoming endocytic vesicles before fusion with early endosomes. Following vesicle fusion with early endosomes, Rab5 facilitates the internalisation and sorting of various proteins, including many GPCRs, such as the dopamine D2 receptors (De Vries *et al*., 2019), the cannabinoid receptor 2 (Grimsey *et al*., 2011), and the FFA1 and FFA4 receptors (Qian *et al*., 2014; Flores-Espinoza *et al*., 2020). Proteins within early endosomes can undergo processing via different trafficking pathways. As endosomes mature, Rab5 is replaced by Rab7 which directs proteins to late endosomes and eventually towards lysosome for degradation (Wartosch *et al*., 2015). Many proteins, including α2δ-1 and α2δ-2 subunits, are recycled back to cell surface through a Rab11-dependent mechanisms (Tran-Van-Minh and Dolphin 2010; Goldenring, 2015; Meyer and Dolphin, 2021). Here, CACHD1 was added to the list of proteins utilising this recycling pathway. Co-localisation studies showed that CACHD1 co-localised with EEA1, Rab5 and Rab11, suggesting early sorting by Rab5-associated endosomes, and subsequent recycling by Rab11-associated recycling endosomes. The initial study describing constitutive internalisation of CACHD1 showed prominent internalisation at 1- and 2-hour timepoints, while at the 4 hour timepoint the levels of intracellular CACHD1 appeared to be decreased, which suggested possible recycling back to cell surface, and this theory was confirmed by the co-localisation of CACHD1 with Rab11.

The Rab11-dependent recycling pathway is also used by α2δ-1 and α2δ-2 subunits, and inhibition of this pathway by introducing dominant-negative Rab11a mutant resulted in α2δ re-routing towards the degradation pathway (Tran-Van-Minh and Dolphin 2010; Meyer and Dolphin, 2021). It is important to note that α2δ subunits, unlike CACHD1, are predicted to be GPI-anchored and do not possess an intracellular C-terminal tail (Davies *et al*., 2010; Wu *et al*., 2016), and therefore it is unlikely they possess a YXXϕ based signal motif that could regulate their internalisation. This suggests that α2δ subunits may use their extracellular domains for mediating the internalisation process. While the Rab5 and Rab11-dependent trafficking pathway was demonstrated for CACHD1, it is possible that alternative trafficking pathways may also be involved.

5.5.3 The transmembrane domain and C-terminal tail comprising YXXϕ signal motif are involved in CACHD1 trafficking

In addition to characterising constitutive internalisation and determining endocytic pathway used by CACHD1, the last two objectives of this chapter aimed to investigate the roles of the TyrIM located on the C-terminal tail, as well as the transmembrane domain and the C-terminal tail itself in mediating CACHD1 internalisation. Previous studies have described the significance of YXXϕ signal motifs, typically situated on the C-terminal tail of membrane proteins (Rohrer *et al*., 1996; Bonifacino and Traub, 2003), in regulating protein internalisation and subsequent processing. Some examples of proteins include the transferrin receptor (YXRF; Girones *et al*., 1991), H^+/K^+-ATPase (FRHY; Courtois-Coutry *et al*., 1997), CD63 (YEVM; Metzelaar *et al*., 1991) and CTLA-4 (YVKM; Chuang *et al*., 1997). Moreover, GPCRs, including 5-HT_{2a}, PAR-1, TRH, and acetylcholine M2 and M4 (Marchese *et al*., 2010), as well as connexin proteins (Cx; Fisher and Falk, 2023) were shown to use their YXXϕ motifs for directing protein endocytosis. For instance, Cx43 utilises its two YXXϕ motifs (Y^{265}AYF and Y^{286}KLV) to recruit clathrin and mediate its endocytosis (Piehl *et al*., 2006; Fong *et al*., 2013), and in PAR-1, the YXXL motif was shown to produce the trafficking signal (Paing *et al*., 2004). Furthermore, in aquaporin-4 (AQP4), the YXXϕ plays a critical role in internalisation, subcellular localisation, and lysosomal degradation, while also generating signal for AQP4 degradation through proteasomes under specific conditions (Wang *et al*., 2023). These studies provide the evidence that YXXϕ signal motifs found in many membrane proteins play critical roles in directing proteins to specific cellular compartments, such as endosomes, lysosomes or back to plasma membrane, through interactions with adaptor proteins, such as AP2 (Traub, 2003).

The tyrosine residue within YXXϕ motifs is considered critical in mediating protein internalisation and subsequent post-endocytic sorting, as evidenced by numerous studies. Mutations of this Tyr residue frequently result in disruptions in protein internalisation caused by the loss or impairment of YXXϕ-associated signal required for effective interaction with the cellular sorting machinery. For example, mutation of the Tyr residue to Ala in the YXXL signal motif of LRP has been shown to decrease the endocytosis rate of LRP mini receptors, leading to their accumulation at the cell surface (Li *et al*., 2000). Similarly, to LRP, mutating Tyr to Ala in the YXXϕ signal motif of H^+/K^+-ATPase and PAR-1 resulted in increased cell surface expression caused by impaired internalisation mechanism (Courtois-Coutry *et al*., 1997; Pain *et al*., 2004; respectively). Additionally, mutations of the Y^{487} and Y^{498} residues to Ala or Phe in two individual YXXϕ signal motifs found in the BVL (bovine leukaemia virus) transmembrane envelope protein resulted in increased cell surface expression due to slower endocytosis rate (Novakovic *et al*., 2004). Interestingly, mutating the Y^{487} residue resulted in slower endocytosis rate in comparison to the Y^{498} mutants (Novakovic *et al*., 2004). Furthermore, studies on SARS-CoV 3a protein revealed it utilised a YXXV motif for intracellular trafficking, and mutations within this motif resulted in lysosomal degradation (Minakshi and Padhan, 2014).

To investigate the role of the Y^{1197}STM signal motif in CACHD1, mutations of the Tyr1197 residue to Ala (Y1197A) or Phe (Y1197F) were introduced. The preliminary findings presented in this chapter suggest differential effects on CACHD1 internalisation dependent on the amino acid residue in place of Y1197. While the Y1197A mutation did not show any apparent effects on CACHD1 internalisation, the Y1197F mutation appeared to slow down the rate of internalisation, which corresponds with the effects observed for LRP (Li *et al*., 2000) and BVL transmembrane envelope protein (Novakovic *et al*., 2004). These results imply the potential involvement of the YSTM signal motif in mediating CACHD1 internalisation. Furthermore, further analysis of cell surface expression of CACHD1-wt, CACHD1-Y1197A and CACHD1-Y1197F by cell surface biotinylation assay showed elevated expression levels of both Y1197A and Y1197 CACHD1 mutants compared to CACHD1-wt, accompanied by significantly increased overall expression levels in whole-cell lysates. The variation in expression levels of could be attributed to many factors, including transfection efficiency, cell confluency, integration into cells, protein stability, and variation in the data, necessitating additional experimentation for a comprehensive understanding on the cell surface expression of CACHD1 TyrIM mutants. To address this issue, regulation of expression to standardise expression levels, as used for

CACHD1 MIDAS motif mutants in Chapter 4, would help determine whether the observed increase in cell surface expression was caused by disrupted internalisation mechanisms of CACHD1 or merely variation in transfection efficiency.

While mutagenesis of Y1197 showed effect on the rate of internalisation, it remains to be determined whether either TyrIM mutant affects CACHD1 post-endocytic sorting. Co-localisation studies with Rab5, Rab7 and Rab11 could shed light on whether CACHD1-Y1197A/F undergo recycling to cell surface or get directed for degradation. Furthermore, co-expression with dominant-negative Rab11 could further elucidate Rab11-dependent recycling mechanism in CACHD1, as in α2δ-1 and α2δ-2 the introduction of dominant-negative Rab11a resulted in a redirection towards the degradation pathway (Tran-Van-Minh and Dolphin 2010; Meyer and Dolphin, 2021). Additionally, using fluorescence-activated cell sorting (FACS) to analyse expression and internalisation could provide insights beyond single-cell analysis.

While the TyrIM may play role in facilitating CACHD1 endocytosis, it is likely not the only mechanism used by CACHD1. This proposal is supported by the finding that truncating CACHD1 by removing its intracellular C-terminal tail did not prevent CACHD1 internalisation. Previous studies have demonstrated the importance of the C-terminal tail in mediating internalisation in various membrane proteins, often facilitated by the short-signal sequence motif (Bonifacino and Dell'gelica, 1999; Miranda *et al*., 2001; Brothers *et al*., 2002; Bonifacino and Traub, 2003). The lack of effect on CACHD1 internalisation upon C-terminal tail removal suggests that CACHD1 may employ additional trafficking mechanisms beyond the YSTM signal motif. Moreover, it would be interesting to investigate the effects of this truncation on the post-endocytic sorting of CACHD1.

On the other hand, further truncation of CACHD1 by removing the transmembrane domain resulted in disruption of CACHD1 trafficking to cell surface as shown by live cell ICC and cell surface biotinylation assay. These results raised the question of whether CACHD1 was not transported to cell surface, or it simply lacked the means to anchor to the membrane leading to secretion out of the cell. Western blot analysis of culture supernatant showed that CACHD1 was not secreted out of the cell, supporting the theory that CACHD1-trunc is not transported to the cell surface at all. The absence of CACHD1-trunc at the cell surface is likely due to potential protein misfolding or the absence of motifs or domains crucial for interacting with proteins mediating CACHD1 transport to cell surface.

5.5.4 Conclusion

The endocytic pathway used by CACHD1, as well as the exact mechanism of CACHD1 internalisation and trafficking remains to be fully elucidated; however, this was the first study to investigate a variety of trafficking pathways used by CACHD1 protein. The post-endocytic processing and recycling of CACHD1 through endosomes positive for EEA1, Rab5 and Rab11 was shown, suggesting that CACHD1 recycles back to cell surface after internalisation. Moreover, mutagenesis of a key Tyr^{1197} residue within the YSTM signal motif to Phe resulted in CACHD1 internalisation that appeared slower compared to CACHD1-wt, suggesting that CACHD internalisation may be mediated through the YSTM signal motif. However, this is likely not the only mechanism used by CACHD1, as the removal of the C-terminal tail had no effect on CACHD1 internalisation, suggesting that CACHD1 internalisation may be mediated by other mechanisms, possibly through its extracellular domains. Interestingly, further removal of the predicted transmembrane domain resulted in intracellular retention of CACHD1, showing no trafficking to cell surface. In conclusion, this chapter has laid the groundwork for further investigations into the regulation of CACHD1 trafficking.

5.6 Limitations

The co-localisation study, which involved tracking the interaction of CACHD1 with endosomal markers (EEA1, Rab5, and Rab11), provided valuable insights into the internalisation and post-endocytic processing of CACHD1. However, there are notable limitations that should be considered. Firstly, light microscopy has a diffraction limit of approx. 200 nm, which restricts the resolution. This means that any interactions occurring within this range may appear as overlapping or co-localised, therefore the close proximity of CACHD1 to EEA1, Rab5, or Rab11 could be misinterpreted as direct interaction when, in reality, the proteins could be in adjacent but distinct endosomal compartments. Secondly, the co-localisation results shown lack quantitative analysis, therefore it is difficult to fully understand the extend of co-localisation or interaction of CACHD1 with EEA1, Rab5, or Rab11. Addressing these limitations with alternative approaches like super-resolution microscopy, PLA, and quantitative co-localisation analysis would provide a more comprehensive understanding of CACHD1 interactions with endosomal pathways.

5.7 Future work

This chapter represents the first study into the trafficking mechanisms governing CACHD1. The results presented here open the doors for future experiments and deeper investigation into these intricate mechanisms, required to fully grasp the trafficking intricacies of CACHD1. Some experiments to consider include the investigation into the potential involvement of alternative endocytic pathways, such as dynamin-dependent pathway or macropinocytosis, using specific inhibitors like dynasore and wortmannin, respectively. Additionally, live cell imaging is a useful method for the characterisation of protein dynamics and movement within a cell over time, which could help determine a more detailed time course by which CACHD1 internalises and recycles back to the membrane. Another technique, FACS, could be useful to study cell population as opposed to single cell. Here, the cell surface is immunolabelled, followed by incubation to allow protein internalisation. Afterward, the cell surface is washed to remove any residual antibodies, allowing the tracking of protein movement for proteins that were internalised during the incubation period, thus facilitating the monitoring of protein recycling. Furthermore, considering the apparent slower internalisation rate caused by the CACHD1-Y1197F mutant, investigating the effects of this mutant on $Ca_V3.1$ channel biophysical properties could shed some light on whether this CACHD1 mutant causes $Ca_V3.1$ retention at the cell surface, thus increasing $Ca_V3.1$ currents.

6. CLONING AND PURIFICATION OF A SOLUBLE FORM OF CACHD1 FOR LIGAND BINDING STUDIES

6.1 Introduction

Protein purification is a fundamental method providing specific protein targets for a wide range of applications, including structural and functional studies, drug development, quality control, and diagnostics assays. Chromatography techniques are often used to separate proteins based on their size, charge, or affinity to specific ligands (Coskun, 2016). The isolation of specific proteins from complex biological mixtures ensures that a protein can be studied without any interference from other cell components. Protein purification plays an essential role in the understanding of cellular processes, disease mechanisms, and protein structure and dynamics.

Once a purified protein is available, a variety of analytical methods are available for an in-depth protein characterisation. These methods include advanced techniques such as X-ray crystallography and nuclear magnetic resonance (NMR) spectroscopy for determination of protein 3D structure and dynamics (Szymczyna *et al*., 2009; Hu *et al*., 2021), enzyme-linked immunosorbent assay (ELISA) for determination of antibody/antigen presence in a sample (Alhazmi and Albratty, 2023), mass spectrometry for measurement of the mass-to-charge ratios important for protein characterisation and post-translational modification analysis (Hermann *et al*., 2022), surface plasmon resonance (SPR), co-immunoprecipitation and fluorescence resonance energy transfer (FRET) assays for investigation of protein-protein and protein-drug interactions (You *et al*., 2006; Rath *et al*., 2020; Wu *et al*., 2022). More conventional techniques include SDS-PAGE, 2D PAGE and western blotting for separation, detection, and quantification of proteins (Magdeldin *et al*., 2014; Mishra *et al*., 2017).

In this chapter, the procedures for the cloning and purification of a soluble CACHD1 protein using affinity column chromatography method are outlined. The aim was to clone and purify a soluble form of CACHD1 protein that could be utilised for a number of future experiments, such as structural or ligand-binding studies. Of particular interest would be the discovery of a small molecule modulator for CACHD1, which would have significant therapeutic implications for diseases associated with Ca_V3 VGCCs and their modulator, CACHD1. These applications include the inhibition of CACHD1-induced effects on Ca_V3 VGCCs and the reversal of physiological responses, such as changes in membrane potential and neurotransmitter

release. Similarly, the generation of soluble α2δ subunits has been instrumental in drug discovery (Brown and Gee, 1998; El-Awaad *et al*., 2019), particularly for gabapentinoids like gabapentin, pregabalin, and mirogabalin. These widely prescribed drugs function by binding to the α2δ-1 and α2δ-2 subunits at the RRR gabapenting binding motif, disrupting the trafficking and Rab11a-dependent recycling of α2δ subunits. This disruption reduces Ca^{2+} currents (Hendrich *et al*., 2008), decreasing excitatory neurotransmission. Producing soluble CACHD1 protein, much like soluble α2δ subunits, could facilitate drug discovery by enabling structural analysis and screening of potential modulators, potentially leading to innovative treatments for hyperexcitability diseases associated with Ca_V3 VGCCs, much like gabapentinoids do for HVA VGCCs. Moreover, an antagonist could be used to confirm the specificity of CACHD1 effects on Ca_V3 VGCCs, further aiding in drug development for hyperexcitability diseases.

6.2 Objective

In Chapter 5, a truncated CACHD1 was generated, however, this protein did not traffic to cell surface, nor was it secreted out of the cell.

- The first objective of this chapter was to determine if the replacement of CACHD1 native signal peptide with an Igκ signal peptide could facilitate the secretion of truncated CACHD1 out of the cell. The Igκ signal peptide was selected due to its capacity to improve protein expression and secretion (Liu *et al*., 2016; Wang *et al*., 2016). Furthermore, modification of signal peptides was previously shown to be successful in enhancing protein production and secretion in mammalian cells (Güler-Gane *et al*., 2016; Peng *et al*., 2016; You *et al*., 2018).

- The second objective was to purify soluble CACHD1 from culture supernatant using affinity column chromatography.

6.3 Experimental approach

6.3.1 Modification of signal peptide and tagging of CACHD1 with Avi and 12-His tags

In Chapter 5, a truncated CACHD1 was generated. After truncation, two tags were added – a 12-His tag for protein purification with Ni-NTA affinity column chromatography, and an Avi tag for ligand screening studies using SPR platform.

Here, Q5 DNA polymerase PCR method was used (section 2.4.6) to replace the native signal peptide (M1-A35: MARQPEEEETAVARARRPPLWLLCLVACWLLGAGA; UniProt, Q5VU97) with Igκ signal peptide (METDTLLLWVLLLWVPGSTGD) to facilitate CACHD1 protein secretion from cell. The cloning procedure is shown in Figure 6.1. All final constructs were sequenced to confirm successful modification of the signal peptide in CACHD1.

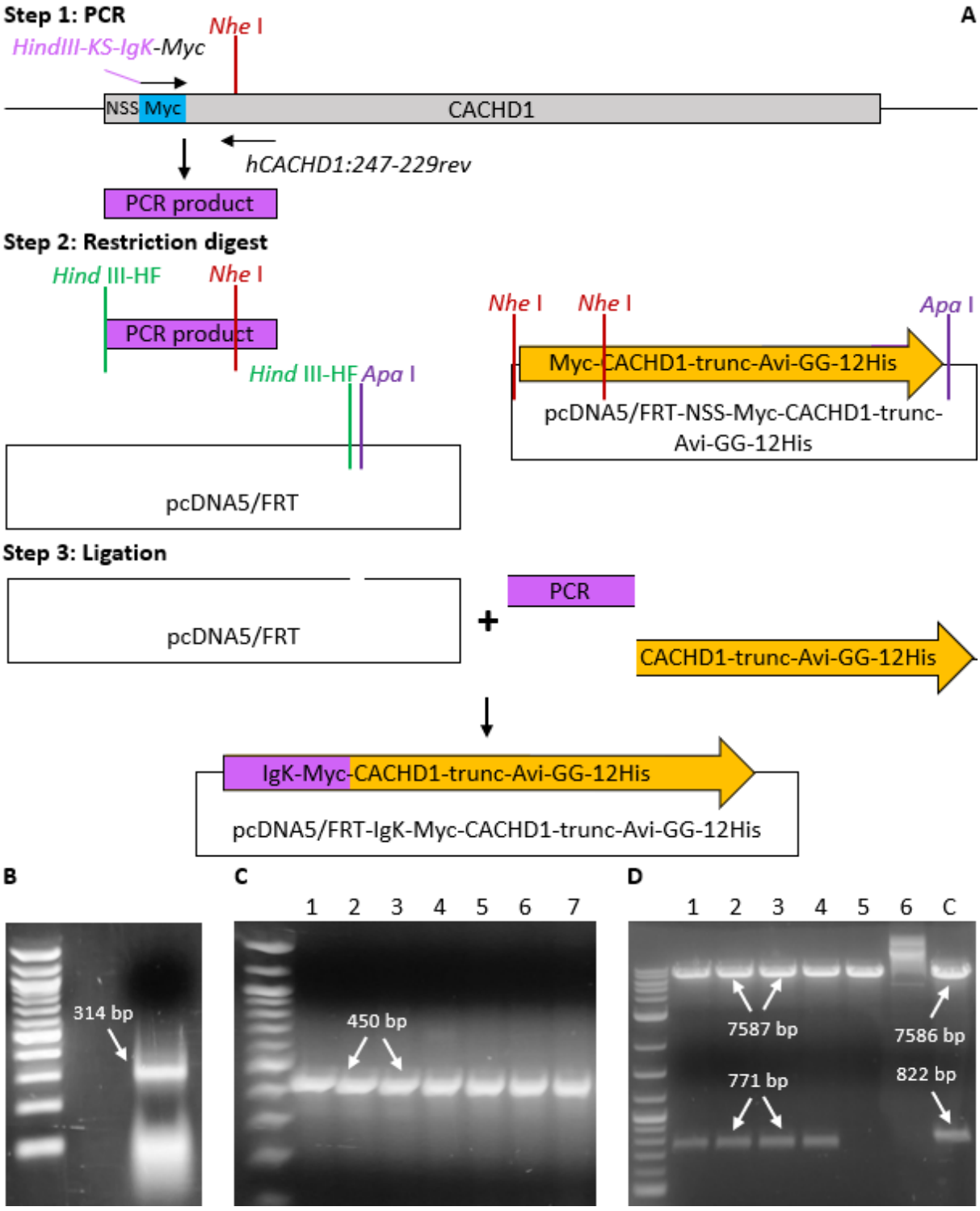

Figure 6.1 Cloning procedure for the modification of the signal peptide in CACHD1. (A) HindIII-KS-Igκ-Myc and hCACHD1:247-229rev primers were used to produce 314 bp Myc-CACHD1 fragment (B) with *Hind* III restriction site and Igκ signal sequence upstream of Myc tag. The PCR product, pcDNA5/FRT-NSS-Myc-CACHD1-trunc-Avi-GG-12His and pcDNA5/FRT were digested with *Hind* III-HF + *Nhe* I, *Nhe* I + *Apa* I, and *Hind* III-HF + *Apa* I respectively to introduce single-stranded overhangs. The final pcDNA5/FRT-Igκ-Myc-CACHD1-trunc-Avi-GG-12His construct was generated by a 3-way ligation with T4 DNA ligase. **(C)** Positive colony PCR with CMV fwd and hCACHD1:247-229rev primers (450bp fragment), **(D)** and restriction digest of final product (lanes 1-4) and pcDNA5/FRT-Igκ-HA-CACHD1-trunc-Avi-GG-12His control (lane C) with *Hind* III-HF + *Cla* I showed expected DNA fragments, suggesting successful modification of the signal peptide in CACHD1. (B-C: 2% agarose gel, 100 bp DNA ladder, NEB; D: 1% agarose gel, 1 kb Plus DNA ladder, NEB).

6.3.2 Validation of Igκ-Myc-CACHD1-trunc-Avi-12His expression and secretion in transiently transfected HEK239 cells

HEK293 cells in a 6-well plate were transiently transfected with 6 µg of pcDNA5/FRT-NSS-Myc-CACHD1-trunc-Avi-12His or pcDNA5/FRT-Igκ-Myc-CACHD1-trunc-Avi-12His construct as described in section 2.1.5 and cultured at 37°C, 5% CO_2, overnight. Culture medium was then discarded, cells were washed 2x with DPBS+CM, and 2 ml of Opti-MEM™ reduced-serum medium (L-glutamine, HEPES, no phenol red; Thermo Fisher Scientific) were added to each well. Cells were allowed to grow at 37°C, 5% CO_2. After 48 h, culture supernatant was collected, concentrated (10x) by centrifugation (4500 *g*, 4°C) using the X12 Membrane Vivaspin 20 concentrator (100 kDa; Sartorius) and resuspended in 10 ml of binding buffer (Table 2.5). The centrifugation-resuspension steps were repeated 3x to remove all serum, and finally concentrated 10x for analysis. Remaining cells were lysed as described in section 2.2.3 to extract non-secreted CACHD1 protein from cells. Western blot was then used to confirm Igκ-Myc-CACHD1-trunc-Avi-12His protein expression and secretion in HEK293 cells (sections 2.2.7-8 and 2.2.10-12).

6.3.3 Generation of stable cell line expressing Igκ-Myc-CACHD1-trunc-Avi-12His protein

To further upscale the production of soluble CACHD1 protein, stable cell line expressing Igκ-Myc-CACHD1-trunc-Avi-12His (section 2.1.1, Table 2.1) was generated using the Flp-In system as outlined in section 2.1.6.

6.3.4 Protein purification method for production of Igκ-Myc-CACHD1-trunc-Avi-12His in mammalian expression system

Stable cells expressing Igκ-Myc-CACHD1-trunc-Avi-12His were plated at $5x10^6$ cells/plate density in five 100 mm cell culture dishes coated with poly-D-lysine and incubated in antibiotic-free DMEM 10% FBS medium at 37°C, 5% CO_2, overnight. The next day, DMEM 10% FBS was removed, and cells were washed 2x with DPBS+CM to remove all serum. 10 ml of Opti-MEM™ reduced-serum medium was then added to each dish and cells were incubated at 37°C, 5% CO_2, for 48 h. Culture supernatant containing secreted proteins was then collected, replaced with 10 ml of fresh Opti-MEM™ medium and cells were incubated for further 24-48 h before supernatant collection. This process was repeated until 500 ml of culture supernatant containing secreted proteins was collected. The culture supernatant was then concentrated

(100x) by centrifugation (4500 *g*, 4°C) using the X12 Membrane Vivaspin 20 concentrator (100 kDa; Sartorius) and resuspended in 50 ml of binding buffer resulting in a 10x concentration. The concentration-resuspension process was repeated 3x to remove all serum and exchange Opti-MEM® medium for binding buffer. After the last concentration step, proteins were resuspended in 20 ml of binding buffer (final Opti-MEM® concentration approx. 0.25%; binding buffer in section 2.2.6, Table 2.5). Following this process, the concentrated protein mixture was stored at -80°C until needed for purification.

Ni-NTA affinity column chromatography method described in section 2.2.6 was used to purify CACHD1 protein from the concentrated protein mixture. A peristaltic pump was used to maintain a flow rate of 1 ml/min (set-up in Figure 6.2). To maintain protein stability and activity throughout the purification procedure, ice cold 20 mM Tris/HCl buffer (pH 8.0) was used because of its stability over a broad pH range (7-9) and ensuring optimal and stable conditions shown in previous studies (Budde *et al*., 2006; Yadav *et al*., 2020). Imidazole was used to elute the 12-His-tagged CACHD1 protein from the column. Imidazole is often used in Ni-NTA affinity chromatography because it competitively binds to the immobilised metal ions on the column, therefore releasing the histidine-tagged proteins, allowing selective protein purification (Bornhorst and Falke, 2000; Vançan *et al*., 2002; Völzke *et al*., 2023). To determine the lowest imidazole concentration required for protein elution, the elution process was optimised by gradually increasing imidazole concentration (10-400 mM). Dot blot (Figure 6.3) showed that 300 mM imidazole was sufficient to elute all CACHD1 protein from the column and was therefore used in the elution buffer. 5 mM and 20 mM imidazole were also used in the binding and wash buffers respectively to reduce binding of non-specific proteins to the Ni-NTA column and thus increasing the purity of the final protein.

The protein purification method consisted of four steps: 1) column equilibration with 20 volumes of binding buffer containing 5 mM imidazole; 2) CACHD1 protein binding to the Ni-NTA agarose column; 3) column wash with wash buffer containing 20 mM imidazole; 4) elution of CACHD1 from the column with 20 ml of elution buffer containing 300 mM imidazole. Purified CACHD1 protein was then concentrated and resuspended in 20 mM Tris/HCl buffer. The concentration-resuspension step was repeated three times to remove residual imidazole that could interfere with further analysis (Kanoh *et al*., 2023). Purified protein was then analysed using western blot (section 2.2.10) and Coomassie Blue staining (section 2.2.9) to

assess the protein size, purity, and degradation levels. A BCA assay (section 2.2.5) was used to determine the final protein yield.

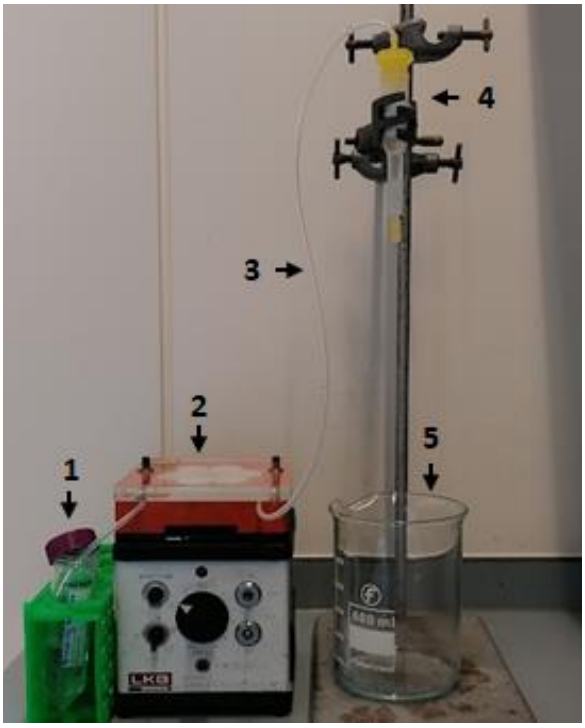

Figure 6.2 Ni-NTA affinity column chromatography set-up for CACHD1 protein purification. (1) Buffer or sample, (2) peristaltic pump maintaining flow rate of 1 ml/min, (3) tubing, (4) Ni-NTA affinity column, (5) vessel for flow-through collection.

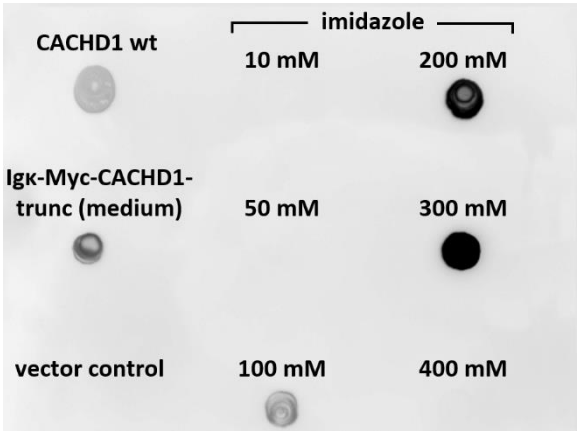

Figure 6.3 Determination of imidazole concentration required for Igκ-CACHD1-trunc protein elution from Ni-NTA chromatography agarose column. Opti-MEM® medium containing secreted proteins underwent a series of concentration-resuspension steps to exchange medium with binding buffer (20 mM Tris/HCl, 5 mM imidazole, pH 8.0). Concentrated protein mixture was put through a Ni-NTA affinity agarose column to allow binding of the 12-His-tagged Igκ-Myc-CACHD1-trunc protein, washed with 20 mM Tris/HCl (pH 8.0), and gradually eluted with 20 mM Tris/HCl (pH 8.0) containing 10-400 mM imidazole. Flow-through was collected for each step (binding, wash, elution). Dot blot analysis was performed by spotting a nitrocellulose membrane with 10 µl of each elution step (10-400 mM imidazole) and controls (CACHD1 wt, culture supernatant, vector control), and dried at 37°C. Blot was blocked for 1 h with 5% milk, followed by incubation with Myc antibody. Immunoreactive Myc-CACHD1 was detected in all controls except the vector control, confirming antibody specificity. The elution of Igκ-Myc-CACHD1-trunc was observed within the 100-300 mM imidazole range, with 300 mM imidazole being sufficient to elute all Igκ-CACHD1-trunc from the chromatography column. No Igκ-Myc-CACHD1-trunc was detected in 10 mM, 50 mM and 400 mM imidazole elution steps. (n=3).

6.4 Results

6.4.1 Igκ signal peptide facilitates Myc-CACHD1-trunc-Avi-12His protein secretion in transiently transfected HEK293 cells

Sub-cellular localisation of Myc-tagged CACHD1 proteins was determined by immunocytochemistry, using rabbit anti-Myc antibody for live cell labelling (section 2.3.4), and mouse anti-Myc antibody for fixed cell labelling (section 2.3.5). Immunoreactive Myc-CACHD1 wild type was expressed at the cell surface and inside the cell (Figure 6.4A). Expression of truncated CACHD1 variants with native and Igκ signal peptides was restricted to only inside the cell, with no detection on cell surface, as shown in Figure 6.4A. No immunoreactive signals were detected for vector control cells, confirming the specificity of detection. Although these results suggested a similar expression pattern for both truncated CACHD1 variants, they did not confirm whether the signal peptide modification facilitated CACHD1-trunc trafficking to cell surface and subsequent secretion.

To address the question of whether modification of the signal peptide in CACHD1 facilitates protein secretion, western blot analysis of cell lysates and culture supernatant was performed. In Figure 6.4B, immunolabelling with rabbit anti-Myc antibody showed the presence of immunoreactive CACHD1-wt, NSS-CACHD1-trunc and Igκ-CACHD1-trunc in cell lysates, with only Igκ-CACHD1-trunc detected in culture supernatant. Notably, no immunoreactive signal was detected in NSS-CACHD1-trunc culture supernatant. Furthermore, Igκ-CACHD1-trunc was detected at the same molecular mass as the NSS-CACHD1-trunc (~140 kDa). These findings confirmed that signal peptide modification in CACHD1 had no effect on the final protein size and it facilitated protein secretion.

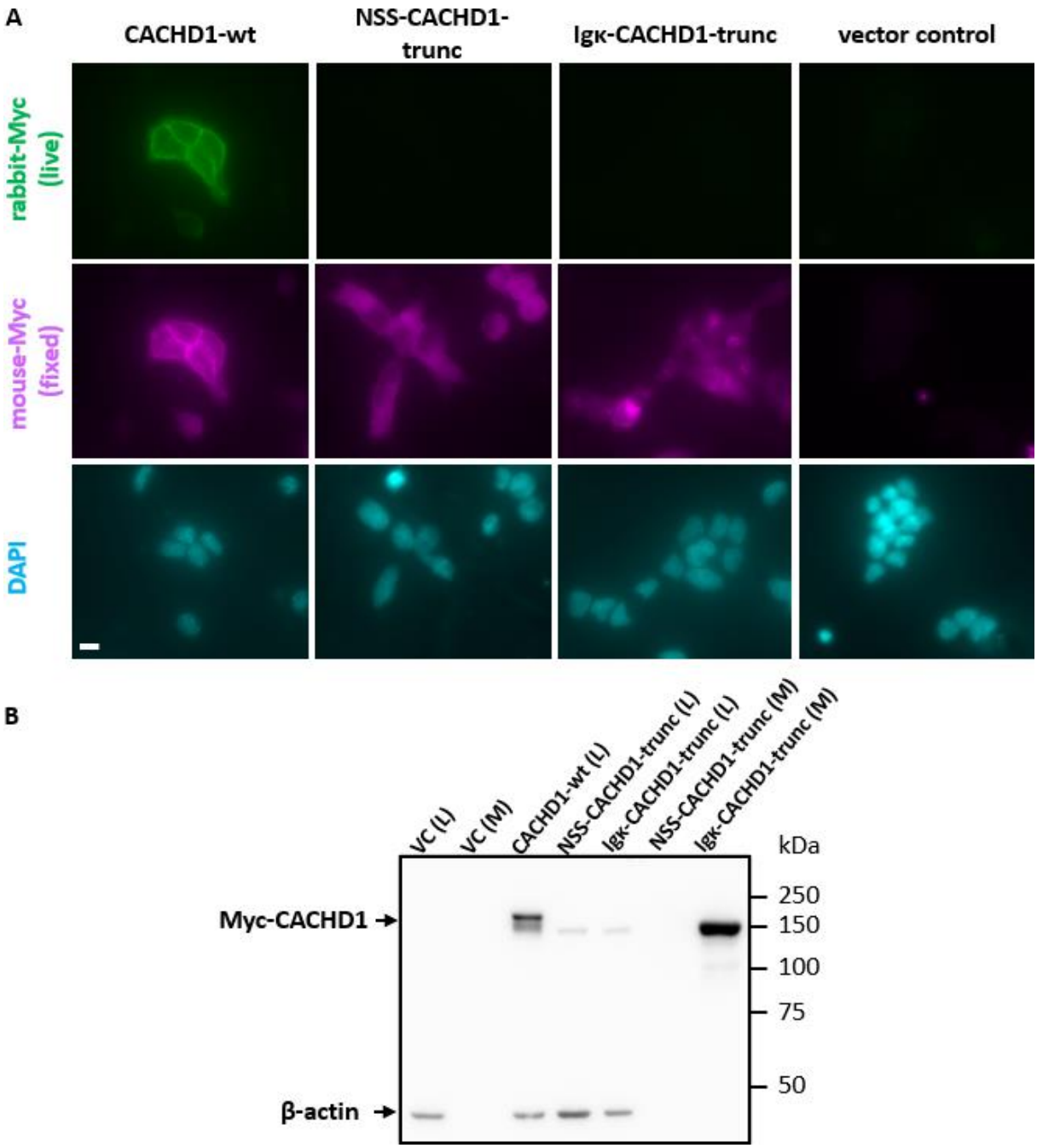

Figure 6.4 Analysis of expression and secretion of truncated Myc-CACHD1 variants by western blotting and immunofluorescence. HEK293 cells were transiently transfected with Myc-CACHD1-wt, NSS-Myc-CACHD1-trunc, Igκ-Myc-CACHD1-trunc, and vector control, and protein expression and secretion were determined by ICC and western blotting. **(A)** Cells were labelled live with rabbit Myc antibody, fixed with 4% PFA and labelled with mouse Myc antibody. Myc-tagged CACHD1-wt was detected at the cell surface and in intracellular compartments by the rabbit and mouse Myc antibodies, respectively. Myc-tagged NSS-CACHD1-trunc and Igκ-Myc-CACHD1-trunc were only detected in intracellular compartments, with no immunofluorescent signals detected at the cell surface. (n=3, Scale bar, 10 µm). **(B)** Culture supernatant containing secreted proteins was collected and remaining cells were lysed. Proteins were separated by SDS-PAGE and blots incubated with antibodies to Myc and β-actin (loading control). Immunoreactive Myc-CACHD1-wt, NSS-Myc-CACHD1-trunc and Igκ-Myc-CACHD1-trunc proteins were detected in cell lysates (L), with only Igκ-Myc-CACHD1-trunc detected in the culture supernatant (M), confirming secretion. Both truncated CACHD1 variants were detected at the same molecular mass, confirming the modification of signal peptide had no effect on final protein size. (9% SDS-PAGE gel, n=3).

6.4.2 Secreted Igκ-Myc-CACHD1-trunc-Avi-12His protein presents at larger molecular mass in comparison to intracellular Igκ-Myc-CACHD1-trunc-Avi-12His protein

Analysis of expression and subsequent secretion of Igκ-Myc-CACHD1-trunc-Avi-12His protein in stable HEK293 Flp-In™ T-REx™ revealed that the secreted Igκ-Myc-CACHD1-trunc exhibited a higher molecular mass (~150 kDa) in comparison to the Igκ-Myc-CACHD1-trunc protein detected in cell lysate (~140 kDa), as shown in Figure 6.5. This difference in molecular mass is most likely to be the result of post-translational modifications, such as glycosylation. Furthermore, the expected molecular mass of Igκ-Myc-CACHD1-trunc is 126 kDa (Uniprot), suggesting that the Myc-CACHD1-trunc present in cell lysate (native and modified signal peptide) may already have undergone some post-translational modifications, and the addition of Igκ signal peptide facilitated further processing and secretion.

In addition to the results showing that modification of the signal peptide to Igκ facilitated secretion of CACHD1-trunc protein (Figure 6.4), the difference in molecular sizes of Igκ-CACHD1-trunc suggested that the modification of the signal peptide may also influence the localisation and subsequent processing of Igκ-CACHD1-trunc protein in stably expressing HEK293 cells. However, the results shown in Figure 6.5 did not confirm that the modification of the signal peptide facilitated glycosylation, and therefore further investigation of the secreted Igκ-Myc-CACHD1-trunc protein glycosylation levels are required.

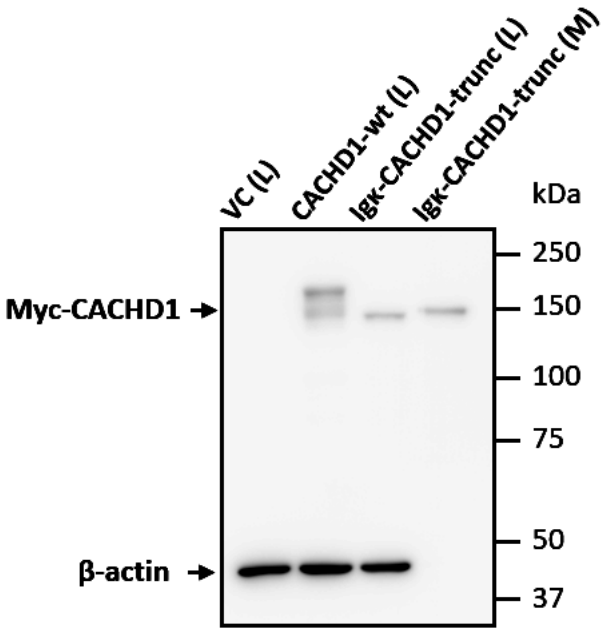

Figure 6.5 Analysis of expression of Igκ-Myc-CACHD1-trunc-Avi-12His protein in stably expressing HEK293 cells. Culture supernatant was collected, and remaining cells were lysed. Proteins were separated by SDS-PAGE and blots incubated with antibodies to Myc and β-actin (loading control). Immunoreactive Myc-CACHD1-wt and Igκ-Myc-CACHD1-trunc proteins were detected at 150-170 kDa and 140-150 kDa, respectively. Secreted Igκ-Myc-CACHD1-trunc (M) was detected at higher molecular mass (~150 kDa) compared to Igκ-Myc-CACHD1-trunc protein detected in cell lysate (~140 kDa), suggesting differential glycosylation.

6.4.3 Ni-NTA affinity column chromatography is an efficient technique for the purification of Igκ-Myc-CACHD1-trunc-Avi-12His protein from mammalian cells

SDS-PAGE followed by western blotting and Coomassie Blue staining were used to confirm isolation and purification of the soluble form of truncated CACHD1 protein from a mammalian expression system.

Figure 6.6A-B shows successful purification of Igκ-Myc-CACHD1-trunc-Avi-12His protein using the method outlined in section 6.3.4, with detection of CACHD1-wt and Igκ-CACHD1-trunc proteins in cell lysates and culture supernatant (140-170 kDa) consistent with previous findings shown in sections 6.4.1 and 6.4.2. Furthermore, a band at approx. 150 kDa was detected by anti-Myc and anti-6His antibodies in the flow-through collected during protein binding step, suggesting that the flow rate was too fast or potential Ni-NTA column overload. No protein bands were detected in the flow-through collected during the wash step. Immunoreactive protein bands were detected by rabbit anti-Myc (Figure 6.6A) and rabbit anti-6His (Figure 6.6B) antibodies, confirming the presence of Igκ-Myc-CACHD1-trunc-Avi-12His in the eluate. Lower molecular mass protein bands at 50-120 kDa were also detected, indicating potential protein degradation. It is important to note that the smaller protein bands showed different patterns when labelled with anti-Myc and anti-6His antibodies (Figure 6.6C). Respective SDS-PAGE gels were stained with Coomassie Blue stain, showing Igκ-Myc-CACHD1-trunc-Avi-12His presence in culture supernatant, binding flow-through, and the eluate. No proteins were detected in the wash flow-through, suggesting that 20 mM imidazole may not be sufficient to elute histidine-rich proteins other than Igκ-Myc-CACHD1-trunc-Avi-12His bound to the column, and therefore these proteins were detected by anti-6His antibody in the final eluate. Increasing imidazole concentration in the wash buffer and size exclusion column (SEC) chromatography could be used to enhance purity of the final protein, and to clarify the nature of the smaller protein bands.

Final protein quantity was assessed by BCA assay, and 500 ml of culture supernatant collected from approx. 25-30x10^7 cells (~1400 cm^2 total growth area) yielded 3.5 mg of Igκ-Myc-CACHD1-trunc-Avi-12His protein (2 ml at 1.75 µg/µl concentration).

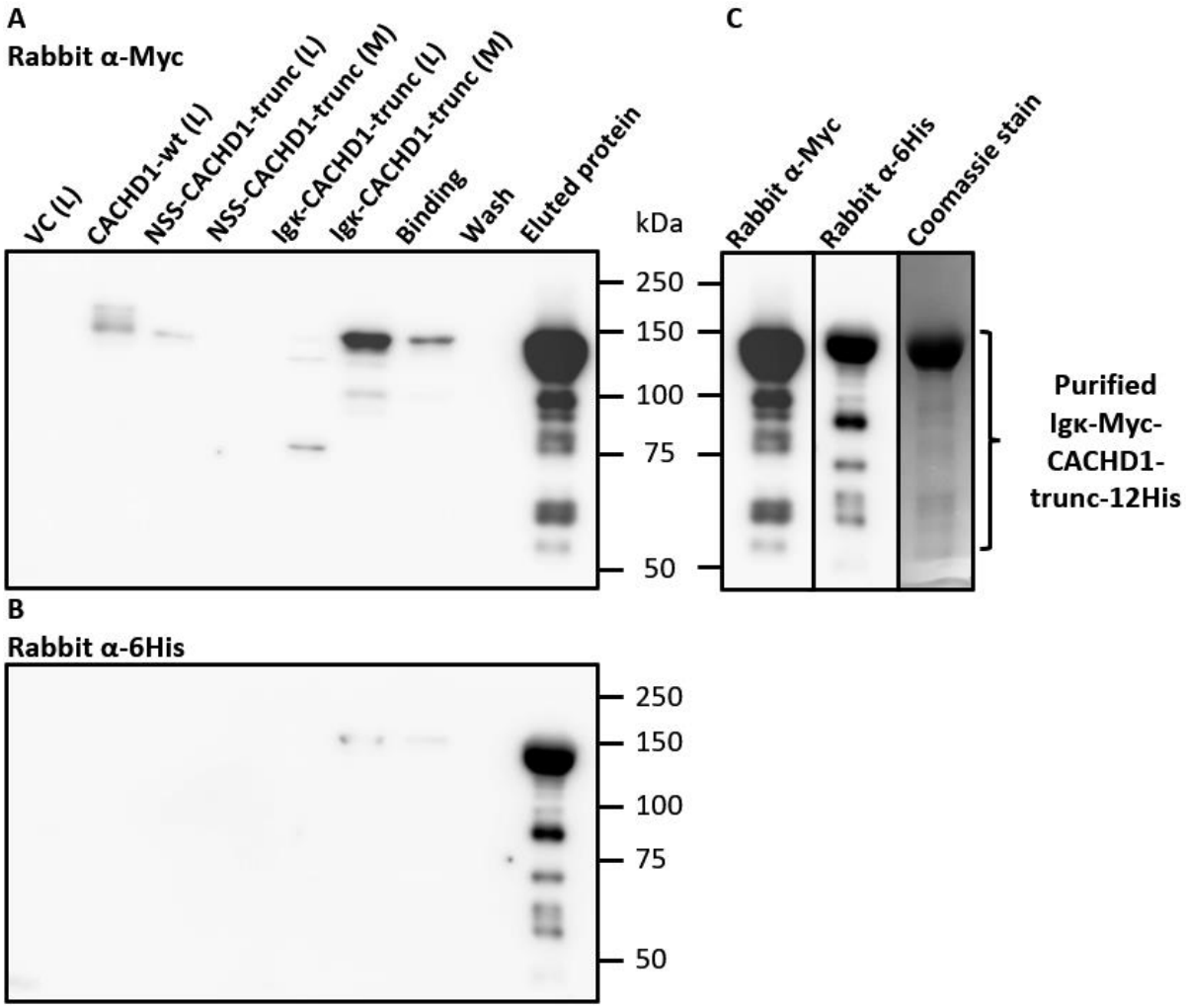

Figure 6.6 Analysis of Igκ-Myc-CACHD1-trunc-Avi-12His protein purification by western blotting. Lysates and culture supernatant were collected from transiently (vectrol control (VC)) and stably expressing cells (CACHD1-wt, NSS-Myc-CACHD1-trunc, Igκ-Myc-CACHD1-trunc). CACHD1-trunc proteins were purified from culture supernatant using Ni-NTA affinity column chromatography. Proteins were separated by SDS-PAGE and blots were incubated with anti-Myc **(A)** and anti-6-His **(B)** antibodies. Immunoreactive CACHD1 proteins were detected at 140-170 kDa in all cell lysate samples, with only Igκ-Myc-CACHD1-trunc detected in culture supenatant (M) and binding flow-through. No immunoreactive proteins were detected in wash flow-through. A strong protein band was detected at 140-150 kDa in the final protein eluate, confirming Igκ-Myc-CACHD1-trunc purification. Smaller protein bands were detected at 50-120 kDa in the final protein eluate **(A, B)**, showing different band pattern when detected with anti-Myc and anti-6-His antibodies **(C)**, indicating protein breakdown or cleavage at different domains. (7% SDS-PAGE gel; Protein loading: lysates 30 µg, culture supernatant, binding and wash flow-through 50 µl, purified protein 10 µg; n=3).

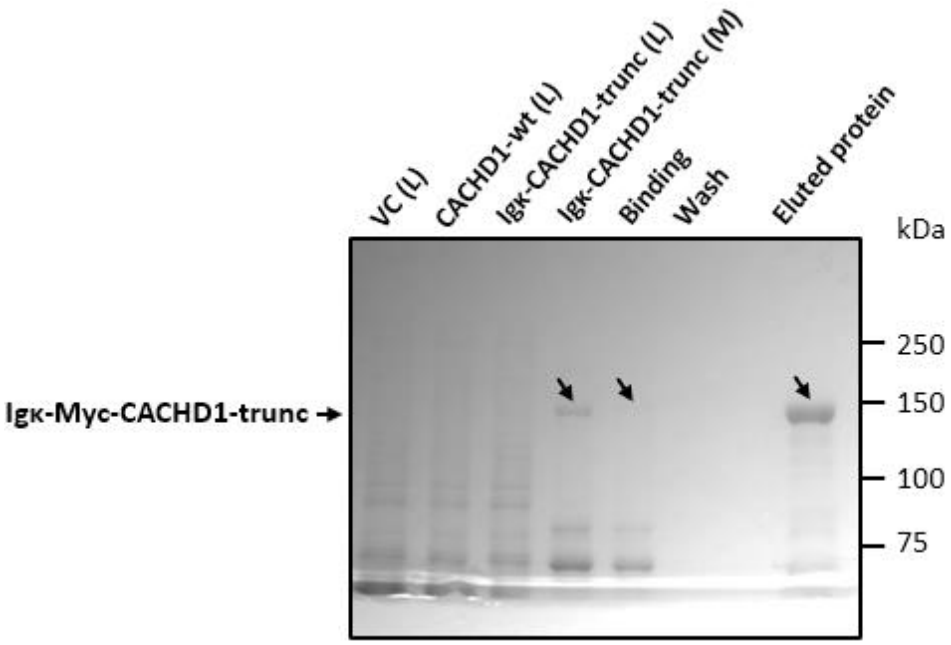

Figure 6.7 Analysis of Igκ-Myc-CACHD1-trunc-Avi-12His protein purification by Coomassie Blue staining. Lysates and culture supernatant were collected from transiently (vectrol control (VC)) and stably expressing cells (CACHD1-wt, NSS-Myc-CACHD1-trunc, Igκ-Myc-CACHD1-trunc). CACHD1-trunc proteins were purified from culture supernatant using Ni-NTA affinity column chromatography. Proteins were separated by SDS-PAGE and gel was stained with Coomassie Blue stain. Igκ-Myc-CACHD1-trunc was detected in culture supernatant (M), binding flow-through and the final protein eluate, confirming successful purification. No CACHD1 protein was detected in lysate samples, possibly due to low protein concentration. (7% SDS-PAGE gel; Protein loading: lysates 30 µg, culture supernatant, binding and wash flow-through 50 µl, purified protein 10 µg; n=3).

6.5 Discussion

Protein purification is an important method that allows the isolation of specific proteins from complex protein mixtures, and affinity column chromatography, in particular Ni-NTA affinity chromatography is a commonly used technique for the isolation of histidine-tagged proteins (Coskun, 2016; Völzke *et al*., 2023). In this chapter, the modification and purification of soluble CACHD1 protein utilising the Ni-NTA affinity chromatography technique was investigated, with the aim to obtain purified CACHD1 protein for future structural and ligand-binding studies.

6.5.1 Signal peptide modification in CACHD1 facilitates protein secretion

Proper localisation and processing are important for the structure and function of proteins in mammalian cells. Signal peptides play an important role in directing and transporting proteins to the correct locations in the endoplasmic reticulum, allowing correct post-translational modifications (Ramazi and Zahiri, 2021). The first objective of this study was to investigate whether the modification of the native signal peptide of CACHD1 to an Igκ signal peptide could facilitate the secretion of truncated CACHD1 protein. Through a series of experiments, it was determined that this modification indeed facilitated the expression and subsequent secretion of truncated CACHD1 in transiently and stably expressing HEK293 cells, corresponding with findings from previous studies showing enhancement of protein expression and secretion by the Igκ signal peptide (Peng *et al*., 2016; Wang *et al*., 2016). Furthermore, the Igκ signal peptide was previously used to secrete proteolytic enzymes (Cottrell *et al*., 2004) and improve expression of GPCRs (Rojas *et al*., 2016). Western blot results revealed that truncated CACHD1 exhibited a higher molecular mass of approximately 140-150 kDa compared to the expected 125 kDa. This difference may be related to post-translational modifications, such as glycosylation, as CACHD1 is known to have up to seven glycosylation sites (Dahimene *et al*., 2018). Furthermore, molecular mass difference of approximately 10 kDa was observed between the intracellular (~140 kDa) and secreted (~150 kDa) truncated CACHD1, suggesting that the addition of Igκ signal peptide facilitated further processing and secretion of CACHD1 protein in HEK293 cells. However, further investigation of CACHD1 glycosylation levels is required, and enzymatic deglycosylation with Peptide-N-Glycosidase F (PNGase F) or Endoglycosidase H (Endo H), or mutagenesis of predicted glycosylation sites could be used to confirm this theory (Kim and Leahy, 2013).

6.5.2 Ni-NTA affinity column chromatography is an effective method for purification of histidine-tagged CACHD1

This study demonstrated efficient production and purification of a soluble truncated form of CACHD1 using HEK293 mammalian expression system and Ni-NTA affinity column chromatography. Western blotting and Coomassie Blue staining confirmed the isolation of truncated CACHD1 from the culture supernatant. However, several smaller protein bands were detected, suggesting protein degradation at some stage during the process. Protein degradation may have occurred during cell culture where enzymes such as proteases cause proteolytic cleavage. To address this concern, lower culture temperature, such as 30°C, could be utilised (Chakrabarti *et al*., 2016). Additionally, protein degradation might have occurred during the concentration of culture supernatant or the purification procedure (Ryan and Henehan, 2016). It is important to note that the smaller protein bands showed different patterns when labelled with anti-Myc and anti-6His antibodies, indicating potential protein cleavage or breakdown at different domains. Additionally, if Igκ-Myc-CACHD1-trunc-Avi-12His polymerised, denaturation during SDS-PAGE would result in monomeric Igκ-Myc-CACHD1-trunc-Avi-12His and partially degraded proteins, explaining the smaller protein bands detected (Lee *et al*., 2011). Furthermore, detection of smaller proteins by anti-6His antibody could indicate presence of other histidine-rich proteins bound to the Ni-NTA agarose column during affinity column chromatography (Rees and Lilley, 2011). More investigation is required to clarify the nature of the smaller proteins present in the final eluate. Methods such as SEC chromatography and high-performance liquid chromatography (SEC-HPLC) could be used to determine the nature of these proteins, as well as detect any impurities present in the final protein eluate. Furthermore, native-PAGE could be used to analyse the native state and size of the purified protein, providing clarity on CACHD1 dimerisation or even oligomerisation.

6.5.3 HEK293 mammalian expression system is effective and efficient for the production of soluble CACHD1 protein

Various expression systems are available for protein production, including bacteria, yeast, and insect cells. However, the recombinant proteins produced in these systems often lack the correct post-translational modifications that are added in eukaryotic cells, or the proteins do not fold properly and/or are inactive (Nosaki *et al*., 2021) and therefore often require further processing, which may result in reduced protein yield (Gomes *et al*., 2018). To overcome the limitations of non-mammalian expression systems, HEK293 cells were used for CACHD1

production due to their capacity to correctly assemble, fold and post-translationally modify proteins (Goh and Ng, 2018). HEK293 cells are often used for initial development and screening before transitioning to scalable systems. To further upscale the production of CACHD1 protein, Chinese hamster ovary (CHO) cells could be used. CHO cells are commonly used for production of recombinant proteins in the biopharmaceutical industry, as they offer advantages such as high productivity, scalability of protein production, and their capacity to be cultured in suspension and in serum-free culture media (Omasa *et al*., 2010; Le Fourn, *et al*., 2014). However, while CHO cells can produce recombinant proteins with human-compatible post-translational modifications, they are not completely able to reproduce human glycostructures, due to the lack of α1,3/4 fucosyl transferase, β-galactoside α2,6-sialyltransferase and β-1,4-N-acetylglucosaminyltransferase III expressed in human cell lines (Goh and Ng, 2018), giving HEK293 cells an advantage of producing recombinant proteins with the desired glycosylation profile. Furthermore, suspension culture HEK293S cells could be used to easily scale up recombinant protein production as they are not limited by surface area like adherent HEK293 cells (Sun *et al*., 2023).

Currently, two human soluble recombinant CACHD1 proteins are commercially available, one produced in insect cells (Antibodies-Online, AA 36-1095) and one in HEK293 cells (BioTechne, 10750-CA). Commercially available CACHD1 can be very costly, costing over £12000 for 1 mg. The method outlined in this chapter demonstrated the feasibility of producing and purifying comparable amount of recombinant CACHD1 protein at a fraction of the cost, with HEK293 expression system yielding 3.5 mg of CACHD1 protein from 500 ml of culture supernatant. While this is a relatively good yield, the purity of the protein needs to be increased, which will likely lead to reduction in the final yield of purified CACHD1.

6.5.4 Conclusion

In conclusion, the modification of native signal peptide to Igκ signal peptide in CACHD1 facilitates protein secretion in HEK293 cells. Moreover, a HEK293 mammalian expression system combined with Ni-NTA affinity column chromatography provided an effective and efficient method for the purification of truncated CACHD1. These findings lay the foundations for future research aimed at exploring the therapeutic potential of CACHD1 as a modulator of Ca_V3 VGCCs.

6.6 Future work

More work is required to further improve the purity of CACHD1 protein generated during this study. SEC chromatography could be used to separate the full size CACHD1-trunc from any degraded proteins present in the final eluate, followed by enzymatic deglycosylation to fully understand the glycosylation profile of the purified Igκ-Myc-CACHD1-trunc-Avi-12His protein. Once the protein is characterised more fully, it could be used for a variety of experiments outlined below.

6.6.1 Ligand identification and characterisation

The aim was to purify a soluble form of CACHD1 protein that could be used for further experiments, such as ligand binding studies. Of particular interest would be the discovery of a small molecule modulator for CACHD1. Such discovery would hold significant therapeutic applications in diseases associated with Ca_V3 VGCCs. SPR could be used to screen for CACHD1 ligands as it allows high throughput screening of large compound libraries, and can detect protein-protein, protein-small molecule, and protein-nucleic acid interactions, providing a wide range of screening opportunities.

Once a ligand is identified, kinetic studies could be performed to characterise its affinity to CACHD1. The Octet platform could be used to quantitively analyse binding kinetics and affinity of CACHD1-ligand interactions. While the Octet platform is useful for studying protein-protein interactions, it also has sensitivity and precision limitations when it comes to studying small molecule-protein interactions (Kamat and Rafique, 2017). Alternatively, the Biacore system could be utilised to study small molecule-protein binding kinetics, affinity, and specificity (Singh, 2016).

Furthermore, identification of CACHD1 ligand, antagonist in particular, could be beneficial in the investigation of CACHD1 effects on Ca_V3 VGCCs expression, trafficking, and their electrophysiological properties.

6.6.2 Further characterisation of CACHD1 MIDAS motif

The next step in the characterisation of CACHD1 MIDAS motif would be the modification of native signal peptide to Igκ signal peptide in CACHD1-AAA MIDAS motif mutant. As shown in Chapter 3, the AAA mutation prevented CACHD1 trafficking to cell surface. It would be of interest to see if modification of the signal peptide facilitated CACHD1-AAA trafficking to cell

surface, subsequently impacting the effect of CACHD1-AAA on T-type currents described in Chapter 4.

Furthermore, other proteins have been shown to contain metal ions within their MIDAS motif, including α2δ subunits (Mg^{2+} or Ca^{2+} ion; Cantí *et al*., 2005), VWA domains (Mg^{2+} ion; Lacy *et al*., 2004), and integrins (Mg^{2+} ion; Carman and Springer, 2003). Techniques like atomic ion spectroscopy (AIS) and atomic absorption spectroscopy (AAS) could be used to identify the metal ion present in the MIDAS motif of CACHD1, and its role in CACHD1 function and structural stability.

6.6.3 CACHD1 antibody production

The purified CACHD1 protein could be used to produce new CACHD1 antibodies. Currently available antibodies against CACHD1 are useful for western blotting; however, there is a lack of reliable antibodies available for immunocytochemistry. The development of new antibodies against CACHD1 could prove beneficial for studying untagged CACHD1 protein, enabling investigation of its sub-cellular localisation and interaction with other proteins.

7. DISCUSSION

This study aimed to address two primary objectives: i) to characterise the variant MIDAS motif in CACHD1 and determine its importance in both, the expression of CACHD1 and CACHD1 function as a modulator of $Ca_V3.1$ VGCCs; ii) to investigate the trafficking and post-endocytic mechanisms employed by CACHD1, with a specific focus on the roles of the transmembrane domain, intracellular C-terminal tail, and the YSTM signal motif located on the C-terminal tail.

Initially identified as a member of the α2δ family by Whittaker and Hynes (2002) using a bioinformatics approach, CACHD1 was later characterised as a modulator of Ca_V3 LVA VGCCs by Cottrell *et al*. (2018). This project sought to expand upon previous findings by investigating the involvement of the variant MIDAS motif (DxGxS) in CACHD1 expression, sub-cellular localisation, and modulation of $Ca_V3.1$. Additionally, this study represents the first investigation into the trafficking mechanisms of CACHD1. Furthermore, a soluble form of CACHD1 was purified during this project, providing a valuable resource for further understanding of the functional and mechanistic aspects of CACHD1 in cellular processes and signalling pathways.

7.1 The variant MIDAS motif in CACHD1 functions similarly to the fully conserved MIDAS motif found in α2δ subunits

The fully conserved MIDAS motif (DxSxS) found in α2δ subunits has been studied extensively and has been shown to be important in the function and trafficking of α2δ and HVA VGCCs (Cantí *et al*., 2005; Hoppa *et al*., 2012; Cassidy *et al*., 2014). Here, the variant MIDAS motif (DxGxS) present in CACHD1 was investigated; specifically its role in CACHD1 expression, sub-cellular localisation, and modulation of $Ca_V3.1$ VGCCs.

Initially, the variant MIDAS motif of CACHD1 was characterised to determine if it has a similar role to the fully conserved MIDAS motif found in α2δ subunits, focusing on CACHD1 expression and sub-cellular localisation in heterologous expression systems in the absence of $Ca_V3.1$. The results reported in Chapter 3 showed that mutating all three key residues (DxGxS) to Ala significantly reduced total CACHD1 expression levels (Figure 3.5) and disrupted CACHD1 trafficking to cell surface (Figure 3.6). Conversely, mutating only the second key residue (G^{236}) to Ser, which led to CACHD1 with a MIDAS motif identical to those found in α2δ subunits, had no significant effects on CACHD1 expression levels or trafficking. Next, the role of the variant MIDAS motif in CACHD1 function as a modulator of $rCa_V3.1$ VGCCs was investigated. To study

the effects of MIDAS motif mutagenesis on CACHD1 modulation of rCa$_V$3.1, stable cell lines where the expression levels of CACHD1-wt, CACHD1-AAA and CACHD1-G236S could be regulated and standardised were generated. The standardisation of expression levels allowed the investigation of CACHD1 functional effects on rCa$_V$3.1 T-type currents associated with MIDAS motif mutagenesis independently of any effects caused by the varying protein expression levels. Both, CACHD1-wt and CACHD1-G236S, significantly increased rCa$_V$3.1 T-type currents and G_{max} by 1.36-fold (Figure 4.9) and 1.49-fold (Figure 4.11), respectively, while the CACHD1-AAA mutant abolished CACHD1-wt-associated current increase and further reduced rCa$_V$3.1 T-type currents by 0.55-fold (Figure 4.10).

The combined results from chapters 3 and 4 mirror the effects seen in α2δ subunits, where the AAA mutation was shown to impair α2δ-1 trafficking to cell surface (Cassidy *et al*., 2014), and abolish the Ca$_V$1 and Ca$_V$2 current increase normally associated with wild-type α2δ-1 (Cantí *et al*., 2005; Hoppa *et al*., 2012; Cassidy *et al*., 2014). Furthermore, the AAA mutation in α2δ-2 was reported to prevent α2δ-2-mediated increase in Ca$_V$2.2 current density (Cantí *et al*., 2005; Hoppa *et al*., 2012). While CACHD1 with a variant (DxGxS) or a fully conserved (DxSxS) MIDAS motif can function equally well, this study demonstrated that CACHD1 modulation of rCa$_V$3.1 is dependent on the MIDAS motif integrity. Taken together, these results indicate that the variant MIDAS motif (DxGxS) in CACHD1 and the fully conserved MIDAS motif in α2δ subunits function in a similar way.

7.1.1 Proposed mechanism of CACHD1-Ca$_V$3.1 interaction

CACHD1 appears to modulate Ca$_V$3.1 VGCCs through two different mechanisms: i) by promoting forward trafficking to cell surface as CACHD1 was shown to promote Ca$_V$3.1 cell surface expression (Cottrell *et al*., 2018), and ii) by a MIDAS motif-dependent interaction between CACHD1 and Ca$_V$3.1, important for modulation of Ca$_V$3.1 function. Figure 7.1 illustrates the two proposed mechanisms of interaction between CACHD1 and Ca$_V$3.1.

Hypothesis 1: CACHD1 and Ca$_V$3.1 interact intracellularly and are trafficked to cell surface as a CACHD1/Ca$_V$3.1 complex.

This hypothesis tests that the variant MIDAS motif of CACHD1 is involved in CACHD1-Ca$_V$3.1 interaction. This hypothesis is based on the reports that the MIDAS motif in other proteins is known to bind Ca^{2+}, Mn^{2+} or Mg^{2+} ions, which then in turn leads to conformational changes within the VWA domain that promote protein function, and mutations in the MIDAS motif

have been reported to disrupt the ion binding, leading to disrupted protein function (Mould *et al*., 2002; Valdramidou *et al*., 2008). Cantí *et al*. (2005) proposed that, in α2δ subunits, the key MIDAS motif residues bind Ca^{2+}/Mg^{2+} when the concentration of divalent cations is high in the endoplasmic reticulum, causing conformational changes in α2δ that allow correct folding and subsequent trafficking of the $Ca_V\alpha1$ complex to cell membrane. Interestingly, the mutagenesis of all three key residues to alanine (DxSxS ⇔ AxAxA) had no effect on α2δ-2 protein folding or trafficking when expressed alone; however, it reduced cell surface expression of its complexes with the pore-forming $Ca_V\alpha1$ and $Ca_V2.2$ subunits (Cantí *et al*., 2005). This suggests that binding of divalent cations in the ER or other intracellular compartments may be critical for CACHD1-$Ca_V3.1$ interaction and trafficking to the cell surface. Disruption of this binding caused by MIDAS motif mutagenesis could alter the intracellular interaction between CACHD1 and $Ca_V3.1$, potentially resulting in intracellular retention of $Ca_V3.1$. PLA could be used to investigate this hypothesis, and to determine whether CACHD1 and $Ca_V3.1$ interact intracellularly. While the mutagenesis of G^{236} residue to Ser, resulting in CACHD1 with a ”fully conserved” MIDAS motif (DxSxS), showed no effect on normal function of CACHD1, mutating the key residues to Ala (AxAxA) resulted in disrupted CACHD1 function, potentially causing intracellular retention of $Ca_V3.1$. If CACHD1 and $Ca_V3.1$ interact intracellularly, the AAA-associated disruption of CACHD1-trafficking to cell surface (Figure 3.6) could account for the observed decrease in $rCa_V3.1$ T-type current (Figure 4.10), similar to the effects reported for α2δ-1-AAA/Ca_V1 and α2δ-1-AAA/Ca_V2 complexes (Cantí *et al*., 2005; Hoppa *et al*., 2012; Cassidy *et al*., 2014).

Hypothesis 2: CACHD1 and $Ca_V3.1$ are trafficked to cell surface separately and then interact at the cell surface.

This hypothesis tests that CACHD1 and $Ca_V3.1$ are trafficked separately to the cell surface where they interact. However, this is an unlikely scenario due to the results presented in Chapter 4, where CACHD1-AAA significantly reduced $rCa_V3.1$ T-type currents in comparison to $rCa_V3.1$ expressed alone (Figure 4.10). Given that CACHD1-AAA could not be detected at the cell surface (Figure 3.6), if CACHD1 and $Ca_V3.1$ only interacted at the cell surface, one would expect no additional decrease in $rCa_V3.1$ T-type currents.

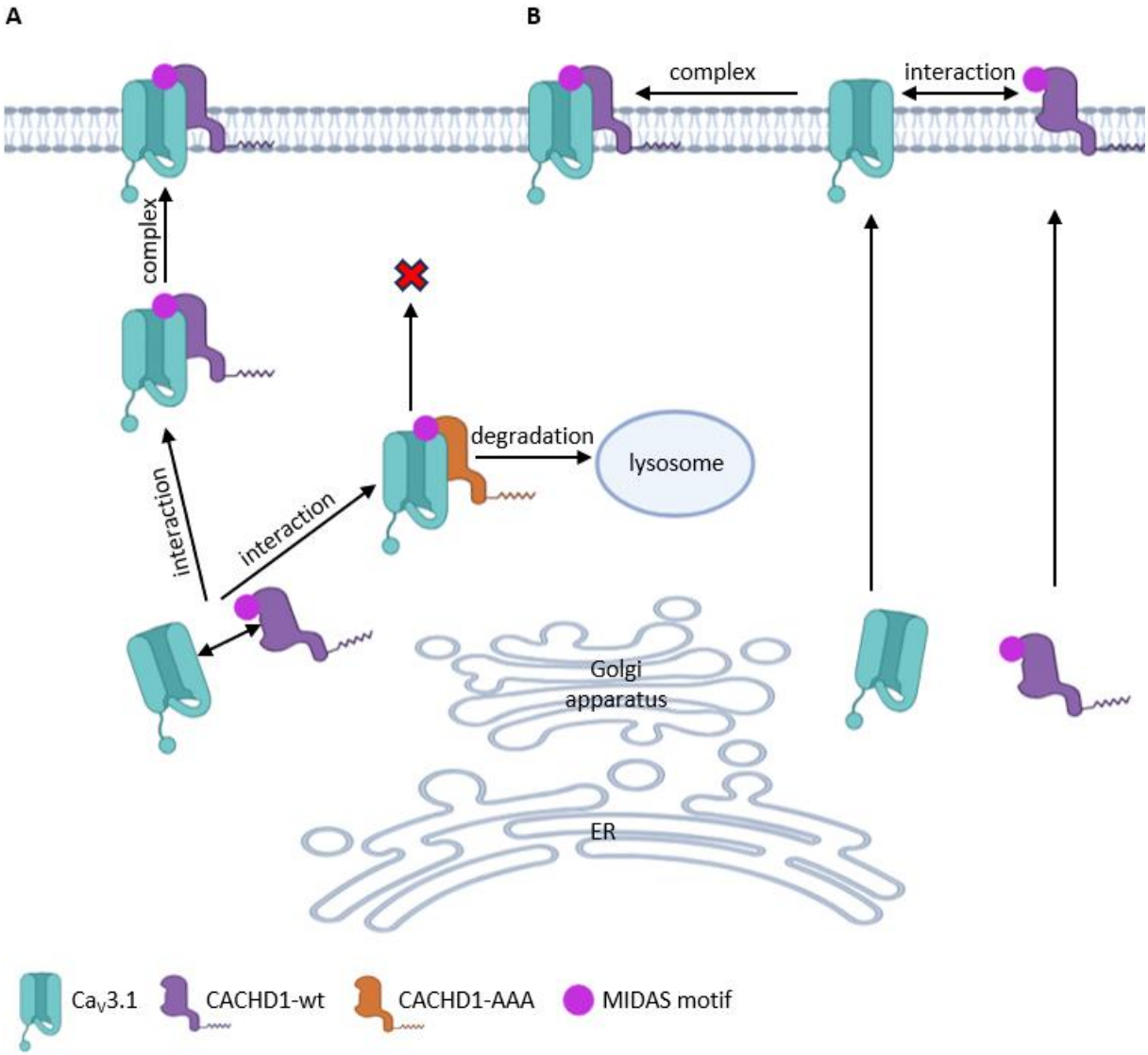

Figure 7.1 Proposed mechanisms of CACHD1-Ca_V3.1 interaction. (A) CACHD1 and Ca_V3.1 interact intracellularly, forming a complex that is trafficked to the membrane. Mutagenesis of the variant MIDAS motif in CACHD1, DxGxS, to AxAxA, disrupts CACHD1 and potentially CACHD1-AAA/Ca_V3.1 complex trafficking to the membrane, possibly due to protein misfolding and subsequent protein degradation by lysosome. **(B)** CACHD1 and Ca_V3.1 traffic to the membrane independently of each other and interact at the membrane. (Made in Biorender.com and Photoshop).

7.2 CACHD1 trafficking

The intricate mechanisms governing protein trafficking in cells have been the subject of this study. As a relatively new protein, CACHD1 research has primarily focused on its functional effects on LVA VGCCs and its potential role in disease, while the mechanisms governing the trafficking and processing of CACHD1 in cells have remained unexplored. This study represents the first attempt to define the internalisation and post-endocytic sorting mechanisms used by CACHD1 in heterologous expression systems.

Starting with the characterisation of CACHD1 constitutive internalisation, the results showed a consistent internalisation pattern of CACHD1 over time, accompanied by an apparent decrease in intracellular CACHD1 levels at the 4-hour timepoint. This observation suggested that CACHD1 was recycled back to the cell surface, as no decrease in cell surface CACHD1 was observed. Furthermore, this is supported by the fact that CACHD1 was detected in Rab11-positive recycling endosomes (Figure 5.12). Notably, if CACHD1 underwent degradation, one would expect the cell surface CACHD1 levels to decrease over time.

Subsequently, two primary endocytic pathways, clathrin-mediated and caveolae-dependent, were investigated as the possible pathways used by CACHD1 for internalisation. Inhibitors, namely hypotonic sucrose, MβCD and nystatin, were used to determine which endocytic pathway is used by CACHD1. Out of the three inhibitors, only MβCD exhibited inhibition of CACHD1 internalisation, suggesting that CACHD1 internalises via caveolae in a cholesterol-dependent manner. This was further supported by the results showing that recovery of cholesterol levels for one hour partially reinstated CACHD1 internalisation, with complete restoration of CACHD1 internalisation after two hours of cholesterol recovery. Similar outcomes were reported for I-transferrin, where restored internalisation post-MβCD treatment was attributed to cholesterol synthesis and restoration in cells (Rodal *et al*., 1999). Moreover, the post-endocytic sorting of CACHD1 was investigated, and the results showed CACHD1 co-localisation with EEA1, Rab5 and Rab11 proteins. This suggests post-endocytic sorting of CACHD1 via Rab5-associated early endosomes followed by recycling back to the membrane via Rab11-associated recycling endosomes. These findings draw further parallels between CACHD1 and α2δ subunits, as α2δ-1 and α2δ-2 subunits have been shown to use a Rab11a-mediated recycling pathway (Tran-Van-Minh and Dolphin, 2010; Meyer and Dolphin, 2021).

In addition to exploring the endocytic and post-endocytic pathways, this study investigated the roles of the transmembrane domain, intracellular C-terminal tail, and the YSTM signal motif identified on the C-terminal tail of CACHD1. The YSTM motif is a tyrosine-based signal motif where, typically, the Tyr residue is critical for its function (Pandey, 2009). To investigate the role of the YSTM motif, mutations of the Tyr^{1197} residue to Ala (Y1197A) and Phe (Y197F) were introduced. Previous studies indicated that such mutations often slow down or inhibit protein internalisation (Li *et al*., 2000; Novakovic *et al*., 2004; Pain *et al*., 2004; Minakshi and Padhan, 2014). Interestingly, while the Y1197F mutation resulted in an apparent slower internalisation rate compared to CACHD1-wt, the Y1197A mutation appeared to have no discernible effect on CACHD1 internalisation; suggesting that CACHD1 internalisation may be mediated by its YSTM signal motif. However, further investigation revealed that a truncated version of CACHD1 lacking the C-terminal tail, thus the YSTM signal motif, internalised in a similar manner to CACHD1-wt. This implies that CACHD1 does not solely rely on the YSTM motif but may also use other motifs, possibly extracellular ones, for internalisation.

Further truncation of CACHD1 by removing its transmembrane domain disrupted CACHD1 trafficking to the cell surface, resulting in intracellular retention of CACHD1. This suggested that the removal of the transmembrane domain resulted in either a misfolded protein or in a loss of interaction sites required by trafficking proteins which may interact with CACHD1. This truncated CACHD1 was further studied in Chapter 6, with the aim of obtaining a soluble form of CACHD1. Initially, the natural signal peptide was replaced with an Igκ signal peptide, which facilitated the secretion of CACHD1-trunc out of the cells. Subsequently, CACHD1-trunc was purified from culture media using the Ni-NTA column chromatography method. Using this method, 3.5 mg of CACHD1-trunc were obtained, although additional work is required to enhance the purity of the final product.

Overall, the findings presented in Chapters 5 and 6 highlight the complexity of CACHD1 trafficking mechanisms and underscore the importance of individual structural motifs and domains in mediating its internalisation and processing. While the exact internalisation and trafficking mechanisms remain to be fully elucidated, Figure 7.2 illustrates the proposed pathways used by CACHD1.

7.2.1 Proposed CACHD1 internalisation and post-endocytic sorting mechanisms

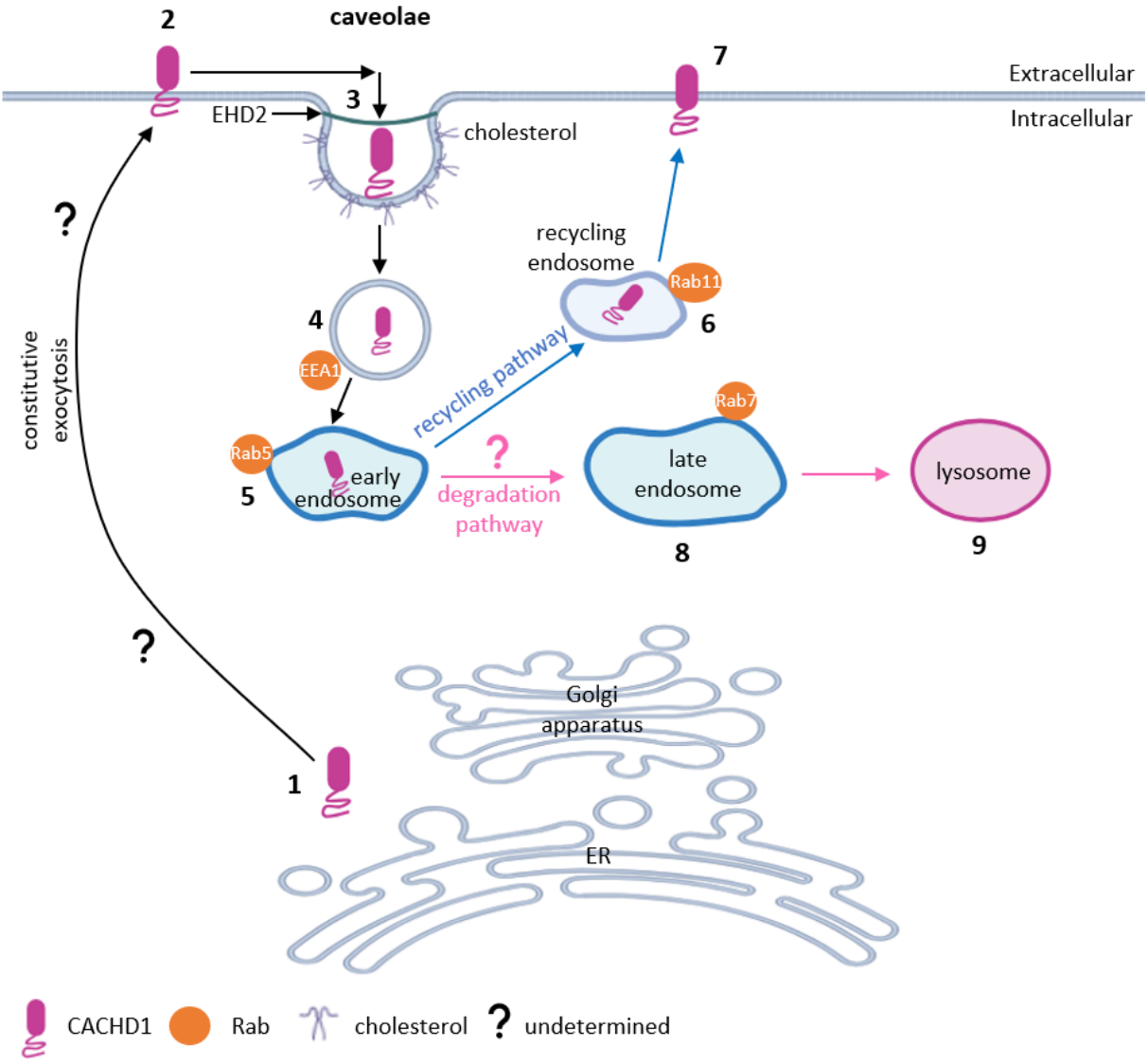

Figure 7.2 Proposed endocytic and post-endocytic sorting mechanisms used by CACHD1. (1-2) CACHD1 is constitutively trafficked to the membrane. **(3)** CACHD1 is internalised via the caveolae-dependent pathway, primarily relying on cholesterol. EHD2 (EH-domain-containing protein 2) constricts the caveolae neck, leading to vesicle separation from the membrane. **(4)** EEA1 (early endosomal antigen 1) is present at the vesicle before fusion with early endosomes. **(5)** The vesicle fuses with Rab5-associated early endosomes. **(6-7)** CACHD1 is recycled back to the membrane through Rab11-associated recycling endosomes. **(8-9)** Alternative pathway: CACHD1 is degraded through the Rab7-associated late endosome and lysosome pathway, but this remains to be determined.

7.3 Conclusions

The findings presented in this study have significant implications for therapeutic interventions targeting Ca_V3 VGCCs, especially in the context of hyperexcitability diseases such as epilepsy, neuropathic pain, and other disorders associated with the dysregulation of neuronal excitability. By characterising the variant MIDAS motif in CACHD1 and identifying its importance in modulating $Ca_V3.1$ VGCCs, this study highlights a new mechanism by which CACHD1 influences calcium currents. Results showing that mutagenesis of the MIDAS motif significantly reduces CACHD1 expression and cell surface trafficking, mirroring effects seen in α2δ subunit, demonstrates the critical role of this motif in Ca_V3 VGCC modulation. Furthermore, the MIDAS-dependent increase in $Ca_V3.1$ currents suggests that CACHD1 could be a novel target for modulating Ca_V3 VGCCs in hyperexcitability conditions. Similar to gabapentinoids targeting α2δ subunits in HVA VGCC associated diseases, drugs could be developed to target CACHD1-Ca_V3 interaction to reduce calcium influx and excitability.

Moreover, the exploration of CACHD1 trafficking mechanisms, particularly its caveolae-mediated internalization and Rab11-dependent recycling, draws parallels to the trafficking mechanisms of α2δ subunits. This opens avenues for therapeutic strategies aimed at disrupting CACHD1 trafficking or recycling to control its regulatory effects on Ca_V3 channels. If specific inhibitors or modulators can be identified to target these processes, they could offer new treatment options for conditions where excessive Ca_V3 VGCC activity contributes to disease pathology. Additionally, the purification of a soluble form of CACHD1 provides a tool for future structural studies and high-throughput screening of potential modulators, accelerating drug discovery in this area. Ultimately, these findings suggest that targeting CACHD1, either by disrupting its surface trafficking or modulating its interaction with Ca_V3 VGCCs, holds therapeutic potential for managing hyperexcitability diseases.

REFERENCES

Ablinger, C., Eibl, C., Geisler, S. M., Campiglio, M., Stephens, G. J., Missler, M., & Obermair, G. J. (2022). α2δ-4 and Cachd1 Proteins Are Regulators of Presynaptic Functions. International Journal of Molecular Sciences, 23(17). https://doi.org/10.3390/ijms23179885.

Ablinger, C., Eibl, C., Roznovcova, M., Cottrell, G. S., Stephens, G. J., & Obermair, G. J. (2024). The presynaptic α2δ protein family and their therapeutic potential. In G. J. Stephens & E. B. tevens (Eds.), Ion Channels as Targets in Drug Discovery. Springer.

Alhazmi, H. A., & Albratty, M. (2023). Analytical Techniques for the Characterization and Quantification of Monoclonal Antibodies. Pharmaceuticals, 16(291). https://doi.org/10.3390/ph16020291.

Anantharaman, V., & Aravind, L. (2000). Cache - A signaling domain common to animal Ca2+-channel subunits and a class of prokaryotic chemotaxis receptors. Trends in Biochemical Sciences, 25(11), 535–537. https://doi.org/10.1016/S0968-0004(00)01672-8.

Antonell, A., Lladó, A., Altirriba, J., Botta-Orfila, T., Balasa, M., Fernández, M., Ferrer, I., Sánchez-Valle, R., & Molinuevo, J. L. (2013). A preliminary study of the whole-genome expression profile of sporadic and monogenic early-onset Alzheimer's disease. Neurobiology of Aging, 34(7), 1772–1778. https://doi.org/10.1016/j.neurobiolaging.2012.12.026.

Anderson, R. G. (1998). The caveolae membrane system. Annu Rev Biochem, 67, 199-225.

Antonescu, C. N., Foti, M., Sauvonnet, N., & Klip, A. (2009). Ready, set, internalize: mechanisms and regulation of GLUT4 endocytosis. Bioscience Reports, 29(1), 1–11. https://doi.org/10.1042/BSR20080105.

Antonny, B., Burd, C., de Camilli, P., Chen, E., Daumke, O., Faelber, K., Ford, M., Frolov, V. A., Frost, A., Hinshaw, J. E., Kirchhausen, T., Kozlov, M. M., Lenz, M., Low, H. H., McMahon, H., Merrifield, C., Pollard, T. D., Robinson, P. J., Roux, A., & Schmid, S. (2016). Membrane fission by dynamin: what we know and what we need to know. The EMBO Journal, 35(21), 2270–2284. https://doi.org/10.15252/embj.201694613.

Apkarian, A. V., Bushnell, M. C., Treede, R. D., & Zubieta, J. K. (2005). Human brain mechanisms of pain perception and regulation in health and disease. European Journal of Pain, 9(4), 463–484. https://doi.org/10.1016/j.ejpain.2004.11.001

Aromolaran, K. A., Benzow, K. A., Cribbs, L. L., Koob, M. D., & Piedras-Rentería, E. S. (2010). T-type current modulation by the actin-binding protein Kelch-like 1. Am J Physiol-Cell Physiol, 298, 1353–1362. https://doi.org/10.1152/ajpcell.00235.2009.

Azizan, E. A. B., Poulsen, H., Tuluc, P., Zhou, J., Clausen, M. v., Lieb, A., Maniero, C., Garg, S., Bochukova, E. G., Zhao, W., Shaikh, L. H., Brighton, C. A., Teo, A. E. D., Davenport, A. P., Dekkers, T., Tops, B., Küsters, B., Ceral, J., Yeo, G. S. H., … Brown, M. J. (2013). Somatic mutations in ATP1A1 and CACNA1D underlie a common subtype of adrenal hypertension. Nature Genetics, 45(9), 1055–1060. https://doi.org/10.1038/ng.2716.

Ba-Abbad, R., Arno, G., Carss, K., Stirrups, K., Penkett, C. J., Moore, A. T., Michaelides, M., Raymond, F. L., Webster, A. R., & Holder, G. E. (2016). Mutations in CACNA2D4 Cause Distinctive Retinal Dysfunction in Humans. Ophthalmology, 123(3), 668-671.e2. https://doi.org/10.1016/j.ophtha.2015.09.045.

Bader, P. L., Faizi, M., Kim, L. H., Owen, S. F., Tadross, M. R., Alfa, R. W., Bett, G. C. L., Tsien, R. W., Rasmusson, R. L., & Shamloo, M. (2011). Mouse model of Timothy syndrome recapitulates triad of autistic traits. Proceedings of the National Academy of Sciences of the United States of America, 108(37), 15432–15437. https://doi.org/10.1073/pnas.1112667108.

Baig, S. M., Koschak, A., Lieb, A., Gebhart, M., Dafinger, C., Nürnberg, G., Ali, A., Ahmad, I., Sinnegger-Brauns, M. J., Brandt, N., Engel, J., Mangoni, M. E., Farooq, M., Khan, H. U., Nürnberg, P., Striessnig, J., & Bolz, H. J. (2011). Loss of Cav 1.3 (CACNA1D) function in a human channelopathy with bradycardia and congenital deafness. Nature Neuroscience, 14(1), 77–86. https://doi.org/10.1038/nn.2694.

Balijepalli, R. C., Foell, J. D., Hall, D. D., Hell, J. W., & Kamp, T. J. (2006). Localization of cardiac L-type Ca 2 channels to a caveolar macromolecular signaling complex is required for 2-adrenergic regulation. PNAS, 103(19). www.pnas.orgcgidoi10.1073pnas.0503465103.

Bannister, R. A., & Beam, K. G. (2013). CaV1.1: The atypical prototypical voltage-gated Ca2 + channel. Biochim Biophys Acta, 1828(7), 1587–1597. https://doi.org/10.1016/j.bbamem.2012.09.007.

Barclay, J., Balaguero, N., Mione, M., Ackerman, S. L., Letts, V. A., Brodbeck, J., Canti, C., Meir, A., Page, K. M., Kusumi, K., Perez-Reyes, E., Lander, E. S., Frankel, W. N., Gardiner, R. M., Dolphin, A. C., & Rees, M. (2001). Ducky Mouse Phenotype of Epilepsy and Ataxia Is Associated with Mutations in the Cacna2d2 Gene and Decreased Calcium Channel Current in Cerebellar Purkinje Cells. Journal of Neuroscience, 21(16), 6095–6104.

Barrett, C. F., & Tsien, R. W. (2008). The Timothy syndrome mutation differentially affects voltage-and calcium-dependent inactivation of Ca V 1.2 L-type calcium channels. PNAS, 105(6), 2157–2162.

Barron, T., & Kim, J. H. (2019). Neuronal input triggers Ca2+ influx through AMPA receptors and voltage-gated Ca2+ channels in oligodendrocytes. GLIA, 67, 1922–1932. https://doi.org/10.1002/glia.23670.

Bauer, C. S., Nieto-Rostro, M., Rahman, W., Tran-Van-Minh, A., Ferron, L., Douglas, L., Kadurin, I., Ranjan, Y. S., Fernandez-Alacid, L., Millar, N. S., Dickenson, A. H., Lujan, R., & Dolphin, A. C. (2009). The increased trafficking of the calcium channel subunit α2δ-l to presynaptic terminals in neuropathic pain is inhibited by the α2δ ligand pregabalin. The Journal of Neuroscience, 29(13), 4076–4088. https://doi.org/10.1523/JNEUROSCI.0356-09.2009.

Benkert, J., Hess, S., Roy, S., Beccano-Kelly, D., Wiederspohn, N., Duda, J., Simons, C., Patil, K., Gaifullina, A., Mannal, N., Dragicevic, E., Spaich, D., Müller, S., Nemeth, J., Hollmann, H., Deuter, N., Mousba, Y., Kubisch, C., Poetschke, C., … Liss, B. (2019). Cav2.3 channels contribute to dopaminergic neuron loss in a model of Parkinson's disease. Nature Communications, 10(5094). https://doi.org/10.1038/s41467-019-12834-x.

Bernstein, G. M., & Jones, O. T. (2007). Kinetics of internalization and degradation of N-type voltage-gated calcium channels: Role of the α2/δ subunit. Cell Calcium, 41, 27–40. https://doi.org/10.1016/j.ceca.2006.04.010.

Berrow, N. S., Campbell, V., Fitzgerald, E. M., Brickley, K., & Dolphin, A. C. (1995). Antisense depletion of/i-subunits modulates the biophysical and pharmacological properties of neuronal calcium channels. Journal of Physiology, 482(3), 481–491.

Beurrier, C., Congar, P., Bioulac, B., & Hammond, C. (1999). Subthalamic Nucleus Neurons Switch from Single-Spike Activity to Burst-Firing Mode. The Journal of Neuroscience, 19(2), 599–609.

Bieber, T., Meissner, W., Kostin, S., Niemann, A., & Elsasser, H.-P. (2002). Intracellular route and transcriptional competence of polyethylenimine–DNA complexes. Journal of Controlled Release, 82, 441–454.

Bonifacino, J. S., & Dell'angelica, E. C. (1999). Mini-Review Molecular Bases for the Recognition of Tyrosine-based Sorting Signals. The Journal of Cell Biology, 145(5), 923–926. http://www.jcb.org.

Bonifacino, J. S., & Traub, L. M. (2003). Signals for sorting of transmembrane proteins to endosomes and lysosomes. Annual Review of Biochemistry, 72, 395–447. https://doi.org/10.1146/annurev.biochem.72.121801.161800.

Bornhorst, J. A., & Falke, J. J. (2000). Purification of Proteins Using Polyhistidine Affinity Tags. Methods in Enzymology, 326, 245-254. Methods in Enzymology, 326, 245–254.

Boroujerdi, A., Zeng, J., Sharp, K., Kim, D., Steward, O., Luo, D. Z. (2011). Calcium channel alpha-2-delta-1 protein upregulation in dorsal spinal cord mediates spinal cord injury-induced neuropathic pain states. Pain, 152(3), 649-655. doi: 10.1016/j.pain.2010.12.014.

Bourinet, E., Francois, A., & Laffray, S. (2016). T-type calcium channels in neuropathic pain. Pain, 157, S15–S22. https://doi.org/10.1097/j.pain.0000000000000469.

Briot, J., Mailhot, O., Bourdin, B., Tétreault, M. P., Najmanovich, R., & Parent, L. (2018). A three-way inter-molecular network accounts for the CaV21-induced functional modulation of the pore-forming CaV1.2 subunit. Journal of Biological Chemistry, 293(19), 7176–7188. https://doi.org/10.1074/jbc.RA118.001902.

Brothers, S. P., Janovick, J. A., Maya-Nunez, G., Cornea, A., Han, X.-B., & Conn, P. M. (2002). Conserved mammalian gonadotropin-releasing hormone receptor carboxyl terminal amino

acids regulate ligand binding, effector coupling and internalization. Molecular and Cellular Endocrinology, 190, 19–27. www.elsevier.com/locate/mce.

Brown, J. P., Gee, N. S. (1998). Cloning and deletion mutagenesis of the alpha2 delta calcium channel subunit from porcine cerebral cortex. Expression of a soluble form of the protein that retains [3H]gabapentin binding activity. Journal of Biological Chemistry, 273(39), 25458-65. doi: 10.1074/jbc.273.39.25458.

Brown, K. L., Banerjee, S., Feigley, A., Abe, H., Blackwell, T. S., Pozzi, A., Hudson, B. G., & Zent, R. (2018). Salt-bridge modulates differential calcium-mediated ligand binding to integrin α1- and α2-I domains. Scientific Reports, 8(2916). https://doi.org/10.1038/s41598-018-21231-1

Budde, C., Schoenfish, M. J., Linder, M. E., & Deschenes, R. J. (2006). Purification and Characterization of Recombinant Protein Acyltransferases. Methods, 40(2),. Methods, 40(2), 143–150.

Burashnikov, E., Pfeiffer, R., Barajas-Martinez, H., Delpón, E., Hu, D., Desai, M., Borggrefe, M., Hissaguerre, M., Kanter, R., Pollevick, G. D., Guerchicoff, A., Laio, R., Marieb, M., Nademanee, K., Nam, G. B., Robles, R., Schimpf, R., Stapleton, D. D., Viskin, S., … Antzelevitch, C. (2010). Mutations in the cardiac L-type calcium channel associated with inherited J-wave syndromes and sudden cardiac death. Heart Rhythm, 7(12), 1872–1882. https://doi.org/10.1016/j.hrthm.2010.08.026.

Cai, S., Tuohy, P., Ma, C., Kitamura, N., Gomez, K., Zhou, Y., Ran, D., Bellampalli, S. S., Yu, J., Luo, S., Dorame, A., Pham, N. Y. N., Molnar, G., Streicher, J. M., Patek, M., Perez-Miller, S., Moutal, A., Wang, J., & Khanna, R. (2020). A modulator of the low-voltage-activated T-type calcium channel that reverses HIV glycoprotein 120-, paclitaxel-, and spinal nerve ligation-induced peripheral neuropathies. Pain, 161(11), 2551–2570. https://doi.org/10.1097/j.pain.0000000000001955.

Cain, S. M., & Snutch, T. P. (2010a). Contributions of T-type calcium channel isoforms to neuronal firing. Channels, 4(6), 475–482. https://doi.org/10.4161/chan.4.6.14106.

Cain, S. M., & Snutch, T. P. (2010b). Voltage-gated calcium channels in epilepsy. Epilepsia, 51(11). https://doi.org/10.1111/j.1528-1167.2010.02797.x.

Calandre E. P., Rico-Villademoros F., Slim M. (2016). Alpha 2 delta ligands, gabapentin, pregabalin and mirogabalin: a review of their clinical pharmacology and therapeutic use. Expert Rev Neurother. 16(11):1263–77.

Cantí, C., Nieto-Rostro, M., Foucault, I., Heblich, F., Wratten, J., Richards, M. W., Hendrich, J., Douglas, L., Page, K. M., Davies, A., & Dolphin, A. C. (2005). The metal-ion-dependent adhesion site in the Von Willebrand factor-A domain of 2 subunits is key to trafficking voltage-gated Ca 2 channels. PNAS, 102(32), 11230–11235. www.pnas.orgcgidoi10.1073pnas.0504183102.

Carabelli, V., Marcantoni, A., Comunanza, V., de Luca, A., Díaz, J., Borges, R., & Carbone, E. (2007). Chronic hypoxia up-regulates α1H T-type channels and low-threshold catecholamine secretion in rat chromaffin cells. Journal of Physiology, 584(1), 149–165. https://doi.org/10.1113/jphysiol.2007.132274.

Carbone, E., & Lux, H. D. (1984). A low voltage-activated, fully inactivating Ca channel in vertebrate sensory neurones. Nature, 310(9).

Carman, C. v., & Springer, T. A. (2003). Integrin avidity regulation: Are changes in affinity and conformation underemphasized? Current Opinion in Cell Biology, 15, 547–556. https://doi.org/10.1016/j.ceb.2003.08.003.

Cassidy, J. S., Ferron, L., Kadurin, I., Pratt, W. S., & Dolphin, A. C. (2014). Functional exofacially tagged N-type calcium channels elucidate the interaction with auxiliary α2δ-1 subunits. PNAS, 111(24), 8979–8984. https://doi.org/10.1073/pnas.1403731111.

Catterall, W. A., Leal, K., & Nanou, E. (2013). Calcium channels and short-term synaptic plasticity. Journal of Biological Chemistry, 288(15), 10742–10749. https://doi.org/10.1074/jbc.R112.411645.

Catterall, W. A., Perez-Reyes, E., Snutch, T. P., & Striessnig, J. (2005). International Union of Pharmacology. XLVIII. Nomenclature and structure-function relationships of voltage-gated calcium channels. Pharmacological Reviews, 57(4), 411–425. https://doi.org/10.1124/pr.57.4.5.

Chandrasekaran, S., & Bonchev, D. (2013). A network view on Parkinson's disease. Computational and Structural Biotechnology Journal, 7(8), e201304004. https://doi.org/10.5936/csbj.201304004.

Chataigner, L. M. P., Leloup, N., & Janssen, B. J. C. (2020). Structural Perspectives on Extracellular Recognition and Conformational Changes of Several Type-I Transmembrane Receptors. Frontiers in Molecular Biosciences, 7(129). https://doi.org/10.3389/fmolb.2020.00129.

Chen, J., Li, L., Chen, S. R., Chen, H., Xie, J. D., Sirrieh, R. E., MacLean, D. M., Zhang, Y., Zhou, M. H., Jayaraman, V., & Pan, H. L. (2018). The α2δ-1-NMDA Receptor Complex Is Critically Involved in Neuropathic Pain Development and Gabapentin Therapeutic Actions. Cell Reports, 22(9), 2307–2321. https://doi.org/10.1016/j.celrep.2018.02.021.

Chen, J., Salas, A., & Springer, T. A. (2003). Bistable regulation of integrin adhesiveness by a bipolar metal ion cluster. Nature Structural & Molecular Biology, 10(12), 995–1001. https://doi.org/10.1038/nsb1011.

Chen, Z., Mondal, A., & Minor, D. L. (2023). Structural basis for CaVα2δ:gabapentin binding. Nature Structural and Molecular Biology, 30(6), 735–739. https://doi.org/10.1038/s41594-023-00951-7.

Cheng, J., Zhou, Q., Fu, J., Wei, C., Zhang, L., Khan, M. S. S., Lv, H., Anuchapreeda, S., & Fu, J. (2021). Novel compound heterozygous missense variants (c.G955A and c.A1822C) of CACNA2D4 likely causing autosomal recessive retinitis pigmentosa in a Chinese patient. 3 Biotech, 11(208). https://doi.org/10.1007/s13205-021-02761-4.

Cheong, E., & Shin, H.-S. (2013). T-type Ca2+ channels in normal and abnormal brain functions. Physiol Rev, 93, 961–992. https://doi.org/10.1152/physrev.00010.2012.

Choudhury, A., Marks, D. L., Proctor, K. M., Gould, G. W., & Pagano, R. E. (2006). Regulation of caveolar endocytosis by syntaxin 6-dependent delivery of membrane components to the cell surface. Nature Cell Biology, 8(4), 317–328. https://doi.org/10.1038/ncb1380.

Chuang, E., Alegre, M. L., Duckett, C. S., Noel, P. J., vander Heiden, M. G., & Thompson, C. B. (1997). Interaction of CTLA-4 with the clathrin-associated protein AP50 results in ligand-

independent endocytosis that limits cell surface expression. The Journal of Immunology, 159(1), 144–151. https://doi.org/10.4049/jimmunol.159.1.144.

Cocucci, E., Aguet, F., Boulant, S., & Kirchhausen, T. (2012). The first five seconds in the life of a clathrin-coated pit. Cell, 150, 495–507. https://doi.org/10.1016/j.cell.2012.05.047.

Cole, R. L., Lechner, S. M., Williams, M. E., Prodanovich, P., Bleicher, L., Varney, M. A., & Gu, G. (2005). Differential distribution of voltage-gated calcium channel alpha-2 delta (α2δ) subunit mRNA-containing cells in the rat central nervous system and the dorsal root ganglia. The Journal of Comparative Neurology, 491, 246–269. https://doi.org/10.1002/cne.20693.

Colloca, L., Ludman, T., Bouhassira, D., Baron, R., Dickenson, A. H., Yarnitsky, D., Freeman, R., Truini, A., Attal, N., Finnerup, N. B., Eccleston, C., Kalso, E., Bennett, D. L., Dworkin, R. H., & Raja, S. N. (2017). Neuropathic pain. Nature Reviews Disease Primers, 3(17002). https://doi.org/10.1038/nrdp.2017.2.

Coskun, O. (2016). Separation Tecniques: CHROMATOGRAPHY. Northern Clinics of Istanbul, 3(2), 156–160. https://doi.org/10.14744/nci.2016.32757.

Cottrell, G. S., Amadesi, S., Grady, E. F., & Bunnett, N. W. (2004). Trypsin IV, a Novel Agonist of Protease-activated Receptors 2 and 4. The Journal of Biological Chemistry, 279(14), 13532–13539. https://doi.org/10.1074/jbc.M312090200.

Cottrell, G. S., Soubrane, C. H., Hounshell, J. A., Lin, H., Owenson, V., Rigby, M., Cox, P. J., Barker, B. S., Ottolini, M., Ince, S., Bauer, C. C., Perez-Reyes, E., Patel, M. K., Stevens, E. B., & Stephens, G. J. (2018). CACHD1 is an α2δ-like protein that modulates Cav3 voltage-gated calcium channel activity. The Journal of Neuroscience, 38(43), 9186–9201. https://doi.org/10.1523/JNEUROSCI.3572-15.2018.

Coultrap, S. J., and Bayer, K. U. (2012). CaMKII regulation in information processing and storage. Trends Neurosci. 35, 607–618. doi: 10.1016/j.tins.2012.05.003.

Courtois-Coutry, N., & Roush, D. (1997). A Tyrosine-Based Signal Targets H/K-ATPase to a Regulated Compartment and Is Required for the Cessation of Gastric Acid Secretion. Cell, 90, 501–510.

Coutelier, M., Blesneac, I., Monteil, A., Monin, M. L., Ando, K., Mundwiller, E., Brusco, A., le Ber, I., Anheim, M., Castrioto, A., Duyckaerts, C., Brice, A., Durr, A., Lory, P., & Stevanin, G. (2015). A recurrent mutation in CACNA1G alters Cav3.1 T-type calcium-channel conduction and causes autosomal-dominant cerebellar ataxia. The American Journal of Human Genetics, 97, 726–737. https://doi.org/10.1016/j.ajhg.2015.09.007.

Cribbs, L. L., Lee, J.-H., Yang, J., Satin, J., Zhang, Y., Daud, A., Barclay, J., Williamson, M. P., Fox, M., Rees, M., & Perez-Reyes, E. (1998). Cloning and Characterization of 1H From Human Heart, a Member of the T-Type Ca 2 Channel Gene Family. American Heart Association. http://ahajournals.org.

Cullen, P. J., & Steinberg, F. (2018). To degrade or not to degrade: mechanisms and significance of endocytic recycling. Nature Reviews Molecular Cell Biology, 19, 679–696. https://doi.org/10.1038/s41580-018-0053-7.

Dahimene, S., Page, K. M., Kadurin, I., Ferron, L., Ho, D. Y., Powell, G. T., Pratt, W. S., Wilson, S. W., & Dolphin, A. C. (2018). The α2δ-like Protein Cachd1 Increases N-type Calcium Currents and Cell Surface Expression and Competes with α2δ-1. Cell Reports, 25, 1610–1621. https://doi.org/10.1016/j.celrep.2018.10.033.

Daniil, G., Fernandes-Rosa, F. L., Chemin, J., Blesneac, I., Beltrand, J., Polak, M., Jeunemaitre, X., Boulkroun, S., Amar, L., Strom, T. M., Lory, P., & Zennaro, M. C. (2016). CACNA1H Mutations Are Associated With Different Forms of Primary Aldosteronism. EBioMedicine, 13, 225–236. https://doi.org/10.1016/j.ebiom.2016.10.002.

David, L. S., Garcia, E., Cain, S. M., Thau, E. M., Tyson, J. R., & Snutch, T. P. (2010). Splice-variant changes of the CaV3.2 T-type calcium channel mediate voltage-dependent facilitation and associate with cardiac hypertrophy and development. Channels, 4(5), 375–389. https://doi.org/10.4161/chan.4.5.12874.

Davies, A., Kadurin, I., Alvarez-Laviada, A., Douglas, L., Nieto-Rostro, M., Bauer, C. S., Pratt, W. S., & Dolphin, A. C. (2010). The α2δ subunits of voltage-gated calcium channels form GPI-anchored proteins, a posttranslational modification essential for function. PNAS, 107(4), 1654–1659. https://doi.org/10.1073/pnas.0908735107.

de Château, M., Chen, S., Salas, A., & Springer, T. A. (2001). Kinetic and mechanical basis of rolling through an integrin and novel Ca2+-dependent rolling and Mg2+-dependent firm adhesion modalities for the α4/β7 - MAdCAM-1 interaction. Biochemistry, 40, 13972–13979. https://doi.org/10.1021/bi011582f.

de Jongh, K. S., Warner, C., & Catterall, W. A. (1990). Subunits of purified calcium channels. Alpha 2 and delta are encoded by the same gene. Journal of Biological Chemistry, 265(25), 14738–14741. https://doi.org/10.1016/s0021-9258(18)77174-3.

de Vries, L., Finana, F., Cathala, C., Ronsin, B., & Cussac, D. (2019). Innovative bioluminescence resonance energy transfer assay reveals differential agonist-induced D2 receptor intracellular trafficking and arrestin-3 recruitment. Molecular Pharmacology, 96, 308–319. https://doi.org/10.1124/mol.119.115998.

del Pozo, M. A., Alderson, N. B., Grande-García, A., Balasubramanian, N., Schwartz, M. A., Kiosses, W. B., & Anderson, R. G. W. (2005). Phospho-Caveolin-1 Mediates Integrin-Regulated Membrane Domain Internalisation. Nature Cell Biology, 7(9), 901–908.

Deng, G. F., Lin Sun, Y., Hamet, P., Inagami, T., & Fu GUO, D. (2001). The angiotensin II type 1 receptor and receptor-associated proteins. Cell Research, 11(3), 165–180.

Deng M., Chen S. R., Pan H.L. (2019). Presynaptic NMDA receptors control nociceptive transmission at the spinal cord level in neuropathic pain. Cell Mol Life Sci. 76(10), 1889–99.

di Guglielmo, G. M., le Roy, C., Goodfellow, A. F., & Wrana, J. L. (2003). Distinct endocytic pathways regulate TGF-β receptor signalling and turnover. Nature Cell Biology, 5(5), 410–421. https://doi.org/10.1038/ncb975.

Dickman, D. K., Kurshan, P. T., & Schwarz, T. L. (2008). Mutations in a Drosophila α2δ voltage-gated calcium channel subunit reveal a crucial synaptic function. Journal of Neuroscience, 28(1), 31–38. https://doi.org/10.1523/JNEUROSCI.4498-07.2008.

Dolphin, A. C. (2003). G Protein Modulation of Voltage-Gated Calcium Channels. Pharmacological Reviews, 55(4), 607–627. https://doi.org/10.1124/pr.55.4.3.

Dolphin, A. C. (2012). Calcium channel auxiliary α 2 δ and β subunits: Trafficking and one step beyond. Nature Reviews Neuroscience, 13, 542–555. https://doi.org/10.1038/nrn3311.

Dolphin, A. C. (2018). Voltage-gated calcium channels: Their discovery, function and importance as drug targets. Brain and Neuroscience Advances, 2, 1–8. https://doi.org/10.1177/2398212818794805.

Dolphin, A. C., Wyatt, C. N., Richards, J., Beattie, R. E., Craig, P., Lee, J.-H., Cribbs, L. L., Volsen, S. G., & Perez-Reyes, E. (1999). The effect of a2-d and other accessory subunits on expression and properties of the calcium channel a1G. Journal of Physiology, 519(1), 35–45.

Domon Y., Kobayashi N., Kubota K., Kitano Y., Ueki H., Shimojo Y., et al. (2023). The novel gabapentinoid mirogabalin prevents upregulation of α2δ-1 subunit of voltage-gated calcium channels in spinal dorsal horn in a rat model of spinal nerve ligation. Drug Res. 73(01), 54–60.

Dreyfus, F. M., Tscherter, A., Errington, A. C., Renger, J. J., Shin, H. S., Uebele, V. N., Crunelli, V., Lambert, R. C., & Leresche, N. (2010). Selective T-type calcium channel block in thalamic neurons reveals channel redundancy and physiological impact of ITwindow. Journal of Neuroscience, 30(1), 99–109. https://doi.org/10.1523/JNEUROSCI.4305-09.2010.

Dubel, S. J., Altier, C., Chaumont, S., Lory, P., Bourinet, E., & Nargeot, J. (2004). Plasma membrane expression of T-type calcium channel α1 subunits is modulated by high voltage-activated auxiliary subunits. The Journal of Biological Chemistry, 279(28), 29263–29269. https://doi.org/10.1074/jbc.M313450200.

Duzhyy, D. E., Viatchenko-Karpinski, V. Y., Khomula, E. v., Voitenko, N. v., & Belan, P. v. (2015). Upregulation of T-type Ca2+ channels in long-term diabetes determines increased excitability of a specific type of capsaicin-insensitive DRG neurons. Molecular Pain, 11(29). https://doi.org/10.1186/s12990-015-0028-z.

Edvardson, S., Oz, S., Abulhijaa, F. A., Taher, F. B., Shaag, A., Zenvirt, S., Dascal, N., & Elpeleg, O. (2013). Early infantile epileptic encephalopathy associated with a high voltage gated calcium channelopathy. Journal of Medical Genetics, 50(2), 118–123. https://doi.org/10.1136/jmedgenet-2012-101223.

Eisfeld, A. J., Kawakami, E., Watanabe, T., Neumann, G., & Kawaoka, Y. (2011). RAB11A Is Essential for Transport of the Influenza Virus Genome to the Plasma Membrane. Journal of Virology, 85(13), 6117–6126. https://doi.org/10.1128/jvi.00378-11.

El-Awaad, E., Pryymachuk, G., Fried, C. et al. (2019). Direct, gabapentin-insensitive interaction of a soluble form of the calcium channel subunit α2δ-1 with thrombospondin-4. Scientific Reports, 9, 16272. https://doi.org/10.1038/s41598-019-52655-y.

Ernst, W. L., Zhang, Y., Yoo, J. W., Ernst, S. J., & Noebels, J. L. (2009). Genetic enhancement of thalamocortical network activity by elevating α1G-mediated low-voltage-activated calcium current induces pure absence epilepsy. The Journal of Neuroscience, 29(6), 1615–1625. https://doi.org/10.1523/JNEUROSCI.2081-08.2009.

Feng, T., Kalyaanamoorthy, S., & Barakat, K. (2018). L-Type Calcium Channels: Structure and Functions. In Ion Channels in Health and Sickness. InTech. https://doi.org/10.5772/intechopen.77305.

Feng, X. J., Ma, L. X., Jiao, C., Kuang, H. X., Zeng, F., Zhou, X. Y., Cheng, X. E., Zhu, M. Y., Zhang, D. Y., Jiang, C. Y., & Liu, T. (2019). Nerve injury elevates functional Cav3.2 channels in superficial spinal dorsal horn. Molecular Pain, 15, 1–12. https://doi.org/10.1177/1744806919836569.

Finnerup, N. B., Kuner, R., & Jensen, T. S. (2021). Neuropathic pain: Frommechanisms to treatment. Physiological Reviews, 101, 259–301. https://doi.org/10.1152/physrev.00045.2019.

Fisher, C. G., & Falk, M. M. (2023). Endocytosis and Endocytic Motifs across the Connexin Gene Family. International Journal of Molecular Sciences, 24(12851). https://doi.org/10.3390/ijms241612851.

Flores-Espinoza, E., Meizoso-Huesca, A., Villegas-Comonfort, S., Reyes-Cruz, G., & García-Sáinz, J. A. (2020). Effect of docosahexaenoic acid, phorbol myristate acetate, and insulin on the interaction of the FFA4 (short isoform) receptor with Rab proteins. European Journal of Pharmacology, 889(173595). https://doi.org/10.1016/j.ejphar.2020.173595.

Fong, J. T., Kells, R. M., & Falk, M. M. (2013). Two tyrosine-based sorting signals in the Cx43 C-terminus cooperate to mediate gap junction endocytosis. Molecular Biology of the Cell, 24, 2834–2848. https://doi.org/10.1091/mbc.E13-02-0111.

Fuentealba, R. A., Liu, Q., Zhang, J., Kanekiyo, T., Hu, X., Lee, J. M., Ladu, M. J., & Bu, G. (2010). Low-density lipoprotein receptor-related protein 1 (LRP1) mediates neuronal Aβ42 uptake and lysosomal trafficking. PLoS ONE, 5(7). https://doi.org/10.1371/journal.pone.0011884.

Gaifullina, A. S., Lazniewska, J., Gerasimova, E. v., Burkhanova, G. F., Rzhepetskyy, Y., Tomin, A., Rivas-Ramirez, P., Huang, J., Cmarko, L., Zamponi, G. W., Sitdikova, G. F., & Weiss, N. (2019). A potential role for T-type calcium channels in homocysteinemia-induced peripheral neuropathy. Pain, 00(00), 1–13. https://doi.org/10.1097/j.pain.0000000000001669.

Gao, B., Sekido, Y., Maximov, A., Saad, M., Forgacs, E., Latif, F., Wei, M. H., Lerman, M., Lee, J.-H., Perez-Reyes, E., Bezprozvanny, I., & Minna, J. D. (2000). Functional Properties of a New Voltage-dependent Calcium Channel α 2 δ Auxiliary Subunit Gene (CACNA2D2)*. J Biol Chem, 275(16), 12237–12242.

García-Caballero, A., Gadotti, V. M., Stemkowski, P., Weiss, N., Souza, I. A., Hodgkinson, V., Bladen, C., Chen, L., Hamid, J., Pizzoccaro, A., Deage, M., François, A., Bourinet, E., & Zamponi, G. W. (2014). The Deubiquitinating Enzyme USP5 Modulates Neuropathic and Inflammatory Pain by Enhancing Cav3.2 Channel Activity. Neuron, 83, 1144–1158. https://doi.org/10.1016/j.neuron.2014.07.036.

Ghazisaeidi, S., Muley, M. M., & Salter, M. W. (2023). Annual Review of Pharmacology and Toxicology Neuropathic Pain: Mechanisms, Sex Differences, and Potential Therapies for a Global Problem. The Annual Review of Pharmacology and Toxicology Is, 63, 565–583. https://doi.org/10.1146/annurev-pharmtox-051421.

Ginés, S., Ciruela, F., Burgueño, J., Casadó, V., Canela, Enric. I., Mallol, J., Lluís, C., & Franco, R. (2001). Involvement of Caveolin in Ligand-Induced Recruitment and Internalization of A 1 Adenosine Receptor and Adenosine Deaminase in an Epithelial Cell Line. Molecular Pharmacology, 59(5), 1314–1323. https://doi.org/10.1124/mol.59.5.1314.

Gironès, N., Alvarez, E., Seth, A., Lin, I. M., Latour, D. A., & Davis, R. J. (1991). Mutational analysis of the cytoplasmic tail of the human transferrin receptor: Identification of a sub-domain that is required for rapid endocytosis. The Journal of Biological Chemistry, 266(28), 19006–19012. https://doi.org/10.1016/s0021-9258(18)55163-2.

Goh, J. B., & Ng, S. K. (2018). Impact of host cell line choice on glycan profile. Critical Reviews in Biotechnology, 38(6), 851–867. https://doi.org/10.1080/07388551.2017.1416577.

Goh, L. K., & Sorkin, A. (2013). Endocytosis of Receptor Tyrosine Kinases. Cold Spring Harbor Perspectives in Biology, 5(5), a017459–a017459. https://doi.org/10.1101/cshperspect.a017459.

Goldenring, J. R. (2015). Recycling endosomes. Current Opinion in Cell Biology, 35, 117–122. https://doi.org/10.1016/j.ceb.2015.04.018.

Goldstein, J. L., Anderson, R. G. W., & Brown, M. S. (1979). review article Coated pits, coated vesicles, and receptor-mediated endocytosis. Nature, 279, 679–685.

Gomes, A. M. V., Carmo, T. S., Carvalho, L. S., Bahia, F. M., & Parachin, N. S. (2018). Comparison of yeasts as hosts for recombinant protein production. Microorganisms, 6(38). https://doi.org/10.3390/microorganisms6020038.

Gomora, J. C., Murbartiá, J., Arias, J. M., Lee, J.-H., & Perez-Reyes, E. (2002). Cloning and Expression of the Human T-Type Channel Ca v 3.3: Insights into Prepulse Facilitation. Biophysical Journal, 83, 229–241.

Gossen, M., & Bujardt, H. (1992). Tight control of gene expression in mammalian cells by tetracycline-responsive promoters. Cell Biology, 89, 5547–5551.

Grant, B. D., & Donaldson, J. G. (2009). Pathways and mechanisms of endocytic recycling. Nature Reviews Molecular Cell Biology, 10(9), 597–608. https://doi.org/10.1038/nrm2755.

Grimsey, N. L., Goodfellow, C. E., Dragunow, M., & Glass, M. (2011). Cannabinoid receptor 2 undergoes Rab5-mediated internalization and recycles via a Rab11-dependent pathway. Biochimica et Biophysica Acta, 1813, 1554–1560. https://doi.org/10.1016/j.bbamcr.2011.05.010.

Groen, J. L., Andrade, A., Ritz, K., Jalalzadeh, H., Haagmans, M., Bradley, T. E. J., Jongejan, A., Verbeek, D. S., Nürnberg, P., Denome, S., Hennekam, R. C. M., Lipscombe, D., Baas, F., & Tijssen, M. A. J. (2015). CACNA1B mutation is linked to unique myoclonus-dystonia syndrome. Human Molecular Genetics, 24(4), 987–993. https://doi.org/10.1093/hmg/ddu513.

Güler-Gane, G., Kidd, S., Sridharan, S., Vaughan, T. J., Wilkinson, T. C. I., & Tigue, N. J. (2016). Overcoming the refractory expression of secreted recombinant proteins in mammalian cells through modification of the signal peptide and adjacent amino acids. PLoS ONE. https://doi.org/10.1371/journal.pone.0155340.

Gulsuner, S., Walsh, T., Watts, A. C., Lee, M. K., Thornton, A. M., Casadei, S., Rippey, C., Shahin, H., Nimgaonkar, V. L., Go, R. C. P., Savage, R. M., Swerdlow, N. R., Gur, R. E., Braff, D. L., King, M. C., & McClellan, J. M. (2013). XSpatial and temporal mapping of de novo mutations in schizophrenia to a fetal prefrontal cortical network. Cell, 154(3), 518–529. https://doi.org/10.1016/j.cell.2013.06.049.

Gumerov, V. M., Andrianova, E. P., Matilla, M. A., Page, K. M., Monteagudo-Cascales, E., Dolphin, A. C., Krell, T., & Zhulin, I. B. (2022). Amino acid sensor conserved from bacteria to humans. PNAS, 119(10). https://doi.org/10.1073/pnas.2110415119/-/DCSupplemental.

Güner, G., & Lichtenthaler, S. F. (2020). The substrate repertoire of γ-secretase/presenilin. Seminars in Cell and Developmental Biology, 105, 27–42. https://doi.org/10.1016/j.semcdb.2020.05.019.

Guo, H., Wang, T., Wu, H., Long, M., Coe, B. P., Li, H., Xun, G., Ou, J., Chen, B., Duan, G., Bai, T., Zhao, N., Shen, Y., Li, Y., Wang, Y., Zhang, Y., Baker, C., Liu, Y., Pang, N., … Xia, K. (2018). Inherited and multiple de novo mutations in autism/developmental delay risk genes suggest a multifactorial model. Molecular Autism, 9(64). https://doi.org/10.1186/s13229-018-0247-z.

Gurnett, C. A., Felix, R., & Campbell, K. P. (1997). Extracellular interaction of the voltage-dependent Ca2+ channel α2δ and α1 subunits. The Journal of Biological Chemistry, 272(29), 18508–18512. https://doi.org/10.1074/jbc.272.29.18508.

Hailstones, D., Sleer, L. S., Parton, R. G., & Stanley, K. K. (1998). Regulation of caveolin and caveolae by cholesterol in MDCK cells. Journal of Lipid Research, 39, 369–379. https://doi.org/10.1016/s0022-2275(20)33898-0.

Hamill, O. P., Marty, A., Neher, E., Sakmann, B., & Sigworth, F. J. (1981). Improved patch-clamp techniques for high-resolution current recording from cells and cell-free membrane patches. Pflügers Archiv - European Journal of Physiology, 391(2), 85–100. https://doi.org/10.1007/BF00656997.

Hanlon, M. R., Berrow, N. S., Dolphin, A. C., & Wallace, B. A. (1999). Modelling of a voltage-dependent Ca2+ channel β subunit as a basis for understanding its functional properties. FEBS Letters, 445, 366–370. https://doi.org/10.1016/S0014-5793(99)00156-8.

Hansen, P. B. L. (2015). Functional importance of T-type voltage-gated calcium channels in the cardiovascular and renal system: news from the world of knockout mice. Am J Physiol Regul Integr Comp Physiol, 308, 227–237. https://doi.org/10.1152/ajpregu.00276.2014.

Harding, E. K., & Zamponi, G. W. (2022). Central and peripheral contributions of T-type calcium channels in pain. Molecular Brain, 15(39). https://doi.org/10.1186/s13041-022-00923-w.

Harraz, O. F., Abd El-Rahman, R. R., Bigdely-Shamloo, K., Wilson, S. M., Brett, S. E., Romero, M., Gonzales, A. L., Earley, S., Vigmond, E. J., Nygren, A., Menon, B. K., Mufti, R. E., Watson, T., Starreveld, Y., Furstenhaupt, T., Muellerleile, P. R., Kurjiaka, D. T., Kyle, B. D., Braun, A. P., & Welsh, D. G. (2014). Cav3.2 channels and the induction of negative feedback in cerebral arteries. Circulation Research, 650–661. https://doi.org/10.1161/CIRCRESAHA.114.304056.

Harraz, O. F., Visser, F., Brett, S. E., Goldman, D., Zechariah, A., Hashad, A. M., Menon, B. K., Watson, T., Starreveld, Y., & Welsh, D. G. (2015). CaV1.2/CaV3.x channels mediate divergent vasomotor responses in human cerebral arteries. Journal of General Physiology, 145(5), 405–418. https://doi.org/10.1085/jgp.201511361.

Hartung, J. E., Moy, J. K., Loeza-Alcocer, E., Nagarajan, V., Jostock, R., Christoph, T., Schroeder, W., & Gold, M. S. (2022). Voltage-gated calcium currents in human dorsal root ganglion neurons. Pain, 163(6), E774–E785. https://doi.org/10.1097/j.pain.0000000000002465.

Harvey, R. D., & Calaghan, S. C. (2012). Caveolae create local signalling domains through their distinct protein content, lipid profile and morphology. Journal of Molecular and Cellular Cardiology, 52(2), 366–375. https://doi.org/10.1016/j.yjmcc.2011.07.007.

Helbig, K. L., Lauerer, R. J., Bahr, J. C., Souza, I. A., Myers, C. T., Uysal, B., Schwarz, N., Gandini, M. A., Huang, S., Keren, B., Mignot, C., Afenjar, A., Billette de Villemeur, T., Héron, D., Nava, C., Valence, S., Buratti, J., Fagerberg, C. R., Soerensen, K. P., … Mefford, H. C. (2018). De Novo Pathogenic Variants in CACNA1E Cause Developmental and Epileptic Encephalopathy with Contractures, Macrocephaly, and Dyskinesias. American Journal of Human Genetics, 103, 666–678. https://doi.org/10.1016/j.ajhg.2018.09.006.

Hemming, M. L., Elias, J. E., Gygi, S. P., & Selkoe, D. J. (2009). Identification of β-secretase (BACE1) substrates using quantitative proteomics. PLoS ONE, 4(12). https://doi.org/10.1371/journal.pone.0008477.

Hendrich, J., Tran, A., Minh, V., Heblich, F., Nieto-Rostro, M., Watschinger, K., Rg Striessnig, J., Wratten, J., Davies, A., & Dolphin, A. C. (2008). Pharmacological disruption of calcium channel trafficking by the 2-ligand gabapentin. PNAS, 105(9), 3628–3633. www.pnas.org/cgi/content/full/.

Hermann, J., Schurgers, L., & Jankowski, V. (2022). Identification and characterization of post-translational modifications: Clinical implications. Molecular Aspects of Medicine, 86. https://doi.org/10.1016/j.mam.2022.101066.

Heron, S. E., Khosravani, H., Varela, D., Bladen, C., Williams, T. C., Newman, M. R., Scheffer, I. E., Berkovic, S. F., Mulley, J. C., & Zamponi, G. W. (2007). Extended spectrum of idiopathic generalized epilepsies associated with CACNA1H functional variants. Annuals of Neurology, 62, 560–568. https://doi.org/10.1002/ana.21169.

Higgins, J. M. G., Cernadas, M., Tan, K., Irie, A., Wang, J. H., Takada, Y., & Brenner, M. B. (2000). The role of α and β chains in ligand recognition by β7 integrins. Journal of Biological Chemistry, 275(33), 25652–25664. https://doi.org/10.1074/jbc.M001228200.

Hino-Fukuyo, N., Kikuchi, A., Arai-Ichinoi, N., Niihori, T., Sato, R., Suzuki, T., Kudo, H., Sato, Y., Nakayama, T., Kakisaka, Y., Kubota, Y., Kobayashi, T., Funayama, R., Nakayama, K., Uematsu, M., Aoki, Y., Haginoya, K., & Kure, S. (2015). Genomic analysis identifies candidate pathogenic variants in 9 of 18 patients with unexplained West syndrome. Human Genetics, 134, 649–658. https://doi.org/10.1007/s00439-015-1553-6.

Hirst, J., Robinson, M. S., & Lindsay, M. R. (2001). GGAs: Roles of the Different Domains and Comparison with AP-1 and Clathrin. Molecular Biology of the Cell, 12, 3573–3588. https://www.researchgate.net/publication/11658989.

Hoda, J. C., Zaghetto, F., Koschak, A., & Striessnig, J. (2005). Congenital stationary night blindness type 2 mutations S229P, G369D, L1068P, and W1440X alter channel gating or functional expression of Ca v1.4 L-type Ca2+ channels. Journal of Neuroscience, 25(1), 252–259. https://doi.org/10.1523/JNEUROSCI.3054-04.2005.

Hodgkin, A. L., & Huxley, A. F. (1952). A quantitative description of membrane current and its application to conduction and excitation in nerve. J. Physiol, 117, 500–544.

Hogg, N., Stewart, M. P., Searth, S. L., Newton, R., Shaw, J. M., Law, S. K. A., & Klein, N. (1999). A novel leukocyte adhesion deficiency caused by expressed but nonfunctional β2 integrins Mac-1 and LFA-1. Journal of Clinical Investigation, 103(1), 97–106. https://doi.org/10.1172/JCI3312.

Homma, Y., Hiragi, S., & Fukuda, M. (2021). Rab family of small GTPases: an updated view on their regulation and functions. FEBS Journal, 288, 36–55. https://doi.org/10.1111/febs.15453.

Hooper, N. M. (2001). Determination of glycosyl-phosphatidylinositol membrane protein anchorage. Proteomics, 1, 748–755. https://doi.org/10.1002/1615-9861(200106)1:6<748::AID-PROT748>3.0.CO;2-T.

Hoppa, M. B., Lana, B., Margas, W., Dolphin, A. C., & Ryan, T. A. (2012). α2δ expression sets presynaptic calcium channel abundance and release probability. Nature, 486(7401), 122–125. https://doi.org/10.1038/nature11033.

Hu, Y., Cheng, K., He, L., Zhang, X., Jiang, B., Jiang, L., Li, C., Wang, G., Yang, Y., & Liu, M. (2021). NMR-Based Methods for Protein Analysis. Analytical Chemistry, 93, 1866–1879. https://doi.org/10.1021/acs.analchem.0c03830.

Huang, X. F., Huang, F., Wu, K. C., Wu, J., Chen, J., Pang, C. P., Lu, F., Qu, J., & Jin, Z. B. (2015). Genotype-phenotype correlation and mutation spectrum in a large cohort of patients with inherited retinal dystrophy revealed by next-generation sequencing. Genetics in Medicine, 17(4), 271–278. https://doi.org/10.1038/gim.2014.138.

Hutagalung, A. H., & Novick, P. J. (2011). Role of Rab GTPases in membrane traffic and cell physiology. Physiological Reviews, 91(1), 119–149. https://doi.org/10.1152/physrev.00059.2009.

Im, J., Maiti, K. K., Kim, W., Kim, K. T., & Chung, S. K. (2011). Cellular uptake properties of the complex derived from quantum dots and G8 molecular transporter. Bulletin of the Korean Chemical Society, 32(4), 1282–1292. https://doi.org/10.5012/bkcs.2011.32.4.1282.

Ince, S. (2018). Characterization of the Role of the CACHD1 MIDAS site in the Trafficking and Localization of CACHD1 and CaV3.1.

Inoue, H., Nojima, H., & Okayama, H. (1990). High efficiency transformation of Escherichia coli with plasmids. Gene, 96(1), 23–28. https://doi.org/10.1016/0378-1119(90)90336-P.

Iossifov, I., O'Roak, B. J., Sanders, S. J., Ronemus, M., Krumm, N., Levy, D., Stessman, H. A., Witherspoon, K. T., Vives, L., Patterson, K. E., Smith, J. D., Paeper, B., Nickerson, D. A., Dea, J., Dong, S., Gonzalez, L. E., Mandell, J. D., Mane, S. M., Murtha, M. T., … Wigler, M. (2014). The contribution of de novo coding mutations to autism spectrum disorder. Nature, 515, 216–221. https://doi.org/10.1038/nature13908.

Islam, S. (2019). Calcium signalling. Advances in Experimental Medicine and Biology. http://www.springer.com/series/5584.

Iversen, T. G., Skotland, T., & Sandvig, K. (2011). Endocytosis and intracellular transport of nanoparticles: Present knowledge and need for future studies. Nano Today, 6, 176–185. https://doi.org/10.1016/j.nantod.2011.02.003.

Jacus, M. O., Uebele, V. N., Renger, J. J., & Todorovic, S. M. (2012). Presynaptic CaV3.2 channels regulate excitatory neurotransmission in nociceptive dorsal horn neurons. Journal of Neuroscience, 32(27), 9374–9382. https://doi.org/10.1523/JNEUROSCI.0068-12.2012.

Jagodic, M. M., Pathirathna, S., Joksovic, P. M., Lee, W. Y., Nelson, M. T., Naik, A. K., Su, P., Jevtovic-Todorovic, V., & Todorovic, S. M. (2008). Upregulation of the T-type calcium current in small rat sensory neurons after chronic constrictive injury of the sciatic nerve. Journal of Neurophysiology, 99(6), 3151–3156. https://doi.org/10.1152/jn.01031.2007.

Jay, S. D., Sharp, A. H., Kahl, S. D., Vedvick, T. S., Harpold, M. M., & Campbell, K. P. (1991). Structural characterization of the dihydropyridine-sensitive calcium channel α2- subunit and the associated δ peptides. Journal of Biological Chemistry, 266(5), 3287–3293. https://doi.org/10.1016/s0021-9258(18)49986-3.

Ji, R. R., Kohno, T., Moore, K. A., & Woolf, C. J. (2003). Central sensitization and LTP: Do pain and memory share similar mechanisms? Trends in Neurosciences, 26(12), 696–705. https://doi.org/10.1016/j.tins.2003.09.017.

Jurkat-Rott, K., Lehmann-Horn, F., Elbaz, A., Heine, R., Gregg, R. G., Hogan, K., Powers, P. A., Laple, P., Vale-Santos, J. E., Weissenbach, J., & Fontaine, B. (1994). A calcium channel mutation causing hypokalemic periodic paralysis. Human Molecular Genetics, 3(8), 1415–1419. https://academic.oup.com/hmg/article/3/8/1415/554876.

Kadurin, I., Rothwell, S. W., Lana, B., Nieto-Rostro, M., & Dolphin, A. C. (2017). LRP1 influences trafficking of N-type calcium channels via interaction with the auxiliary α2δ-1 subunit. Scientific Reports, 7(43802). https://doi.org/10.1038/srep43802.

Kakehashi, A., Chariyakornkul, A., Suzuki, S., Khuanphram, N., Tatsumi, K., Yamano, S., Fujioka, M., Gi, M., Wongpoomchai, R., & Wanibuchi, H. (2021). Cache domain containing 1 is a novel marker of non- alcoholic steatohepatitis-associated hepatocarcinogenesis. Cancers, 13(1216), 1–19. https://doi.org/10.3390/cancers13061216.

Kaksonen, M., & Roux, A. (2018). Mechanisms of clathrin-mediated endocytosis. Nature Reviews Molecular Cell Biology, 19, 313–326. https://doi.org/10.1038/nrm.2017.132.

Kamat, V., & Rafique, A. (2017). Designing binding kinetic assay on the bio-layer interferometry (BLI) biosensor to characterize antibody-antigen interactions. Analytical Biochemistry, 536, 16–31. https://doi.org/10.1016/j.ab.2017.08.002.

Kelly, B. T., McCoy, A. J., Späte, K., Miller, S. E., Evans, P. R., Höning, S., & Owen, D. J. (2008). A structural explanation for the binding of endocytic dileucine motifs by the AP2 complex. Nature, 456(7224), 976–979. https://doi.org/10.1038/nature07422.

Kerckhove, N., Pereira, B., Soriot-Thomas, S., Alchaar, H., Deleens, R., Hieng, V. S., Serra, E., Lanteri-Minet, M., Arcagni, P., Picard, P., Lefebvre-Kuntz, D., Maindet, C., Mick, G., Balp, L., Lucas, C., Creach, C., Letellier, M., Martinez, V., Navez, M., … Eschalier, A. (2018). Efficacy and safety of a T-type calcium channel blocker in patients with neuropathic pain: A proof-of-concept, randomized, double-blind and controlled trial. European Journal of Pain, 22, 1321–1330. https://doi.org/10.1002/ejp.1221.

Kim, M. S., & Leahy, D. (2013). Enzymatic deglycosylation of glycoproteins. In Methods in Enzymology (Vol. 533, pp. 259–263). Academic Press Inc. https://doi.org/10.1016/B978-0-12-420067-8.00019-2.

Kimura, M., Yabe, I., Hama, Y., Eguchi, K., Ura, S., Tsuzaka, K., Tsuji, S., & Sasaki, H. (2017). SCA42 mutation analysis in a case series of Japanese patients with spinocerebellar ataxia. Journal of Human Genetics, 62, 857–859. https://doi.org/10.1038/jhg.2017.51.

Klocke, B., Krone, K., Tornes, J., Moore, C., Ott, H., & Pitychoutis, P. M. (2023). Insights into the role of intracellular calcium signaling in the neurobiology of neurodevelopmental disorders. Frontiers in Neuroscience, 17(1093099). https://doi.org/10.3389/fnins.2023.1093099.

Kornfeld, R., & Kornfeld, S. (1985). Assembly of asparagine-linked oligosaccharides. Ann. Rev. Biochem, 54, 631–664. www.annualreviews.org/aronline.

Kozik, P., Francis, R. W., Seaman, M. N. J., & Robinson, M. S. (2010). A Screen for Endocytic Motifs. Traffic, 11, 843–855. https://doi.org/10.1111/j.1600-0854.2010.01056.x.

Kuo, I. Y. T., Howitt, L., Sandow, S. L., McFarlane, A., Hansen, P. B., & Hill, C. E. (2014). Role of T-type channels in vasomotor function: Team player or chameleon? Pflugers Archiv European Journal of Physiology, 466, 767–779. https://doi.org/10.1007/s00424-013-1430-x.

Kurzchalia, T. V., Parton, R. G. (1999). Membrane microdomains and caveolae. Curr Opin Cell Biol, 11, 424-431.

Lacy, B. D., Wigelsworth, D. J., Scobie, H. M., Young, J. A. T., & Collier, R. J. (2004). Crystal structure of the von Willebrand factor A domain of human capillary morphogenesis protein 2: An anthrax toxin receptor. PNAS, 101(17), 6367–6372. www.pnas.orgcgidoi10.1073pnas.0401506101.

Lana, B., Page, K. M., Kadurin, I., Ho, S., Nieto-Rostro, M., Dolphin, A. C. (2016). Thrombospondin-4 reduces binding affinity of [(3)H]-gabapentin to calcium-channel α2δ-1-subunit but does not interact with α2δ-1 on the cell-surface when co-expressed. Sci Rep. 6, 24531. doi: 10.1038/srep24531.

Lauzadis, J., Liu, H., Lu, Y., Rebecchi, M. J., Kaczocha, M., & Puopolo, M. (2020). Contribution of T-type calcium channels to spinal cord injury-induced hyperexcitability of nociceptors. Journal of Neuroscience, 40(38), 7229–7240. https://doi.org/10.1523/JNEUROSCI.0517-20.2020.

Lay, L. S., Hajduch, E., Lindsay, M. R., le Lièpvre, X., Thiele, C., Ferré, P., Parton, R. G., Kurzchalia, T., Simons, K., & Dugail, I. (2006). Cholesterol-induced caveolin targeting to lipid droplets in adipocytes: A role for caveolar endocytosis. Traffic, 7, 549–561. https://doi.org/10.1111/j.1600-0854.2006.00406.x.

le Fourn, V., Girod, P. A., Buceta, M., Regamey, A., & Mermod, N. (2014). CHO cell engineering to prevent polypeptide aggregation and improve therapeutic protein secretion. Metabolic Engineering, 21, 91–102. https://doi.org/10.1016/j.ymben.2012.12.003.

Lee, A., Tang, S. K. Y., MacE, C. R., & Whitesides, G. M. (2011). Denaturation of proteins by SDS and tetraalkylammonium dodecyl sulfates. Langmuir, 27(18), 11560–11574. https://doi.org/10.1021/la201832d.

Lee, J. M., Hammarén, H. M., Savitski, M. M., & Baek, S. H. (2023). Control of protein stability by post-translational modifications. Nature Communications, 14(201). https://doi.org/10.1038/s41467-023-35795-8.

Lee, J.-H., Daud, A. N., Cribbs, L. L., Lacerda, A. E., Pereverzev, A., Klö, U., Schneider, T., & Perez-Reyes, E. (1999). Cloning and Expression of a Novel Member of the Low Voltage-Activated T-Type Calcium Channel Family. The Journal of Neuroscience, 19(6), 1912–1921.

Li, K. W., Kim, D. S., Zaucke, F., Luo, Z. D. (2014). Trigeminal nerve injury-induced thrombospondin-4 up-regulation contributes to orofacial neuropathic pain states in a rat model. Eur J Pain, 18(4), 489-95. doi: 10.1002/j.1532-2149.2013.00396.x.

Li, Y., Marzolo, M. P., van Kerkhof, P., Strous, G. J., & Bu, G. (2000). The YXXL motif, but not the two NPXY motifs, serves as the dominant endocytosis signal for low density lipoprotein receptor-related protein. Journal of Biological Chemistry, 275(22), 17187–17194. https://doi.org/10.1074/jbc.M000490200.

Lillis, A. P., van Duyn, L. B., Murphy-Ullrich, J. E., & Strickland, D. K. (2008). LDL receptor-related protein 1: Unique tissue-specific functions revealed by selective gene knockout studies. Physiological Reviews, 88(3), 887–918. https://doi.org/10.1152/physrev.00033.2007.

Liu, H., Zou, X., Li, T., Wang, X., Yuan, W., Chen, Y., & Han, W. (2016). Enhanced production of secretory glycoprotein VSTM1-v2 with mouse IgGκ signal peptide in optimized HEK293F

transient transfection. Journal of Bioscience and Bioengineering, 121(2), 133–139. https://doi.org/10.1016/j.jbiosc.2015.05.016.

Lucchesi, W., Mizuno, K., and Giese, K. P. (2011). Novel insights into CaMKII function and regulation during memory formation. Brain Res. Bull. 85, 2–8. doi: 10.1016/j.brainresbull.2010.10.009.

Luo, Z. D., Chaplan, S. R., Higuera, E. S., Sorkin, L. S., Stauderman, K. A., Williams, M. E., Yaksh, T. L. (2001). Upregulation of dorsal root ganglion (alpha)2(delta) calcium channel subunit and its correlation with allodynia in spinal nerve-injured rats. J Neurosci, 21(6), 1868-75. doi: 10.1523/JNEUROSCI.21-06-01868.2001.

Luscher, C., & Malenka, R. C. (2012). NMDA Receptor-Dependent Long-Term Potentiation and Long-Term Depression (LTP/LTD). Cold Spring Harbor Perspectives in Biology, 4(6), a005710–a005710. https://doi.org/10.1101/cshperspect.a005710.

Magdeldin, S., Enany, S., Yoshida, Y., Xu, B., Zhang, Y., Zureena, Z., Lokamani, I., Yaoita, E., & Yamamoto, T. (2014). Basics and recent advances of two dimensional-polyacrylamide gel electrophoresis. Clinical Proteomics, 11(16). http://www.clinicalproteomicsjournal.com/content/11/1/16.

Mahammad, S., & Parmryd, I. (2008). Cholesterol homeostasis in T cells. Methyl-β-cyclodextrin treatment results in equal loss of cholesterol from Triton X-100 soluble and insoluble fractions. Biochimica et Biophysica Acta - Biomembranes, 1778, 1251–1258. https://doi.org/10.1016/j.bbamem.2008.02.010.

Maksemous, N., Blayney, C. D., Sutherland, H. G., Smith, R. A., Lea, R. A., Tran, K. N., Ibrahim, O., McArthur, J. R., Haupt, L. M., Cader, M. Z., Finol-Urdaneta, R. K., Adams, D. J., & Griffiths, L. R. (2022). Investigation of CACNA1I Cav3.3 Dysfunction in Hemiplegic Migraine. Frontiers in Molecular Neuroscience, 15. https://doi.org/10.3389/fnmol.2022.892820.

Mangoni, M. E., Traboulsie, A., Leoni, A. L., Couette, B., Marger, L., le Quang, K., Kupfer, E., Cohen-Solal, A., Vilar, J., Shin, H. S., Escande, D., Charpentier, F., Nargeot, J., & Lory, P. (2006). Bradycardia and slowing of the atrioventricular conduction in mice lacking CaV3.1/α1G T-type calcium channels. Circulation Research, 1422–1430. https://doi.org/10.1161/01.RES.0000225862.14314.49.

Marais, E., Klugbauer, N., & Hofmann, F. (2001). Calcium Channel α 2 δ Subunits—Structure and Gabapentin Binding. Molecular Pharmacology, 59(5), 1243–1248. https://doi.org/10.1124/mol.59.5.1243.

Marchese, A., Paing, M. M., Temple, B. R. S., & Trejo, J. A. (2008). G protein-coupled receptor sorting to endosomes and lysosomes. Annual Review of Pharmacology and Toxicology, 48, 601–629. https://doi.org/10.1146/annurev.pharmtox.48.113006.094646.

Marger, F., Gelot, A., Alloui, A., Matricon, J., Sanguesa Ferrer, J. F., Barrère, C., Pizzoccaro, A., Muller, E., Nargeot, J., Snutch, T. P., Eschalier, A., Bourinet, E., & Ardid, D. (2011). T-type calcium channels contribute to colonic hypersensitivity in a rat model of irritable bowel syndrome. PNAS, 108(27), 11268–11273. https://doi.org/10.1073/pnas.1100869108.

Marinus, M. G., & Løbner-Olesen, A. (2014). DNA Methylation. EcoSal Plus, 6(1). https://doi.org/10.1128/ecosalplus.esp-0003-2013.

Marks, M. S., Woodruff, L., Ohno, H., & Bonifacino, J. S. (1996). Protein Targeting by Tyrosine- and Di-leucine-based Signals: Evidence for Distinct Saturable Components. The Journal of Cell Biology, 135(2), 341–354.

Martinez-Morales, J. C., Teresa Romero-Avila, M., Reyes-Cruz, G., & Garcia-Sainz, J. A. (2022). Roles of Receptor Phosphorylation and Rab Proteins in G Protein-Coupled Receptor Function and Trafficking. Molecular Pharmacology, 101, 144–153. https://doi.org/10.1124/molpharm.121.000429.

Matilla, M. A., Velando, F., Martín-Mora, D., Monteagudo-Cascales, E., & Krell, T. (2022). A catalogue of signal molecules that interact with sensor kinases, chemoreceptors and transcriptional regulators. In FEMS Microbiology Reviews (Vol. 46). Oxford University Press. https://doi.org/10.1093/femsre/fuab043.

Maue, R. A. (2007). Understanding ion channel biology using epitope tags: Progress, pitfalls, and promise. Journal of Cellular Physiology, 618–625. https://doi.org/10.1002/jcp.21259.

McKay, B. E., McRory, J. E., Molineux, M. L., Hamid, J., Snutch, T. P., Zamponi, G. W., & Turner, R. W. (2006). CaV3 T-type calcium channel isoforms differentially distribute to somatic and

dendritic compartments in rat central neurons. European Journal of Neuroscience, 24, 2581–2594. https://doi.org/10.1111/j.1460-9568.2006.05136.x.

Mefford, H. C., Yendle, S. C., Hsu, C., Cook, J., Geraghty, E., McMahon, J. M., Eeg-Olofsson, O., Sadleir, L. G., Gill, D., Ben-Zeev, B., Lerman-Sagie, T., MacKay, M., Freeman, J. L., Andermann, E., Pelakanos, J. T., Andrews, I., Wallace, G., Eichler, E. E., Berkovic, S. F., & Scheffer, I. E. (2011). Rare copy number variants are an important cause of epileptic encephalopathies. Annuals of Neurology, 70(6), 974–985. https://doi.org/10.1002/ana.22645.

Meir, A., Bell, D. C., Stephens, G. J., Page, K. M., & Dolphin, A. C. (2000). Calcium Channel Subunit Promotes Voltage-Dependent Modulation of 1B by G. Biophysical Journal, 79, 731–746.

Meiser, A., Mueller, A., Wise, E. L., Mcdonagh, E. M., Petit, S. J., Saran, N., Clark, P. C., Williams, T. J., Pease, J. E., & Pease, J. (2008). The chemokine receptor CXCR3 is degraded following internalisation and is replenished at the cell surface by de novo synthesis of receptor. Europe PMC Funders Group. J Immunol, 180(10), 6713–6724. www.jimmunol.org.

Mesirca, P., Torrente, A. G., & Mangoni, M. E. (2014). T-type channels in the sino-atrial and atrioventricular pacemaker mechanism. European Journal of Physiology, 466, 791–799. https://doi.org/10.1007/s00424-014-1482-6.

MetzelaarS, M. J., Wijngaardg, P. L., Petersll, P. J., Sixma, J. J., Karel NieuwenhuisS, H., & CleversB, H. C. (1991). A novel lysosomal membrane glycoprotein, cloned by a screening procedure for intracellular antigens in eukaryotic cells. The Journal of Biological Chemistry, 266(5), 3239–3245.

Meyer, J. O., & Dolphin, A. C. (2021). Rab11-dependent recycling of calcium channels is mediated by auxiliary subunit α2δ-1 but not α2δ-3. Scientific Reports, 11(10256). https://doi.org/10.1038/s41598-021-89820-1.

Minakshi, R., & Padhan, K. (2014). The YXXΦ motif within the severe acute respiratory syndrome coronavirus (SARS-CoV) 3a protein is crucial for its intracellular transport. Virology Journal, 11(75). https://doi.org/10.1186/1743-422X-11-75.

Miranda, K. C., Khromykh, T., Christy, P., Le, T. L., Gottardi, C. J., Yap, A. S., Stow, J. L., & Teasdale, R. D. (2001). A Dileucine Motif Targets E-cadherin to the Basolateral Cell Surface in Madin-Darby Canine Kidney and LLC-PK1 Epithelial Cells. Journal of Biological Chemistry, 276(25), 22565–22572. https://doi.org/10.1074/jbc.M101907200.

Mishra, M., Tiwari, S., & Gomes, A. v. (2017). Protein purification and analysis: Next generation western blotting techniques. Expert Review of Proteomics, 14(11), 1037–1053. https://doi.org/10.1080/14789450.2017.1388167.

Monier, S., Dietzen, D. J., Hastings, W. R., Lublin, D. M., & Kurzchalia, T. v. (1996). Oligomerization of VIP21-caveolin in vitro is stabilized by long chain fatty acylation or cholesterol. FEBS Letters, 388, 143–149. https://doi.org/10.1016/0014-5793(96)00519-4.

Mould, A. P., Askari, J. A., Barton, S., Kline, A. D., McEwan, P. A., Craig, S. E., & Humphries, M. J. (2002). Integrin activation involves a conformational change in the α1 helix of the β subunit A-domain. Journal of Biological Chemistry, 277(22), 19800–19805. https://doi.org/10.1074/jbc.M201571200.

Nagase, T., Kikuno, R., Nakayama, M., Hirosawa, M., Ohara, O. (2000). Prediction of the coding sequences of unidentified human genes. XVIII. The complete sequences of 100 new cDNA clones from brain which code for large proteins *in vitro*. DNA Research, 7, 273-281.

Neely, G. G., Hess, A., Costigan, M., Keene, A. C., Goulas, S., Langeslag, M., Griffin, R. S., Belfer, I., Dai, F., Smith, S. B., Diatchenko, L., Gupta, V., Xia, C. ping, Amann, S., Kreitz, S., Heindl-Erdmann, C., Wolz, S., Ly, C. v., Arora, S., … Penninger, J. M. (2010). A Genome-wide Drosophila screen for heat nociception identifies α2δ3 as an evolutionarily conserved pain gene. Cell, 143, 628–638. https://doi.org/10.1016/j.cell.2010.09.047.

Nguyen, H. du, Okada, T., Sekiguchi, F., Tsubota, M., Nishikawa, H., Kawabata, A., & Toyooka, N. (2019). Prenylflavanones as Novel T-Type Calcium Channel Blockers Useful for Pain Therapy. Natural Product Communications. https://doi.org/10.1177/1934578X19873441.

Ning, L., Ma, L.-Q., Wang, Z.-R., & Wang, Y.-W. (2013). Experimental Trial Chronic Constriction Injury Induced Long-Term Changes in Spontaneous Membrane-Potential Oscillations in Anterior Cingulate Cortical Neurons in Vivo. Pain Physician, 16, E577–E589. www.painphysicianjournal.com.

Njavro, J. R., Klotz, J., Dislich, B., Wanngren, J., Shmueli, M. D., Herber, J., Kuhn, P. H., Kumar, R., Koeglsperger, T., Conrad, M., Wurst, W., Feederle, R., Vlachos, A., Michalakis, S., Jedlicka, P., Müller, S. A., & Lichtenthaler, S. F. (2020). Mouse brain proteomics establishes MDGA1 and CACHD1 as in vivo substrates of the Alzheimer protease BACE1. FASEB Journal, 2465–2482. https://doi.org/10.1096/fj.201902347R.

Nosaki, S., Hoshikawa, K., Ezura, H., & Miura, K. (2021). Transient protein expression systems in plants and their applications. Plant Biotechnology, 38, 297–304. https://doi.org/10.5511/plantbiotechnology.21.0610a.

Novakovic, S., Sawai, E. T., & Radke, K. (2004). Dileucine and YXXL Motifs in the Cytoplasmic Tail of the Bovine Leukemia Virus Transmembrane Envelope Protein Affect Protein Expression on the Cell Surface. Journal of Virology, 78(15), 8301–8311. https://doi.org/10.1128/jvi.78.15.8301-8311.2004.

Ohno, H., Stewart, J., Fournier, M.-C., Bosshart, H., Rhee, I., Miyatake, S., Saito, T., Gallusser, A., Kirchhausen, T., & Bonifacino, J. S. (1995). Interaction of Tyrosine-Based Sorting Signals with Clathrin-Associated Proteins. Science, 269(5232), 1872–1875. https://doi.org/10.1126/science.7569928.

Omasa, T., Onitsuka, M., & Kim, W.-D. (2010). Cell Engineering and Cultivation of Chinese Hamster Ovary (CHO) Cells. Current Pharmaceutical Biotechnology, 11(3), 233–240. https://doi.org/10.2174/138920110791111960.

Ortega, Á., Zhulin, I. B., & Krell, T. (2017). Sensory Repertoire of Bacterial Chemoreceptors. Microbiology and Molecular Biology Reviews, 81(4). https://doi.org/10.1128/MMBR.

Ottolia, M., Torres, N., Bridge, J. H. B., Philipson, K. D., & Goldhaber, J. I. (2013). Na/Ca exchange and contraction of the heart. Journal of Molecular and Cellular Cardiology, 61, 28–33. https://doi.org/10.1016/j.yjmcc.2013.06.001.

Paing, M. M., Temple, B. R. S., & Trejo, J. A. (2004). A tyrosine-based sorting signal regulates intracellular trafficking of protease-activated reeeptor-1: Multiple regulatory mechanisms for agonist-induced G protein-coupled receptor internalization. Journal of Biological Chemistry, 279(21), 21938–21947. https://doi.org/10.1074/jbc.M401672200.

Palade, G. . E. (1953). Fine Structure of Blood Capillaries. Journal of Applied Physics, 24, 1424–1432.

Pan, B., Yu, H., Park, J., Yu, Y. P., Luo, Z. D., Hogan, Q. H. (2015). Painful nerve injury upregulates thrombospondin-4 expression in dorsal root ganglia. J Neurosci Res, 93(3), 443-53. doi: 10.1002/jnr.23498.

Pandey, K. N. (2009). Functional roles of short sequence motifs in the endocytosis of membrane receptors. Front Biosci, 14, 5339–5360.

Pandey, K. N., Nguyen, H. T., Sharma, G. D., Shi, S. J., & Kriegel, A. M. (2002). Ligand-regulated internalization, trafficking, and down-regulation of guanylyl cyclase/atrial natriuretic peptide receptor-A in human embryonic kidney 293 cells. Journal of Biological Chemistry, 277(7), 4618–4627. https://doi.org/10.1074/jbc.M106436200.

Pani, B., Singh, B .B. (2009). Lipid rafts/caveolae as microdomains of calcium signalling. Cell Calcium, 45(6), 625-633.

Parkinson, J. S., Hazelbauer, G. L., & Falke, J. J. (2015). Signaling and sensory adaptation in Escherichia coli chemoreceptors: 2015 update. Trends in Microbiology, 23(5), 257–266. https://doi.org/10.1016/j.tim.2015.03.003.

Parkyn, C. J., Vermeulen, E. G. M., Mootoosamy, R. C., Sunyach, C., Jacobsen, C., Oxvig, C., Moestrup, S., Liu, Q., Bu, G., Jen, A., & Morris, R. J. (2008). LRP1 controls biosynthetic and endocytic trafficking of neuronal prion protein. Journal of Cell Science, 121(6), 773–783. https://doi.org/10.1242/jcs.021816.

Parton, R. G. (2018). Caveolae: Structure, Function, and Relationship to Disease. Annual Review of Cell and Developmental Biology, 34, 111–136. https://doi.org/10.1146/annurev-cellbio-100617.

Patel, H. H., Murray, F., Insel, P. A. (2008). Caveolae are organizers of pharmacologically relevant signal transduction molecules. Annu Rev Pharmacol Toxicol, 48, 359-391.

Peng, L., Yu, X., Li, C., Cai, Y., Chen, Y., He, Y., Yang, J., Jin, J., & Li, H. (2016). Enhanced recombinant factor VII expression in Chinese hamster ovary cells by optimizing signal peptides

and fed-batch medium. Bioengineered, 7(3), 189–197. https://doi.org/10.1080/21655979.2016.1176656.

Perez-Reyes, E. (2003). Molecular Physiology of Low-Voltage-Activated T-type Calcium Channels. Physiol Rev, 83, 117–161. https://doi.org/10.1152/physrev.00018.2002.-T-type.

Perez-Reyes, E., Cribbs, L. L., Daud, A., Lacerda, A. E., Barclays, J., Williamson, M. P., Fox, M., Rees, M., & Lee, J. H. (1998). Molecular characterization of a neuronal low-voltage-activated T-type calcium channel. Nature, 391, 896–900. https://doi.org/10.1038/36110.

Piehl, M., Lehmann, C., Gumpert, A., Denizot, J.-P., Segretain, D., & Falk, M. M. (2007). Internalization of Large Double-Membrane Intercellular Vesicles by a Clathrin-dependent Endocytic Process. Molecular Biology of the Cell, 18, 337–347. https://doi.org/10.1091/mbc.E06.

Pike, L. J. (2006). Rafts defined: a report on the Keystone Symposium on lipid rafts and cell function. J lipid Res, 47, 1597-8.

Pike, L. J., Han, X., Chung, K. N., Gross, R. W. (2002). Lipid rafts are enriched in arachidonic acid and plasmenylethanolamine and their composition is independent of caveolin-1 expression: a quantitative electrospray ionization/mass spectrometric analysis. Biochemistry, 41, 2075-88.

Pippucci, T., Parmeggiani, A., Palombo, F., Maresca, A., Angius, A., Crisponi, L., Cucca, F., Liguori, R., Valentino, M. L., Seri, M., & Carelli, V. (2013). A novel null homozygous mutation confirms CACNA2D2 as a gene mutated in epileptic encephalopathy. PLoS ONE, 8(12). https://doi.org/10.1371/journal.pone.0082154.

Poteser, M., Graziani, A., Rosker, C., Eder, P., Derler, I., Kahr, H., Zhu, M. X., Romanin, C., & Groschner, K. (2006). TRPC3 and TRPC4 associate to form a redox-sensitive cation channel: Evidence for expression of native TRPC3-TRPC4 heteromeric channels in endothelial cells. Journal of Biological Chemistry, 281(19), 13588–13595. https://doi.org/10.1074/jbc.M512205200.

Powell, K. L., Cain, S. M., Ng, C., Sirdesai, S., David, L. S., Kyi, M., Garcia, E., Tyson, J. R., Reid, C. A., Bahlo, M., Foote, S. J., Snutch, T. P., & O'Brien, T. J. (2009). A Cav3.2 T-type calcium

channel point mutation has splice-variant-specific effects on function and segregates with seizure expression in a polygenic rat model of absence epilepsy. Journal of Neuroscience, 29(2), 371–380. https://doi.org/10.1523/JNEUROSCI.5295-08.2009.

Pragnell, M., de Waard, M., Mori, Y., Tanabe, T., Snutch, T. P., & Campbell, K. P. (1994). Calcium channel B-subunit binds to a conserved motif in the I-II cytoplasmic linker of the a1-subunit. Nature, 368.

Pragnell, M., Sakamoto, J., Jay, S. D., & Campbell, K. P. (1991). Cloning and tissue-specific expression of the brain calcium channel β-subunit. FEBS Letters, 291(2), 253–258. https://doi.org/10.1016/0014-5793(91)81296-K.

Proft, J., Rzhepetskyy, Y., Lazniewska, J., Zhang, F. X., Cain, S. M., Snutch, T. P., Zamponi, G. W., & Weiss, N. (2017). The Cacna1h mutation in the GAERS model of absence epilepsy enhances T-type Ca2+ currents by altering calnexin-dependent trafficking of Cav3.2 channels. Scientific Reports, 7(11513). https://doi.org/10.1038/s41598-017-11591-5.

Qian, J., Wu, C., Chen, X., Li, X., Ying, G., Jin, L., Ma, Q., Li, G., Shi, Y., Zhang, G., & Zhou, N. (2014). Differential requirements of arrestin-3 and clathrin for ligand-dependent and -independent internalization of human G protein-coupled receptor 40. Cellular Signalling, 26, 2412–2423. https://doi.org/10.1016/j.cellsig.2014.07.019.

Qin, N., Platano, D., Olcese, R., Costantin, J. L., Stefani, E., & Birnbaumer, L. (1998). Unique regulatory properties of the type 2a Ca 2 channel subunit caused by palmitoylation. Neurobiology, 95, 4690–4695. www.pnas.org.

Qin, N., Yagel, S., Momplaisir, M.-L., Codd, E. E., & D'Andrea, M. R. (2002). Molecular Cloning and Characterization of the Human Voltage-Gated Calcium Channel α 2 δ-4 Subunit. Molecular Pharmacology, 62(3), 485–496. https://doi.org/10.1124/mol.62.3.485.

Ramazi, S., & Zahiri, J. (2021). Post-translational modifications in proteins: Resources, tools and prediction methods. Database, 00. https://doi.org/10.1093/database/baab012.

Rangel-Galván, M., Rangel, A., Romero-Méndez, C., Dávila, E. M., Castro, M. E., Caballero, N. A., Meléndez Bustamante, F. J., Sanchez-Gaytan, B. L., Meza, U., & Perez-Aguilar, J. M. (2021).

Inhibitory Mechanism of the Isoflavone Derivative Genistein in the Human CaV3.3 Channel. ACS Chemical Neuroscience, 12, 651–659. https://doi.org/10.1021/acschemneuro.0c00684.

Rangel-Galván, M., Rangel-Galván, V., & Rangel-Huerta, A. (2023). T-type calcium channel modulation by hydrogen sulfide in neuropathic pain conditions. Frontiers in Pharmacology. https://doi.org/10.3389/fphar.2023.1212800.

Rassi, D. M., Junta, C. M., Fachin, A. L., Sandrin-Garcia, P., Mello, S., Silva, G. L., Evangelista, A. F., Magalhães, D. A., Wastowski, I. J., Crispim, J. O., Martelli-Palomino, G., Fernandes, A. P. M., Deghaide, N. N. H. S., Foss-Freitas, M. C., Foss, M. C., Soares, C. P., Sakamoto-Hojo, E. T., Passos, G. A. S., & Donadi, E. A. (2008). Gene expression profiles stratified according to type 1 diabetes mellitus susceptibility regions. Annals of the New York Academy of Sciences, 1150, 282–289. https://doi.org/10.1196/annals.1447.064.

Rath, P. P., Anand, G., & Agarwal, S. (2020). Surface Plasmon Resonance Analysis of the Protein-protein Binding Specificity Using Autolab ESPIRIT. Bio-Protocol, 10(4). https://doi.org/10.21769/BioProtoc.3519.

Ray, P., Torck, A., Quigley, L., Wangzhou, A., Neiman, M., Rao, C., Lam, T., Kim, J. Y., Kim, T. H., Zhang, M. Q., Dussor, G., & Price, T. J. (2018). Comparative transcriptome profiling of the human and mouse dorsal root ganglia: An RNA-seq-based resource for pain and sensory neuroscience research. Pain, 159(7), 1325–1345. https://doi.org/10.1097/j.pain.0000000000001217.

Redin, C., Brand, H., Collins, R. L., Kammin, T., Mitchell, E., Hodge, J. C., Hanscom, C., Pillalamarri, V., Seabra, C. M., Abbott, M. A., Abdul-Rahman, O. A., Aberg, E., Adley, R., Alcaraz-Estrada, S. L., Alkuraya, F. S., An, Y., Anderson, M. A., Antolik, C., Anyane-Yeboa, K., … Talkowski, M. E. (2017). The genomic landscape of balanced cytogenetic abnormalities associated with human congenital anomalies. Nature Genetics, 49(1), 36–45. https://doi.org/10.1038/ng.3720.

Rees, J. S., & Lilley, K. S. (2011). Method for suppressing non-specific protein interactions observed with affinity resins. Methods, 54, 407–412. https://doi.org/10.1016/j.ymeth.2011.06.004.

Remy, J.-S., Abdallah, B., Antonietta Zanta, M., Boussif, O., Paul Behr, J., & Demeneix, B. (1998). Gene transfer with lipospermines and polyethylenimines. Advanced Drug Delivery Reviews, 30, 85–95.

Rennick, J. J., Johnston, A. P. R., & Parton, R. G. (2021). Key principles and methods for studying the endocytosis of biological and nanoparticle therapeutics. Nature Nanotechnology, 16, 266–276. https://doi.org/10.1038/s41565-021-00858-8.

Reynders, A., Mantilleri, A., Malapert, P., Rialle, S., Nidelet, S., Laffray, S., Beurrier, C., Bourinet, E., & Moqrich, A. (2015). Transcriptional Profiling of Cutaneous MRGPRD Free Nerve Endings and C-LTMRs. Cell Reports, 10, 1007–1019. https://doi.org/10.1016/j.celrep.2015.01.022.

Risher, W. C., Kim, N., Koh, S., Choi, J. E., Mitev, P., Spence, E. F., Pilaz, L. J., Wang, D., Feng, G., Silver, D. L., Soderling, S. H., Yin, H. H., Eroglu, C. (2018). Thrombospondin receptor α2δ-1 promotes synaptogenesis and spinogenesis via postsynaptic Rac1. J Cell Biol, 217(10), 3747-3765. doi: 10.1083/jcb.201802057.

Rodal, S. K., Skretting, G., Garred, Ø., Vilhardt, F., van Deurs, B., & Sandvig, K. (1999). Extraction of Cholesterol with Methyl-Cyclodextrin Perturbs Formation of Clathrin-coated Endocytic Vesicles. Molecular Biology of the Cell, 10, 961–974.

Rodríguez-López, J., Sobrino, B., Amigo, J., Carrera, N., Brenlla, J., Agra, S., Paz, E., Carracedo, Á., Páramo, M., Arrojo, M., & Costas, J. (2018). Identification of putative second genetic hits in schizophrenia carriers of high-risk copy number variants and resequencing in additional samples. European Archives of Psychiatry and Clinical Neuroscience, 268, 585–592. https://doi.org/10.1007/s00406-017-0799-5.

Rohrer, J., Schweizer, A., Russell, D., & Kornfeld, S. (1996). The Targeting of Lampl to Lysosomes Is Dependent on the Spacing of its Cytoplasmic Tail Tyrosine Sorting Motif Relative to the Membrane. The Journal of Cell Biology, 132(4), 565–576.

Rojas, E. P., Maceira, F. I. G., Guerrero, V. I. L., Penalvo, M. G. M., Maceira, T. G., Martinez, J. A. M., Gomez, A. B. A., Molina, A. Q., & Morales, A. M. M. (2012). GPCR with improved cell surface expression (US9499584B2).

Rothberg, K. G., Heuser, J. E., Donzell, W. C., Ying, Y.-S., Glenney, J. R., & Anderson, R. G. W. (1992). Caveolin, a protein component of caveolae membrane coats. Cell, 68(4), 673–682. https://doi.org/10.1016/0092-8674(92)90143-Z.

Ruth, P., Röhrkasten, A., Biel, M., Bosse, E., Regulla, S., Meyer, H. E., Flockerzi, V., & Hofmann, F. (1989). Primary Structure of the β Subunit of the DHP-Sensitive Calcium Channel from Skeletal Muscle. Science, 245(4922), 1115–1118. https://doi.org/10.1126/science.2549640.

Ryan, B. J., & Heneban, G. T. (2016). Avoiding Proteolysis During Protein Purification. Methods in Molecular Biology, 4, 53–70. http://www.springer.com/series/7651.

Rzhepetskyy, Y., Lazniewska, J., Blesneac, I., Pamphlett, R., & Weiss, N. (2016). CACNA1H missense mutations associated with amyotrophic lateral sclerosis alter Cav3.2 T-type calcium channel activity and reticular thalamic neuron firing. Channels, 10(6), 466–477. https://doi.org/10.1080/19336950.2016.1204497.

Rzhepetskyy, Y., Lazniewska, J., Proft, J., Campiglio, M., Flucher, B. E., & Weiss, N. (2016). A Cav3.2/Stac1 molecular complex controls T-type channel expression at the plasma membrane. Channels, 10(5), 346–354. https://doi.org/10.1080/19336950.2016.1186318.

Sabin, J., Alatorre-Meda, M., Miñones, J., Domínguez-Arca, V., & Prieto, G. (2022). New insights on the mechanism of polyethylenimine transfection and their implications on gene therapy and DNA vaccines. Colloids and Surfaces B: Biointerfaces, 210. https://doi.org/10.1016/j.colsurfb.2021.112219.

Sacharok, A. L., Porsch, E. A., & st. Geme, J. W. (2023). The Kingella kingae PilC1 MIDAS Motif Is Essential for Type IV Pilus Adhesive Activity and Twitching Motility. Infection and Immunity, 91(1). https://doi.org/10.1128/iai.00338-22.

Saheki, Y., & Bargmann, C. I. (2009). Presynaptic CaV2 calcium channel traffic requires CALF-1 and the alpha2-delta subunit UNC-36. Nature Neuroscience, 12(10), 1257–1265. http://www.nature.com/authors/editorial_policies/license.html#terms.

Sakmann, B., & Neher, E. (1976). Single-channel currents recorded from membrane of denervated frog muscle fibres. Nature, 260.

Sauvonnet, N., Dujeancourt, A., & Dautry-Varsat, A. (2005). Cortactin and dynamin are required for the clathrin-independent endocytosis of γc cytokine receptor. Journal of Cell Biology, 168(1), 155–163. https://doi.org/10.1083/jcb.200406174.

Shajahan, A. N., Timblin, B. K., Sandoval, R., Tiruppathi, C., Malik, A. B., & Minshall, R. D. (2004). Role of Src-induced Dynamin-2 Phosphorylation in Caveolae-mediated Endocytosis in Endothelial Cells. Journal of Biological Chemistry, 279(19), 20392–20400. https://doi.org/10.1074/jbc.M308710200.

Sharma, D. K., Brown, J. C., Cheng, Z., Holicky, E. L., Marks, D. L., & Pagano, R. E. (2005). The Glycosphingolipid, Lactosylceramide, Regulates β1-Integrin Clustering and Endocytosis. Cancer Research, 65(18), 8233–8241. https://doi.org/10.1158/0008-5472.CAN-05-0803.

Sharma, S., Schiller, M. R. (2019). The carboxy-terminus, a key regulator of protein function. Crit Rev Biochem Mol Biol, 54(2), 85-102. doi: 10.1080/10409238.2019.1586828.

Shen, F. Y., Chen, Z. Y., Zhong, W., Ma, L. Q., Chen, C., Yang, Z. J., Xie, W. L., & Wang, Y. W. (2015). Alleviation of Neuropathic Pain by Regulating T-Type Calcium Channels in Rat Anterior Cingulate Cortex. Molecular Pain, 11(7). https://doi.org/10.1186/s12990-015-0008-3.

Simons, K., Toomre, D. (2000). Lipid rafts and signal transduction. Nat Rev Mol Cell Biol, 1, 31-39.

Singh, P. (2016). SPR Biosensors: Historical Perspectives and Current Challenges. Sensors and Actuators, B: Chemical, 229, 110–130. https://doi.org/10.1016/j.snb.2016.01.118.

Song, I., Kim, D., Choi, S., Sun, M., Kim, Y., & Shin, H. S. (2004). Role of the α1G T-type calcium channel in spontaneous absence seizures in mutant mice. Journal of Neuroscience, 24(22), 5249–5257. https://doi.org/10.1523/JNEUROSCI.5546-03.2004.

Sorkina, T., Hoover, B. R., Zahniser, N. R., Sorkin, A., & Munksgaard, B. (2005). Constitutive and Protein Kinase C-Induced Internalization of the Dopamine Transporter is Mediated by a Clathrin-Dependent Mechanism. Traffic, 6, 157–170. https://doi.org/10.1111/j.1600-0854.2004.00259.x.

Soubrane, C. H., Stevens, E. B., & Stephens, G. J. (2012). Poster Communications: Expression and functional studies of the novel CNS protein CACHD1. Proc Physiol Soc.

Splawski, I., Yoo, D. S., Stotz, S. C., Cherry, A., Clapham, D. E., & Keating, M. T. (2006). CACNA1H mutations in autism spectrum disorders. Journal of Biological Chemistry, 281(31), 22085–22091. https://doi.org/10.1074/jbc.M603316200.

Stephens, G. J., & Cottrell, G. S. (2019). CACHD1: A new activity-modifying protein for voltage-gated calcium channels. In Channels (Vol. 13, pp. 120–123). Taylor and Francis Inc. https://doi.org/10.1080/19336950.2019.1600968.

Stephens, G. J., Page, K. M., Bogdanov, Y., & Dolphin, A. C. (2000). The a1B Ca2+ channel amino terminus contributes determinants for B subunit-mediated voltage-dependent inactivation properties. Journal of Physiology, 525(2), 377–390.

Sun, H., Wang, S., Lu, M., Tinberg, C. E., & Alba, B. M. (2023). Protein production from HEK293 cell linederived stable pools with high protein quality and quantity to support discovery research. PLoS ONE, 18. https://doi.org/10.1371/journal.pone.0285971.

Szymczyna, B. R., Taurog, R. E., Young, M. J., Snyder, J. C., Johnson, J. E., & Williamson, J. R. (2009). Synergy of NMR, Computation, and X-Ray Crystallography for Structural Biology. Structure, 17(4), 499–507. https://doi.org/10.1016/j.str.2009.03.001.

Takahashi, M., Seagart, M. J., Jones, J. F., Reber, B. F. X., & Catterallt, W. A. (1987). Subunit structure of dihydropyridine-sensitive calcium channels from skeletal muscle (calcium antagonists/protein phosphorylation/glycoproteins/ion channels). Neurobiology, 84, 5478–5482.

Talley, E. M., Cribbs, L. L., Lee, J.-H., Daud, A., Perez-Reyes, E., & Bayliss, D. A. (1999). Differential Distribution of Three Members of a Gene Family Encoding Low Voltage-Activated (T-Type) Calcium Channels. The Journal of Neuroscience, 19(6), 1895–1911.

Taylor, C. P., & Garrido, R. (2008). Immunostaining of rat brain, spinal cord, sensory neurons and skeletal muscle for calcium channel alpha2-delta (α2-δ) type 1 protein. Neuroscience, 155(2), 510–521. https://doi.org/10.1016/j.neuroscience.2008.05.053.

Taylor, D. R., & Hooper, N. M. (2007). The low-density lipoprotein receptor-related protein 1 (LRP1) mediates the endocytosis of the cellular prion protein. Biochemical Journal, 402, 17–23. https://doi.org/10.1042/BJ20061736.

Templin, C., Ghadri, J. R., Rougier, J. S., Baumer, A., Kaplan, V., Albesa, M., Sticht, H., Rauch, A., Puleo, C., Hu, D., Barajas-Martinez, H., Antzelevitch, C., Lüscher, T. F., Abriel, H., & Duru, F. (2011). Identification of a novel loss-of-function calcium channel gene mutation in short QT syndrome (SQTS6). European Heart Journal, 32, 1077–1088. https://doi.org/10.1093/eurheartj/ehr076.

Tian, C., Johnson, K. R., Lett, J. M., Voss, R., Salt, A. N., Hartsock, J. J., Steyger, P. S., & Ohlemiller, K. K. (2021). CACHD1-deficient mice exhibit hearing and balance deficits associated with a disruption of calcium homeostasis in the inner ear. Hearing Research, 409(108327). https://doi.org/10.1016/j.heares.2021.108327.

Tolomeo, D., Agostini, A., Macchia, G., L'Abbate, A., Severgnini, M., Cifola, I., Frassanito, M. A., Racanelli, V., Solimando, A. G., Haglund, F., Mertens, F., & Storlazzi, C. T. (2021). BL1391: an established cell line from a human malignant peripheral nerve sheath tumor with unique genomic features. Human Cell, 34, 238–245. https://doi.org/10.1007/s13577-020-00418-7.

Tomita, S., Chen, L., Kawasaki, Y., Petralia, R. S., Wenthold, R. J., Nicoll, R. A., & Bredt, D. S. (2003). Functional studies and distribution define a family of transmembrane AMPA receptor regulatory proteins. Journal of Cell Biology, 161(4), 805–816. https://doi.org/10.1083/jcb.200212116.

Tottene, A., Conti, R., Fabbro, A., Vecchia, D., Shapovalova, M., Santello, M., van den Maagdenberg, A. M. J. M., Ferrari, M. D., & Pietrobon, D. (2009). Enhanced Excitatory Transmission at Cortical Synapses as the Basis for Facilitated Spreading Depression in CaV2.1 Knockin Migraine Mice. Neuron, 61, 762–773. https://doi.org/10.1016/j.neuron.2009.01.027.

Tran-Van-Minh, A., & Dolphin, A. C. (2010). The α2δ ligand gabapentin inhibits the Rab11-dependent recycling of the calcium channel subunit α 2δ-2. Journal of Neuroscience, 30(38), 12856–12867. https://doi.org/10.1523/JNEUROSCI.2700-10.2010.

Traub, L. M. (2003). Sorting it out: AP-2 and alternate clathrin adaptors in endocytic cargo selection. Journal of Cell Biology, 163(2), 203–208. https://doi.org/10.1083/jcb.200309175.

Uebele, V. N., Gotter, A. L., Nuss, C. E., Kraus, R. L., Doran, S. M., Garson, S. L., Reiss, D. R., Li, Y., Barrow, J. C., Reger, T. S., Yang, Z. Q., Ballard, J. E., Tang, C., Metzger, J. M., Wang, S. P., Koblan, K. S., & Renger, J. J. (2009). Antagonism of T-type calcium channels inhibits high-fat

diet-induced weight gain in mice. Journal of Clinical Investigation, 119(6), 1659–1667. https://doi.org/10.1172/JCI36954.

Ungewickell, E. J., & Hinrichsen, L. (2007). Endocytosis: clathrin-mediated membrane budding. Current Opinion in Cell Biology, 19, 417–425. https://doi.org/10.1016/j.ceb.2007.05.003.

Urao, T., Yamaguchi-Shinozaki, K., & Shinozaki, K. (2001). Plant Histidine Kinases: An Emerging Picture of Two-Component Signal Transduction in Hormone and Environmental Responses. Science's STKE, 2001(109). https://doi.org/10.1126/stke.2001.109.re18.

Valdramidou, D., Humphries, M. J., & Mould, A. P. (2008). Distinct roles of β1 metal ion-dependent adhesion site (MIDAS), adjacent to MIDAS (ADMIDAS), and ligand-associated metal-binding site (LIMBS) cation-binding sites in ligand recognition by integrin α2β1. Journal of Biological Chemistry, 283(47), 32704–32714. https://doi.org/10.1074/jbc.M802066200.

Valence, S., & Burglen, L. (2019). Exome sequencing in congenital ataxia identifies two new candidate genes and highlights a pathophysiological link between some congenital ataxias and early infantile epileptic encephalopathies. Genetics in Medicine, 21(3). https://doi.org/10.1038/s41436.

van den Bossche, M. J., Strazisar, M., de Bruyne, S., Bervoets, C., Lenaerts, A. S., de Zutter, S., Nordin, A., Norrback, K. F., Goossens, D., de Rijk, P., Green, E. K., Grozeva, D., Mendlewicz, J., Craddock, N., Sabbe, B. G., Adolfsson, R., Souery, D., & Del-Favero, J. (2012). Identification of a CACNA2D4 deletion in late onset bipolar disorder patients and implications for the involvement of voltage-dependent calcium channels in psychiatric disorders. American Journal of Medical Genetics, Part B: Neuropsychiatric Genetics, 159 B(4), 465–475. https://doi.org/10.1002/ajmg.b.32053.

van der Sluijs, P., Hull, M., Webster, P., Mâle, P., Goud, B., & Mellman, I. (1992). The small GTP-binding protein rab4 controls an early sorting event on the endocytic pathway. Cell, 70(5), 729–740. https://doi.org/10.1016/0092-8674(92)90307-X.

van Petegem, F., Clark, K. A., Chatelain, F. C., & Minor, D. L. (2004). Structure of a complex between a voltage-gated calcium channel β-subunit and an α-subunit domain. Nature, 429(6992), 671–675. https://doi.org/10.1038/nature02588.

van Petegem, F., Duderstadt, K. E., Clark, K. A., Wang, M., & Minor, D. L. (2008). Alanine-Scanning Mutagenesis Defines a Conserved Energetic Hotspot in the CaVα1 AID-CaVβ Interaction Site that Is Critical for Channel Modulation. Structure, 16(2), 280–294. https://doi.org/10.1016/j.str.2007.11.010.

Vançan, S., Alves Miranda, E., & Alves Bueno, S. M. (2002). IMAC of human IgG: studies with IDA-immobilized copper, nickel, zinc, and cobalt ions and different buffer systems. Process Biochemistry, 37, 573–579. www.elsevier.com/locate/procbio.

Vangeel, L., & Voets, T. (2019). Transient receptor potential channels and calcium signaling. Cold Spring Harbor Perspectives in Biology, 11. https://doi.org/10.1101/cshperspect.a035048.

Vercauteren, D., Vandenbroucke, R. E., Jones, A. T., Rejman, J., Demeester, J., de Smedt, S. C., Sanders, N. N., & Braeckmans, K. (2010). The use of inhibitors to study endocytic pathways of gene carriers: Optimization and pitfalls. Molecular Therapy, 18(3), 561–569. https://doi.org/10.1038/mt.2009.281.

Vogl, C., Tanifuji, S., Danis, B., Daniels, V., Foerch, P., Wolff, C., Whalley, B. J., Mochida, S., & Stephens, G. J. (2015). Synaptic vesicle glycoprotein 2A modulates vesicular release and calcium channel function at peripheral sympathetic synapses. European Journal of Neuroscience, 41, 398–409. https://doi.org/10.1111/ejn.12799.

Völzke, J. L., Smatty, S., Döring, S., Ewald, S., Oelze, M., Fratzke, F., Flemig, S., Konthur, Z., & Weller, M. G. (2023). Efficient Purification of Polyhistidine-Tagged Recombinant Proteins Using Functionalized Corundum Particles. BioTech, 12(2), 31. https://doi.org/10.3390/biotech12020031.

von Zastrow, M., & Sorkin, A. (2007). Signaling on the endocytic pathway. Current Opinion in Cell Biology, 19(4), 463–445.

Wang, M., Offord, J., Oxender, D. L., & Su, T.-Z. (1999). Structural requirement of the calcium-channel subunit α 2 δ for gabapentin binding. Biochem. J, 342, 313–320.

Wang, X., Liu, H., Yuan, W., Cheng, Y., & Han, W. (2016). Efficient production of CYTL1 protein using mouse IgGκ signal peptide in the CHO cell expression system. Acta Biochimica et Biophysica Sinica, 48(4), 391–394. https://doi.org/10.1093/abbs/gmw007.

Wang, Y., Fehlhaber, K. E., Sarria, I., Cao, Y., Ingram, N. T., Guerrero-Given, D., Throesch, B., Baldwin, K., Kamasawa, N., Ohtsuka, T., Sampath, A. P., & Martemyanov, K. A. (2017). The Auxiliary Calcium Channel Subunit α2δ4 Is Required for Axonal Elaboration, Synaptic Transmission, and Wiring of Rod Photoreceptors. Neuron, 93(6), 1359-1374.e6. https://doi.org/10.1016/j.neuron.2017.02.021.

Wang, Y., Suzuki, R., Fujii, A., Ieki, K., Goda, W., Yasui, M., & Abe, Y. (2023). A tyrosine-based YXXΦ motif regulates the degradation of aquaporin-4 via both lysosomal and proteasomal pathways and is functionally inhibited by a 10-amino-acid sequence within its C-terminus. FEBS Journal, 290, 2616–2635. https://doi.org/10.1111/febs.16717.

Wartosch, L., Bright, N. A., & Luzio, J. P. (2015). Lysosomes. Current Biology, 25, R315–R316. https://doi.org/10.1016/j.cub.2015.02.027.

Watanabe, I., Zhu, J., Recio-Pinto, E., & Thornhill, W. B. (2004). Glycosylation affects the protein stability and cell surface expression of Kv1.4 but not Kv1.1 potassium channels: A pore region determinant dictates the effect of glycosylation on trafficking. Journal of Biological Chemistry, 279(10), 8879–8885. https://doi.org/10.1074/jbc.M309802200.

Wei, F., Qiu, C.-S., Kim, S. J., Muglia, L., Maas, J. W., Pineda, V. v, Xu, H.-M., Chen, Z.-F., Storm, D. R., Muglia, L. J., & Zhuo, M. (2002). Genetic elimination of behavioural sensitisation in mice lacking calmodulin-stimulated adenylyl cyclases. Neuron, 36, 713–726.

Weiss, N., & Zamponi, G. W. (2019). T-type calcium channels: From molecule to therapeutic opportunities. International Journal of Biochemistry and Cell Biology, 108, 34–39. https://doi.org/10.1016/j.biocel.2019.01.008.

Weiss, N., & Zamponi, G. W. (2020). Genetic T-type calcium channelopathies. Journal of Medical Genetics, 57, 1–10. https://doi.org/10.1136/jmedgenet-2019-106163.

Whittaker, C. A., & Hynes, R. O. (2002). Distribution and evolution of von Willebrand/integrin A domains: Widely dispersed domains with roles in cell adhesion and elsewhere. Molecular Biology of the Cell, 13, 3369–3387. https://doi.org/10.1091/mbc.E02-05-0259.

Wiechelman, K. J., Braun, R. D., & Fitzpatrick, J. D. (1988). Investigation of the bicinchoninic acid protein assay: Identification of the groups responsible for color formation. Analytical Biochemistry, 175(1), 231–237. https://doi.org/10.1016/0003-2697(88)90383-1.

Williams, S. R., Toth, T. I., Turner, J. P., Hughes, S. W., & Crunelli, V. (1997). The "window" component of the low threshold Ca2+ current produces input signal amplification and bistability in cat and rat thalamocortical neurones. Journal of Physiology, 505(3), 689–705.

Williams, T. M., & Lisanti, M. P. (2004). The caveolin proteins. Genome Biology, 5(214). http://genomebiology.com/2004/5/3/214.

Woll, K. A., & van Petegem, F. (2022). Calcium-release channels: Structure and function of IP3 receptors and ryanodine receptors. Physiological Reviews, 102, 209–268. https://doi.org/10.1152/PHYSREV.00033.2020.

Woodman, S. E., Park, D. S., Cohen, A. W., Cheung, M. W. C., Chandra, M., Shirani, J., Tang, B., Jelicks, L. A., Kitsis, R. N., Christ, G. J., Factor, S. M., Tanowitz, H. B., & Lisanti, M. P. (2002). Caveolin-3 knock-out mice develop a progressive cardiomyopathy and show hyperactivation of the p42/44 MAPK cascade. Journal of Biological Chemistry, 277(41), 38988–38997. https://doi.org/10.1074/jbc.M205511200.

Wu, J., Yan, Z., Li, Z., Qian, X., Lu, S., Dong, M., Zhou, Q., & Yan, N. (2016). Structure of the voltage-gated calcium channel Cav1.1 at 3.6 Å resolution. Nature, 537, 191–196. https://doi.org/10.1038/nature19321.

Wu, X., Zhang, Q., Guo, Y., Zhang, H., Guo, X., You, Q., & Wang, L. (2022). Methods for the Discovery and Identification of Small Molecules Targeting Oxidative Stress-Related Protein–Protein Interactions: An Update. Antioxidants, 11(619). https://doi.org/10.3390/antiox11040619.

Xu, H., & van Remmen, H. (2021). The SarcoEndoplasmic Reticulum Calcium ATPase (SERCA) pump: a potential target for intervention in aging and skeletal muscle pathologies. Skeletal Muscle, 11(25). https://doi.org/10.1186/s13395-021-00280-7.

Xu, H., Wu, L. J., Wang, H., Zhang, X., Vadakkan, K. I., Kim, S. S., Steenland, H. W., & Zhuo, M. (2008). Presynaptic and postsynaptic amplifications of neuropathic pain in the anterior cingulate cortex. Journal of Neuroscience, 28(29), 7445–7453. https://doi.org/10.1523/JNEUROSCI.1812-08.2008.

Yadav, S., Srivastava, A., Biswas, S., Chaurasia, N., Singh, S. K., Kumar, S., Srivastava, V., & Mishra, Y. (2020). Comparison and optimization of protein extraction and two-dimensional gel electrophoresis protocols for liverworts. BMC Research Notes, 13(60). https://doi.org/10.1186/s13104-020-4929-1.

Yagami, T., Kohma, H., & Yamamoto, Y. (2012). L-Type Voltage-Dependent Calcium Channels As Therapeutic Targets for Neurodegenerative Diseases. Current Medicinal Chemistry, 19(28), 4816–4827. https://doi.org/10.2174/092986712803341430.

Yarotskyy, V., & Dirksen, R. T. (2014). Cav1.1 in Malignant Hyperthermia. Pathologies of Calcium Channels.

Yarwood, R., Hellicar, J., Woodman, P. G., & Lowe, M. (2020). Membrane trafficking in health and disease. Disease Models and Mechanisms, 13. https://doi.org/10.1242/dmm.043448.

You, M., Yang, Y., Zhong, C., Chen, F., Wang, X., Jia, T., Chen, Y., Zhou, B., Mi, Q., Zhao, Q., An, Z., Luo, W., & Xia, N. (2018). Efficient mAb production in CHO cells with optimized signal peptide, codon, and UTR. Applied Microbiology and Biotechnology, 102, 5953–5964. https://doi.org/10.1007/s00253-018-8986-5.

Yu, Y., Zhu, J., Mi, L. Z., Walz, T., Sun, H., Chen, J. F., & Springer, T. A. (2012). Structural specializations of α 4β 7, an integrin that mediates rolling adhesion. Journal of Cell Biology, 196(1), 131–146. https://doi.org/10.1083/jcb.201110023.

Yuan, W., & Song, C. (2020). The Emerging Role of Rab5 in Membrane Receptor Trafficking and Signaling Pathways. Biochemistry Research International. https://doi.org/10.1155/2020/4186308.

Zamponi, G. W. (2016). Targeting voltage-gated calcium channels in neurological and psychiatric diseases. Nature Reviews Drug Discovery, 15, 19–34. https://doi.org/10.1038/nrd.2015.5.

Zamponi, G. W., Lewis, R. J., Todorovic, S. M., Arneric, S. P., & Snutch, T. P. (2009). Role of voltage-gated calcium channels in ascending pain pathways. Brain Research Reviews, 60(1), 84–89. https://doi.org/10.1016/j.brainresrev.2008.12.021.

Zamponi, G. W., Striessnig, J., Koschak, A., & Dolphin, A. C. (2015). The physiology, pathology, and pharmacology of voltage-gated calcium channels and their future therapeutic potential. Pharmacological Reviews, 67, 821–870. https://doi.org/10.1124/pr.114.009654.

Zhang, H., Links, P. H., Ngsee, J. K., Tran, K., Cui, Z., Ko, K. W. S., & Yao, Z. (2004). Localization of Low Density Lipoprotein Receptor-related Protein 1 to Caveolae in 3T3-L1 Adipocytes in Response to Insulin Treatment. Journal of Biological Chemistry, 279(3), 2221–2230. https://doi.org/10.1074/jbc.M310679200.

Zhang, J., Jiang, Z., & Shi, A. (2022). Rab GTPases: The principal players in crafting the regulatory landscape of endosomal trafficking. Computational and Structural Biotechnology Journal, 20, 4464–4472. https://doi.org/10.1016/j.csbj.2022.08.016.

Zhang, K., & Chen, J. F. (2012). The regulation of integrin function by divalent cations. Cell Adhesion and Migration, 6(1), 20–29. https://doi.org/10.4161/cam.18702.

Zhi, Y. R., Cao, F., Su, X. J., Gao, S. W., Zheng, H. N., Jiang, J. Y., Su, L., Liu, J., Wang, Y., Zhang, Y., & Zhang, Y. (2022). The T-Type Calcium Channel Cav3.2 in Somatostatin Interneurons in Spinal Dorsal Horn Participates in Mechanosensation and Mechanical Allodynia in Mice. Frontiers in Cellular Neuroscience, 16. https://doi.org/10.3389/fncel.2022.875726.

Zhu, X. D., Zhuang, Y., Ben, J. J., Qian, L. L., Huang, H. P., Bai, H., Sha, J. H., He, Z. G., & Chen, Q. (2011). Caveolae-dependent endocytosis is required for class a macrophage scavenger receptor-mediated apoptosis in macrophages. Journal of Biological Chemistry, 286(10), 8231–8239. https://doi.org/10.1074/jbc.M110.145888.

8. APPENDICES

8.1 Appendix I: Materials information

Antibodies		
Target	**Source (cat. no.)**	**Batch no.**
HA	BioLegend (901502)	B220767, B326653
c-Myc	Sigma (C3956)	087M4765V
	Sigma (M4439)	016M4762V, 0000085774
6-His	Sigma (SAB4301134)	492635533
TFR	Invitrogen (136800)	136800, 1100424A
Donkey anti-mouse IgG (H+L) Alexa Fluor ™ 546	Invitrogen (A10036)	1078784
Donkey anti-mouse IgG (H+L) Alexa Fluor ™ 647	Invitrogen (A31571)	1069838
Donkey anti-rabbit IgG (H+L) Alexa Fluor ™ 555	Invitrogen (A31572)	1891766
Donkey anti-rabbit IgG (H+L) Alexa Fluor ™ 488	Invitrogen (A21206)	1110071

Cell culture		
Item	**Source (cat. no.)**	**Batch no.**
FBS	Lonza (DE14-801FH)	1SB011H2
	Sigma (F7524)	0001662869
	Biowest (S181T-500)	S00JW
	Biowest (S1810-500)	S00GT
	Biowest (S181H-500)	S00FL

8.2 Appendix II: Chapter 4 supplementary data

```
human      MDEEEDGAGAEESGQPRSFMRLNDLSGAGGRPGPGSAEKDPGSADSEAEGLPYPALAPVV 60
rat        MDEEEDGAGAEESGQPRSFTQLNDLSGAGGRQGPGSTEKDPGSADSEAEGLPYPALAPVV 60
           ****************** :********** ****:************************

human      FFYLSQDSRPRSWCLRTVCNPWFERISMLVILLNCVTLGMFRPCEDIACDSQRCRILQAF 120
rat        FFYLSQDSRPRSWCLRTVCNPWFERVSMLVILLNCVTLGMFRPCEDIACDSQRCRILQAF 120
           *************************:**********************************

human      DDFIFAFFAVEMVVKMVALGIFGKKCYLGDTWNRLDFFIVIAGMLEYSLDLQNVSFSAVR 180
rat        DDFIFAFFAVEMVVKMVALGIFGKKCYLGDTWNRLDFFIVIAGMLEYSLDLQNVSFSAVR 180
           ************************************************************

human      TVRVLRPLRAINRVPSMRILVTLLLDTLPMLGNVLLLCFFVFFIFGIVGVQLWAGLLRNR 240
rat        TVRVLRPLRAINRVPSMRILVTLLLDTLPMLGNVLLLCFFVFFIFGIVGVQLWAGLLRNR 240
           ************************************************************

human      CFLPENFSLPLSVDLERYYQTENEDESPFICSQPRENGMRSCRSVPTLRGDGGGGPPCGL 300
rat        CFLPENFSLPLSVDLEPYYQTENEDESPFICSQPRENGMRSCRSVPTLRGEGGGGPPCSL 300
           *************** ********************************:*******.*

human      DYEAYNSSSNTTCVNWNQYYTNCSAGEHNPFKGAINFDNIGYAWIAIFQVITLEGWVDIM 360
rat        DYETYNSSSNTTCVNWNQYYTNCSAGEHNPFKGAINFDNIGYAWIAIFQVITLEGWVDIM 360
           ***:********************************************************

human      YFVMDAHSFYNFIYFILLIIVGSFFMINLCLVVIATQFSETKQRESQLMREQRVRFLSNA 420
rat        YFVMDAHSFYNFIYFILLIIVGSFFMINLCLVVIATQFSETKQRESQLMREQRVRFLSNA 420
           ************************************************************

human      STLASFSEPGSCYEELLKYLVYILRKAARRLAQVSRAAGVRVGLLSSPAPLGGQETQPSS 480
rat        STLASFSEPGSCYEELLKYLVYILRKAARRLAQVSRAIGVRAGLLSSPVARSGQEPQPSG 480
           ************************************ ***.******.  .*** ***.

human      SCSRSHRRLSVHHLVHHHHHHHHHYHLGNGTLRAPRASPEIQDRDANGSRRLMLPPPSTP 540
rat        SCTRSHRRLSVHHLVHHHHHHHHHYHLGNGTLRVPRASPEIQDRDANGSRRLMLPPPSTP 540
           **:*******************************.*************************

human      ALSGAPPGGAESVHSFYHADCHLEPVRCQAPPPRSPSEASGRTVGSGKVYPTVHTSPPPE 600
rat        TPSGGPPRGAESVHSFYHADCHLEPVRCQAPPPRCPSEASGRTVGSGKVYPTVHTSPPPE 600
           : **.** *************************.************************

human      TLKEKALVEVAASSGPPTLTSLNIPPGPYSSMHKLLETQSTGACQSSCKISSPCLKADSG 660
rat        ILKDKALVEVAPSPGPPTLTSFNIPPGPFSSMHKLLETQSTGACHSSCKISSPCSKADSG 660
            **:******* * *******:******:***************:********* *****

human      ACGPDSCPYCARAGAGEVELADREMPDSDSEAVYEFTQDAQHSDLRDPHSR-RQRSLGPD 719
rat        ACGPDSCPYCARTGAGEPESADHVMPDSDSEAVYEFTQDAQHSDLRDPHSRRRQRSLGPD 720
           ***********:**** * **: ************************** ********

human      AEPSSVLAFWRLICDTFRKIVDSKYFGRGIMIAILVNTLSMGIEYHEQPEELTNALEISN 779
rat        AEPSSVLAFWRLICDTFRKIVDSKYFGRGIMIAILVNTLSMGIEYHEQPEELTNALEISN 780
           ************************************************************

human      IVFTSLFALEMLLKLLVYGPFGYIKNPYNIFDGVIVVISVWEIVGQQGGGLSVLRTFRLM 839
rat        IVFTSLFALEMLLKLLVYGPFGYIKNPYNIFDGVIVVISVWEIVGQQGGGLSVLRTFRLM 840
           ************************************************************

human      RVLKLVRFLPALQRQLVVLMKTMDNVATFCMLLMLFIFIFSILGMHLFGCKFASERDGDT 899
rat        RVLKLVRFLPALQRQLVVLMKTMDNVATFCMLLMLFIFIFSILGMHLFGCKFASERDGDT 900
           ************************************************************

human      LPDRKNFDSLLWAIVTVFQILTQEDWNKVLYNGMASTSSWAALYFIALMTFGNYVLFNLL 959
rat        LPDRKNFDSLLWAIVTVFQILTQEDWNKVLYNGMASTSSWAALYFIALMTFGNYVLFNLL 960
           ************************************************************
```


human VAILVEGFQAEEISKREDASGQLSCIQLPVDSQGGDANKSESEPDFFSPSLDGDGDRKKC 1019
rat VAILVEGFQAE----------GDATKSESEPDFFSPSVDGDGDRKKR 997
human LALVSLGEHPELRKSLLPPLIIHTAATPMSLPKSTSTGLGEALGPASRRTSSSGSAEPGA 1079
rat LALVALGEHAELRKSLLPPLIIHTAATPMSHPKSSSTGVGEALGSGSRRTSSSGSAEPGA 1057
human A-HEMKSPPSARSSPHSPWSAASSWTSRRSSRNSLGRAPSLKRRSPSGERRSLLSGEGQE 1138
rat AHHEMKCPPSARSSPHSPWSAASSWTSRRSSRNSLGRAPSLKRRSPSGERRSLLSGEGQE 1117
human SQDEEESSEEERASPAGSDHRHRGSLEREAKSSFDLPDTLQVPGLHRTASGRGSASEHQD 1198
rat SQDEEESSEEDRASPAGSDHRHRGSLEREAKSSFDLPDTLQVPGLHRTASGRSSASEHQD 1177
human CNGKSASGRLARALRPDDPPLDGDDADDEGNLSKGERVRAWIRARLPACCLERDSWSAYI 1258
rat CNGKSASGRLARTLRTDDPQLDGDDDNDEGNLSKGERIQAWVRSRLPACCRERDSWSAYI 1237
human FPPQSRFRLLCHRIITHKMFDHVVLVIIFLNCITIAMERPKIDPHSAERIFLTLSNYIFT 1318
rat FPPQSRFRLLCHRIITHKMFDHVVLVIIFLNCITIAMERPKIDPHSAERIFLTLSNYIFT 1297
human AVFLAEMTVKVVALGWCFGEQAYLRSSWNVLDGLLVLISVIDILVSMVSDSGTKILGMLR 1378
rat AVFLAEMTVKVVALGWCFGEQAYLRSSWNVLDGLLVLISVIDILVSMVSDSGTKILGMLR 1357
human VLRLLRTLRPLRVISRAQGLKLVVETLMSSLKPIGNIVVICCAFFIIFGILGVQLFKGKF 1438
rat VLRLLRTLRPLRVISRAQGLKLVVETLMSSLKPIGNIVVICCAFFIIFGILGVQLFKGKF 1417
human FVCQGEDTRNITNKSDCAEASYRWVRHKYNFDNLGQALMSLFVLASKDGWVDIMYDGLDA 1498
rat FVCQGEDTRNITNKSDCAEASYRWVRHKYNFDNLGQALMSLFVLASKDGWVDIMYDGLDA 1477
human VGVDQQPIMNHNPWMLLYFISFLLIVAFFVLNMFVGVVVENFHKCRQHQEEEEARRREEK 1558
rat VGVDQQPIMNHNPWMLLYFISFLLIVAFFVLNMFVGVVVENFHKCRQHQEEEEARRREEK 1537
human RLRRLEKKRRNLMLDDVIASGSSASAASEAQCKPYYSDYSRFRLLVHHLCTSHYLDLFIT 1618
rat RLRRLEKKRRSK----------EKQMAEAQCKPYYSDYSRFRLLVHHLCTSHYLDLFIT 1586
human GVIGLNVVTMAMEHYQQPQILDEALKICNYIFTVIFVLESVFKLVAFGFRRFFQDRWNQL 1678
rat GVIGLNVVTMAMEHYQQPQILDEALKICNYIFTVIFVFESVFKLVAFGFRRFFQDRWNQL 1646
human DLAIVLLSIMGITLEEIEVNASLPINPTIIRIMRVLRIARVLKLLKMAVGMRALLDTVMQ 1738
rat DLAIVLLSIMGITLEEIEVNLSLPINPTIIRIMRVLRIARVLKLLKMAVGMRALLHTVMQ 1706
human ALPQVGNLGLLFMLLFFIFAALGVELFGDLECDETHPCEGLGRHATFRNFGMAFLTLFRV 1798
rat ALPQVGNLGLLFMLLFFIFAALGVELFGDLECDETHPCEGLGRHATFRNFGMAFLTLFRV 1766
human STGDNWNGIMKDTLRDCDQESTCYNTVISPIYFVSFVLTAQFVLVNVVIAVLMKHLEESN 1858
rat STGDNWNGIMKDTLRDCDQESTCYNTVISPIYFVSFVLTAQFVLVNVVIAVLMKHLEESN 1826
human KEAKEEAELEAELELEMKTLSPQPHSPLGSPFLWPGVEGPDSPDSPKPGALHPAAHARSA 1918
rat KEAKEEAELEAELELEMKTLSPQPHSPLGSPFLWPGVEGVNSTDSPKPGAPHTTAHIGAA 1886

Figure 8.1 Amino acid sequence alignment of hCa$_V$3.1 and rCa$_V$3.1. Alignment was performed in Clustal Omega multiple sequence alignment tool using amino acid sequences from UniProt (hCa$_V$3.1: O434497; rCa$_V$3.1: O54898).

Power Analysis Table

	N1	N2	Actual Power[b]	Test Assumptions Power	Std. Dev.[c]	Effect Size	Sig.
Test for Mean Difference[a]	15	15	.805	.8	.48	-.937	.05

a. One-sided test.

b. Based on noncentral t-distribution.

c. Group variances are assumed to be equal.

Figure 8.2 Power calculations to determine optimal sample size for CACHD1-wt.

Power Analysis Table

	N1	N2	Actual Power[b]	Test Assumptions Power	Std. Dev.[c]	Effect Size	Sig.
Test for Mean Difference[a]	16	16	.809	.8	.34	.912	.05

a. One-sided test.

b. Based on noncentral t-distribution.

c. Group variances are assumed to be equal.

Figure 8.3 Power calculations to determine optimal sample size for CACHD1-AAA.

Power Analysis Table

	N1	N2	Actual Power[b]	Test Assumptions Power	Std. Dev.[c]	Effect Size	Sig.
Test for Mean Difference[a]	14	14	.824	.8	.19	-1.000	.05

a. One-sided test.

b. Based on noncentral t-distribution.

c. Group variances are assumed to be equal.

Figure 8.4 Power calculations to determine optimal sample size for CACHD1-G236S.

8.3 Appendix IV: List of publications

The MIDAS motif of voltage-gated calcium channel CACHD1 subunit contributes to protein trafficking. Selected Abstracts from Pharmacology 2022 (conference abstract). *British Journal of Pharmacology*. Accepted Author Manuscript. (https://doi.org/10.1111/bph.15944).

Ablinger, C., Eibl, C., Roznovcova, M., Cottrell, G. S., Stephens, G. J., Obermair, G. J. (2024). The presynaptic α2δ protein family and their therapeutic potential. In: Ion Channels as Targets in Drug Discovery. Eds: Stephens, G. J., Stevens, E. B.. Springer.

8.4 Appendix V: List of posters, presentations and conferences attended

- *The MIDAS motif of voltage-gated calcium channel CACHD1 subunit contributes to protein trafficking*; Pharmacology 2022, Liverpool; 15 min presentation

- *The 'AAA' MIDAS motif mutation reduces expression and impairs trafficking of CACHD1 in HEK293 cells*, UoR Doctoral Research Conference 2022, Reading; Poster (People's choice prize)

- *The 'AAA' MIDAS motif mutation reduces expression and impairs trafficking of CACHD1 in HEK293 cells*; European Calcium Channel Conference 2022, Alpbach; Poster

- *The 'AAA' MIDAS motif mutation reduces expression and impairs trafficking of CACHD1 in HEK293 cells*; Calcium Channels in Excitable Cells Symposium 2022, Innsbruck; Poster

- *The 'AAA' MIDAS motif mutation reduces expression and impairs trafficking of CACHD1 in HEK293 cells*; Cambridge Ion Channel Forum 2022, Cambridge; Poster (2nd place for best poster)

- *The effects of MIDAS motif mutations on the expression and function of CACHD1 protein*; UoR School of Pharmacy PhD Showcase 2022, Reading; 10 min presentation

- *The novel role of the CACHD1 protein in hyperexcitability disease*; UoR School of Pharmacy PhD showcase 2021, Reading; 5 min presentation